Université catholique de Louvain
Ecole Polytechnique de Louvain
Institute of Condensed Matter and Nanosciences
Division of Bio and Soft Matter

Synthesis and Dynamics of Metallo-Supramolecular Polymeric Assemblies

Flanco Zhuge

Jury members:

Prof. Jacques Devaux (UCL), Chairman
Prof. Evelyne van Ruymbeke (UCL), Supervisor
Prof. Jean-François Gohy (UCL), Co-supervisor
Prof. Charles-André Fustin (UCL)
Prof. Dimitris Vlassopoulos (FORTH)
Prof. Michel Cloître (EPSCI)

Thesis submitted in fulfillment of the degree
of Doctor in Engineering Science and Technology

Louvain-la-Neuve 2018

1

Abstract

Associating polymers, based on the dynamic metal-ligand (M-L) coordination, form an interesting class of materials because of the richness in their tunable properties and the design of various self-assembled materials. These adaptable systems have potential applications in various domains such as tissue engineering, coatings, adhesives or shock absorbers. Regardless of the final application, the possible exploitation of the transient nature hinges on the rheological behavior and resulting processability. In this respect, the design of responsive entangled supramolecular polymers is dependent on our fundamental understanding of their structure and dynamics in the melt state. This thesis addresses this grand challenge, and aims at a deeper understanding of how the combination of M-L interactions with entanglements impacts the structure, the relaxation dynamics and the mechanical properties of well-defined entangled metallo-supramolecular polymers over a wide timescale or temperature range. The structure-property relationships are established based on several experimental techniques (RAFT polymerization, shear and extensional rheology, DSC, DRS and X-ray scattering) combined with theoretical tube-based models (upgraded TMA). Results showed that the viscoelasticity of these systems are affected by both the disentanglement process of the polymers and the dissociation mechanism of the metal-ligand complexes. By altering the temperature, we systematically vary the relative importance of the M-L interactions, which allows us to determine their specific contribution to the viscoelastic properties. Through this systematic investigation, general guidelines are achieved to unambiguously control the design of supramolecular materials with specific rheological features that can be engineered over a wide window of mechanical properties.

Table of contents

List of acronyms

A	Acceptor
AFM	Atomic force microscopy
AIBN	2,2'-azobis(isobutyronitrile)
BA	Butyl acrylate
BMA	Butyl methacrylate
Bpy	Bipyridine
Btp	Bistriazolypyridine
CBMAT	2-(2-Carboxyethylsulfanylthiocarbonylsulfanyl)-2-methylpropionic acid
CLF	Contour length fluctuation
CPP	Cone partitioned plate
CR	Constraint release
CRR	Constraints release Rouse
CTA	Chain transfer agent
D	Donor
DCM	Dichloromethane
DDMAT	2-(Dodecylthiocarbonothioylthio)-2-methylpropionic acid
DMA	N,N-dimethylacrylamide
DMF	dimethylformamide
DMSO	Dimethylsulfoxide
DP	Degree of polymerization
DPTZ	3,6-di-2-pyridinyl-1,2,4,5-tetrazine
DRS	Dielectric relaxation spectroscopy
DSC	Differential scanning calorimetry

DSP	Degree of supramolecular polymer
DTD	Dynamic tube dilatation
EDCI	N-(3-dimethyl-aminopropyl)-N'-ethylcarbodiimide hydrochloride
EP	Electrode polarization
FSR	Filament stretching rheometer
HB	Hydrogen bonding
His	Histidine
HN	Havriliak-Negami
HOBT	1-hydroxybenzotriazole
I	Initiator
IB	Ionic bond
ICP	Imidazole containing polymers
L/M	Ligand/Metal ratio
LAOS	Large amplitude oscillatory shear
LMA	Lauryl methacrylate
M	Molar concentration (mol/L ≡ M)
Mebip	2,6-bis(1-metyhlbenzimidazolyl)pyridine
M-L	Metal-ligand
MMA	Methyl methacrylate
MSBN	Metallo-supramolecular polymer network
MSBP	Metallo-supramolecular bulk polymer
MSP	Metallo-supramolecular polymer
***n*BA**	*n*-butyl acrylate
NIPAM	N-isopropylacrylamide
NMP	Nitroxide mediated polymerization
NMR	Nuclear magnetic resonance

Norb	Norbornene
P3HT	Poly(3-hexylthiophene)
PBMA	Poly(butyl methacrylate)
PDCPD	Poly(dicyclopentadiene)
PDMA	Poly(N,N-dimethylacrylamide)
PDMS	Poly(dimethylsiloxane)
PEG	Poly(ethylene glycol)
PEO	Poly(ethylene oxide)
Phen	Phenanthroline
PLMA	Poly(lauryl methacrylate)
P*n*BA	Poly(*n*-butyl acrylate)
PS	Polystyrene
PTC	Phase transfer catalyzed
PTMAT	Pentaerythritoltetrakis-(2-(2-Carboxyethylsulfanylthio-carbonylsulfanyl)-2-methylpropionic acid)
Pybox	Thiophene functionalized norbornene
RAFT	Reversible addition-fragmentation transfer
RDRP	Reversible deactivation radical polymerization
Ref	Reference
ROMP	Ring opening metathesis polymerization
SAOS	Small amplitude oscillatory shear
SAXS	Small angle X-ray scattering
SEC	Size exclusion chromatography
THF	Tetrahydrofuran
TMA	Time marching algorithm
TPA	Terpyridine acrylate
Tpy	Terpyridine

Tpy-A	Terpyridine acrylate
TTC	Trithiocarbonate
TTS	Time temperature superposition
Upy	Ureidopyrimidinone
UV/Vis	Ultra-violet/visible
VDM	2-vinyl-4,4-dimethyl-azlactone
vdW	van der Waals
VFT	Vogel-Fulcher-Tammann
VPR	Vinylpyridine
WAXS	Wide angle X-ray scattering
WLF	William-Landel-Ferry
XB	Halogen bonding

General Introduction

Inspired by Nature, supramolecular chemistry has become a powerful tool to form associating building blocks with interesting properties. There are several non-covalent interactions that can be used in supramolecular chemistry. Among them, the metal-ligand coordinations are particularly promising because these interactions are stimuli-responsive and they are highly directional, meaning that the M-L interaction occurs in specific orientation between the metal atom and the ligand. Moreover, the dynamics of metal-ligand coordinations can be finely tailored due to their versatilities in which various metal ions can react with multiple ligands. These interactions were first used to assemble small chemical entities or oligomers with relatively low molar masses, forming supramolecular polymers in which monomers are linked together via metal-ligand interactions. Later on this concept was expanded to the incorporation of metal-ligand coordination into polymers with higher molar masses.

Indeed, the use of these interactions into usual polymers has led to the development of a broad range of associating polymers with featuring properties that can be dynamically tuned. Thus to achieve this complete mastery, one of the main challenge is to incorporate these associating units within high molar mass polymeric chains in a well-controlled way. The first used approach was post-functionalization of already synthesized polymers. However, this method does not lead to a total control over the inclusion of metal-ligand coordination into polymers. The post-functionalization approach is not always fully quantitative especially when polymers with high molar masses are used, resulting into partially functionalized associating systems. During the past ten years, the controlled polymerization techniques have allowed to precisely incorporate the metal-ligand interactions within polymer chains at specific locations. In fact, a characteristic point of these polymerization techniques is the use of a precursor (initiator or chain transfer agent) in which its chemical structure is embodied into the formed polymer chains. By functionalizing these precursors with metal-

ligand coordination groups, it is then possible to specifically incorporate these associating units within polymer chains with a quantitative yield.

The resulting metallo-supramolecular polymers can self-assemble into well-organized nanostructures, improving the mechanical properties of polymers. The development of such associating systems gives access to polymeric materials with a wide range of upgraded mechanical properties that can be engineered. In parallel, these materials can be easily processed by tuning the association/dissociation mechanism of metal-ligand coordination with external stimuli such as temperature, irradiation, shear or elongation. The reversibility of these interactions can also be exploited in the elaboration of stimuli-responsive materials with healing features. Plethora of studies have been reported on metallo-supramolecular polymers. However, most of these works are essentially focused on the healing properties of the unentangled associating materials at the expense of fundamentally understanding their mechanical features. Rheological properties and dynamics of these systems have not been deeply studied and a good understanding on the topological effects within the bulk materials is unfortunately not fully established.

In the framework of this thesis, a systematic investigation over the fundamental relationships between rheological properties and structures of the entangled associating metallo-supramolecular polymers is conducted. Herein, the contribution of entanglements originating from the high molar mass polymers combined with the metal-ligand coordination is considered and its influence on the structure, the relaxation dynamics and the mechanical properties of the well-defined associating materials is studied, so that the structure-property relationships can be well-established to provide a design guideline of associating polymers. In this manuscript, the elaboration of different entangled supramolecular polymeric models is reported. The influence of the structural design of these associating polymers on the resulting mechanical properties is systematically investigated. The selected associating unit is based on the tridentate terpyridine ligand. The latter is incorporated into the poly(*n*-butyl acrylate) polymer. Different transition metal cations are used to modulate the dynamics of

metal-ligand coordination and consequently the mechanical properties of the entangled metallo-supramolecular polymers under load.

Chapter 1 describes a state of the art on polymers containing associating units based on metal-ligand coordination. The advent of supramolecular chemistry, the incorporation of these interactions within polymers, the resulting mechanical properties and theoretical models on associating polymers are succinctly described.

Chapter 2 reports on the synthesis of different entangled supramolecular poly(*n*-butyl acrylate) building blocks bearing terpyridine ligands. The pre-modification approach coupled with the RAFT polymerization strategy is explained. The influence of the associating units and the topology of the polymers is exploited.

In Chapter 3, a systematic investigation on the linear viscoelastic properties of the metallo-supramolecular bulk polymers is conducted. The properties of the obtained associating systems can be finely tailored depending on the topology, the length of the polymer chains and the nature of added metal ions.

Chapter 4 presents a modified version of the tube-based time marching algorithm model to describe the linear dynamics of metallo-supramolecular polymers. The latter reveals that the dissociation events of metal-ligand complexes occur via ligand exchange process. The results are found to be consistent with experimental data.

In Chapter 5, the systematic investigation is extended to nonlinear viscoelastic properties of metallo-supramolecular bulk networks. The influence of the metal-ligand complex combined with polymer entanglements and the fraction of uncoordinated chains on the capacity of the transient network to resist large deformation is established.

Chapter 6 is an attempt to experimentally determine the lifetime of the metal-ligand complexes in the poly(*n*-butyl acrylate) matrix. Dielectric relaxation spectroscopy is used to probe this timescales at different temperatures.

In Chapter 7, early results on the linear viscoelastic properties of binary blends based on metallo-supramolecular networks are also

15

investigated. Precisely, the transient networks are diluted in two different linear poly(*n*-butyl acrylate) matrices. The results reveals the influence of the length and the ratio of linear matrices over the dynamics of the metallo-supramolecular polymers.

In the last part of this manuscript, general conclusions are drawn and possible perspectives for future investigations are presented.

Chapter 1

State of the art

Abstract

In this Chapter, some fundamentals on supramolecular chemistry, polymers and rheology basics are reminded. During these past five years, several studies have been reported in the literature on the synthesis and the mechanical properties of supramolecular polymers and selected examples are presented herein. A supramolecular polymer is a complex assembly of molecules held together by noncovalent, relatively weak and reversible associations, such as van der Waals interactions, π-π stacking, hydrogen bonding, host-guest interactions or coordinative bonds. The last few decades, great achievements have been made in the field of supramolecular polymers, and plethora supramolecular polymers have been designed with different synthetic strategies. The mechanical features of these systems are also widely investigated using a range of experimental techniques and several theoretical models are introduced.

1.1 Synthesis of metallo-supramolecular polymer

1.1.1 Supramolecular chemistry

In 1987 Jean-Marie Lehn, Charles Pedersen and Donald Cram were awarded the Nobel Prize for their pioneering contributions to supramolecular chemistry. Supramolecular chemistry has been defined by Lehn[1] as:

"the chemistry beyond the molecule bearing on the organized entities of higher complexity that result from the association of two or more chemical species held together by intermolecular forces"

Hence, in classical molecular chemistry the molecules are built through atoms connected by covalent bonds. Whereas the supramolecular compounds are built by connecting molecules with non-covalent intermolecular forces to form supramolecules. The formation of these supramolecular components through reversible interactions gives access to new chemical entities with interesting properties that behave in entirely novel ways and respond towards external stimuli. There are a variety of well-established non-covalent interactions which can be distinguished by their natures or by their binding energies such as:

- van der Waals interactions ($E \leq 5$ kJ.mol^{-1}).

van der Waals (vdW) interaction occurs from the polarization of an electron cloud of an atom or a molecule by the vicinity of an adjacent atom or molecule.[2,3] Resulting in an electrostatic attraction or repulsion between atomic or molecular entities. The vdW interaction encompasses the electrostatic (dipole-dipole) interaction between permanent dipoles in polar systems, the induction (dipole-induced dipole) interaction between polar and non-polar systems and the dispersion interaction between induced dipoles in non-polar systems.[4] vdW forces are short-range, non-directional (meaning that the interaction can occur in any orientation) and they are considered as extremely weak interactions compared to other interactions.[5]

- π-π stacking interaction (E = 2-50 kJ.mol^{-1}).

π-π stacking interaction is a weak, directional intermolecular interaction in molecules with aromatic conjugated groups.[6] The effect of aromaticity is that, by drawing electron density into orbitals bonded to the carbon atoms, the hydrogen atoms of the molecules are polarized. This results in an electron rich region linked to the π system and an electron poor region associated with the hydrogen atoms. By overlapping the π-electron cloud in two aromatic molecules, π-π stacking interaction occurs where one molecule lies above the other so that the complementary electron rich and electron poor regions match up. There are at least three types of conformations in π stacking interaction for the benzene dimer, parallel, displaced parallel and T-shaped configurations as illustrated in Figure 1.1.[7]

----- Electrostatic repulsion   ----- Electrostatic attraction
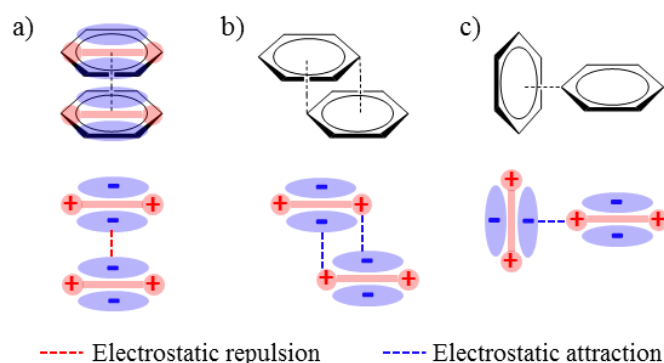
Figure 1.1: Three stacking patterns of benzene dimers a) parallel face-to-face, b) displaced parallel and c) T-shaped edge-to face.[7]

- Hydrogen bonding (E = 4-120 kJ.mol^{-1}).

The hydrogen bond (HB) is an attractive intra- or intermolecular interaction between an electron-deficient hydrogen atom covalently bonded to an electronegative atom (donor) from a molecule and another electronegative atom (acceptor) in the same or a different molecule.[8] The atoms, with lone pair of electrons and with electronegativity greater than hydrogen, have the capacity to form hydrogen bonds.[9] Both the strength and the directionality of HB can be fine-tuned when multiple hydrogen bonding arrays are used by varying the number or the order of the donor (D) and acceptor in the arrays (A) as schematized in Figure

1.2. Depending on the sequences of the multiple hydrogen bonding arrays, the binding constant can be low or significantly high.[10]
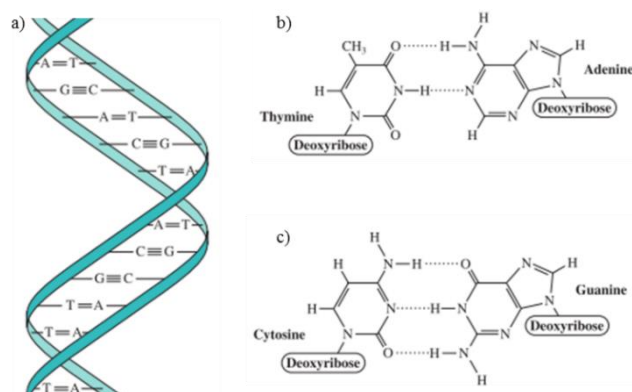
Figure 1.2: a) The DNA double helix held together by HB between complementary nucleobases. Chemical structures of b) Thymine-Adenine and c) Cytosine-Guanine pairs.[11]

- Halogen bonding (E = 10-180 kJ.mol^{-1}).

The halogen bond (XB) arises from a net attractive interaction between an electrophilic region associated with a halogen atom, in a molecular entity and a nucleophilic region in another (or the same) molecular entity as depicted in Figure 1.3.[12–14] In another words, a halogen bond occurs through a transfer of electron density between the Lewis basic site (i.e. XB acceptor, electron donor) and the Lewis acidic site (i.e. XB donor, electron acceptor). The strength of XB can be finely tailored by varying the nature of halogen atom and the moiety to which it is covalently linked. Indeed when the electron-withdrawing capacity of the substituent increases, it leads to an increase of halogen-bond donor strength.[15]
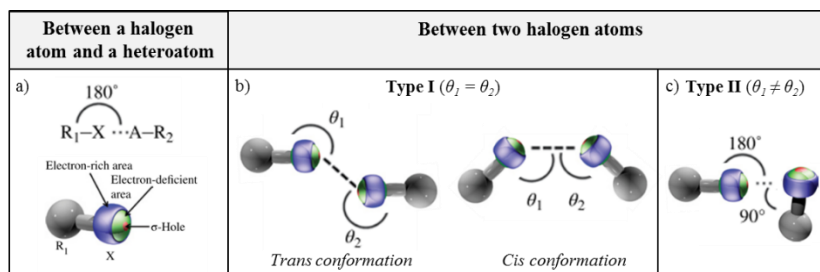
Figure 1.3: a) Halogen bond involving a XB donor and a heteroatom acceptor. XB between two halogen atoms b) Type I and c) Type II.[16,17]

- Metal-ligand coordination (E = 100-300 kJ.mol^{-1}).

The metal-ligand (M-L) coordination occurs when an orbital with lone pair of electrons originated from an atom associated to a ligand overlaps with an empty orbital with specific directional preferences coming from a metal atom as illustrated in Figure 1.4. More precisely, a stable M-L complex is formed via a transfer of a pair (or pairs) of electrons between a Lewis base (i.e. ligand, electron-pair donor) and a Lewis acid (i.e. metal atom, electron-pair acceptor). M-L coordinative bonding displays high directionality and their binding strength offers great versatility due to diverse transition metal atoms and various polydentate ligands. These interactions, while strong, can also be labile and reversible.[18,19]

Electron-pair donor   Metal   Metal-ligand coordination
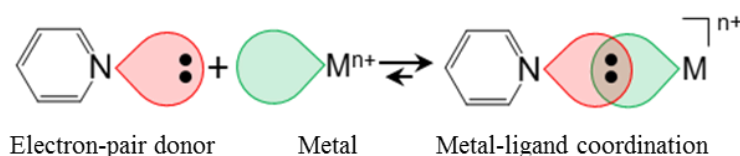
Figure 1.4: M-L coordination via electron-pair transfer from a ligand to a transition metal atom with specific directional preferences.

- Ionic interactions (E = 100-350 kJ.mol^{-1}).

An ionic bond (IB) is a strong electrostatic attraction between two oppositely charged ions (i.e. cations and anions). It is originated from a complete transfer of electrons from one atom to another to form ions. Hence, IBs are formed when there is a large difference in electronegativity between the two atoms bonding together. A large amount of energy is required to disrupt these interactions and to separate the ions. Indeed complementary non-directional cation-anion interactions can be as strong as covalent bonds. However, since the ions are charged, they can be easily disrupted in presence of polar molecules as shown in Figure 1.5.
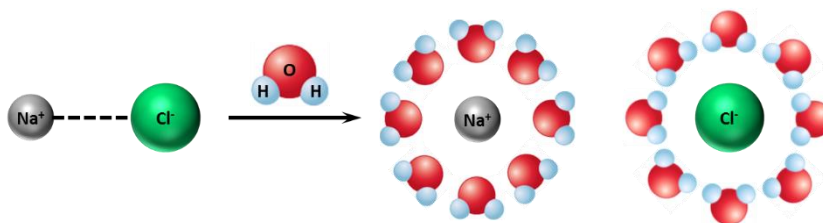
Figure 1.5: Ionic interaction between sodium Na$^+$, chloride Cl$^-$ ions in absence and in presence of polar water molecules.

21

In general, reversible non-covalent interactions listed in Table 1.1, allowing the association of molecules, are characterized by binding energies smaller than those of typical covalent chemical bonds (E = 200-400 kJ.mol^{-1}). Individually these supramolecular interactions are often weaker than covalent bonds but their cumulative effects can drive the formation of complex functional molecular systems with unique properties. Both the reversibility and the flexibility of non-covalent interactions are favored to construct supramolecular compounds which involve molecular recognition or self-assembly of constituent components. The existence of these multicomponent entities is due to reversible interactions which can dissociate and reform towards particular external, chemical or environmental stimuli. It is important to emphasize the different levels of complexity to design high affinity reversible host-guest interactions at molecular scale and to target specific dynamic molecular assembly, i.e. the thermodynamic and kinetic reversibility of non-covalent interactions between supramolecular components.

Interactions	Directionality	Binding energy (kJ.mol^{-1})
van der Waals	Non-directional	< 5
π-π stacking	Directional	$2 - 50$
Hydrogen bonds	Directional	$4 - 120$
Halogen bonds	Directional	$10 - 180$
Metal-ligand bonds	Directional	$100 - 300$
Ionic	Directional	$100 - 350$
Covalent bonds	Directional	$200 - 400$

Table 1.1: List of common supramolecular interactions.

Following these principles, it appears that the reversible metal-ligand coordination complexes are excellent non-covalent candidates to focus on because they are based on highly directional interactions that can be dynamically tailored by varying the types of ligands or by altering the nature of metal atoms.[18] In M-L coordination, the thermodynamic as well as the kinetic stabilities of a host-guest complex are enhanced by the chelating effects originating from the ligands. The donor ligand atoms are the host binding sites and the acceptor metal

atoms act as the guests. Self-assembly of molecules through M-L complexation is generally spontaneous and the most thermodynamically stable structure is formed. This is why the structural integrity of the self-assembled macromolecules is maintained with a constant balance between enthalpy and entropy. Hence, controlling the dynamics of M-L coordination to dictate the molecular organization (or recognition) is a key point in the elaboration of materials in which these host-guest interactions are incorporated. The application of metal-ligand complexes to materials science is an emerging domain. Coordination bonds have been significantly developed to offer a variety of highly functionalized polymeric materials in which it is possible to modify the properties of supramolecular structures through the panoply of tools supplied by the fields of organic polymers and inorganic chemistry.

1.1.2 Supramolecular polymers

Supramolecular polymers are at the crossroad between polymer science and supramolecular chemistry. Meijer[20] defined supramolecular polymers as:

"polymeric arrays of monomeric units that are brought together by reversible and highly directional secondary interactions, resulting in polymeric properties in dilute and concentrated solutions, as well as in the bulk".

The directionality and strength of the supramolecular bonding are important features. Due to their dynamic and reversible properties supramolecular polymers have been studied and have brought new vigor in material science. As previously mentioned, there is a variety of non-covalent interactions, e.g. aromatic stacking, hydrogen bonding, metal-ligand coordination and ionic interaction that have been employed as driving forces to construct supramolecular polymers. Herein, the focus will essentially be on metal-ligand containing polymers. Metallo-supramolecular polymers (MSPs) originating from building blocks with chelating groups linked to chains through reversible metal-ligand coordination as depicted in Figure 1.6, have

been extensively studied because they represent an important class of soft supramolecular materials.[21]
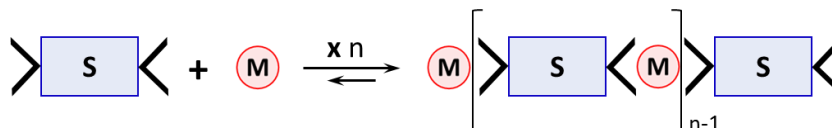
Figure 1.6: A supramolecular coordination polymer with M as a metal ion, and S as an organic spacer bridging two ligand moieties.

The macromolecular metal-containing systems exhibit the properties of organic polymers but also potential redox, magnetic, electrochromic, optical and catalytic properties of metallic complexes.[22,23] Additionally, these systems can reversibly dissociate and re-associate leading to the development of environment-adaptable materials.[24] Therefore, MSPs are promising systems for the development of functional self-organized architectures with tunable properties. The physical, chemical and mechanical properties of these coordinating polymers can be tailored by (i) the structure of the polymers itself, (ii) the choice of chelating groups and (iii) the choice of metal ions.[25–27] Due to the high variety of ligands and metal ions, the binding strength, the coordination and the reversibility can be adjusted widely. To achieve a high degree of supramolecular polymerization (DSP), a wise choice of complexation system with high binding strength is necessary along with other parameters such as solvents, temperature and concentrations. For reversible MSPs, the degree of supramolecular polymerization can be estimated with the following equation:

$$DSP \; \alpha \; (K[M])^{1/2} \tag{1.1}$$

Where K is the binding constant (or binding strength) and M is the monomer concentration (or precursor concentration). Hence according to equation 1.1, to obtain MSPs with a high DSP, large binding strength and high concentration are of paramount importance. An increase of binding constant K can be achieved by using multidentate ligands and different metal ions. Dobrawa and Würthner demonstrated this strategy by a comparison of Zn^{2+} complexation with different types of pyridine

donor ligands in specific solvents as summarized in Table 1.2.[18,28] According to different pyridine derivatives, the binding constant significantly increased from $K = 10^3$ M^{-1} for monodentate pyridine-Zn^{2+} complex to $K > 10^{14}$ M^{-2} for tridentate terpyridine-Zn^{2+} complex. Following equation 1.1, the DSP of metallo-supramolecular polymers constructed from 1 mM solution of precursors can be estimated. In the case of binding constant of $K = 10^5$ M^{-1}, it is expected to obtain only oligomers with a DSP $\sim$ 10. Whereas in the case of binding constant $K = 10^7$ M^{-1}, polymers with DSP $\sim$ 100 can be obtained. The rational design of the molecular structure of ligands and the directionality of the coordination bonding are of prime importance since both play a key roles in the construction of MSPs. With the development of MSPs, a great diversity of ligands has been designed. Among these ligands, pyridine (monodentate, bidentate, tridentate or multidentate) derivatives are especially interesting for their high binding affinity with various metal cations.

In the following, several metallo-supramolecular polymers will be presented based on the aforementioned ligands with different metal cations. First the pyridine based monodentate ligands will be introduced, followed by bidentate and tridentate ligands. Herein the development of metallo-supramolecular polymers during these past five years will be presented. The plethora examples of associating polymers based on metal-ligand coordination and the different synthetic strategies to elaborate these materials will be highlighted.
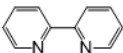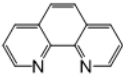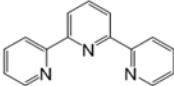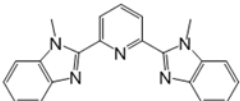
Chemical structure	Ligand Name	Binding constant	Solvent
	Pyridine	$4.1 \times 10^3 \ M^{-1}$	Chloroform
	Bipyridine	$10^{13} \ M^{-3}$	Water
	Phenanthroline	$10^{17} \ M^{-3}$	Water
	Terpyridine	$2.0 \times 10^{14} \ M^{-2}$	Acetonitrile
	Methylbenzimidazolyl pyridine	$10^6 \ M^{-3}$	Chloroform/ Acetonitrile

Table 1.2: Binding constants of zinc(II) complexes with different types of pyridine based ligands.[29–32]

Khlobystov et al. reported that the coordination of pyridine based ligands to silver Ag(I) ions (Figure 1.7(a)) tends to connect two ligands into linear one-dimensional structures because the Ag$^+$-pyridine complexes do not display high binding constant.[33] Indeed, due to the high lability of Ag(I) metal ion, the process of coordination polymer formation is completely reversible. Würthner et al. developed a highly soluble diazadibenzoperylene-based dye capable of forming a coordination polymer in presence of silver Ag(I) ions as depicted in Figure 1.7(b).[34] The tetraphenoxy-diazadibenzoperylene ligand forms a complex with Ag$^+$, as confirmed by an increased viscosity of the system suggesting the presence of one-dimensional coordination polymer at an equimolar ratio of the ligand and AgOTf.
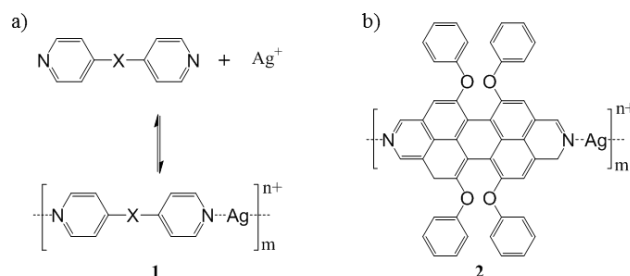
Figure 1.7: Reversible metal-ligand coordination binding molecular components with X an organic spacer between pyridyl ligands.[33,34]

Recently Martínez-Calvo et al. generated luminescent MSP by combining pyridine-2,6-dicarboxylic acid based ligands that can bind to lanthanides and transition metal ions as shown in Figure 1.8.[35] The ligand was designed to facilitate the formation of three-dimensional structures of high order. The presence of carboxylic acid groups plays an important role in the coordination of Eu(III) or Tb(III) lanthanides ions by providing the necessary platform for the formation of highly organized and large self-assembled coordinating polymer.
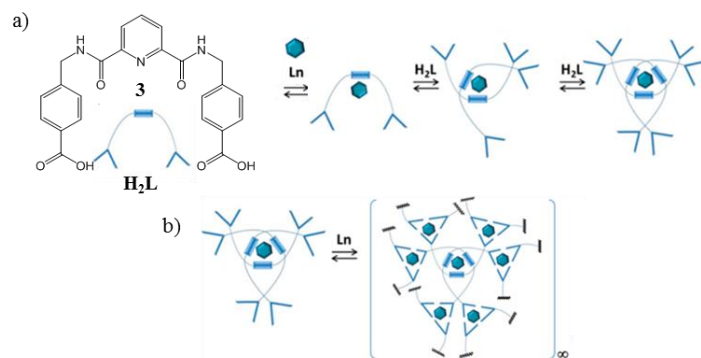
Figure 1.8: a) Self-assembly of pyridine-2,6-dicarboxylic acid derivative ligand in presence of lanthanide ions. b) Formation of high order metallo-supramolecular polymers.[35]

The pyridine moiety is the simplest ligand type for the elaboration of coordination polymers. However, monodentate pyridine ligand-metal complexes are not strong enough to form materials with polymeric properties. The self-assembly of MSPs can be achieved if the binding

constants (K) are increased. To do so, additional interactions need to be taken into account such as the chelating effect of multidentate ligands.

As already mentioned, the application of chelating complexes is an effective method to aim higher binding constants for metallo-supramolecular polymeric assemblies. Rehahn et al. reported the first example of a high molar mass MSP that is soluble and inert in organic non-coordinating solvents.[36] A coordinating polymer with a DSP higher than 30 was obtained based on a bidentate phenanthroline ligand monomer, 4,4''-bis[(9-aryl)-2-*o*-phenanthroline]-2',5'-di-*n*-hexyl-*p*-terphenyl, which was mixed with a equimolar amount of [Cu(MeCN)$_4$]PF$_6$. However, when a coordinating solvent such as acetonitrile was added to the MSP, the resulting system decomposed into oligomers because it became more dynamic with rapid exchange of ligands. Based on this results, Rehahn et al. also developed a set of MSPs based on different structures of *o*-phenanthroline bidentate ligands with copper (I) ions and silver (I) ions as represented in Figure 1.9(a).[37,38]

Higuchi et al. employed unsubstituted phenanthroline with a dioctylfluorene group as spacer to elaborate a copper containing supramolecular polymer as shown in Figure 1.9(b).[39] A high molar mass (M_n = 7600 kg.mol^{-1}) supramolecular polymer was obtained. Compared to substituted phenanthroline-based ligands, the unsubstituted ones display a higher coordination affinity with metal ions due to the lack of steric hindrance. Higuchi et al. also developed electrochromic and ionic conductive materials based on the unsubstituted phenanthroline ligand chelated with copper Cu(II) ions and with nickel Ni(II) ions.[40,41]
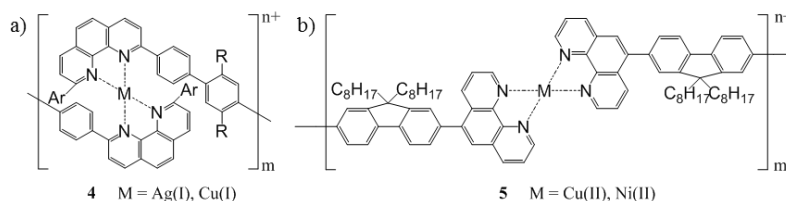
Figure 1.9: a) Formation of MSP based on a) a ditopic substituted phenanthroline and b) a phenanthroline with a fluorene spacer.[37–39]

Since then, many excellent reviews encompass a great number of metal-containing polymers which have been synthesized either by incorporating ligands into the main chain or by attaching them as pendant groups at the side chain.[21,42–46] This chapter will essentially focus on the emerging metallo-supramolecular polymers which have been synthesized during the past five years. Recently Rao et al. designed a dielectric elastomer which is achieved by incorporation of metal-ligand coordination as cross-linking sites in the backbone of poly(dimethylsiloxane) (PDMS) polymers.[47] The resulting coordination PDMS (with a $M_n \sim 70$ kg.mol^{-1}, dispersity Đ = 2.2) is based on the bidentate 2,2'-bipyridine-5,5'-dicarboxylic amide ligand while the metal ions are iron Fe(II) and zinc Zn(II) cations as illustrated in Figure 1.10(a). Additionally, Rao et al. also studied the effects of coordinating counter anions which directly affect the cross-linker dynamics and consequently the dynamic of the resulting MSPs.[48]
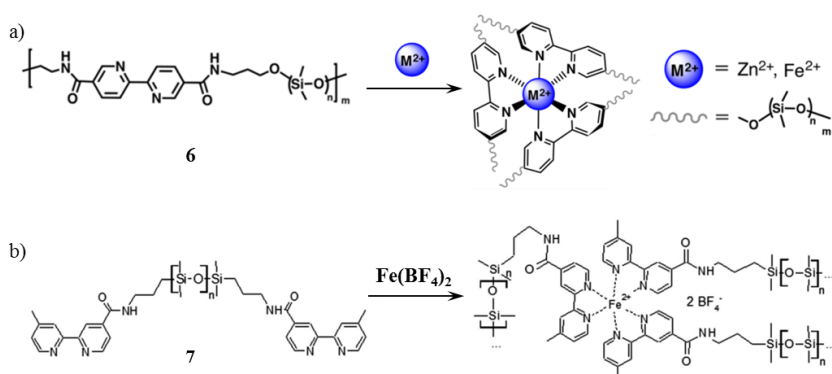
Figure 1.10: The structures of bpy-PDMS polymer and of metal ions-bpy cross-linked polymers with bpy ligand incorporated a) in the polymer backbone and b) at the polymer extremity.[47–49]

Williams et al. elaborated linear 2,2'-bipyridine-terminated poly(dimethylsiloxanes)s (bpy-PDMS) with four different PDMS chain lengths ($M_n = 3.3 – 50$ kg.mol^{-1}).[49] When bpy-PDMS are mixed with Fe(BF$_4$)$_2$, crosslinked PDMS elastomeric networks are obtained through tris(bipyridine)metal complexes. While these systems resemble to the work of Rao. et al, the major distinction is in the position of bipyridine-based ligands located at the termini of PDMS polymers as depicted in Figure 1.10(b). The present system allows the self-assembly

of well-defined metal-containing polymers and it is shown that the stiffness of these materials increases as the molar mass between cross-links decreases.

Similar works were pursued using histidine as a promising bidentate ligand for the elaboration of metallo-supramolecular polymers. For instance Grindy et al. studied a model system based on four-arm poly(ethylene glycol) (PEG) polymers with different molar masses (10, 20 and 40 kg.mol^{-1}) and functionalized with the histidine (His) ligand at the extremity of each arm to obtain 4PEG-His.[50] When mixed with transition metal ions such as Ni(II) ions at physiologic pH, the His:Metal complexes behave as transient cross-links between telechelic polymers to form hydrogel networks as shown in Figure 1.11(a).

Tang et al. worked on transient networks which are based on histidine-nickel coordination bonds as pendant groups on a poly(N,N-dimethyl-acrylamide) (PDMA) based polymer (M_n = 36.2 kg.mol^{-1}, dispersity Đ = 1.06) as illustrated in Figure 1.11(b).[51] When nickel Ni(II) ions are added to the functionalized PDMA, bis(histidine)nickel complexes are formed in aqueous solution to give reversible metallo-supramolecular hydrogel network with a well-characterized His-Ni^{2+} binding constants.[52]
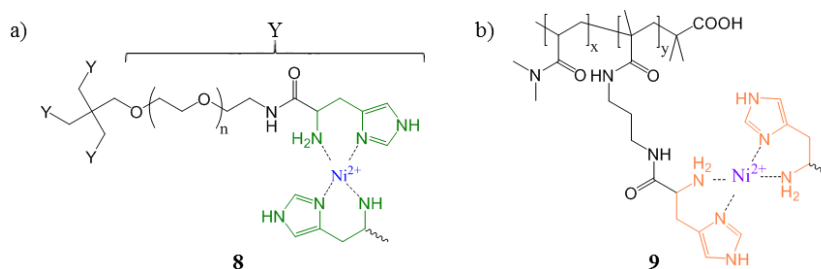
Figure 1.11: Chemical structure of a) telechelic 4-arm PEG end-capped with histidine ligand and b) PDMA functionalized with histidine ligands as pendant groups.[50,51]

The chelating effect can be enhanced by using various bidentate pyridine-based ligands such a phenanthroline (phen), bipyridine (bpy) or histidine (his) derivatives to elaborate building blocks which are then used for the formation of metallo-supramolecular polymers as reviewed above. In order to improve the stiffness, the strength or the stability of

MSPs, further investigations were conducted to form coordination polymers based on ligands with higher chelating properties, i.e. with higher binding constants such as tridentate (also called tweezer or claw) ligands that are in the focus of current research.[21]

The 2,6-bis(1-methylbenzimidazolyl)pyridine ligand is one of the most important ligands which is used for fabricating MSPs. Wang et al. reported coordination polymers consisting of poly(*n*-butyl acrylate-*co*-methyl methacrylate)s functionalized with Mebip side groups along the polymer chains as shown in Figure 1.12.[53] The P(BA-MMA-Mebip) precursors with different molar masses (M_n = 9.8–13.5 kg.mol^{-1}, Đ = 1.79 – 2.14) are dynamically cross-linked by the $Zn(OTf_2)_2$ and $Eu(OTf_2)_3$ metal ions to form a set of MSPs which micro-phase separate. The latter was exploited to develop a triple shape memory associating polymers combined with healing ability by heating and cooling. Jackson et al. pursued the same work by engineering metal-containing robust polymer films with well-defined linear poly(*n*-butyl acrylate) (M_n = 77 kg.mol^{-1}, Đ = 1.13) backbone functionalized with the same metal binding ligands which were randomly located along the polymer backbone.[54,55] P(BA-co-Mebip) polymer was mixed with different metal ions such as $Cu(ClO_4)_2$, $Zn(ClO_4)_2$ or $Co(ClO_4)_2$ to form MSPs and the influence of metal-Mebip binding strength on the associating systems was tested.
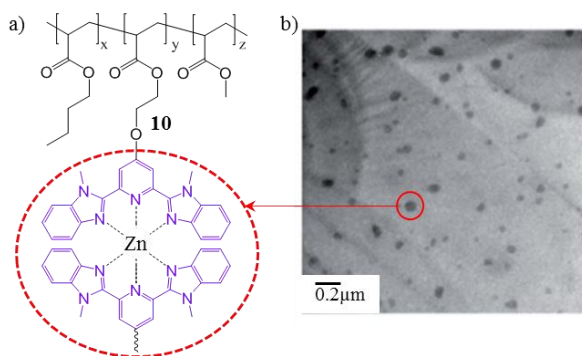
Figure 1.12: a) Chemical structure of a) metallo-supramolecular poly(BA-MMA) copolymers containing bis(Mebip)-Zn complexes b) TEM image of MSP showing microphase-separation.[53]

The 2,2',6'2"-terpyridine (tpy) ligand is one of the most important ligands for elaborating MSPs. Tpy, which is analogous to the Mebip ligand, contains three nitrogen atoms and each nitrogen has a lone electron-pair, so the tpy moiety can act as a claw ligand, i.e. a tridentate ligand. Constable et al. first proposed that MSPs can be obtained by combining tpy-functionalized monomers with metal ions.[56] Then Colbran et al. reported a series of bis(terpyridine) ligands spaced by small chemical entities and chain-extended metallo-polymers through a synthetic route involving the supramolecular polyaddition mechanism.[57,58] Following the same strategy, Schütte et al. prepared multi layers metallo-supramolecular thin polyelectrolyte films based on the complexation between 1,4-bis-(2,2,6,2"-terpyrid-4'-yl)benzene and iron(II) ions.[59] However, early research on these tpy ligand containing MSPs suffered from restricted solubility and in some cases the dissolution has to be achieved by complicated procedures or harsh conditions. To overcome this restriction, Schubert et al. designed water soluble MSPs using poly(diethylene glycol) or poly(ethylene oxide) as spacers to bridge two tpy moieties as illustrated in Figure 1.13.[60,61]
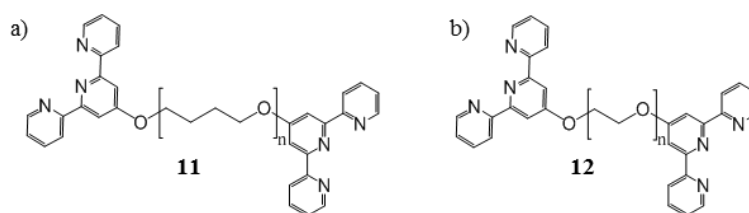
Figure 1.13: a) Chemical structure of telechelic water-soluble a) poly(diethylene glycol) and b) poly(ethylene oxide) both end-functionalized with terpyridine ligands.[60,61]

The addition of octahedral coordinating metal ions such as Co(II), Fe(II) or Zn(II) to these terpyridine ligands leads to the formation of metal-containing supramolecular polymers. The reversibility of bis(terpyridine)-metal complexes can be enhanced by changing the pH, by applying an electrochemical potential or even thermal treatment. Schubert et al. also developed well-defined linear metallo-supramolecular chain-extended polymers using telechelic poly(styrene)s (PS) end-capped by terpyridine ligands at each termini, as represented in Figure 1.14(a), with M_n = 9.5-12 kg.mol^{-1} and Đ =

1.16-1.18.[62] Since then, further studies of MSPs based on terpyridine-metal complex system were significantly extended.

Yang et al. designed metallo-polymer networks using a set of linear polymer (M_n = 19.4-21.2 kg.mol^{-1}) containing terpyridine acrylate (Tpy-A) with methyl methacrylate (MMA) and butyl acrylate (BA) with varying the molar amount of tpy groups as depicted in Figure 1.14(b).[63] A stoichiometric amount of NiCl$_2$ was added to the precursors in order to form metallo-supramolecular polymer networks displaying a gradient thermal plasticity.
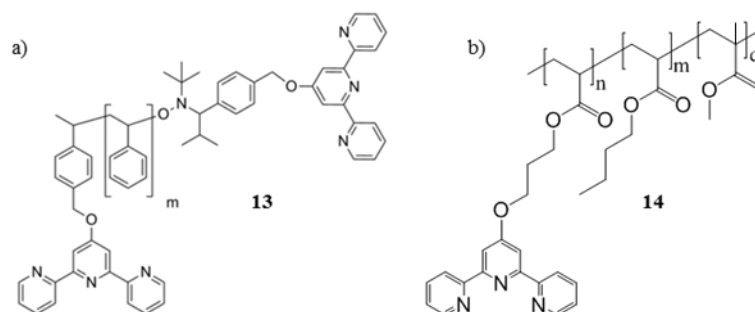
Figure 1.14: Chemical structure of linear a) telechelic PS end-capped with tpy ligand b) random P(*n*BA-*co*-MMA) functionalized with tpy ligands as pendant groups.[62,63]

The dynamic nature of the metal−ligand coordination is one of the key features of MSPs. Plethora M-L combination can be done using different metal ions combined with various ligands. Hence M-L interactions can exhibit different binding kinetics and thermodynamic stabilities, which makes coordination polymeric systems even more versatile. Depending on the selected combination, the resulting metal-containing polymers display diverse interesting properties such as smart electrochromic materials with optical memory[25,64,65], shape morphing devices[63], organic electronic accessories[66] or building nanocomposites where the reinforcing phase is ensured by reversible metal-ligand.[55] In this chapter, only a part of recent researches on MSPs based on metal-ligand coordination is reviewed. Indeed it is important to highlight that there is a great variety of coordination polymers with structural diversity reported in the literature.[19,21] MSPs presented above are mainly constructed by employing M-L coordination only, while in

parallel the combination of multiple non-covalent interactions, e.g. metal-ligand complexes combined with another supramolecular interaction, to fabricate MSPs is emerging. Only few works are presented below to highlight the possibility to elaborate associative polymers with multiple driving forces.

Mansfeld et al. designed a responsive amphiphilic supramolecular triblock copolymer by combining two of the most widely used supramolecular moieties.[67,68] The terpyridine ligand as well as a self-complementary quadruple hydrogen bonding array based on ureido-pyrimidinone (Upy) moiety have been incorporated and spaced by polystyrene blocks of different lengths (tpy-PS-Upy). The linear well-defined hetero-telechelic polymer (M_n = 4.8-13.7 kg.mol^{-1}, Đ = 1.07-1.18) can self-assemble via two orthogonal binding sites, as illustrated in Figure 1.15(a, b), and gives access to extended stimuli responsiveness materials. Furthermore, a supramolecular amphiphilic copolymer is achieved by mixing tpy-PS-Upy with nickel Ni(II) ions and a chain stopper based on poly(ethylene glycol) end-capped by a tpy ligand at one extremity (PEG-tpy, M_n = 2.1 kg.mol^{-1}, Đ = 1.13). The blocks are linked together by self-complementary hydrogen bonding and by bis(terpyridine)-metal complexes as represented in Figure 1.15(c).
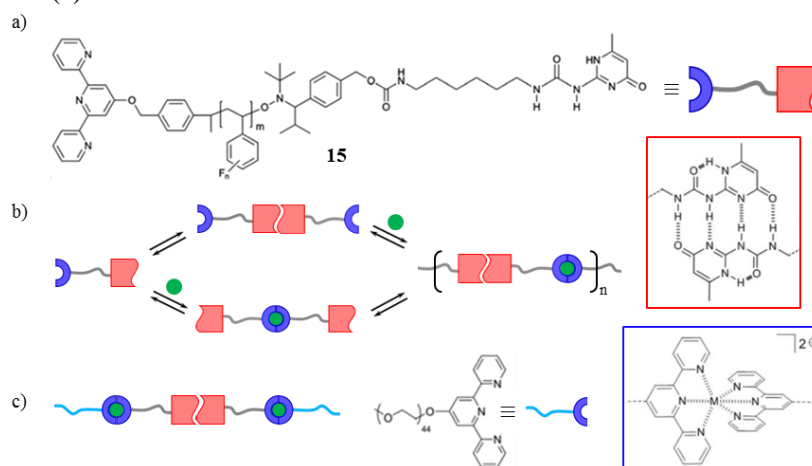
Figure 1.15: Chemical structure and schematic representation of a) the hetero-telechelic PS end-capped with terpyridine ligand at one extremity and Upy at the other end, b) the self-assembly of the hetero-telechelic associating polymer via the two supramolecular orthogonal

binding sites and c) the supramolecular amphiphilic quasi-triblock PEG-[Ni]-PS-[Upy/Upy]-PS-[Ni]-PEG polymer.[67,68]

He et al. elaborated a facile construction of metallo-supramolecular diblock copolymers via a combination of self-assembled nanostructures, π-π stacking interactions and complementary coordination.[66] More precisely, they predesigned complementary coordination between a terpyridine ligand and an anthracene substituted terpyridine-based ligand which are respectively mono-functionalized on the well-defined poly(3-hexylthiophene)s (P3HT, M_n = 6.3-8.9 kg.mol^{-1}, Đ = 1.21-1.26) and poly(ethylene oxide)s (PEO, M_n = 1.2-2.4 kg.mol^{-1}, Đ = 1.08-1.13) chain ends. A set of metallo-supramolecular rod-coil diblock copolymers P3HT-b-PEO was fabricated using π-π stacking interactions between anthracene moieties and the complementary ligand pair upon treatment with zinc Zn(II) ions.
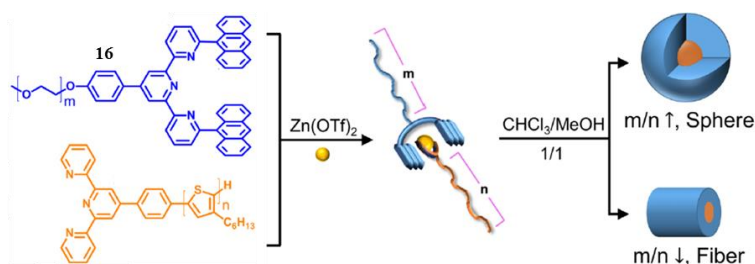
Figure 1.16: Chemical structure and schematic representation of terpyridine-functionalized homopolymers for the construction of MS P3HT-b-PEO self-assembled into nanostructures.[66]

As summarized in this chapter, the wide range of available metal ions and ligand moieties provides a strong tool for the fabrication of polymeric materials with diverse length, stability and reversibility. Based on M-L coordination only or a combination or M-L complexes with an additional non-covalent interaction, there is a variety of synthetic methods which can be used to elaborate MSPs. From a synthesis point of view, functionalized polymers can be classified between (i) those obtained by post-functionalization of polymers and (ii) associating systems obtained by pre-functionalization methods.

Polymers post-functionalization methods are usually the first strategy conducted to synthesize associating polymers. The procedure

consists in chemically incorporating the coordinating ligands in an already formed polymer. The synthetic route associated to this strategy appears to be simple. But in general, it is quite complicated because the reactivity between small chemical entities and a macromolecular polymer strongly differs from the reactivity between two small chemical entities. Indeed, one need to consider the steric hindrance parameter, the high dilution effect on the active groups linked to the polymers and also the solubility effect where the polymers are usually non-polar and oppositely the associating moieties are polar.

In spite of this, Burnworth et al. synthesized their associating systems via Mitsunobu reaction between the hydroxyl-terminated poly(ethylene-*co*-butylene) and hydroxyl-Mebip as illustrated in Figure 1.17.[69] After purification, a poly(ethylene-*co*-butylene) end-capped Mebip is obtained with a molar mass of 4.8 kg.mol^{-1} and Đ = 1.02. The resulting systems are dynamic and optically healable through the reversible formation of the metal-ligand complexes. However, these coordination polymers micro-phase separate to form structures with lamellar morphology where metal-ligand complexes assemble into a hard phase surrounded by the soft phase originated from the poly(ethylene-co-butyle) cores. Later on, Balkenende et al. extended the development of such systems by studying the dissociation of tris(Mebip)-Eu^{3+} complexes upon ultrasonication and also the metal exchange mechanism within coordination polymers.[70]
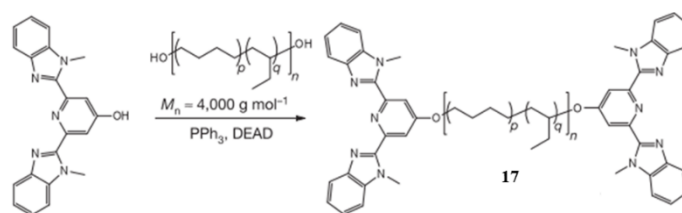
Figure 1.17: Post-functionalization of linear poly(butadiene-*co*-butylene) with Mebip ligand at chain extremity.[69]

Chen et al. used a two-step post-functionalization process in order to obtain terpyridine-end-capped four-arm poly(ethylene glycol) polymer of molar mass M_n = 5.3 kg.mol^{-1}.[71] First step is to obtain an amino-terpyridine molecule bearing NH$_2$ group (tpy-NH$_2$) via an alkoxylation reaction between 4-chloro-2,2:6,2″-terpyridine (tpy-Cl) and 6-amino-1-

hexanol. Then the tpy-NH$_2$ moieties are coupled with an active 4-arm-PEG N-hydroxysuccinimydil NHS ester via amidation reaction as shown in Figure 1.18(a). The accordingly obtained light-emitting MSP displays interesting optical properties which can be modulated by simply tuning the lanthanide metal ion stoichiometry and also leads to stimuli-responsive properties via dynamically reversible bis(terpyridine)-lanthanide complexes. For the synthesis of poly(ethylene-*co*-butylene) functionalized with pyridyl groups at the termini, Razgoniaev et al. obtained the polymer via nucleophilic aromatic substitution of *sim*-trichlorotriazine with hydroxyl-terminated poly(ethylene-*co*-butylene).[65] The resulting triazine-terminated poly(ethylene-*co*-butylene) is subject to further nucleophilic substitution to achieve the associating polymer with a molar mass $M_n =$ 3.1 kg.mol^{-1} as illustrated in Figure 1.18(b). The incorporation of pyridine-chromium Cr(III) interactions within poly(ethylene-*co*-butylene) enables the formation photo-responsive materials that can respond to irradiation in specific ways with unique optical properties.
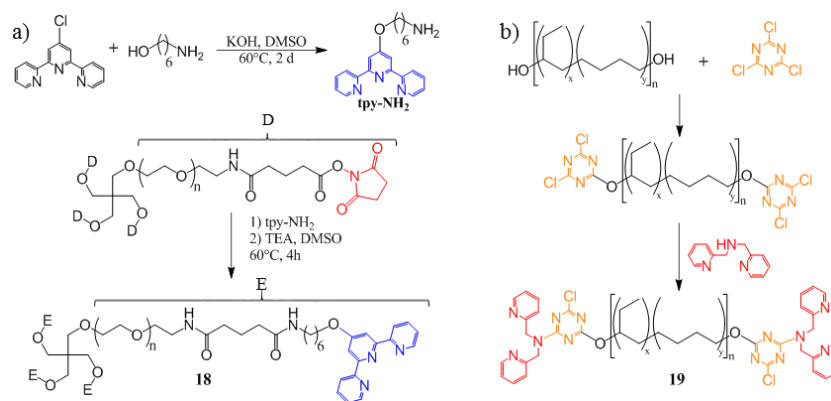
Figure 1.18: Synthesis of a) a four-arm poly(ethylene glycol) end-capped with terpyridine ligand and b) a metallo-polymer using poly(ethylene-*co*-butylene) and pyridyl ligand termini.[65,71]

Post-functionalization methods are sufficient and efficient to elaborate functionalized polymers with associating moieties linked at the termini or bonded as pendant groups along the polymeric backbone. However, it is difficult to achieve a complete functionalization, i.e. a functionalization yield of 100% through these techniques. Therefore self-assembly of such associating systems may be hampered by the

presence of non-functionalized polymers. Moreover, the post-functionalized polymers presented here are limited in chain length and present low molar masses, e.g. $M_n < 10$ kg.mol^{-1}. Beyond this value, the post-functionalization becomes extremely difficult, uncontrolled and often incomplete. The limitations of post-functionalization techniques have led to the development of a new synthetic approach which consists in incorporating associating moieties on the monomers, the initiators or the transfer agents before the polymerization step. Once the monomers, the initiators or the transfer agents are chemically functionalized with associating units, they are used in classical polymerization techniques such as polycondensation, radical and ring opening polymerizations. The pre-modification methods allow to easily incorporate stickers within polymeric chains and to ensure an almost complete functionalization with minimum fraction of non-functionalized polymer chains.
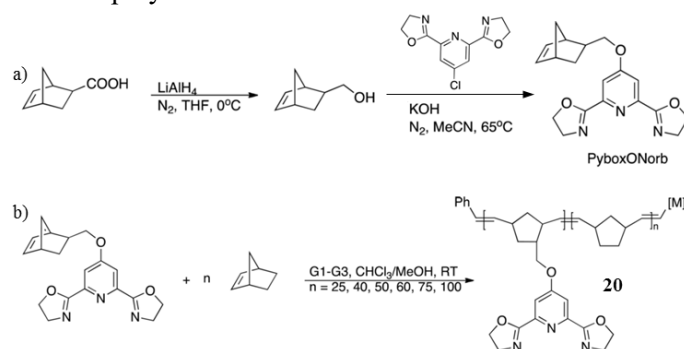
Figure 1.19: Synthesis of a) norbornene monomer functionalized with thiophene based tridentate ligand and b) copolymers with varying ratios of PyboxONorb and norbornene repeating units.[72]

For instance, Bettencourt-Dias et al. reported a set of metal-containing polymers by using a monomer functionalization method.[72] To do so, they first functionalized norbornene (Norb) monomer with thiophene based tridentate ligand (Pybox) in a three-step reaction as illustrated in Figure 1.19 to yield PyboxONorb monomer. Then PyboxONorb was copolymerized with Norb through ring opening metathesis polymerization (ROMP) to obtain poly(PyboxONorb-*co*-Norb)s. The obtained associating systems with Pybox as pendant groups along the polymeric backbone are promising for application as light-emitting-diode materials.

Similarly, Enke et al. functionalized a methacrylamide monomer with histidine ligands and the resulting associating monomers were copolymerized via radical reversible addition-fragmentation transfer (RAFT) polymerization.[73] Transient metallo-supramolecular polymeric networks, which exhibit healing properties, are obtained based on histidine-zinc complexes as pendant groups and poly(butyl methacrylate) (PBMA) and poly(lauryl methacrylate) (PLMA). There are many other examples of monomer functionalization in which ligands with various binding constants have been used such as triazole-pyridine ligands functionalized with methacrylate monomers[74], Mebip ligands with (meth)acrylate monomers[53,54], terpyridine ligands with acrylamide[75] methacrylate[76] or carbazole[77] monomers. Hence, monomer functionalization seems to be an excellent method to incorporate associating moieties within polymers. However, this technique does not allow to precisely assign the stickers at specific locations such as the extremity or the center of polymer chains. This is why the functionalization of initiators or transfer agents has been developed to overcome this limitation.

Nitroxide mediated polymerization (NMP) uses an alkoxyamine as an initiator that decomposes into an initiating radical and a nitroxide one. The nitroxide radical is unable to initiate any polymerization but it can trap the radical species by recombination. This termination reaction is not irreversible because the covalent bond NO-C is thermally reversible and extremely labile. Schubert et al. first developed an alkoxyamine chemically modified with terpyridine ligand which was then used in NMP in order to build different well-defined tpy end-functionalized polymers with a high end-functionality.[78] Later on, they pursued the work by designing a NMP initiator containing both the terpyridine ligand and the self-complementary quadruple hydrogen bonding 2-ureido-4[1H]-pyrimidinone (UPy) synthesized in a three-step reaction to prepare heterodifunctional telechelic polystyrene as described above and as reported by Mansfeld et al.[79] Supramolecular polymers can be obtained via the combination of hydrogen bonding and metal-ligand complexes. Likewise, Mugemana et al. used this polymerization technique with a tpy functionalized unimolecular initiator to build a terpyridine end-capped polystyrene-*block*-poly(*tert*-butyl acrylate) block copolymer with a M_n = 30.4 kg.mol^{-1} and Đ =

1.26.[80] The latter was then used for the preparation of micellar gels in selective solvents as represented in Figure 1.20.
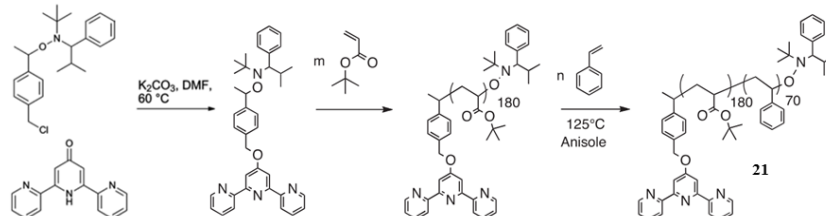
Figure 1.20: Synthetic strategy to terpyridine functionalized alkoxyamine NMP initiator and polymerization of polystyrene followed by poly(*tert*-butyl acrylate).[79,80]

Herein, the synthesis is well-controlled and a narrow dispersity and a high molar mass, e.g. 30.4 kg.mol^{-1}, are achieved. The functionalization of NMP initiators is an advantageous approach to obtain associating polymers with higher molar mass compared to the post-functionalization methods in which it is more difficult to attain such lengthy polymeric systems. While NMP provides numerous advantages for the elaboration of coordination polymers, several limitations such as slow polymerization kinetics that require high temperatures or the inability to easily polymerize methacrylate monomers in a controlled way have led to the more widespread use of RAFT polymerization in polymer pre-modification synthesis.[81]

The development of RAFT polymerization has proven to be more versatile and easier to carry out. Indeed, it offers faster polymerization kinetics, lower polymerization temperatures and a broader range of monomers to be polymerized compared to NMP technique. Thanks to this method which relies on thiocarbonylthio based chain transfer agents, well-defined polymers can be obtained. Hence, the functionalization of the RAFT agent with a moiety able to self-assemble by metal-ligand coordination can lead to the elaboration of metallo-supramolecular polymers with high yields of functionality at the center or the extremity of polymer chains. Harruna et al. first established the terpyridine-functionalized chain-transfer agent (CTA) that can produce well-defined macromolecular structures with tpy functionalities at one chain end via RAFT polymerization.[82] The tpy-modified dithioester as

illustrated in Figure 1.21(a) is synthesized in a three-step reaction with a relative good yield.
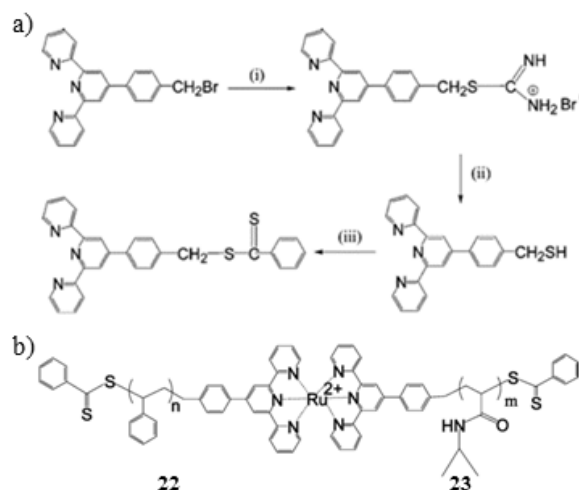
Figure 1.21: a) Synthetic route of the terpyridine functionalized chain transfer agent. b) Elaboration of bis(terpyridine)-ruthenium complex-connected diblock copolymers.[82]

The functionalized CTA was then used for the polymerization of styrene and N-isopropylacrylamide (NIPAM) to generate respectively a set of tpy end-functionalized and low dispersity PS (M_n = 3.4-9.8 kg.mol^{-1}, Đ = 1.04-1.18) and PNIPAM (M_n = 4.8-12.5 kg.mol^{-1}, Đ = 1.06-1.11) polymers. The resulting systems were further used for the elaboration of supramolecular diblock metallo-polymers by bis(terpyridine)-ruthenium complexation as shown in Figure 1.21(b). Additionally, surface observation by atomic force microscopy (AFM) showed the presence of amphiphilic diblock metallo-polymers which are able to form spherical particles.

Similarly, Zhang et al. developed a symmetric bisterpyridine-functionalized trithiocarbonate (TTC) as a chain transfer agent to synthesize higher molar mass polymers based on styrene and n-butyl acrylate (nBA) monomers.[83] As a result, a series of well-defined telechelic PS (M_n = 25.8-44.5 kg.mol^{-1}, Đ = 1.12-1.16) or PnBA (M_n = 12.3-31.5 kg.mol^{-1}, Đ = 1.28-1.34) homopolymers and triblock PS-

41

PnBA-PS or PnBA-PS-PnBA (M_n = 38.4-309.6 kg.mol^{-1}, Đ = 1.14-1.19) copolymers were obtained as illustrated in Figure 1.22.
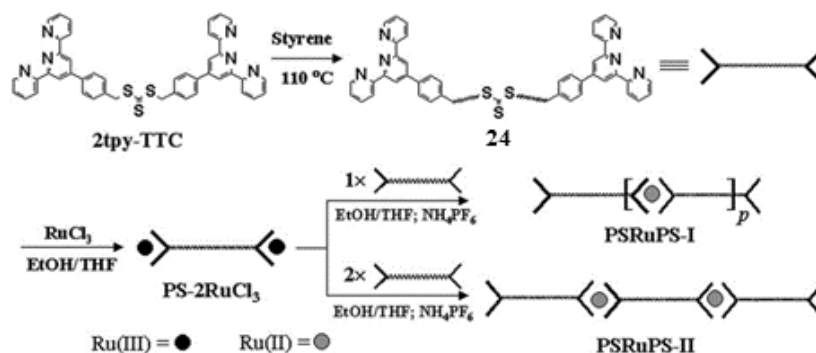
Figure 1.22: The synthetic strategy of bisterpyridine functionalized poly(styrene) and formation of MSPs based on bis(terpyridine)-ruthenium complexes.[83]

In this context, O'Reilly et al. reported two bistriazolylpyridine (btp) containing initiators for the RAFT polymerization.[84] These particular CTAs allow the growing of two polymeric chains in two active sites bonded to a central tridentate core which has the capability to form metal-ligand complexes at the center of the associating polymers as depicted in Figure 1.23. Well-defined homopolymers based on methyl methacrylate (MMA), *tert*-butyl acrylate or styrene monomers were obtained with a molar mass ranging from 17.2 to 40.9 kg.mol^{-1} and a dispersity between 1.09 to 1.29. The coordination of the macro-ligands to ruthenium or europium metal ions yielded respectively four- and six-armed star-shaped metallo-polymers.
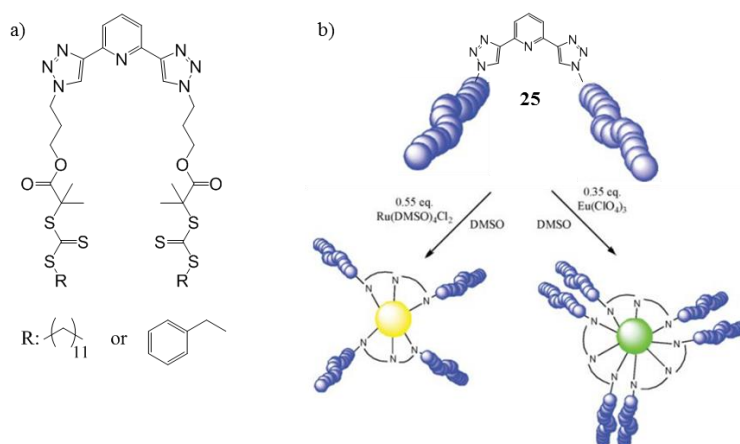
Figure 1.23: a) Chemical structure of bis-RAFT agents. b) Formation of 4 and 6 arm metallopolymers.[84]

Piogé et al. elaborated a terpyridine-terminated trithiocarbonate agent which was obtained in a two-step reaction.[85,86] Several monomers such as *N,N*-dimethylacrylamide (DMA), *N*-isopropylacrylamide (NIPAM) and 2-vinyl-4,4-dimethyl-azlactone (VDM) were polymerized with this functionalized CTA via RAFT polymerization. A well-defined (M_n = 35 kg.mol^{-1}, Đ = 1.42) thermoresponsive double hydrophilic block copolymer Tpy-PDMA-*b*-P(NIPAM-*co*-VDM) end-capped with a terpyridine unit was obtained and dynamic metallo-supramolecular flower-like micelles were formed by addition of iron ions as represented in Figure 1.24.
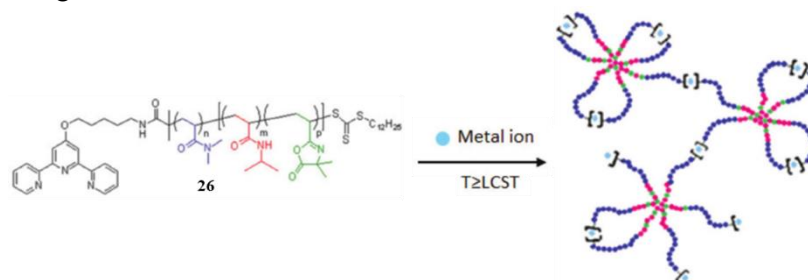
Figure 1.24: Schematic representation of dynamic metallo-supramolecular hydrogels based on the thermoresponsive terpyridine functionalized copolymer Tpy-PDMA-*b*-P(NIPAM-*co*-VDM).[86]

The incorporation of associating moieties within polymers can be achieved through several methods. Depending on the location of the sticker, one approach can be more suitable compared to the other one.

Indeed, the functionalization of initiators or chain transfer agents is more appropriate in the case where the stickers are specifically assigned at the extremity or at the center of polymer chains. On the other hand, incorporation of associating units as pendant groups along polymer backbones is more appropriate by monomer functionalization followed by their polymerization. The post-modification approaches of already synthesized polymers are also interesting. However, these procedures are extremely limited because there is a high risk to obtain non-functionalized chains which directly disrupt the self-assembly of associating polymers. Plus, there is an additional limitation in terms of polymer lengths where high molar mass polymers (M_n > 10 kg.mol^{-1}) cannot be correctly functionalized because the concentration of reactive groups is extremely low.

This section briefly summarizes the possibility to synthesize plethora metallo-supramolecular polymers with well-defined structures. Depending on the desired chemical structure and topology of the associating system, different synthetic routes can be considered. Besides elementary characterizations which define the physical and chemical properties of these materials, the rheological study of these systems is also useful to determine their mechanical properties.

1.2 Dynamics of metallo-supramolecular polymers

1.2.1 Rheology of molten polymers

Rheology is the science that studies the way materials deform when forces are applied to them. It is commonly applied to the study of liquids and liquid-like materials such as paint, ketchup, oil, blood, polymer solutions and melts, i.e. materials that flow. But it also includes the study of elastic materials that do not flow, such as cross-linked materials. To investigate the rheological properties of a material, one must either measure the force required to produce a given deformation or the deformation resulting from a given force. Through this investigation, rheology allows the development of relationships that show how rheological properties such as the viscosity or the relaxation

modulus are directly influenced by molecular structure and composition of the molten polymers but also by temperature and pressure.

From an industrial point of view, molten polymers which are processed as liquids are converted to end-use products by means of melt forming operations, including profile extrusion and several molding methods. In all these techniques, the rheological properties of the molten polymers play a key role and must be considered in the design of processing equipment and in the definition of operating conditions for the development of new products. For instance, in an extruder, the dependence of viscosity on shear rate and temperature is of interest, but once a melt leaves a shaped die, its viscoelastic properties govern its behavior. In the case of blow molding, the amount of swelling that the melt undergoes as it exits the die before being expanded into the mold is a crucial point because there are various flow instabilities that can cause havoc in melt processing. In summary, the melt flow behaviors are governed by their rheological properties and the latter have important applications in molten polymer development, quality control, and the numerical simulation of forming processes. In this work, the general examined types of rheological behavior are elasticity, viscosity, viscoelasticity and structural time dependency that are exhibited by molten polymers.

Elasticity corresponds to a type of behavior in which a deformed material returns to its original shape whenever a deforming stress is removed. This implies that a stress deformation is necessary to generate and to maintain any deviation in shape from the original unstressed shape. The simplest type of elastic behavior is when the stress required to produce a given amount of deformation is directly proportional to the strain associated with that deformation. For instance, in simple shear this can be expressed as follows.

$$\sigma = G.\gamma \qquad (1.2)$$

Where σ is the stress, G is the shear modulus, γ is the strain and this relationship is called Hooke's law. For simple extension, the corresponding form of Hooke's law is:

$$\sigma_E = E(L-L_0)/L_0 \qquad (1.3)$$

Where σ_E is the tensile stress, E is the Young's modulus, L and L_0 is the length of polymer for extensional test a time t and time $t = t_0$ (i.e. initial length) respectively. For a pure elastic material, all the produced stress to deform the material is stored as elastic energy and it is fully recovered when the material returns to its initial equilibrium unstressed state as the stress is removed.

Viscosity describes the resistance of a material to continuous deformation. In this case, the stress is related to the rate of deformation and it is a particular property of materials that flow. The deformation is permanent, irreversible when stress is removed and the energy produced by the stress is completely dissipated into heat. For simple shear, this type of behavior is defined by a linear relationship between the shear stress and the shear rate as follows.

$$\sigma = \eta . \dot{\gamma} \tag{1.4}$$

Where η is the viscosity and $\dot{\gamma}$ is the shear rate. A material that obeys this relationship with the viscosity being independent of shear rate is called a Newtonian fluid. For uniaxial extension, the net tensile stress σ_E is measured and is related to the viscosity as:

$$\sigma_E = 3\eta . \dot{\varepsilon} \tag{1.5}$$

Where $\dot{\varepsilon}$ corresponds to the Hencky strain rate. The latter is multiplied by the Trouton ratio 3 which is used to normalize extensional data. Trouton who found that the extensional viscosity is equal to three times the shear viscosity. Hence for a Newtonian fluid, the viscosity does not depend on the rate or amount of strain but it is dependent on temperature and pressure.

Molten polymers are viscoelastic. Their rheological response to a change in stress or strain is time dependent and they display both the elastic storage of energy and the viscous dissipation. At relative long timescale, a viscoelastic polymer will flow and consequently dissipate all the energy originated from the generated stress or strain into heat. At short timescale, molten polymers can behave as an elastic solid able to restitute the given energy. The short time response to stress or strain of flexible molten polymers with high molar mass is similar to the response of cross-linked rubbers. This similarity highlights the presence of temporary network that exists within the melt. Unlike permanently

cross-linked network, herein the junctions can slip over relative long timescale and they permit flow. In melts, this temporary network arises from entanglements which is originated from the constraints, the motion limitation and the degree of special overlap of one molecule by its neighbors. Rubbery behavior takes place within molten polymers when their molar masses are high enough to sufficiently generate the number of entanglements necessary to mimic the effect of chemical cross-links over a certain period of time. From a macroscopic point of view, the effect of entanglements includes high viscosity, high elastic recoil and the elastic properties of the transient network are related to the elastic plateau modulus G_N^0 as follows.

$$G_N^0 = \frac{4}{5} \frac{\rho.R.T}{M_e} \qquad (1.6)$$

Where ρ is the melt density, R is the gas constant, T is the absolute temperature and M_e is the molecular weight between entanglements.

Linear viscoelasticity can be described by the relaxation modulus which is determined by measuring the mechanical response of the melt to a small deformation. In small amplitude oscillatory shear (SAOS), it can be characterized in terms of the storage (G') and loss (G") moduli by imposing a given shear strain and tracking the stress or vice-versa. The resulting linear viscoelastic data are a source of fruitful information about molecular structure such average molecular weight and molecular weight distribution and also on mechanical flowing properties of viscoelastic materials. In the following, the main parameters, which are used in rheology studies to describe linear viscoelastic properties of molten polymers, are introduced.

For instance, during stress relaxation experiment, a sample is deformed under a constant strain γ at time $t = 0$ and the evolution of shear stress σ is tracked as function of time. In shear strain, the shear relaxation modulus G(t) is defined as follows.

$$G(t) = \frac{\sigma(t)}{\gamma} \qquad (1.7)$$

In extensional strain, the tensile relaxation modulus E(t) is defined as:

$$E(t) = \frac{\sigma_E(t)}{\varepsilon} \qquad (1.8)$$

Where σ_E is the net tensile stress and ε is magnitude of extensional strain. In linear regime, the stress at any particular value of t is proportional to the strain in both shear and extensional.

While it is convenient to use relaxation experiments to introduce elementary parameters, SAOS measurements are the typically used experiments to describe the linear viscoelastic properties of molten polymers. In a controlled strain experiment, a sample is subjected to a constant homogenous shear deformation and the shear strain is related to time as follows.

$$\gamma(t) = \gamma_0.\sin(\omega.t) \qquad (1.9)$$

Where γ_0 is the strain amplitude and is ω the frequency. The shear rate $\dot{\gamma}(t)$ as function of time and shear rate amplitude $\dot{\gamma}_0$ defined as:

$$\dot{\gamma}(t) = \gamma_0.\omega.\cos(\omega.t) = \dot{\gamma}_0.\cos(\omega.t) \qquad (1.10)$$

If the strain amplitude is small that the response is linear, the stress response is periodic, sinusoidal and is measured as function of time.

$$\sigma(t) = \sigma_0.\sin(\omega.t + \delta) \qquad (1.11)$$

Where σ_0 is the stress amplitude and δ is the phase shift or the loss angle. The results obtained via an oscillatory shear measurement can be defined in terms of the amplitude ratio $G_d = \sigma_0/\gamma_0$ and of the loss angle which are function of frequency. Hence, the results can be reported in terms of storage and loss moduli in function of frequency as follows.

$$\sigma(t) = \gamma_0[G'(\omega).\sin(\omega.t) + G''(\omega).\cos(\omega.t)] \qquad (1.12)$$

Where G' and G" are related to the amplitude ratio and the loss angle.

$$G' = G_d.\cos(\delta) \qquad (1.13)$$

$$G'' = G_d.\sin(\delta) \qquad (1.14)$$

In the case of the pure elastic solid with a shear modulus G, the stress is proportional to strain and it is defined in oscillatory shear as:

$$\sigma = G.\gamma = \gamma_0.G[\sin(\omega.t)] \qquad (1.15)$$

With G' = G, G" = 0 and δ = 0. Therefore, stress and strain are in phase to describe the elastic aspect of the response wave.

In the case of a viscous fluid, the stress is proportional to strain rate as:

$$\sigma = \eta.\dot{\gamma} = \gamma_0.\eta[\cos(\omega.t)] \tag{1.16}$$

With G' = 0, G" = $\eta.\omega$ and $\delta = \pi/2$. Consequently, the strain and the stress are out of phase which derives from the Newton's law where the stress is in phase with the shear rate to describe the viscous aspect of the response wave. The ratio of the storage and loss moduli is the tangent of the phase shift, $\tan(\delta)$.

$$\tan(\delta) = G"/G' \tag{1.17}$$

The equation 1.17 allows to determine the ratio of dissipated lost energy to stored elastic one. Phase shift approaches to zero when energy storage predominates, and when dissipation predominates, the loss angle approaches $\pi/2$.

In the case of viscoelastic materials, the stress response displays a phase shift value between 0 and $\pi/2$ with respect to strain wave and from equation 1.11, the response can be redefined as follows.

$$\sigma(t) = \sigma_0[\sin(\omega.t).\cos(\delta) + \cos(\omega.t).\sin(\delta)] \tag{1.18}$$

$$\frac{\sigma(t)}{\gamma_0} = \frac{\sigma_0.\cos(\delta)}{\gamma_0}\sin(\omega.t) + \frac{\sigma_0.\sin(\delta)}{\gamma_0}\cos(\omega.t) \tag{1.19}$$

$$\frac{\sigma(t)}{\gamma_0} = G'.\sin(\omega.t) + G".\cos(\omega.t) \tag{1.20}$$

With G' = $\frac{\sigma_0}{\gamma_0}\cos(\delta)$ and G" = $\frac{\sigma_0}{\gamma_0}\sin(\delta)$.

A frequency sweep experiment consists in probing G' and G" as function of the frequency ω which allows one to measure the amount of energy stored and dissipated during an oscillation cycle in the form of linear viscoelastic moduli.

An alternative illustration of SAOS results is based on the complex viscosity η^* which is defined as follows.

$$\eta^*(\omega) = \frac{\sqrt{G'^2 + G''^2}}{\omega} \qquad (1.21)$$

Note that when the complex viscosity is plotted against frequency, it often matches with a plot of viscosity as function of shear rate:

$$\eta^*(\omega) = \eta(\dot{\gamma}) \qquad (1.22)$$

This empirical relationship is referred as the Cox-Merz rule.[87] Since measuring the viscosity at low shear rates by using a rotational rheometer is more difficult than by employing an oscillatory shear rheometer, the complex viscosity $\eta^*(\omega)$ is often used in the plastics industry instead of $\eta(\dot{\gamma})$. While linear viscoelastic properties provide the most fruitful source of information about the structure of melts of all shear flows, non-linear behavior is more relevant to industrial processing. Indeed, the deformations that occur during processing are large and rapid. The response to a shear deformation does not provide a complete description of melt rheological behavior. Several large and rapid deformations processes such as large amplitude oscillatory shear (LAOS), transient start up shear or uniaxial extensional flow are used to describe the non-linear viscoelastic properties of molten polymers.

In LAOS measurements such as strain sweep tests where the applied strain or stress on a sample is increased from small to large at a given frequency, the shear strain amplitude is large enough that the stress wave remains periodic but not sinusoidal anymore. Hence, the resulting stress cannot be interpreted in terms of in phase and out of phase components. However, the obtained responses are still relevant to reveal diverse characteristics of the non-linear viscoelastic properties of melts. At least four types of strain amplitude dependence can be highlighted which are reported in Figure 1.25.[88]
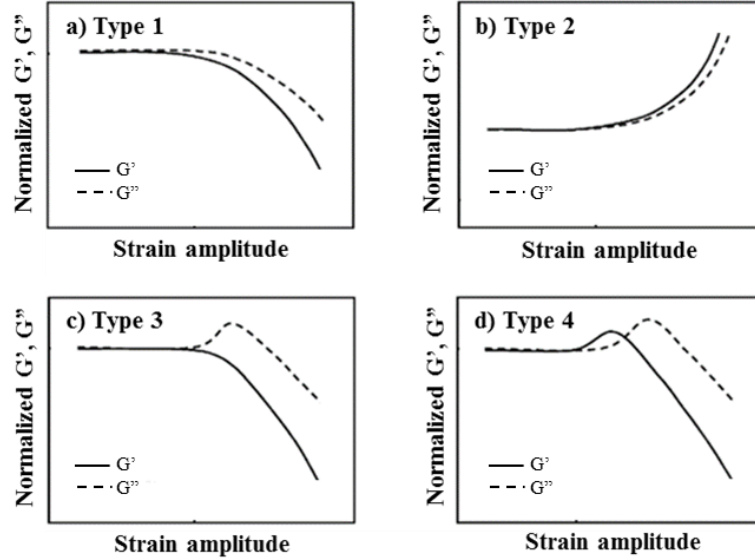
Figure 1.25: The types of LAOS behavior a) strain thinning, b) strain hardening, c) weak strain overshoot and d) strong strain overshoot.[88]

▪ Type 1 – *Strain thinning*. This type of behavior, where G' and G" decrease upon increase of strain, is commonly observed in molten polymers. It is originating from chain orientation or microstructure alignment along the shear flow direction.[89] For entangled polymers, the chains disentangle and align with the flow field when the shear strain increases and consequently the shear stress decreases.

▪ Type 2 – *Strain hardening*. Oppositely to type 1, strain hardening occurs when there are strong interactions between some segments of the chain. The polymer chains can form complex microstructures such as gelation, elaboration of shear induced network or strain stiffening network components that resist to flow alignment.[90] This strong resistance is the origin of the strain hardening behavior.

▪ Type 3 – *Weak strain overshoot*. Depending on the studied material, there are different explanations on the origin of the strain overshoot behavior in loss modulus G". For instance, it can be a structural rearrangement of microstructures under large shear or a balance between the formation and the destruction of flow induced microstructures to resist the deformation up to a certain strain where

G" increases.[91] Then over a critical strain, the microstructures are destroyed and the polymer chains align with the flow field.

- Type 4 – *Strong strain overshoot*. This type of behavior arises from the intermolecular interactions which enable the formation of micellar microstructures. The latter is considered as a network with interaction energy weaker than type 2 but stronger than type 3.

Additional non-linear shear tests can be conducted to obtain further information about the viscoelastic properties of melts. A transient start-up shear test consists in applying a constant shear rate to a melt during a certain time and the evolution of the stress is monitored as a function of time. The shear stress growth coefficient (η^+) is then obtained by dividing the measured stress by the imposed shear rate as follows.

$$\eta^+(t, \dot{\gamma}) = \sigma(t, \dot{\gamma}) \, / \, \dot{\gamma} \qquad (1.23)$$

At short times during which the deformation is small, it is expected that the shear stress growth coefficient increases linearly and follows the linear viscoelastic behavior. At longer times, the shear stress reaches a plateau. If the shear rate is low compared to the characteristic time of chain diffusion, the entire transient viscosity is the same as the linear viscoelastic envelope because the polymer chain has the time to diffuse while being sheared. Oppositely, if the shear rate is high enough that the diffusion does not occur and consequently the entanglements behave as permanent cross-links, the polymer coils are subjected to strong orientation and stretch. Hence, the polymer reaches a new equilibrium state with lower transient viscosity due to lower density of entanglements. The resulting stress relaxation upon flow cessation concerns the recovery of polymer coil configuration from the orientation and stretch in non-linear shear rheology.

While many tests are conducted in shear to study the non-linear viscoelastic properties of molten polymers, uniaxial extension tests provide further information. The latter is different and in a way simpler than the shear experiments since there is not rotation. Indeed, uniaxial extension is extremely sensitive to long chain branching polymers and it applies deformation in which strain hardening behavior is most apparent. Uniaxial extension is an axisymmetric flow in which a tensile

stress is applied to the melt in one direction of the axis of symmetry usually named z-direction and the net tensile stress σ_E is measured. Steady simple extension is a typical experiment which is carried out by imposing a constant Hencky strain rate $\dot{\varepsilon}$ to the melt. The latter corresponds to the speed at which the material is subjected to extensional deformation and is defined as:

$$\dot{\varepsilon} = \frac{d \ln L}{dt} \qquad (1.24)$$

Where L is the length of the sample. In simple extension, the sample length increases exponentially with time at constant $\dot{\varepsilon}$ such as:

$$L(t) = L_0 \exp(\dot{\varepsilon}.t) \qquad (1.25)$$

Where $L(t)$ and L_0 are respectively the length at time t and the initial length. During the test, the evolution of extensional stress (σ_E) is measured as function of time and the tensile stress growth coefficient η_E^+ is obtained as follows.

$$\eta_E^+(t, \dot{\varepsilon}) = \sigma_E \, (t, \dot{\varepsilon}) \, / \, \dot{\varepsilon} \qquad (1.26)$$

Like transient start up shear, linear viscoelastic response can be exhibited if the Hencky strain rate is sufficiently low and is equal to three times the viscosity obtained from SAOS measurements:

$$\eta_E^+(t) = 3\eta^+(t) \qquad (1.27)$$

Similarly to transient start-up shear measurements, the $\eta_E^+(t, \dot{\varepsilon})$ can be compared to the linear response and both results are accurate if they match at short times and low strain rates. At longer times, the molten polymer is said to be strain hardening if the non-linear viscoelastic response rise above the linear one. And oppositely, it is strain thinning if they fall below the linear viscoelastic response.

Molten polymers are rheologically complex viscoelastic materials that exhibit both viscous flow and elastic recoil. A general molecular constitutive model to explain the entire behavior for these materials has not been yet developed. While linear viscoelastic properties of melts are extensively studied and well-known, it is not the case for the non-linear viscoelastic properties where the rheological behaviors of molten

53

polymers are empirical. This is why rheology of classic polymeric melts is an interesting and challenging field of study.

1.2.2 Shear and extensional rheology of associating polymers

Recently, with the advent of supramolecular polymers where the incorporation of associating units able to self-assemble via metal-ligand coordination, additional interesting rheological properties can be obtained within these associating polymeric materials. Due to metal-ligand dynamics, attractive features such as self-healing or shape-memory[24,53] properties can be achieved. Depending on the location of the associating moieties within the polymer, the resulting mechanical properties can differ from stickers incorporated as pendant groups, located at the center or at the extremity of polymer chains. In section 1.1.2 the different synthetic strategies are summarized. In the following, the resulting rheological properties of such materials will be reviewed.

1.2.2.1 Shear measurements

Fullenkamp et al. studied transient network hydrogels based on poly(ethylene glycol) cross-linked via bis(histidine)-metal complexes.[52] Histidine functionalized star PEG, e.g. compound 8 presented in section 1.1.2, were used to alter the rheological properties of these materials. Hydrogels were formed for a fixed polymer concentration at physiological pH and at stoichiometric ratio with different transition metal ions such as nickel (Ni^{2+}), cobalt (Co^{2+}), copper (Cu^{2+}) or zinc (Zn^{2+}). While the precursor polymer solution without metal ions behaves as a free-flowing solution, gel-like materials are formed upon addition of metal ions and their linear viscoelastic properties are investigated by oscillatory shear. As shown in Figure 1.26, results demonstrate the formation of bis(histidine)-metal complexes as physical cross-links to form the transient hydrogels. The influence of the nature of metal ions on the elaboration of hydrogels is highlighted with the relaxation times of these gels which follow the order $Ni^{2+} > Co^{2+} > Cu^{2+} > Zn^{2+}$ when the inverse of the cross-over is considered as the terminal relaxation time. The latter is found to be in correlation with a previous work about divalent metal kinetics where

Ni^{2+} hydrogels relax more slowly than the other materials.[92] Consequently, transient networks based on bis(histidine)-nickel complexes have the longest self-repair rate time because the healing of the materials needs breakage and reformation of coordination bonds.
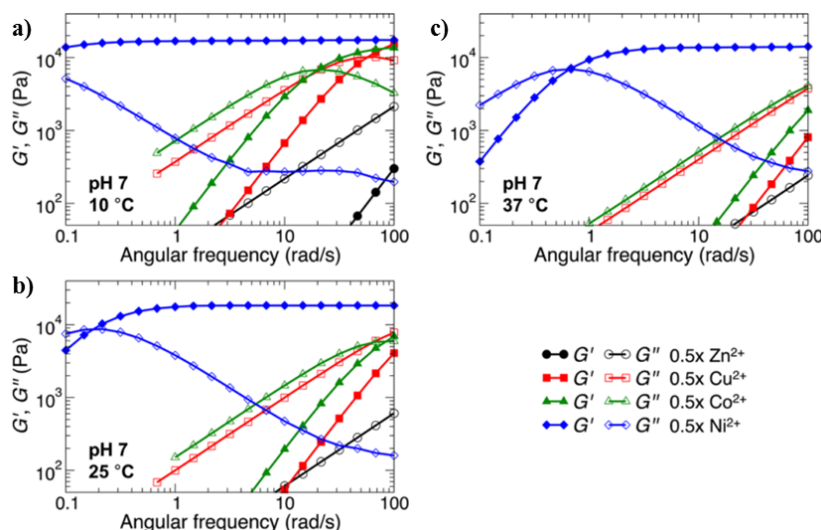
Figure 1.26: Frequency sweeps of four-arm star PEG-His coordination gels with 0.5 divalent metal/polymer end-group at pH = 7. Storage (G') and loss (G") moduli are reported at a) 10°C, b) 25°C and c) 37°C.[52]

Moreover, the influence of polymer concentration is also investigated for hydrogels formed with nickel metal ions. The concentration dependence of the material is studied for concentrations ranging from 10 to 150 mg.mL^{-1} of polymeric precursor. In Figure 1.27(a), it is shown that both the relaxation time and the moduli increase when the concentration increases. According to Fullenkamp et al., this increase in moduli is related to the cross-linking density as the modulus is proportional to it. The decrease in relaxation time is attributed to an increase in chain stretching capacity as the concentration decreases which may influence the relaxation dynamics of the coordinating interactions. Additionally, the effect of pH on the transient gel is also investigated in step strain measurements at a given concentration with Ni^{2+} ions. Results reveal that the gel relaxation follows the order pH 7 > pH 8 > pH 6 > pH 9 where pH 7 seems to be the ideal pH to elaborate gel with optimum coordination bond stability as represented in Figure 1.27(b). Beyond or below this optimum pH, it appears that the bond

relaxation time decreases due to proton or hydroxide concentration. In fact, at low pH, protonation of imidazole or amine from the histidine ligand can occur and consequently the chelating effect between histidine-metal coordination is destabilized. At high pH, it is the hydroxide ions that can interact with metal ions and hence directly affect the histidine-metal coordination.
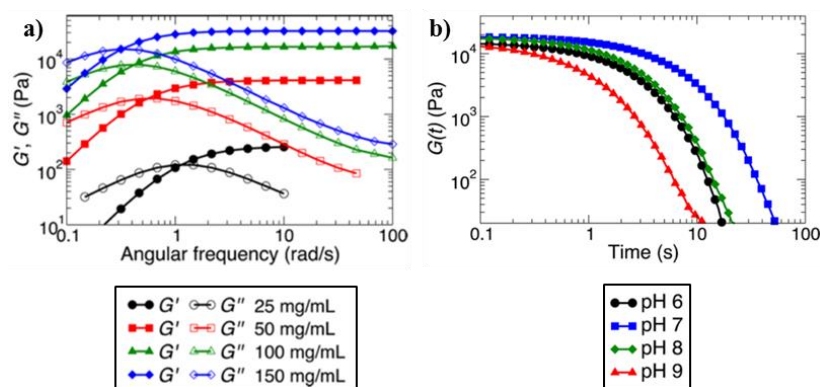
Figure 1.27: a) Influence of polymer concentration of four-arm star PEG-His coordinated with 0.5 equivalents of Ni^{2+} at pH = 8. b) Influence of pH on gel relaxation for PEG-His + $0.50Ni^{2+}$, 100 mg/mL gel subjected to a 10% step strain.[52]

Grindy et al. pursued the study of such systems to provide additional control by varying the active cross-linker concentration over or under the stoichiometry.[50] More precisely, a window of highly tunable stiffness and relaxation time can be obtained by altering the His:Ni^{2+} ratio. The influence of metal-ligand concentration ratios on the viscoelastic properties of 4-PEG-His:Ni^{2+} associating systems is investigated with His:Ni^{2+} ratios between 1:4 and 1:1. The mechanical properties of the resulting systems are reported in Figure 1.28. Results show that the concentration of nickel ions is found to strongly influence the dynamics of the resulting hydrogels where the stiffest transient network is achieved with a His:Ni^{2+} ratio of 3:1 instead of 2:1 as used by Fullenkamp et al. Compared to bis(histidine)-Ni^{2+} complex obtained with a 2:1 ratio, 3:1 ratio leads to formation of tris(histidine)-Ni^{2+} complex. The latter acts as a branching points with an additional active chain that participates to the elasticity of the gel. The linear viscoelastic properties of these transient networks are governed by the dynamics of

metal-ligand coordination by simply adjusting the concentration of the coordinating metal ions.
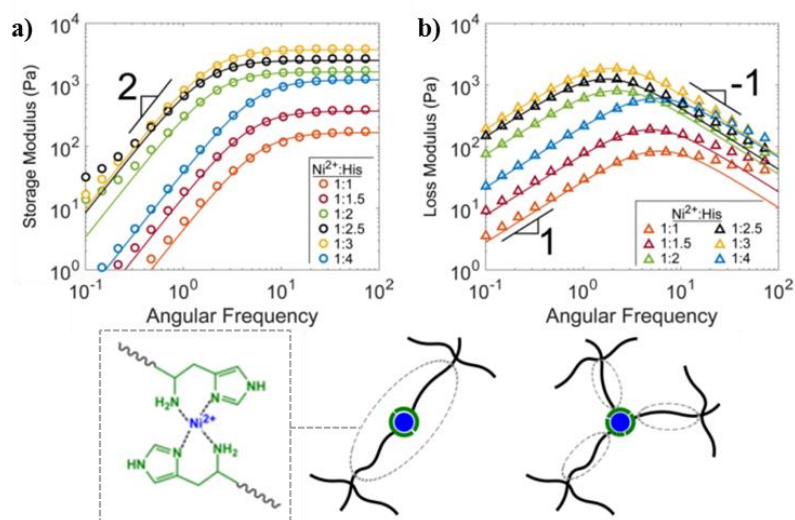
Figure 1.28: Influence of metal ion concentration on four-arm star PEG-His coordinated at varying His:Ni^{2+} ratios. Frequency sweep of the transient networks with a) storage modulus and b) loss modulus reported at 25°C.The formation of bis(histidine)-Ni^{2+} complex creates one elastically active chain. A tris(histidine)-Ni^{2+} complex creates three elastically active chains and therefore contribute more to the storage modulus.[50]

Using the same associating system with a molar mass of 10 kg.mol^{-1}, Wagner et al. reported a redox-responsive hydrogel with cobalt ions to form His:$Co^{2+/3+}$ as cross-linkers.[93] The physical state of the formed hydrogel can be switched from self-healing viscoelastic liquids to stable elastic solids by a simple oxidation step of Co^{2+} into Co^{3+}. Like previous works, different ratios of His:$Co^{2+/3+}$, e.g. 2:1 and 3:1, were used to highlight the formation of different cobalt-histidine based cross-linkers which directly alter the viscoelastic properties of the transient polymer networks as shown in Figure 1.29. While Co^{2+} forms kinetically labile coordination bonds, Co^{3+} forms kinetically inert with high binding strength coordination bonds because d^6 cobalt(III) ion forms complexes with higher formation constant than the d^7 cobalt(II) ion.[94,95] Consequently, cross-links based on cobalt(II) ions undergo fast

ligand exchange and the binding strength is relatively weak which results in a viscoelastic liquid where flowing regime is probed and the cross-over between G' and G" is already passed as shown in Figure 1.29. Upon oxidation, cross-links formed via cobalt(III) ions form stable complexes and are kinetically inert which results in an elastic solid where no cross-over between storage and loss moduli is probed within the measured range. The influence of polymer concentration is also investigated because it also affects the gel properties as it controls the cross-linking density.
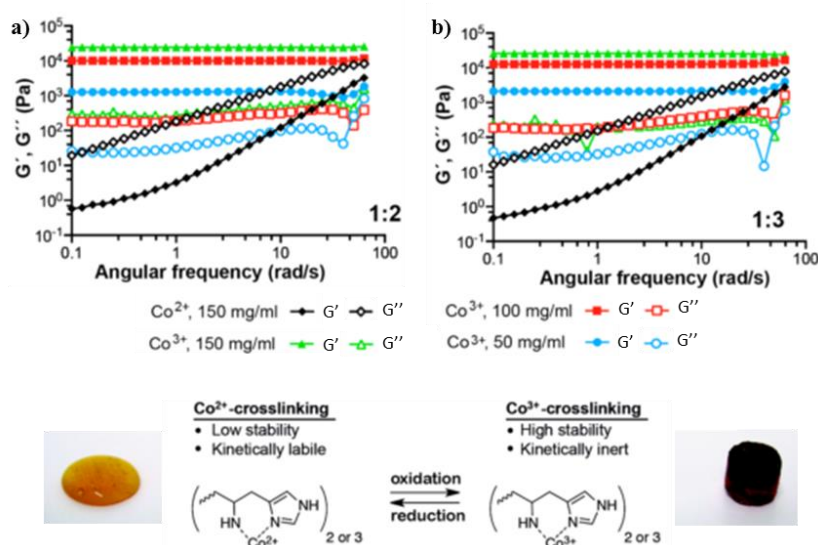
Figure 1.29: Influence of cobalt ions ratio with respect to histidine ligand and influence of polymer concentration of four-arm star PEG-His coordinated with Co^{2+} or Co^{3+} ions with histine:cobalt ratio of a) 2:1 and b) 3:1 at 25°C. The 4arm-PEG-His with Co^{2+} or Co^{3+} results in hydrogels with different rheological features due to the different coordination bond properties. With the Co^{2+}-mediated cross-links, the coordination bonds result in a viscoelastic liquid. In the Co^{3+}-mediated cross-links, the coordination bonds result in an elastic solid. The properties of the hydrogel can be switched from liquid to solid by oxidation of the Co^{2+} to Co^{3+}.[93]

Seiffert el al. also investigated the linear viscoelastic properties of four-arm star PEG (M_w = 10 kg.mol^{-1}, Đ = 1.03) end-capped with terpyridine moieties that can transiently coordinate to different metal

ions.[96,97] The latter was used to form temporary supramolecular polymeric networks in aqueous media or organic solvents with homogeneous architectures and determined binding strength. Their studies reveal that these networks in dilute and semi-dilute solutions display connectivity with temporal detachment of one of the star arms, which permits its relocation within the polymeric networks. Hence, it allows the relaxation of these systems. Depending on the nature of the metal ions, different organo-gels or hydrogels with varying binding strength are obtained and their corresponding relaxation times are ranged between ten to hundreds of seconds at a stoichiometric ratio, i.e. 2:1.

While several investigations have been conducted on linear rheology of associating polymers based on metal-ligand coordination, only a few works are reported on non-linear viscoelastic properties of metallo-supramolecular polymers. This is especially true for shear rheology where LAOS measurements are commonly performed.[98–102] For instance Cao et al. conducted strain sweep measurements on metallogels originated from the coordination of the 3,6-di-2- pyridinyl-1,2,4,5-tetrazine (DPTZ) functionalized poly(dicyclopentadiene) (sPDCPD) macromolecular ligands with zinc and nickel salt as shown in Figure 1.30.[103]
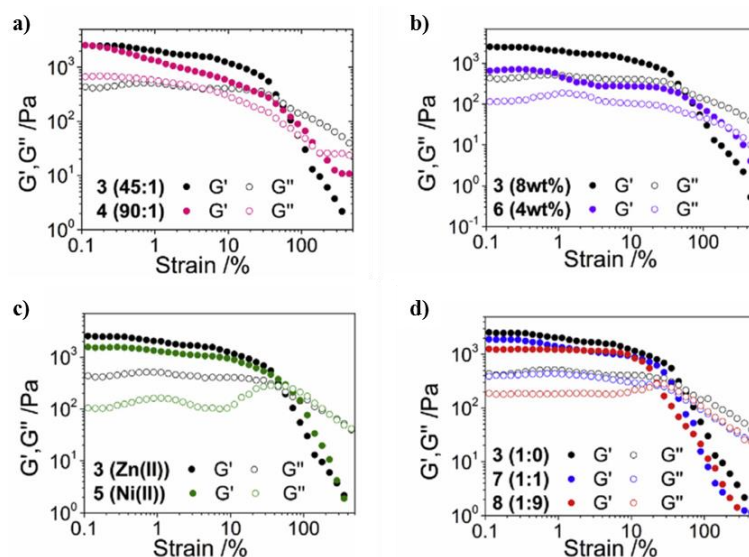
Figure 1.30: LAOS measurements of metallogels at f = 1Hz, T = -20°C with varying a) crosslinking density, b) sPDCPD polymer

59

concentration, c) different metal ions and d) different solvent THF:toluene mixtures.[103]

Their studies reveal that their materials displayed dynamic mechanical properties which are characteristic of metallogels. The shear thinning properties of such systems can be manipulated by varying different parameters such as the crosslinking density (ratio of PDCPD with respect to DPTZ or polymeric concentration with respect to the solvent), the nature of the solvent (THF, THF:toluene mixtures) or the type of metal ions (zinc, nickel). Figure 1.30 results appear to fit to type 3 of strain amplitude dependence. However, no further details were explained by the authors on the weak strain overshoot observed with such metallogels.

1.2.2.2 Shear and extension measurements

Besides LAOS measurements, tensile test experiments can also be conducted to investigate the non-linear elongation viscoelastic properties of metallo-supramolecular polymers. Liu et al. pursued such kind of work by reinforcing covalently cross-linked elastomers based on butadiene-styrene-vinylpyridine (VPR) with bis(pyridine)-zinc(II) coordination bonds.[102] Since M-L bonds are capable of breaking and re-forming, they are used as sacrificial bonds under external load to dissipate energy. The latter also facilitates rubber chains orientation and improves the mechanical properties of the resulting materials. First, the authors started by performing dynamic rheological measurements at various strain and frequency to have more information about the network structure of the samples as show in Figure 1.31
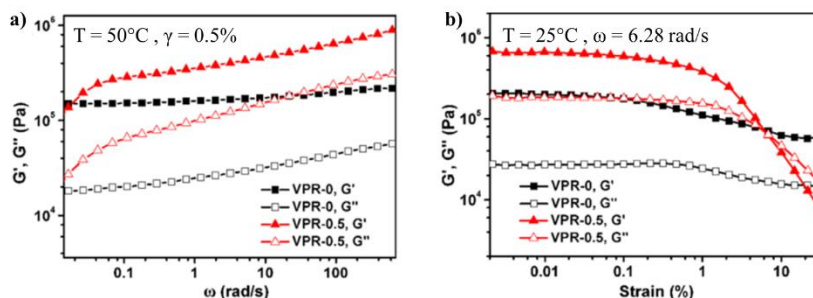
Figure 1.31: Dynamic a) frequency and b) strain sweeps of butadiene-styrene-vinylpyridine rubber with and without $ZnCl_2$ ions.[102]

From SAOS and LAOS data, the incorporation of physical bis(pyridine)-zinc crosslinks within covalently crosslinked elastomers increases the stiffness of the materials. This is highlighted by the general increase in moduli (G', G") for the elastomer additionally cross-linked with M-L complexes (VPR-0.5) compared to the rubber without metal salts (VPR-0). When LAOS measurement is performed, moduli of VPR-0.5 decreases with increasing strain and a cross-over between G' and G" is probed. Showing that the additionally cross-linked rubber exhibits fluid character at high strain because of the rupture of the sacrificial coordination bonds. Whereas for VPR-0, only a slight decrease in moduli is observed which is due to the disentanglements of rubber chains at high shear strain. Then Liu et al. studied the mechanical response of these materials without $ZnCl_2$ and with different ratio of zinc salts under tensile tests and results are reported in Figure 1.32.
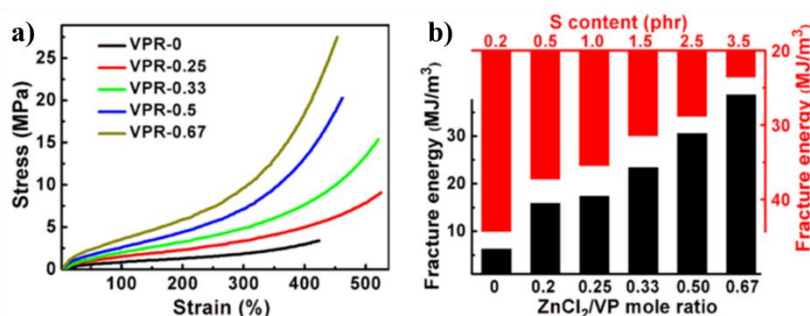
Figure 1.32: a) Tensile stress-strain curves of VPR-x and b) fracture energy of VPR-x, x corresponding to the different ratios of zinc salts.[102]

In the resulting VPR material, the elastomeric architecture is held together by dual cross-links of covalent cross-links and transient Zn^{2+}-pyridine complexes. While the covalent network imparts elasticity and keeps the shape of the material, the zinc-pyridine coordination serves as physical cross-links to increase the elasticity and improves the modulus. M-L complexes reversibly rupture-reform and act as sacrificial bonds to dissipate energy during stretching. After the rupture of physical cross-links, previously protected chains by the sacrificial bonds from the applied stress are released to sustain large deformation. Compared to the VPR without metal ions, the modulus, the tensile strength and fracture energy of VPR with zinc ions are significantly improved without scarifying the extensibility of the material. Hence, it

is demonstrated that the mechanical properties (moduli, strength, toughness, extensibility) of biomimetic diene-rubber can be tuned by adjusting the structural parameters of the covalently cross-linked network. Their mechanical features is also modulated by varying the incorporated ratio of metal-ligand coordination that act as physical cross-links and rupture under external load.

Similarly, Guan et al. investigated the bulk mechanical properties in shear and tensile tests of imidazole-containing polymers (ICPs) using styrene and acrylate monomers.[104] These polymers are dynamically cross-linked by addition of cobalt(II), zinc(II) or copper(II) ions with systematic variation in the ligand/metal (L/M) ratio. Upon addition of metal salt, an increase in the viscosity of the material is noted in shear rheology. This indicates that dynamic M-L cross-links are the major contributors to the viscoelastic properties of these systems and their dynamic viscoelastic properties increase by addition of metal salts as shown in Figure 1.33.
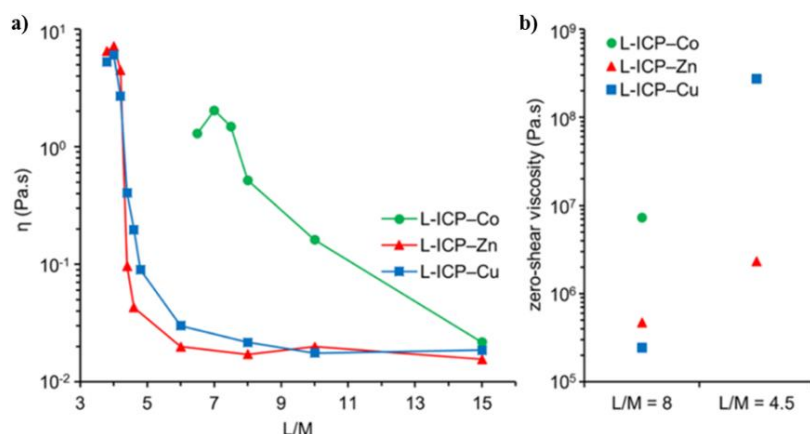
Figure 1.33: Linear dynamic shear viscosities of linear imidazole-containing polymers, a) in acetonitrile and b) in bulk, cross-linked with different types and amounts of metal.[104]

As more physical cross-links are formed within the polymeric network, it is expected that its resistance towards flow increases. These cross-link properties can be tailored by the type of metal ions which directly influences preferred coordination number (e.g. tetrahedral ML_4 or

octahedral ML_6) as depicted in Figure 1.34 and ligand exchange mechanism.
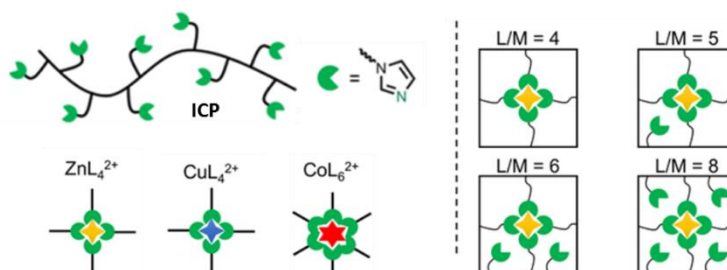
Figure 1.34: Tuning metal-imidazole cross-links properties through metal complex topology and ligand to metal (L/M) stoichiometry.[104]

They can also be tuned by the ligand to metal stoichiometric ratio which simultaneously adjusts the density of cross-links and the uncoordinated ligands. The presence of unbound ligands plays an active role in facilitating cross-links exchange dynamics depending of the M-L complex. Specifically, the presence of dangling arms/ligands affects the network relaxation behavior and consequently the dynamic mechanical properties of the resulting materials. Then Guan et al. pursued their work by investigating the extension mechanical properties of these ICP systems in bulk using static tensile tests. While linear ICP based on acrylate monomers are used to investigate dynamic shear rheology properties, brushed ICP based on styrene and acrylates monomers are designed to perform tensile tests because linear ICPs are not sufficient to produce mechanically strong materials for such kind of experiments. However, brushed ICP has multiphasic structure where glassy polystyrene domains acts as physical cross-links and soft domains are originated from poly(n-butyl acrylate). The Young's modulus (E) and the ultimate extensibility (ε_{ult}) are extracted from tensile data and reported in Figure 1.35 to compare the transient networks obtained with different types and amounts of metal ions.
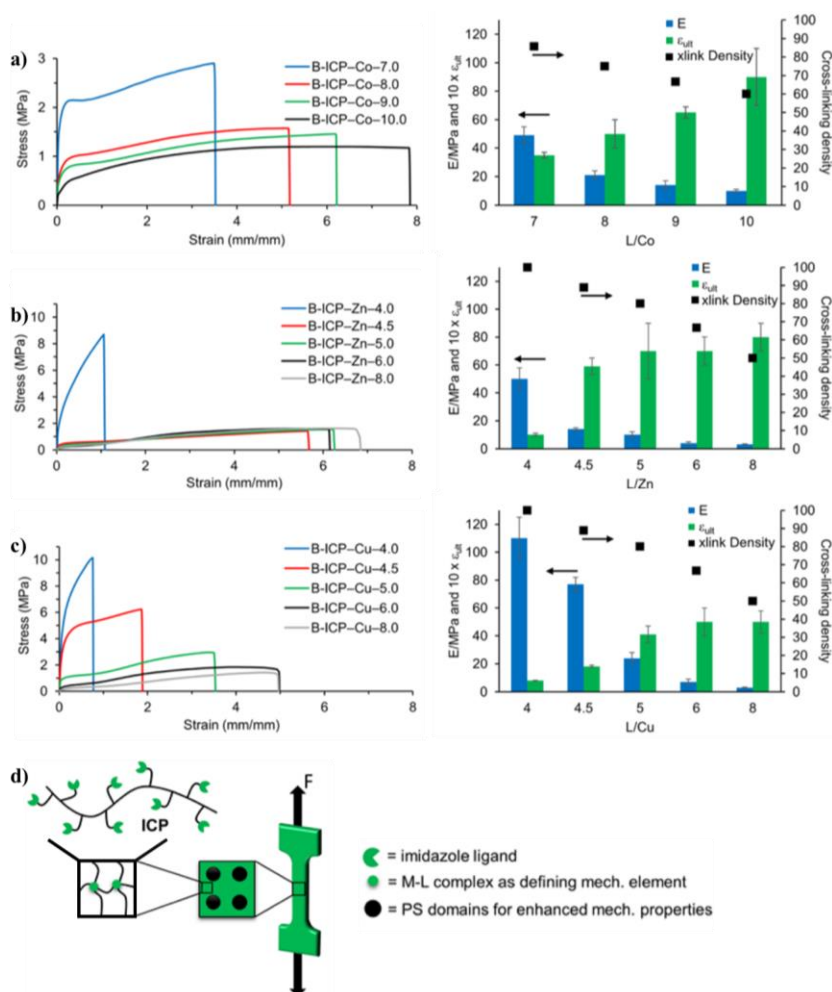
Figure 1.35: Static tensile stress-strain curves for B-ICP-M samples with different L/M ratios, where M = a) $Co^{2+,}$ b) Zn^{2+} and c) Cu^{2+} (strain rate: 100mm/min at 25°C). Young's modulus (E) and strain-at-break (ε_{ult}) plotted with cross-linking density at each L/M ratio. d) Schematic representation of the imidazole containing polymers (ICPs).[104]

For all three metals (Zn^{2+}, Cu^{2+}, Co^{2+}) the Young's modulus increases with increasing cross-linking density via addition of more metal salts. For a similar L/M ratio, the Co^{2+} networks have a higher E compared to Zn^{2+} and Cu^{2+} systems due to the preference of cobalt to form octahedral complexes ML_6 whereas zinc and copper prefer to form tetrahedral complexes ML_4. The ultimate extensibility (strain at break)

changes significantly when the L/M ratio lowers from 8 to 4 for ML_4 complexes and from 10 to 7 for ML_6 complexes. This is related to the fact that the M-L cross-links density increases upon addition of more metal ions. Consequently, a drastic reduction of uncoordinated imidazole groups in the bulk network occurs which dramatically slows down the ligand exchange mechanism. The latter impedes the transient network relaxation and dramatically increases the network rigidity. This is why the extensibility decreases while the tensile strength increases when L/M ratio decreases.

Through this investigation, Guan et al. show that there is a dependence of the bulk tensile properties on the M-L content. At low strain, the mechanical properties are governed by the structural topology of the network, the metal content and the coordination number of M-L cross-links. As the polymer network is stretched further, the dynamics of ligand exchange plays a role and influences the outcome of overstretched chains where the rupture of M-L cross-links can occur to help relaxing chains under stress. Their results clearly demonstrate that a large window of bulk mechanical properties under both static and dynamic loads is accessible by tailoring the metal ion type and amount. Indeed, it is possible to control the structure of the transient networks and the temporal response by regulating the population of active cross-links and the dynamics of ligand exchange rate.[105–107] However, one must note that phase-separation occurs in their brushed ICP which participates to the formation of physical cross-links in the bulk samples. The authors have not compared the mechanical properties under static and dynamic loads of the precursor system without metal ion in order to check the contribution of the phase-separation with respect to the M-L dynamics.

The incorporation of metal-ligand interactions within polymeric systems clearly has an effect on the rheological properties for the resulting materials. Transient networks can be formed with linear telechelic polymeric precursors where the sticker functionality has to be no less than three. In the case of telechelic branched polymeric precursors or linear polymers with multiple stickers distributed along their backbones, a sticker functionality no less than two is necessary to form supramolecular networks. In general, most of the studies are conducted on transient networks formed by these polymeric precursors

(linear or branched, telechelic or randomly attached) which tend to form large aggregates of stickers or flower-like micelles bridged by flexible polymer chains. Hence, phase-separation is promoted due to the fact that the stickers are hydrophilic whereas the polymeric matrix are hydrophobic.

Despite of this, the results obtained from the rheological investigations demonstrate that a large window of mechanical properties is accessible by tailoring the metal-ligand interactions which are incorporated within most of the time unentangled polymers. In order to have a better understanding on the rheological properties of associating polymers, the elaboration of theoretical models is also important to consider.

1.3 Molecular models for associative polymers

1.3.1 Tube theory for classical polymers

Polymer melts and solutions display complex flow behavior and stress relaxation in response to a deformation. In order to interpret such behavior and understand the viscoelastic data beyond phenomenological description, the development of a quantitative molecular theory is needed that correlates rheological properties of a polymer to its molecular structure. In this section, a quick overview of molecular dynamics theories will be essentially focused on dilute polymer solutions and entangled polymers.

The development of the tube model has been one of the most noteworthy accomplishments in polymer physics to predict polymer dynamics at mesoscopic scale. Developed by Doi, Edwards and de Gennes, the tube-model theory considers that a polymer chain is confined in a virtual tube originated from the average effect of all topological constraints between different chains.[108,109] These topological constraints are usually referred to as entanglements as illustrated in Figure 1.36.
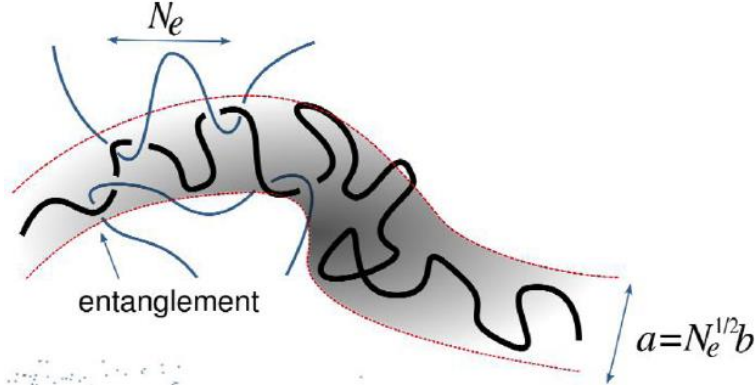
Figure 1.36: Schematic representation of a polymer chain confined by entanglements to a tube region of diameter a.[110]

The latter reflects the topological interaction between one polymer chain and its surrounding neighbors. This interaction can significantly hinder the motion of the chain and thus its ability to relax after a deformation (or a stress) is applied. In presence of entanglements, the polymer chain has to go through unusual motions to move and relax with other polymer molecules. Because of these unusual motions, entangled polymers can have relatively long relaxation times and high viscosities. One of the key idea of the tube model is to investigate the motion of the test chain which moves along the tube. Through this study, different relaxation mechanisms are implemented to the tube model to successfully describe the dynamics of entangled polymers.

1.3.1.1 Rouse model to entangled chains

The Rouse model was intended to describe the dynamics of a polymer molecule in a dilute solution.[111] The model is based on bead-spring models in which a flexible linear chain is mapped as a collection of N beads of size b (considered to be the Kuhn length) and with a friction coefficient ζ. Each bead is connected to each other by N-1 springs with Hookean spring constants equal to $3k_BT/b^2$, where k_B is the Boltzmann constant and T the temperature.

The bead-spring model takes into account the viscous interaction between a solid spherical particle and a liquid medium originated from the random movements of the small particle in a liquid medium. As a particle explore its surrounding, it diffuses from its initial position $r(0)$ at $t = 0$ to another position $r(t)$ at time t. On average, the distance between these two positions can be defined as:

$$< [r(t) - r(0)]^2 > = 6D.t \qquad (1.28)$$

Where D is the diffusion coefficient which characterizes the Brownian motion. The latter is defined by Einstein relation as follows:

$$D = \frac{k_B.T}{\zeta} \qquad (1.29)$$

The friction coefficient ζ is defined by Stokes' law for a sphere as:

$$\zeta = 6\pi.\eta.R \qquad (1.30)$$

Where η is the viscosity of the surrounding liquid medium and R is the radius of the spherical body. Hence, equation 1.29 can be written as:

$$D = \frac{k_B.T}{6\pi.\eta.R} \qquad (1.31)$$

Which is known as the Stokes-Einstein-Sutherland expression. The combination of equations 1.28 and 1.31 provides the duration of a particle to travel a distance comparable to its own size R.

$$\tau \sim \frac{R^2}{D} \sim \frac{\eta.R^3}{k_B.T} \qquad (1.32)$$

In the case of unentangled chains, the R^2 is the length of the primitive path composed of N Kuhn segments of length b^2. The diffusion coefficient of the chain is equal to $k_B.T/N.\zeta$, where $N.\zeta$ corresponds to

the total coefficient friction of the chain. Therefore, the Rouse relaxation time is defined as:

$$\tau_R = \frac{R^2}{D} = \frac{N.b^2}{D} = \frac{N.b^2}{\frac{k_B.T}{N.\zeta}} = \frac{N^2.b^2.\zeta}{k_B.T} = \tau_0.N^2 \qquad (1.33)$$

Where τ_0 is the relaxation time of one Kuhn segment and is defined as:

$$\tau_0 = \frac{b^2.\zeta}{k_B.T} \qquad (1.34)$$

Since the entire chain is composed of N Kuhn segments as illustrated in Figure 1.38, each portion of the chain (or sub-chain) with N/p Kuhn segments relaxes similarly to the whole chain with a specific relaxation time τ_p defined as follow:

$$\tau_p = \tau_0.\left(\frac{N}{p}\right)^2 = \frac{\tau_R}{p^2} \qquad (p = 1,2,3,..., N) \qquad (1.35)$$

From Equation 1.35, the relaxation time by Rouse mode associated to p-1 mode is longer than the relaxation time of p mode ($\tau_{p-1} > \tau_p$). At time $t = \tau_p$ there are p unrelaxed modes which contribute $k_B.T$ to the relaxation modulus $G(t)$. The latter is defined at $t = \tau_p$ as:

$$G(t = \tau_p) = k_B.T.\nu.p \qquad (1.36)$$

Where ν is the number density of active chains. From Equation 1.35, the temporal dependence of p modes is given by:

$$p = N\left(\frac{\tau_p}{\tau_0}\right)^{-\frac{1}{2}} \qquad (1.37)$$

By implementing Equation 1.37 into Equation 1.36, the following relaxation modulus is obtained for $\tau_0 < t < \tau_R$:

$$G(t) \cong k_B.\text{T}.v.\ N\left(\frac{t}{\tau_0}\right)^{-\frac{1}{2}} \tag{1.38}$$

For $t > \tau_R$, an additional exponential term is added to the relaxation modulus as follows:

$$G(t) \cong k_B.\text{T}.v.\ N\left(\frac{t}{\tau_0}\right)^{-\frac{1}{2}}.exp\left(-\frac{t}{\tau_R}\right) \tag{1.39}$$

The explicit formula for the relaxation modulus of the Rouse model is:

$$G(t) = k_B.T.v \sum_{p=1}^{N} exp\left(-\frac{t}{\tau_p}\right) \tag{1.40}$$

In the presence of entanglements, the Rouse mode allows the relaxation of sub-chains shorter than the molecular weight between two entanglements. Therefore, M_e can be considered as the longest sub-chains able to relax via Rouse process. The relaxation time of the sub-chains between two entanglements (τ_e) is defined as:

$$\tau_e = \frac{b^2.\zeta}{k_B.T} N_e^2 = \tau_0.N_e^2 \tag{1.41}$$

Where N_e is the number of Kuhn segments in the sub-chain of molecular weight M_e. For an entangled polymer melt, the global relaxation modulus is given by:

$$G(t) = G_N^0 + G_{Rouse}(t) = G_N^0 + \frac{\rho.R.T}{M} \sum_{p=Z}^{N} exp\left(-\frac{t}{\tau_p}\right) \tag{1.42}$$

In oscillatory shear, the Rouse model predicts that both the storage and loss moduli are proportional to $\omega^{1/2}$ at high frequencies. Once the sub-chains shorter than M_e have completely relaxed, the rubbery plateau and the terminal relaxation zones are reached. The Rouse mode is not sufficient anymore to describe these regions because the entirety of the chains is considered. Hence, additional relaxation processes are needed.

1.3.1.2 Reptation mechanism of de Gennes

Introduced by de Gennes, the reptation process describes how the polymer chain escapes from its virtual tube by sliding back and forth in it.[109] This unidimensional thermal diffusion gradually evacuates the mass of the chain outside the tube. Every time a portion of the chain is out of its tube, the chain is free and randomly orients itself to create a new tube section. The creation of the new tube section is random and its correlation to the initially vacated tube portion is forgotten. Hence, the chain progressively loses the memory of its initial orientation (or original entanglements). When the whole chain is completely out of its initial tube, the polymer chain is said to be relaxed. This reptation mechanism is characterized by the curvilinear diffusion coefficient D_e and is defined as:

$$D_e = \frac{k_B.T}{N.\zeta} \tag{1.43}$$

Where $N.\zeta$ is the total friction coefficient of the chain. In order to relax, the chain has to diffuse out of its tube and move a distance L. A representation of a polymer chain confined in its virtual tube is illustrated in Figure 1.37 along with its parameters.
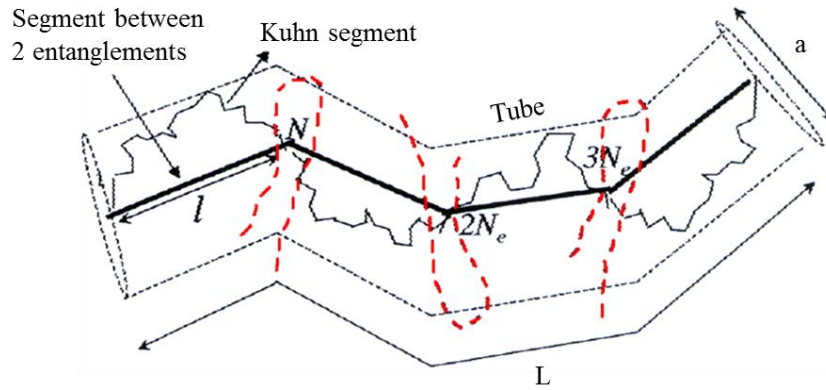
Figure 1.37: Coarse grained model of a chain in its tube. Sub-chains of mass M_e are considered as segments of length l. N_e is the number of Kuhn segments between two entanglements, L is the length of the primitive path and a is the tube diameter.

71

At equilibrium the tube diameter a is equal to the length between two entanglements l and is determined as:

$$a = l \cong N_e^{1/2}.b \tag{1.44}$$

From Figure 1.37, the tube can be considered of being composed of N/N_e sections of size a and each section contains N_e monomers. The chain can be thought of as a random walk of entanglement strands, i.e. N/N_e strands of size a, or as a random walk of monomers, i.e. N monomers of size b. The length of the primitive path L is proportional to the chain length between two entanglements l and it is defined as:

$$L = Z.l = \frac{N}{N_e}.l = \frac{N.b}{\sqrt{N_e}} \tag{1.45}$$

The relaxation time τ_d required for the center of mass of the chain to diffuse a distance L is defined as follows:

$$\tau_d = \frac{L^2}{D_e} = \frac{N^3.b^2.\zeta}{N_e.k_B.T} = \tau_0.\frac{N^3}{N_e} \tag{1.46}$$

By implementing τ_e from Equation 1.41 into the Equation 1.46 the relaxation time τ_d becomes:

$$\tau_d = \tau_0.\frac{N^3}{N_e} = \tau_e.\left(\frac{N}{N_e}\right)^3 = \tau_e.Z^3 \tag{1.47}$$

Where Z is the number of sub-chains of molecular weight M_e in one entire chain or also defined as the number of entanglements per chain.

The reptation mechanism by which a chain would diffuses back and forth along the tube axis, satisfies a one-dimensional diffusion equation. To solve this equation, Doi and Edwards calculated the survival probability P(s,t) as the fraction of the tube located at position s that survives at time t which is given by:

$$\frac{\partial P_{rept}(s,t)}{\partial t} = D_e \frac{\partial^2 P_{rept}(s,t)}{\partial s^2}$$

(1.48)

With the following boundary conditions:

$$\begin{cases} P_{rept}(0,t) = P(L,t) = 0 \\ P_{rept}(s,0) = 1 \quad for \ s \in [0,L] \end{cases}$$

(1.49)

The first condition means that the survival probability of the initial tube fractions localized at the chain ends is zero. The second one involves that the survival probability for any initial tube is one at the beginning.

The general solution for the tube survival probability is defined as:

$$P_{rept}(s,t) = \sum_{p,odd} \frac{4}{p\pi} . \sin\left(\frac{p\pi s}{L}\right) . \exp\left(\frac{-p^2.\pi^2.D_e.t}{L^2}\right)$$

(1.50)

By integrating Equation 1.51, the proportion of unrelaxed segments $\Phi(t)$ at time t is determined as:

$$\Phi(t) = \int_0^L P_{rept}(s,t).ds = \frac{8}{\pi^2} \sum_{p,odd} \frac{1}{p^2} exp\left(\frac{-p^2.D_e.t}{L^2}\right)$$

(1.51)

This survival probability is defined as the fraction of the tube that remains occupied by the chain at time t by assuming that the whole chain is in the tube at time $t = 0$. By including the reptation process with the Rouse motion, the relaxation modulus of entangled polymers is defined as follows:

$$G(t) = G_{Rouse}(t) + G_N^0 . \Phi(t)$$

(1.52)

73

$$G(t) = G_{Rouse}(t) + G_N^0 \cdot \frac{8}{\pi^2} \sum_{p,odd} \frac{1}{p^2} exp\left(\frac{-p^2 \cdot D_e \cdot t}{L^2}\right)$$

In spite of the success of the Doi-Edwards tube model in predicting the linear viscoelasticity of linear entangled polymers, additional relaxation mechanisms are implemented to refine the tube theory so that predictions in good agreements with experimental data can be obtained.

1.3.1.3 Contour length fluctuation (CLF)

The CLF originates from the thermal diffusion that allows the chain to meander within the tube.[112] Consequently, the chain is shrunk in its tube as represented in Figure 1.38. When the polymer chain pulls back its end inside the tube, the ends of the tube are vacated and the stress associated with the now-vacated end tube segments is relaxed. Upon re-expansion, the chain end randomly explores new regions and creates new tube segments. The degree of chain end shrinkage varies constantly due to the Brownian motion. As one can already imagine, contour length fluctuation relaxes the chain ends rapidly whereas the relaxation of the center of the chain by this process is slow because the chain has to be highly shrunk to vacate the center of the tube. Therefore CLF can be divided into two different mechanisms which are:

▪ The early fluctuation is associated to the wrinkling of chain ends where the chain easily fluctuates inside the tube without any topological constraints and the retraction energy is lower than the thermal energy $k_B . T$.

▪ The activated fluctuation refers to shrinkage of the inner part of the chain which requires deep fluctuation to reach it due to topological constraints. Consequently, the retraction energy exceeds the thermal energy.
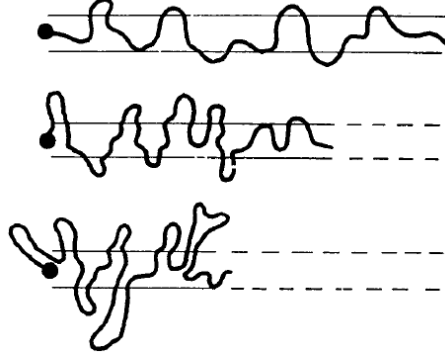
Figure 1.38: Illustration of the primitive path fluctuations, in which the chain ends randomly wrinkle from the ends of the tube.[113]

The potential energy U(x) helps to know which fluctuations process takes place.[114–116] This potential corresponds to the energy generated during the retraction of a chain which is initially at equilibrium and whose ends are retracted to a position x. The formula of U(x) is given by:

$$U(x) = \frac{3k_B.T}{2} Z.x^2 + C$$

(1.53)

Where $x = s/L$ is the normalized distance at which a chain end is retracted and C is a constant. When U(x) $< k_B.T$, the early fluctuation process takes place and its relaxation time is defined as:

$$\tau_{CLF}(x) = \tau_{early,fluc}(x) = \frac{9\pi^3}{16} \left(\frac{M_a}{M_e}\right)^2 . \tau_{R,chain}.x^4$$

(1.54)

Where M_a is the molecular weight of an arm and $\tau_{R,chain}$ is the Rouse relaxation time for an arm. The linear chains are considered as two arms structures with M_a equals to half of M_n. The chain extremities are not affected by the tube constraints. Therefore, the chain ends can freely move and relax by Rouse process.

When $U(x) > k_B.T$, the activated fluctuation occurs where the chain retraction is affected by the topological constraints of the tube and its relaxation time is characterized by:

$$\tau_{CLF}(x) = \tau_{activated,fluc}(x) = \tau_0 . \exp\left(\frac{U(x)}{k_B.T}\right)$$

(1.55)

To summarize, fluctuation time for chain segment being retracted in small depth is described by the early mechanism and fluctuation time corresponding to deeper segment depth is described by the activated process. In between, the segment depth x_{trans} corresponds to the transition between these two mechanisms where $U(x_{trans}) = k_B.T$. So the general fluctuation time can be written as:

$$\tau_{CLF}(x) = \begin{cases} \tau_{early,fluc}(x) & for\ x < x_{trans} \\ \tau_{activated,fluc}(x).\exp\left(\frac{\Delta U_{x_{trans}\to x}}{k_B.T}\right) & for\ x > x_{trans} \end{cases}$$

(1.56)

From Equation 1.56, the general solution for the tube survival probability is defined as:

$$P_{CLF}(x,t) = \exp\left(\frac{-t}{\tau_{CLF}(x,t)}\right)$$

(1.57)

Note that, for linear entangled polymers the time required to relax the inner part of chain via fluctuation process is relatively long that this fraction of the chain will have already relaxed by reptation mechanism. Then the global proportion of unrelaxed segments $\Phi(t)$ at time t is determined as:

$$\Phi(t) = \int_0^1 P_{rept}(x,t).P_{CLF}(x,t).dx$$

(1.58)

By including the CLF mechanism with the reptation and the Rouse motion, the relaxation modulus of entangled polymers becomes:

76

$$G(t) = G_{Rouse}(t) + G_N^0 . \Phi(t)$$

$$G(t) = G_{Rouse}(t) + G_N^0 . \int_0^1 P_{rept}(x,t) . P_{CLF}(x,t) . dx$$

(1.59)

The inclusion of CLF improves the prediction of the tube theory with respect to the scaling exponent for viscosity as function of molecular weight of the polymer chain. However, this inclusion is not sufficient to perfectly describe the dynamics of polymer melts. This implies the existence of other relaxation mechanisms.

1.3.1.4 Constraint release (CR)

The relaxation of a chain not only depends on its own fluctuation and reptation but also on the relaxation of the matrix chains surrounding the test chain in the tube which also undergo similar motions. While the test chain is constrained by entanglements originating from surrounding matrix chains, it also imposes topological constraints on these chains. When the test chain fluctuates and reptates, it releases these constraints on the matrix chains. Similarly, when the matrix chains fluctuate and reptate, they also release their constraints on the test chain. Hence, the CR process can be considered as a global relaxation process where the test chain and its entire environment can release topological constraints.

The CR mechanism can be described by the double reptation theory developed by Tuminello, Tsenoglou and des Cloizeaux.[117–119] The latter considers a blend of two polymers A and B with v_A and v_B being respectively the volume fraction of chain A and B in the blend. $P_A(t)$ and $P_B(t)$ are respectively the remaining fraction of the initial tube from the chain A and B at time t. The total survival fraction of the initial oriented tube segments is given by:

$$\Phi(t) = \sum_{A,B} v_A . v_B . P_A(t) . P_B(t)$$

(1.60)

77

Where $\nu_A.\nu_B$ is the probability to have an entanglement between a chain A and a chain B. The product $P_A(t).P_B(t)$ represents the probability that such an entanglement still exists at time t. By implementing this mechanism, the relaxation modulus is defined as follows:

$$G(t) = G_N^0 \sum_{A,B} \nu_A.\nu_B.P_A(t).P_B(t) = G_N^0 \sum_A \left(\nu_A.P(t)\right)^2 = G_N^0.\Phi(t)^2$$

(1.61)

In the case of a monodisperse system, $\nu_A = 1$, $\nu_B = 0$ and the Equation 1.61 can be simplified into:

$$G(t) = G_N^0.P_A(t)^2$$

(1.62)

The CR mechanism can also be described by the dynamic tube dilation (DTD) mechanism which takes into account the relaxation of the test chain environment.[120,121] If a part this environment has relaxed, then it does not contribute anymore to the stress imposed on the test chain. Therefore, this relaxed environmental polymer fraction can be considered as solvent for the test chain. Consequently, the test chain is less constrained in the tube due to less entanglements that hinder the motion of the chain. Since there are less entanglements, it means that the size of tube confining the test chain needs to be rescaled accordingly. Since the dimensions of the tube and M_e change with time, only the unrelaxed fraction of the polymer plays an effective role in the relaxation mechanism. The DTD theory takes into account the rescaling of the tube parameters such as the increase of M_e due to the loss of entanglements. The rescale of M_e is defined as:

$$M_e(t) = \frac{M_{e,0}}{\Phi(t)^\alpha}$$

(1.63)

Where $M_{e,0}$ is the molecular weight between entanglements at the initial equilibrium state and α is the dynamic dilution exponent. The primitive path length and the rescale of the tube diameter are redefined as follows:

$$L(t) = L_0(t).\Phi(t)^{\alpha/2}$$

(1.64)

$$a(t) = \frac{a_0}{\Phi(t)^{\alpha/2}} \tag{1.65}$$

Equations 1.64 and 1.65 highlight the polymer environment contribution increases with t where the primitive path length becomes shorter and the tube diameter becomes wider. By implementing this mechanism, the relaxation modulus can be written as:

$$G(t) = G_{Rouse}(t) + \frac{\rho.R.T}{M_e(t)}.\Phi(t) = G_{Rouse}(t) + \frac{\rho.R.T}{M_{e,0}(t)}.\Phi(t)^{\alpha+1} \tag{1.66}$$

Note that the Equation 1.66, which is similar to the double reptation process, is the general formula that takes into account the constraints release mechanism. Besides altering the parameters of the tube, DTD also influences the reptation and fluctuation times given by:

$$\tau_{rept}(t) = \frac{L(t)^2}{D_e} = \frac{L_0^2}{D_e}.\Phi(t)^\alpha = \tau_{rept,0}.\Phi(t)^\alpha \tag{1.67}$$

$$\frac{\partial log\tau_{activated,fluc}(x)}{\partial x} = 3\left(\frac{M}{M_e}\right)x = 3\left(\frac{M}{M_{e,0}}\right)x.\Phi(t)^2 \tag{1.68}$$

While DTD has mainly an effect on the activated fluctuation, it has nearly no effect on the early fluctuation process because the sub-chains are not affected by the topological constraints, i.e. the entanglements. This section briefly summarizes the tube theory refined with additional mechanisms. The latter is to build an algorithm to predict the relaxation modulus of classical/conventional polymer melts. By combining the refined tube model with additional concepts describing the kinetics of supramolecular interactions, it is then possible to build theoretical models for associating polymers as well.

1.3.2 Models for associating polymers

From the plethora systems listed above, the associating polymers can be classified into two categories based on the chemical distribution of the associating moieties, i.e. stickers. In one group, the supramolecular polymers have multiple stickers attached along their polymeric backbones. Each polymer can thus form transient cross-links with several other polymers. In the other group, the associating polymers have the stickers located at their extremities such as telechelic polymers. The combination, between the dynamics of the parent polymer chains and the breaking/reforming kinetics of the non-covalent bonds, gives access to a wide window of rich mechanical properties emerging from supramolecular polymers.

Theoretical models have been developed to better understand the rheological properties of these associating polymers in accordance with their structural classification. For instance Rubinstein, Semenov, Leibler and Colby developed the sticky Rouse model for unentangled associating polymer solutions with many pairwise stickers per chain.[122,123] The model reveals that there are few unassociated stickers at a high degree of association. Therefore it is difficult for a sticker to find a new partner to associate with after breaking the bond with an old one. Typically a sticker experiences many breaking and reforming events with its old partner before finding a new one to associate with. Consequently, it extends the effective lifetime of reversible bonds. Due to this series of unsuccessful search for a new partner, the sticker lifetime τ_b is then normalized into τ_b^* where $\tau_b^* \gg \tau_b$. The sticky Rouse model predicts that the Rouse relaxation time is proportional to τ_b^* times the square of the number of inter-chain bonds per polymer. Colby et al. has found great success in modeling the dynamics of ionomers.[124,125] They showed that the relaxation modulus has contributions from the normal Rouse modes and the sticky Rouse modes. While the Rouse modes are unaffected for segments with size smaller than the chains between stickers, the relaxation motion of chains larger than the size of a sticky Rouse segment is contrained by the association of the stickers.

The sticky reptation model extends this idea to entangled associating polymer solutions, where the search for a new partner is

further restricted by a part of the confining tube on the test chain. The model considers that the polymer chains performs sticky Rouse motion along the contour of the virtual confining tube.[122] The reptation time is therefore defined as the sticky Rouse time τ_b^* multiplied by the number of entanglements per chain. The sticky reptation model reveals a strong concentration dependence of viscosity due to the increase of inter-chain associations at the expense of intra-chain ones with increasing polymer concentration. In these two sticky models, the kinetics of breaking and reforming transient bonds dominates the dynamics of associating polymer solutions. More precisely, the intermolecular associations act as dissipative friction points dominating the long-time dynamics. At timescales shorter than the sticker lifetime τ_b the solution behaves as a network. As stickers break and reform, the associating polymers rearrange and begin to flow.

Besides pairwise associating moieties, the stickers are also able to aggregate into large clusters. In this case, formation of interconnected micelles can occur to create reversible networks. Two processes such as chain diffusion and positional rearrangement of the micelles are considered to collectively relax the stress. Herein, it is assumed that the sticker hopping proceeds by dissociating from one micellar core and reform into another core. Marrucci et al. predicted that the relaxation time of unentangled telechelic chains has a power-law dependence on the polymer concentration and molecular weight.[126] Similarly, Semenov and Rubinstein showed that for unentangled and strongly entangled associating polymers, the relaxation time has, respectively, a power-law and exponential polymer concentration dependence.[127] Additionally, the terminal relaxation time for these systems is governed by the micellar positional rearrangements.

Recently, Hawke et al. suggested a model to describe the viscoelasticity of linear entangled associating polymers with stickers randomly attached to the polymer backbone.[128] By implementing the idea of sticky junctions, they showed the emergence of several relaxation steps and also the presence of a second plateau G' at low frequency which is attributed to the formation of stickers aggregates having extremely long lifetime as shown in Figure 1.40.
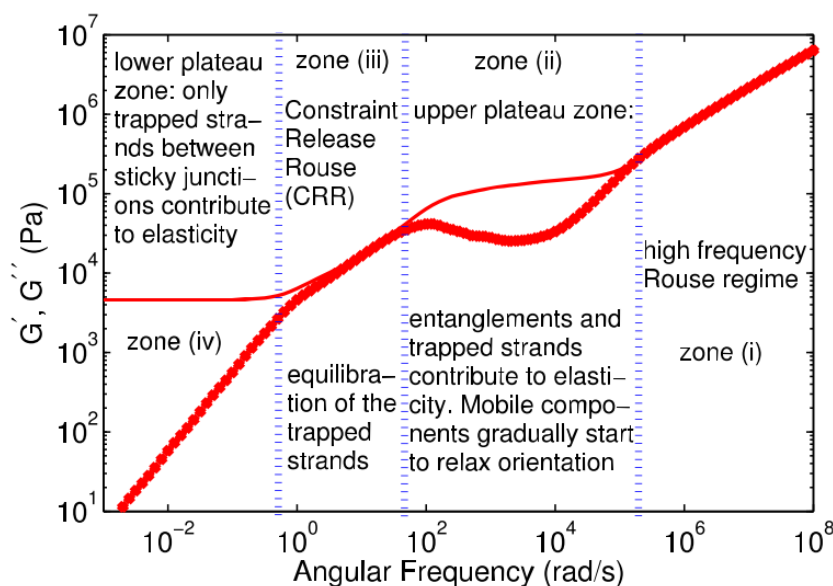
Figure 1.40: Representation of different relaxation regimes. The line curve is the theoretical prediction for the storage modulus G' and the full symbols are the experimental data.[128]

At short timescale, zone (i) corresponds to the Rouse motion described earlier which involves the motion of sub-chains of increasing length. This motion is typically characterized by the slope of -1/2. The transition into zone (ii) indicates the saturation of the Rouse modes where the sub-chains have reached the average spacing between two entanglements or stickers with long lifetime.

Then zone (ii) is attributed to the relaxation of linear chains and the free dangling chains, i.e. chains that are not trapped between two sticky junctions as illustrated in Figure 1.41. Moreover, the linear chains relax via reptation and CLF processes.
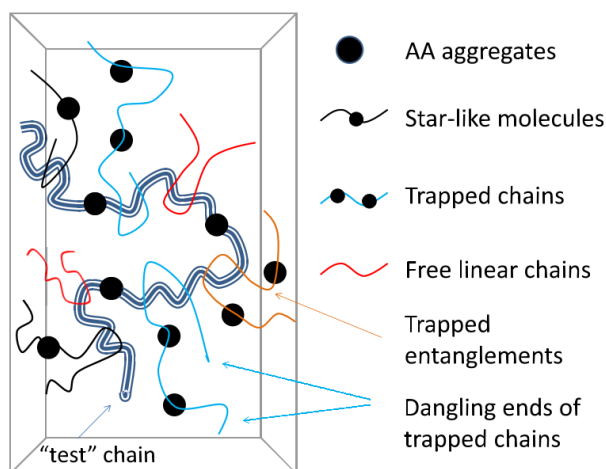
Figure 1.41: Illustration of test chain surrounded by free linear chains not attached to junctions and trapped chains between two sticky junctions.[128]

Once all the entanglements of the mobile chains are relaxed, zone (iii) is reached and the authors attribute this section to the constraints release Rouse (CRR) process. The latter occurs in binary blends of long and short linear chains where the portions of the long chains located between two long-long entanglements use the extra freedom originated from the reptation of short chains. In such case, the fraction of long chains undertakes local hops and renews its local conformation at the rhythm of entanglements and disentanglement of the short chain.[129–131] CRR process takes place for chains trapped between two sticky junctions to partially renew their configurations. Afterwards, the final zone (iv) corresponds to the relaxation time of the trapped chains. The latter is delayed until the sticky junctions dissociate. However, such time is considered extremely long in their model to properly predict the first three relaxation zones.

During the past five years, several theoretical models have been developed to better interpret the rheological properties of various associating systems.[132–135] However, most of these works are related to associating systems that tend to form aggregates or clusters. Moreover, the supramolecular interactions used in the associating polymers are not

the metal-ligand coordination but rather multiple hydrogen bonding or ionic interactions.

1.4 Objectives and structure of the thesis

The state of the art on metallo-supramolecular polymers highlights the existence of plethora associating systems based on metal-ligand coordination. Depending on the desired macromolecular structure/topology and the location of the stickers within the polymeric matrix, different synthetic strategies can be applied to synthesize monodisperse well-defined MSPs or polydisperse uncontrolled MSPs.

Several rheological studies were conducted on these systems to characterize their mechanical properties. Investigations reveal that the thermodynamic stabilities and the kinetics of M-L interactions definitely play a key role on the dynamics of metallo-supramolecular polymers. These M-L complexes restrict the motion of the chain by providing a second source of friction for the polymer. Hence, they lead to a delay on the stress relaxation in associating systems compared to their neutral polymer counterparts. However, most of these studies are limited to unentangled associating polymers where M-L interactions mainly dictate the mechanical properties. In the molten state, large aggregates/clusters of hydrophilic metal-ligand stickers are formed within hydrophobic polymeric matrix, which leads to phase separation. The latter has also an influence on the mechanical properties by restricting the motion of the M-L complexes and it may screen the advantages of pairwise association effect. This is why several studies of MSPs are conducted in solution to avoid aggregation.

In parallel, numerous models are elaborated to predict the viscoelasticity of associating polymers. The majority of them is applied for unentangled supramolecular systems which phase separate and form aggregates of stickers rather than forming pairwise stickers. Furthermore, these systems are based on multiple hydrogen bonding or ionic interactions. The development of theoretical models for metallo-supramolecular polymers is very limited in the literature.[136]

Only few works are reported to date on the investigations of entangled metallo-supramolecular polymers where both the reversible M-L interactions and the structure of the polymer matrix play a role on the rheological features. Furthermore, the molten state is the state of matter in which the majority of polymers are used in different applications. Therefore, it is reasonable to consider that development of entangled metallo-supramolecular could lead to the greatest significant impact in polymer engineering or polymer science.

In this context, the objectives of this thesis are (i) to fundamentally understand the structure and dynamics of entangled metallo-supramolecular bulk polymers (MSBPs) based on well-defined building block models. Precisely, we focus on monodisperse entangled linear and star-like polymers of various lengths. (ii) To investigate the role/influence of the combined effect between the dynamics of metal-ligand coordination and the dynamics of the macromolecules on the rheological behavior. (iii) To study the effect of external stimuli such as shear and temperature on the dynamic responses of MSBPs.

This thesis addresses this grand challenge, and aims at a deeper understanding of how the combination of M-L interactions with entanglements impacts the structure, the relaxation dynamics and the mechanical properties of well-defined entangled metallo-supramolecular polymers over a wide timescale or temperature range. Through this investigation, the structure-property relationships are established, providing general guidelines to unambiguously control the design of supramolecular polymers with specific rheological properties that can be engineered over a wide window of mechanical properties.

To fulfill those objectives, this thesis is constructed as follows:

▪ In Chapter 2 the synthesis of linear and star-like associating polymeric precursors is presented. These precursors are then used for the elaboration of entangled metallo-supramolecular polymers.

▪ The linear viscoelastic properties of these associating systems is studied in Chapter 3 using a strain-controlled shear rheometry. A systematic investigation is conducted by varying the topology of the building blocks and the type of metal ions under external stimuli such a temperature.

▪ Chapter 4 deals with the development of a theoretical model that is capable to predict the linear flow at bulk level by using an upgraded version of time marching algorithm (TMA). The latter takes into account both the dynamics of the metal-ligand interactions and the dynamics of the building blocks.

▪ In Chapter 5, the systematic investigation is extended to non-linear shear and extensional rheology. To achieve this goal, viscoelastic properties are studied by using a cone partitioned plate geometry for shear tests and a filament stretching rheometer for uniaxial extension tests.

▪ Chapter 6 is an attempt to experimentally determine the lifetime of the metal-ligand coordination within the polymeric matrix by performing dielectric relaxation spectroscopy measurements.

▪ Chapter 7 presents early results on binary blends based on metallo-supramolecular bulk networks which are diluted in linear poly(n-butyl acrylate) matrices. This investigation highlights the impact of the linear chains on the viscoelastic properties on the transient networks.

Finally, few conclusions are drawn from these studies and possible perspectives are also highlighted.

Bibliography

(1)   Lehn, J. -M. Supramolecular Chemistry—Scope and Perspectives Molecules, Supermolecules, and Molecular Devices (Nobel Lecture). *Angew. Chemie Int. Ed. English* **1988**, *27*, 89–112.

(2)   Langbein, D. W. *Theory of Van Der Waals Attraction*; Springer: New York, 1974.

(3)   Parsegian, A. V. *Van Der Waals Forces: A Handbook for Biologists, Chemists, Engineers, and Physicists*; Press, C. U., Ed.; Cambridge University Press: Cambridge, 2005.

(4)   Hermann, J.; DiStasio, R. A.; Tkatchenko, A. First-Principles Models for van Der Waals Interactions in Molecules and Materials: Concepts, Theory, and Applications. *Chem. Rev.* **2017**, *117*, 4714–4758.

(5)   Loskill, P.; Hähl, H.; Faidt, T.; Grandthyll, S.; Müller, F.; Jacobs, K. Is Adhesion Superficial? Silicon Wafers as a Model System to Study van Der Waals Interactions. *Adv. Colloid Interface Sci.* **2012**, *179– 182*, 107–113.

(6)   Hunter, C. A.; Lawson, K. R.; Perkins, J.; Urch, C. J. Aromatic Interactions. *J. Chem. Soc. Perkin Trans. 2* **2001**, *2*, 651–669.

(7)   Jennings, W. B.; Farrell, B. M.; Malone, J. F. Attractive Intramolecular Edge-to-Face Aromatic Interactions in Flexible Organic Molecules. *Acc. Chem. Res.* **2001**, *34*, 885–894.

(8)   Arunan, E.; Desiraju, G. R.; Klein, R. A.; Sadlej, J.; Scheiner, S.; Alkorta, I.; Clary, D. C.; Crabtree, R. H.; Dannenberg, J. J.; Hobza, P.; et al. Definition of the Hydrogen Bond (IUPAC Recommendations 2011). *Pure Appl. Chem.* **2011**, *83*, 1637–1641.

(9)   Kollman, P. A.; Allen, L. C. The Theory of the Hydrogen Bond. *Chem. Rev.* **1972**, *72*, 283–303.

(10)   Murray, T. J.; Zimmerman, S. C. New Triply Hydrogen Bonded Complexes with Highly Variable Stabilities. *J. Am. Chem. Soc.* **1992**, *114*, 4010–4011.

(11)   Zumdahl, S. S.; DeCoste, D. J. *Chemical Principles*, 8th ed.; Cengage Learning: Boston, 2015.

(12)   Lommerse, J. P. M.; Stone, A. J.; Taylor, R.; Allen, F. H. The Nature and Geometry of Intermolecular Interactions between Halogens and Oxygen or Nitrogen. *J. Am. Chem. Soc.* **1996**, *118*, 3108–3116.

(13)   Metrangolo, P.; Neukirch, H.; Pilati, T.; Resnati, G. Halogen Bonding Based Recognition Processes: A World Parallel to Hydrogen Bonding. *Acc. Chem. Res.* **2005**, *38*, 386–395.

(14)   Desiraju, G. R.; Ho, P. S.; Kloo, L.; Legon, A. C.; Marquardt, R.; Metrangolo, P.; Politzer, P.; Resnati, G.; Rissanen, K. Definition of the Halogen Bond (IUPAC Recommendations 2013). *Pure Appl. Chem.* **2013**, *85*, 1711–1713.

(15)   Gilday, L. C.; Robinson, S. W.; Barendt, T. A.; Langton, M. J.; Mullaney, B. R.; Beer, P. D. Halogen Bonding in Supramolecular Chemistry. *Chem. Rev.* **2015**, *115*, 7118–7195.

(16)   Mukherjee, A.; Tothadi, S.; Desiraju, G. R. Halogen Bonds in Crystal

Engineering: Like Hydrogen Bonds yet Different. *Acc. Chem. Res.* **2014**, *47*, 2514–2524.

(17)   Wang, W.; Zhao, Y.; Zhang, Y.; Wang, Y. bo. The Nature of the I···I Interactions and a Comparative Study with the Nature of the Π···π Interactions. *Comput. Theor. Chem.* **2014**, *1030*, 1–8.

(18)   Dobrawa, R.; Würthner, F. Metallosupramolecular Approach toward Functional Coordination Polymers. *J. Polym. Sci. Part A Polym. Chem.* **2005**, *43*, 4981–4995.

(19)   Yang, L.; Tan, X.; Wang, Z.; Zhang, X. Supramolecular Polymers: Historical Development, Preparation, Characterization, and Functions. *Chem. Rev.* **2015**, *115*, 7196–7239.

(20)   Brunsveld, L.; Folmer, B. J. B.; Meijer, E. W.; Sijbesma, R. P. Supramolecular Polymers. *Chem. Rev.* **2001**, *101*, 4071–4098.

(21)   Winter, A.; Schubert, U. S. Synthesis and Characterization of Metallo-Supramolecular Polymers. *Chem. Soc. Rev.* **2016**, *45*, 5311–5357.

(22)   Bernhard, S.; Goldsmith, J. I.; Takada, K.; Abruña, H. D. Iron(II) and Copper(I) Coordination Polymers: Electrochromic Materials with and without Chiroptical Properties. *Inorg. Chem.* **2003**, *42*, 4389–4393.

(23)   Vitvarová, T.; Svoboda, J.; Hissler, M.; Vohlídal, J. Conjugated Metallo-Supramolecular Polymers Containing a Phosphole Unit. *Organometallics* **2017**, *36*, 777–786.

(24)   Kumpfer, J. R.; Rowan, S. J. Thermo-, Photo-, and Chemo-Responsive Shape-Memory Properties from Photo-Cross-Linked Metallo-Supramolecular Polymers. *J. Am. Chem. Soc.* **2011**, *133*, 12866–12874.

(25)   Hrma, M.; Šichová, K.; Svoboda, J.; Vohlídal, J. Assembling of Bis(Tpy)Fluorenes with Zn2+ and Fe2+ Ions into Metallo-Supramolecular Polymers with Highly Efficient White-Light Emission. *Polymer (Guildf).* **2017**, *122*, 22–33.

(26)   Hofmeier, H.; Schubert, U. S. Recent Developments in the Supramolecular Chemistry of Terpyridine-Metal Complexes. *Chem. Soc. Rev.* **2004**, *33*, 373–399.

(27)   Wild, A.; Winter, A.; Schlütter, F.; Schubert, U. S. Advances in the Field of π-Conjugated 2,2′:6′,2″-Terpyridines. *Chem. Soc. Rev.* **2011**, *40*, 1459–1511.

(28)   Dobrawa, R.; Lysetska, M.; Ballester, P.; Grüne, M.; Würthner, F. Fluorescent Supramolecular Polymers: Metal Directed Self-Assembly of Perylene Bisimide Building Blocks. *Macromolecules* **2005**, *38*, 1315–1325.

(29)   Yamasaki, K.; Yasuda, M. Stability of Zinc and Cadmium Complexes with 2,2′-Bipyridine and 1,10-Phenanthroline. *J. Am. Chem. Soc.* **1956**, *78*, 1324.

(30)   Zielenkiewicz, W.; Lebedeva, N. S.; Antina, E.; Vyugin, A.; Kami\'niski, M. Titration Calorimetric Investigation of Interactions of Zinc (II), Nickel (II), and Copper (II) Tetraphenylporphine Complexes with Pyridine in Three Solvents. *J. Solution Chem.* **1998**, *27*, 879–886.

(31)   Goze, C.; Ulrich, G.; Charbonnière, L.; Cesario, M.; Prangé, T.; Ziessel, R. Cation Sensors Based on Terpyridine-Functionalized

Boradiazaindacene. *Chem. - A Eur. J.* **2003**, *9*, 3748–3755.

(32)   Rowan, S. J.; Beck, J. B. Metal–ligand Induced Supramolecular Polymerization: A Route to Responsive Materials. *Faraday Discuss.* **2005**, *128*, 43–53.

(33)   Khlobystov, A. N.; Blake, A. J.; Champness, N. R.; Lemenovskii, D. A.; Majouga, A. G.; Zyk, N. V.; Schröder, M. Supramolecular Design of One-Dimensional Coordination Polymers Based on Silver(I) Complexes of Aromatic Nitrogen-Donor Ligands. *Coord. Chem. Rev.* **2001**, *222*, 155–192.

(34)   Würthner, F.; Sautter, A.; Thalacker, C. Substituted Diazadibenzoperylenes: New Functional Buildung Blocks for Supramolecular Chemistry. *Angew. Chemie Int. Ed.* **2000**, *39*, 1243–1245.

(35)   Martínez-Calvo, M.; Kotova, O.; Möbius, M. E.; Bell, A. P.; McCabe, T.; Boland, J. J.; Gunnlaugsson, T. Healable Luminescent Self-Assembly Supramolecular Metallogels Possessing Lanthanide (Eu/Tb) Dependent Rheological and Morphological Properties. *J. Am. Chem. Soc.* **2015**, *137*, 1983–1992.

(36)   Velten, U.; Rehahn, M. First Synthesis of Soluble, Well Defined Coordination Polymers from Kinetically Unstable Copper(I) Complexes. *Chem. Commun.* **1996**, *0*, 2639–2640.

(37)   Velten, U.; Lahn, B.; Rehahn, M. Soluble, Well-Defined Copper(1) and Silver(1) Coordination Polymers From. *Macromol. Chem. Phys.* **1997**, *198*, 2789–2816.

(38)   Lahn, B.; Rehahn, M. Coordination Polymers from Kinetically Labile Copper(I) and Silver(I) Complexes: True Macromolecules or Solution Aggregates? *Macromol. Symp.* **2001**, *163*, 157–176.

(39)   Hossain, M. D.; Sato, T.; Higuchi, M. A Green Copper-Based Metallo-Supramolecular Polymer: Synthesis, Structure, and Electrochromic Properties. *Chem. - An Asian J.* **2013**, *8*, 76–79.

(40)   Pandey, R. K.; Hossain, M. D.; Moriyama, S.; Higuchi, M. Ionic Conductivity of Ni(Ii)-Based Metallo-Supramolecular Polymers: Effects of Ligand Modification. *J. Mater. Chem. A* **2013**, *1*, 9016–9018.

(41)   Pandey, R. K.; Hossain, M. D.; Moriyama, S.; Higuchi, M. Real-Time Humidity-Sensing Properties of Ionically Conductive Ni(Ii)-Based Metallo-Supramolecular Polymers. *J. Mater. Chem. A* **2014**, *2*, 7754–7758.

(42)   Dong, Q.; Meng, Z.; Ho, C. L.; Guo, H.; Yang, W.; Manners, I.; Xu, L.; Wong, W. Y. A Molecular Approach to Magnetic Metallic Nanostructures from Metallopolymer Precursors. *Chem. Soc. Rev.* **2018**, *47*, 4934–4953.

(43)   Yan, Y.; Zhang, J.; Ren, L.; Tang, C. Metal-Containing and Related Polymers for Biomedical Applications. *Chem. Soc. Rev.* **2016**, *45*, 5232–5263.

(44)   Whittell, G. R.; Hager, M. D.; Schubert, U. S.; Manners, I. Functional Soft Materials from Metallopolymers and Metallosupramolecular Polymers. *Nat. Mater.* **2011**, *10*, 176–188.

(45)   Xiang, J.; Ho, C. L.; Wong, W. Y. Metallopolymers for Energy Production, Storage and Conservation. *Polym. Chem.* **2015**, *6*, 6905–6930.

(46)   Li, H.; Wu, L. Metallo/Clusto Hybridized Supramolecular Polymers. *Soft Matter* **2014**, *10*, 9038–9053.

(47)   Rao, Y.-L.; Chortos, A.; Pfattner, R.; Lissel, F.; Chiu, Y.; Feig, V.; Xu, J.; Kurosawa, T.; Gu, X.; Wang, C.; et al. Stretchable Self-Healing Polymeric Dielectrics Cross-Linked Through Metal − Ligand Coordination. *J. Am. Chem. Soc.* **2016**, *138*, 6020–6027.

(48)   Rao, Y. L.; Feig, V.; Gu, X.; Nathan Wang, G. J.; Bao, Z. The Effects of Counter Anions on the Dynamic Mechanical Response in Polymer Networks Crosslinked by Metal–ligand Coordination. *J. Polym. Sci. Part A Polym. Chem.* **2017**, *55*, 3110–3116.

(49)   Williams, Z. H.; Burwell, E. D.; Chiomento, A. E.; Demsko, K. J.; Pawlik, J. T.; Harris, S. O.; Yarolimek, M. R.; Whitney, M. B.; Hambourger, M.; Schwab, A. D. Rubber-Elasticity and Electrochemical Activity of Iron(<scp>ii</Scp>) Tris(Bipyridine) Crosslinked Poly(Dimethylsiloxane) Networks. *Soft Matter* **2017**, *13*, 6542–6554.

(50)   Grindy, S. C.; Lenz, M.; Holten-Andersen, N. Engineering Elasticity and Relaxation Time in Metal-Coordinate Cross-Linked Hydrogels. *Macromolecules* **2016**, *49*, 8306–8312.

(51)   Tang, S.; Olsen, B. D. Relaxation Processes in Supramolecular Metallogels Based on Histidine-Nickel Coordination Bonds. *Macromolecules* **2016**, *49*, 9163–9175.

(52)   Fullenkamp, D. E.; He, L.; Barrett, D. G.; Burghardt, W. R.; Messersmith, P. B. Mussel-Inspired Histidine-Based Transient Network Metal Coordination Hydrogels. *Macromolecules* **2013**, *46*, 1167–1174.

(53)   Wang, Z.; Fan, W.; Tong, R.; Lu, X.; Xia, H. Thermal-Healable and Shape Memory Metallosupramolecular Poly(n-Butyl Acrylate-Co-Methyl Methacrylate) Materials. *RSC Adv.* **2014**, *4*, 25486.

(54)   Jackson, A. C.; Beyer, F. L.; Price, S. C.; Rinderspacher, B. C.; Lambeth, R. H. Role of Metal-Ligand Bond Strength and Phase Separation on the Mechanical Properties of Metallopolymer Films. *Macromolecules* **2013**, *46*, 5416–5422.

(55)   Jackson, A. C.; Walck, S. D.; Strawhecker, K. E.; Butler, B. G.; Lambeth, R. H.; Beyer, F. L. Metallopolymers Containing Excess Metal-Ligand Complex for Improved Mechanical Properties. *Macromolecules* **2014**, *47*, 4144–4150.

(56)   Constable, E. C. Towards Helical Coordination Polymers: Molecular Wires in Chiral Coats. *Macromol. Symp.* **1995**, *98*, 503–524.

(57)   Storrier, G. D.; Colbran, S. B. Transition-Metal Complexes of 4′(4-Anilino)-2,2′ : 6′,2″-Terpyridine (and Derivatives): Versatile Building Blocks for Construction of Metallooligomers and Macromolecules. *J. Chem. Soc. Dalt. Trans.* **1996**, *0*, 2185–2186.

(58)   Storrier, G. D.; Colbran, S. B.; Craig, D. C. Bis[4′-(4-Anilino)-2,2′:6′,2″-   Terpyridine]Transition-Metal   Complexes:

Electrochemically Active Monomers with a Range of Magnetic and Optical Properties for Assembly of Metallo Oligomers and Macromolecules. *J. Chem. Soc. Dalt. Trans.* **1997**, *2*, 3011–3028.

(59) Schütte, M.; Kurth, D. G.; Linford, M. R.; Cölfen, H.; Möhwald, H. Metallosupramolecular Thin Polyelectrolyte Films. *Angew. Chemie - Int. Ed.* **1998**, *37*, 2891–2893.

(60) Schmatloch, S.; González, M. F.; Schubert, U. S. Metallo-Supramolecular Diethylene Glycol: Water-Soluble Reversible Polymers. *Macromol. Rapid Commun.* **2002**, *23*, 957–961.

(61) Schmatloch, S.; Van Den Berg, A. M. J.; Alexeev, A. S.; Hofmeier, H.; Schubert, U. S. Soluble High-Molecular-Mass Poly(Ethylene Oxide)s via Self-Organization. *Macromolecules* **2003**, *36*, 9943–9949.

(62) Mansfeld, U.; Winter, A.; Hager, M. D.; Günther, W.; Altuntaş, E.; Schubert, U. S. A Homotelechelic Bis-Terpyridine Macroligand: One-Step Synthesis and Its Metallo-Supramolecular Self-Assembly. *J. Polym. Sci. Part A Polym. Chem.* **2013**, *51*, 2006–2015.

(63) Yang, L.; Zhang, G.; Zheng, N.; Zhao, Q.; Xie, T. A Metallosupramolecular Shape-Memory Polymer with Gradient Thermal Plasticity. *Angew. Chemie - Int. Ed.* **2017**, *56*, 12599–12602.

(64) Sato, T.; Pandey, R. K.; Higuchi, M. Fluorescent Colour Modulation in Zn(Ii)-Based Metallo-Supramolecular Polymer Films by Electronic-State Control of the Ligand. *Dalt. Trans.* **2013**, *42*, 16036.

(65) Razgoniaev, A. O.; Butaeva, E. V.; Iretskii, A. V.; Ostrowski, A. D. Changing Mechanical Strength in Cr(III)- Metallosupramolecular Polymers with Ligand Groups and Light Irradiation. *Inorg. Chem.* **2016**, *55*, 5430–5437.

(66) He, Y. J.; Tu, T. H.; Su, M. K.; Yang, C. W.; Kong, K. V.; Chan, Y. T. Facile Construction of Metallo-Supramolecular Poly(3-Hexylthiophene)-Block-Poly(Ethylene Oxide) Diblock Copolymers via Complementary Coordination and Their Self-Assembled Nanostructures. *J. Am. Chem. Soc.* **2017**, *139*, 4218–4224.

(67) Mansfeld, U.; Hager, M. D.; Hoogenboom, R.; Ott, C.; Winter, A.; Schubert, U. S. Advanced Supramolecular Initiator for Nitroxide-Mediated Polymerizations Containing Both Metal-Ion Coordination and Hydrogen-Bonding Sites. *Chem. Commun. (Camb).* **2009**, *0*, 3386–3388.

(68) Mansfeld, U.; Winter, A.; Hager, M. D.; Festag, G.; Hoeppener, S.; Schubert, U. S. Amphiphilic Supramolecular A(B)2A Quasi-Triblock Copolymers. *Polym. Chem.* **2013**, *4*, 3177.

(69) Burnworth, M.; Tang, L.; Kumpfer, J. R.; Duncan, A. J.; Beyer, F. L.; Fiore, G. L.; Rowan, S. J.; Weder, C. Optically Healable Supramolecular Polymers. *Nature* **2011**, *472*, 334–337.

(70) Balkenende, D. W. R.; Coulibaly, S.; Balog, S.; Simon, Y. C.; Fiore, G. L.; Weder, C. Mechanochemistry with Metallosupramolecular Polymers. *J. Am. Chem. Soc.* **2014**, *136*, 10493–10498.

(71) Chen, P.; Li, Q.; Grindy, S.; Holten-Andersen, N. White-Light-Emitting Lanthanide Metallogels with Tunable Luminescence and Reversible Stimuli-Responsive Properties. *J. Am. Chem. Soc.* **2015**,

137, 11590–11593.

(72)   De Bettencourt-Dias, A.; Rossini, J. S. K. Ligand Design for Luminescent Lanthanide-Containing Metallopolymers. *Inorg. Chem.* **2016**, *55*, 9954–9963.

(73)   Enke, M.; Bode, S.; Vitz, J.; Schacher, F. H.; Harrington, M. J.; Hager, M. D.; Schubert, U. S. Self-Healing Response in Supramolecular Polymers Based on Reversible Zinc-Histidine Interactions. *Polymer (Guildf).* **2015**, *69*, 274–282.

(74)   Sandmann, B.; Happ, B.; Kupfer, S.; Schacher, F. H.; Hager, M. D.; Schubert, U. S. The Self-Healing Potential of Triazole-Pyridine-Based Metallopolymers. *Macromol. Rapid Commun.* **2015**, *36*, 604–609.

(75)   Zhou, H.; Liang, F.; Li, J.; Ding, X.; Ma, A.; Chen, W.; Luo, C.; Zhang, G.; Tian, W.; Cheng, M.; et al. RAFT Polymerization and Dually Responsive Behaviors of Terpyridine-Containing PNIPAAm Copolymers in Dilute Solutions. *React. Funct. Polym.* **2016**, *106*, 62–68.

(76)   Bode, S.; Enke, M.; Bose, R. K.; Schacher, F. H.; Garcia, S. J.; van der Zwaag, S.; Hager, M. D.; Schubert, U. S. Correlation between Scratch Healing and Rheological Behavior for Terpyridine Complex Based Metallopolymers. *J. Mater. Chem.* **2015**, *3*, 22145–22153.

(77)   Juang, R. S.; Yang, P. C.; Wen, H. W.; Lin, C. Y.; Lee, S. C.; Chang, T. W. Synthesis and Chemosensory Properties of Terpyridine-Containing Diblock Polycarbazole through RAFT Polymerization. *React. Funct. Polym.* **2015**, *93*, 130–137.

(78)   Lohmeijer, B. G. G.; Schubert, U. S. The LEGO Toolbox: Supramolecular Building Blocks by Nitroxide-Mediated Controlled Radical Polymerization. *J. Polym. Sci. Part A Polym. Chem.* **2005**, *43*, 6331–6344.

(79)   Mansfeld, U.; Winter, A.; Hager, M. D.; Hoogenboom, R.; Günther, W.; Schubert, U. S. Orthogonal Self-Assembly of Stimuli-Responsive Supramolecular Polymers Using One-Step Prepared Heterotelechelic Building Blocks. *Polym. Chem.* **2013**, *4*, 113–123.

(80)   Mugemana, C.; Joset, A.; Guillet, P.; Appavou, M.-S.; De Souza, N.; Fustin, C.-A.; Leyh, B.; Gohy, J.-F. Structure of Metallo-Supramolecular Micellar Gels. *Macromol. Chem. Phys.* **2013**, *214*, 1699–1709.

(81)   Grubbs, R. B. Nitroxide-Mediated Radical Polymerization: Limitations and Versatility. *Polym. Rev.* **2011**, *51*, 104–137.

(82)   Zhou, G.; Harruna, I. I. Synthesis and Characterization of Bis(2,2′:6′,2″-Terpyridine)Ruthenium(II)-Connected Diblock Polymers via RAFT Polymerization. *Macromolecules* **2005**, *38*, 4114–4123.

(83)   Zhang, L.; Zhang, Y.; Chen, Y. Synthesis of Bis(2,2′:6′,2″-Terpyridine)-Terminated Telechelic Polymers by RAFT Polymerization and Ruthenium-Polymer Complexation Thereof. *Eur. Polym. J.* **2006**, *42*, 2398–2406.

(84)   Munuera, L.; O'Reilly, R. K. Using Metal–ligand Interactions for the Synthesis of Metallostar Polymers. *Dalt. Trans.* **2010**, *39*, 388–391.

(85) Piogé, S.; Fustin, C. A.; Gohy, J. F. Temperature-Responsive Aqueous Micelles from Terpyridine End-Capped Poly(N-Isopropylacrylamide)-Block-Polystyrene Diblock Copolymers. *Macromol. Rapid Commun.* **2012**, *33*, 534–539.

(86) Le Bohec, M.; Banère, M.; Piogé, S.; Pascual, S.; Benyahia, L.; Fontaine, L. Sol–gel Reversible Metallo-Supramolecular Hydrogels Based on a Thermoresponsive Double Hydrophilic Block Copolymer. *Polym. Chem.* **2016**, *7*, 6834–6842.

(87) Cox, W. P.; Merz, E. H. Correlation of Dynamic and Steady Flow Viscosities of Food Materials. *J. Polym. Sci.* **1958**, *28*, 619–622.

(88) Hyun, K.; Kim, S. H.; Ahn, K. H.; Lee, S. J. Large Amplitude Oscillatory Shear as a Way to Classify the Complex Fluids. *J. Nonnewton. Fluid Mech.* **2002**, *107*, 51–65.

(89) Harrison, G.; Franks, G. Suspensions and Polymers–common Links in Rheology. *Aust. Rheol.* **1999**, *11*, 197–218.

(90) Storm, C.; Pastore, J. J.; MacKintosh, F. C.; Lubensky, T. C.; Janmey, P. A. Nonlinear Elasticity in Biological Gels. *Nature* **2005**, *435*, 191–194.

(91) Sim, H. G.; Ahn, K. H.; Lee, S. J. Three-Dimensional Dynamics Simulation of Electrorheological Fluids under Large Amplitude Oscillatory Shear Flow. *J. Rheol. (N. Y. N. Y).* **2003**, *47*, 879–895.

(92) Sundberg, R. J.; Martin, R. B. Interactions of Histidine and Other Imidazole Derivatives with Transition Metal Ions in Chemical and Biological Systems. *Chem. Rev.* **1974**, *74*, 471–517.

(93) Wegner, S. V.; Schenk, F. C.; Witzel, S.; Bialas, F.; Spatz, J. P. Cobalt Cross-Linked Redox-Responsive PEG Hydrogels: From Viscoelastic Liquids to Elastic Solids. *Macromolecules* **2016**, *49*, 4229–4235.

(94) Bond, J.; Hobson, D. B. The Stability Constants of Cobalt(III) Chelates of Polyaminopolycarboxylic Acids. *J. Chem. Soc. A* **1965**, *0*, 2155–2157.

(95) Ogino, H.; Ogino, K. Redox Potentials and Related Parameters of Cobalt(III/II) Complexes Containing Aminopolycarboxylates. *Inorg. Chem.* **1983**, *22*, 2208–2211.

(96) Rossow, T.; Habicht, A.; Seiffert, S. Relaxation and Dynamics in Transient Polymer Model Networks. *Macromolecules* **2014**, *47*, 6473–6482.

(97) Tang, S.; Habicht, A.; Li, S.; Olsen, B. D. Self-Diffusion of Associating Star-Shaped Polymers. *Macromolecules* **2016**, *49*, 5599–5608.

(98) Kawamoto, K.; Grindy, S. C.; Liu, J.; Holten-Andersen, N.; Johnson, J. A. Dual Role for 1,2,4,5-Tetrazines in Polymer Networks: Combining Diels-Alder Reactions and Metal Coordination to Generate Functional Supramolecular Gels. *ACS Macro Lett.* **2015**, *4*, 458–461.

(99) Yu, X.; Wang, Z.; Li, Y.; Geng, L.; Ren, J.; Feng, G. Fluorescent and Electrochemical Supramolecular Coordination Polymer Hydrogels Formed from Ion-Tuned Self-Assembly of Small Bis-Terpyridine Monomer. *Inorg. Chem.* **2017**, *56*, 7512–7518.

(100) Kim, C.; Kim, K. Y.; Lee, J. H.; Ahn, J.; Sakurai, K.; Lee, S. S.; Jung,

93

J. H. Chiral Supramolecular Gels with Lanthanide Ions: Correlation between Luminescence and Helical Pitch. *ACS Appl. Mater. Interfaces* **2017**, *9*, 3799–3807.

(101) Li, Y.; Guo, J.; Dai, B.; Geng, L.; Shen, F.; Zhang, Y.; Yu, X. Facile Construction of Terpridine-Based Metallo-Polymers in Hydrogels, Crystals and Solutions Directed by Metal Ions. *J. Colloid Interface Sci.* **2018**, *521*, 190–196.

(102) Tang, Z.; Huang, J.; Guo, B.; Zhang, L.; Liu, F. Bioinspired Engineering of Sacrificial Metal-Ligand Bonds into Elastomers with Supramechanical Performance and Adaptive Recovery. *Macromolecules* **2016**, *49*, 1781–1789.

(103) Yao, Z.; Wang, Z.; Yu, Y.; Zeng, C.; Cao, K. Facile Synthesis and Properties of the Chemo-Reversible and Highly Tunable Metallogels Based on Polydicyclopentadiene. *Polym. (United Kingdom)* **2017**, *119*, 98–106.

(104) Mozhdehi, D.; Neal, J. A.; Grindy, S. C.; Cordeau, Y.; Ayala, S.; Holten-Andersen, N.; Guan, Z. Tuning Dynamic Mechanical Response in Metallopolymer Networks through Simultaneous Control of Structural and Temporal Properties of the Networks. *Macromolecules* **2016**, *49*, 6310–6321.

(105) Yount, W. C.; Loveless, D. M.; Craig, S. L. Small-Molecule Dynamics and Mechanisms Underlying the Macroscopic Mechanical Properties of Coordinatively Cross-Linked Polymer Networks. *J. Am. Chem. Soc.* **2005**, *127*, 14488–14496.

(106) Loveless, D. M.; Jeon, S. L.; Craig, S. L. Rational Control of Viscoelastic Properties in Multicomponent Associative Polymer Networks. *Macromolecules* **2005**, *38*, 10171–10177.

(107) Yount, W. C.; Loveless, D. M.; Craig, S. L. Strong Means Slow: Dynamic Contributions to the Bulk Mechanical Properties of Supramolecular Networks. *Angew. Chemie - Int. Ed.* **2005**, *44*, 2746–2748.

(108) Doi, M.; Edwards, S. F. *The Theory of Polymer Dynamics*; Oxford University Press: New York, 1986.

(109) De Gennes, P. G. Reptation of a Polymer Chain in the Presence of Fixed Obstacles. *J. Chem. Phys.* **1971**, *55*, 572–579.

(110) Qin, J.; Milner, S. T. Tubes, Topology, and Polymer Entanglement. *Macromolecules* **2014**, *47*, 6077–6085.

(111) Rouse, P. E. A Theory of the Linear Viscoelastic Properties of Dilute Solutions of Coiling Polymers. *J. Chem. Phys.* **1953**, *21*, 1272–1280.

(112) Doi, M. Explanation for the 3.4-Power Law for Viscosity of Polymeric Liquids on the Basis of the Tube Model. *J. Polym. Sci. Polym. Phys. Ed.* **1981**, *19*, 265–273.

(113) Dealy, J. M.; Larson, R. G. *Structure and Rheology of Molten Polymers*; Hanser, 2006.

(114) Pearson, D. S.; Helfand, E. Viscoelastic Properties of Star-Shaped Polymers. *Macromolecules* **1984**, *17*, 888–895.

(115) van Ruymbeke, E.; Keunings, R.; Bailly, C. Prediction of Linear Viscoelastic Properties for Polydisperse Mixtures of Entangled Star

and Linear Polymers: Modified Tube-Based Model and Comparison with Experimental Results. *J. Nonnewton. Fluid Mech.* **2005**, *128*, 7–22.

(116) Milner, S. T.; McLeish, T. C. B. Parameter-Free Theory for Stress Relaxation in Star Polymer Melts. *Macromolecules* **1997**, *30*, 2159–2166.

(117) Tuminello, W. H. Molecular Weight and Molecular Weight Distribution From Dynamic Measurements of Polymer Melts. *Polym. Eng. Sci.* **1986**, *26*, 1339–1347.

(118) Tsenoglou, C. Viscoelasticity of Binary Polymer Blends. *ACS Polym. Prepr.* **1987**, *28*, 185–186.

(119) des Cloizeaux, J. Double Reptation vs Simple Reptation in Polymer Melts. *Europhys. Lett.* **1988**, *5*, 437–442.

(120) Marrucci, G. Relaxation by Reptation and Tube Enlargement : A Model for Polydisperse Polymers. *J. Polym. Sci. Polym. Phys. Ed.* **1985**, *23*, 159–177.

(121) Viovy, J. L.; Rubinstein, M.; Colby, R. H. Constraint Release in Polymer Melts: Tube Reorganization versus Tube Dilation. *Macromolecules* **1991**, *24*, 3587–3596.

(122) Rubinstein, M.; Semenov, A. N. Dynamics of Entangled Solutions of Associating Polymers. *Macromolecules* **2001**, *34*, 1058–1068.

(123) Leibler, L.; Rubinstein, M.; Colby, R. H. Dynamics of Reversible Networks. *Macromolecules* **1991**, *24*, 4701–4707.

(124) Chen, Q.; Tudryn, G. J.; Colby, R. H. Ionomer Dynamics and the Sticky Rouse Model. *J. Rheol. (N. Y. N. Y).* **2013**, *57*, 1441–1462.

(125) Chen, Q.; Liang, S.; Shiau, H.; Colby, R. H. Linear Viscoelastic and Dielectric Properties of Phosphonium Siloxane Ionomers. *ACS Macro Lett.* **2013**, *2*, 970–974.

(126) Marrucci, G.; Bhargava, S.; Cooper, S. L. Models of Shear-Thickening Behavior in Physically Crosslinked Networks. *Macromolecules* **1993**, *26*, 6483–6488.

(127) Semenov, A. N.; Rubinstein, M. Dynamics of Entangled Associating Polymers with Large Aggregates. *Macromolecules* **2002**, *35*, 4821–4837.

(128) Hawke, L. G. D.; Ahmadi, M.; Gondansaz, H.; van Ruymbeke, E. Viscoelastic Properties of Linear Associating Poly(n-Butyl Acrylate) Chains. *J. Rheol. (N. Y. N. Y).* **2016**, *60*, 297–310.

(129) Read, D. J.; Jagannathan, K.; Sukumaran, S. K.; Auhl, D. W. A Full-Chain Constitutive Model for Bidisperse Blends of Linear Polymers. *J. Rheol. (N. Y. N. Y).* **2012**, *56*, 823–873.

(130) Shivokhin, M. E.; Van Ruymbeke, E.; Bailly, C.; Kouloumasis, D.; Hadjichristidis, N.; Likhtman, A. E. Understanding Constraint Release in Star/Linear Polymer Blends. *Macromolecules* **2014**, *47*, 2451–2463.

(131) Van Ruymbeke, E.; Shchetnikava, V.; Matsumiya, Y.; Watanabe, H. Dynamic Dilution Effect in Binary Blends of Linear Polymers with Well-Separated Molecular Weights. *Macromolecules* **2014**, *47*, 7653–7665.

(132) Zhang, Z.; Chen, Q.; Colby, R. H. Dynamics of Associative Polymers.

Soft Matter **2018**, *14*, 2961–2977.

(133) Metri, V.; Louhichi, A.; Yan, J.; Baeza, G. P.; Matyjaszewski, K.; Vlassopoulos, D.; Briels, W. J. Physical Networks from Multifunctional Telechelic Star Polymers: A Rheological Study by Experiments and Simulations. *Macromolecules* **2018**, *51*, 2872–2886.

(134) Ahmadi, M.; Hawke, L. G. D.; Goldansaz, H.; Van Ruymbeke, E. Dynamics of Entangled Linear Supramolecular Chains with Sticky Side Groups: Influence of Hindered Fluctuations. *Macromolecules* **2015**, *48*, 7300–7310.

(135) Stukalin, E. B.; Cai, L. H.; Kumar, N. A.; Leibler, L.; Rubinstein, M. Self-Healing of Unentangled Polymer Networks with Reversible Bonds. *Macromolecules* **2013**, *46*, 7525–7541.

(136) Ramirez, J.; Dursch, T. J.; Olsen, B. D. A Molecular Explanation for Anomalous Diffusion in Supramolecular Polymer Networks. *Macromolecules* **2018**, *51*, 2517–2525.

Chapter 2

Synthesis of metallo-supramolecular polymers

Abstract

During the last decade numerous developments have been conducted in the research and application of supramolecular polymers. Using different synthetic routes, a variety of supramolecular polymers has been developed. While the majority of these associating systems are unentangled, only few works have been reported on the synthesis of well-defined entangled supramolecular system. Herein, this Chapter presents the synthesis and characterization of different entangled associating polymeric precursors based on poly(n-butyl acrylate) building blocks and terpyridine ligands. The first set of systems is based on linear (semi-)telechelic polymeric systems, the second set comprises four-arm star terpyridine end-functionalized polymers and finally a series of linear sticky copolymers is elaborated to which a random distribution of terpyridine ligands along the polymer backbone is added. All these well-defined precursors are synthesized using a pre-modification approach combined with the reversible addition fragmentation chain transfer polymerization.

2.1 Introduction

2.1.1 Design of associating polymers

In order to fulfill the previously defined objectives, the design of metallo-supramolecular polymers is the first essential task to address. Indeed, it is important to properly tailor the molecular structure of the MSPs in which a total control over the position of the stickers, the topology, the architecture, the molar mass and the dispersity of the macromolecules has to be achieved. Since their mechanical features will be systematically investigated, it is necessary to know these structural parameters to properly establish a correlation between them and the rheological properties. As mentioned in section 1.1.2, there are several types of metal-ligand coordination and different methods to incorporate these interactions within a polymeric matrix.

In the framework of this thesis, the metal-ligand interactions are based on the tridentate terpyridine ligand and different transition metal ions such as zinc(II), copper(II), cobalt(II) or nickel(II) ions. Initiated by Schubert et al, the terpyridine molecule is subjected to extensive works.[1–3] Followed by Gohy's group who prepared a wide range of block copolymers to form different micelles in solution.[4–11] Terpyridine functionalized polymers were connected via bis(terpyridine)-ruthenium(II) complexes, that are as strong as covalent bonds, but also with other transition metal ions to form weaker transient bonds. In most of these studies, tpy moieties were incorporated in polystyrene or poly(ethylene oxide) building blocks.

2.1.1.1 2,2':6',2"-terpyridine ligand

Morgan and Burstall discovered the terpyridine ligand by heating pyridine with anhydrous iron(III) chloride at 340°C in an autoclave.[12] Among the twenty products of this reaction, the 2,2':6',2"-terpyridine molecule (depicted in Figure 2.1) was produced at relatively low yield. Subsequently, it was discovered that the addition of iron(II) ions to a solution of terpyridine compounds results into a purple color. The latter gave the first indication for the formation of a $[Fe(tpy_2)]^{2+}$ complex. The tpy molecule acts as a "claw" chelating

ligand which displays high binding affinity and rich coordination chemistry with various metal ions in different oxidation states.[13–16] The ligand brings a certain degree of versatility and it gives control and stability on the resulting supramolecular structure.[17] Moreover, it is thermally stable up to 180°C at least.[18] Above this temperature, it starts to degrade. Hence, it is interesting to use it for reversible interactions within entangled polymeric materials.
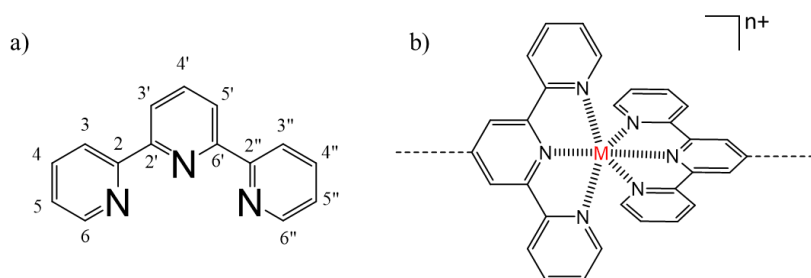
Figure 2.1 a) Chemical structure of the 2,2':6',2"-terpyridine ligand with ring atom numbering. b) Overall arrangement of terpyridine metal complex. The lone pair of electrons donors on nitrogen allows to form strong interactions with the metal ion.

Once the nature of the metal-ligand coordination is fixed, the next step is to select the appropriate macromolecules in which M-L interactions will be incorporated.

2.1.1.2 Poly(*n*-butyl acrylate) polymer model

The poly(*n*-butyl acrylate) (P*n*BA) which belongs to the acrylic polymer family has been selected as macromolecule model system. P*n*BA as represented in Figure 2.2, is a tacky, rubbery polymer which has a relatively low glass transition temperature (T_g = -55°C).[19] Its low T_g allows us to investigate mechanical properties of molten/bulk MSPs at low temperature, room temperature or moderate high temperature.
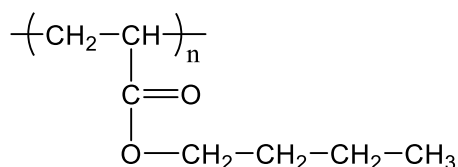
Figure 2.2 Chemical structure of P*n*BA homopolymer.

Hence, a wide range of mechanical responses can be covered where both M-L and macromolecule dynamics play an effective role. If PS or PEO were used as macromolecules, the study would have to be conducted at elevated temperature to reach molten state, for instance, at temperature higher than 100°C to be above polystyrene T_g or higher than 65°C to be above the melting temperature of PEO. However, at such elevated temperatures, the M-L dynamic contribution can be severely weakened in such a way that these stickers will not be efficient anymore and could be neglected.

This is why P*n*BA is an excellent candidate to overcome this limitation. Moreover, the latter displays great resistance towards temperature (stable up to 300°C) and also towards humidity and its environment, e.g. it is unaffected by oxygen, or ultra-violet light. Unlike polymethacrylates, P*n*BA does not depolymerize on heating to high temperatures. It only degrades and decomposes slowly under extreme conditions where the temperature is above 300°C.[20] The latter can be synthesized via controlled radical polymerizations where different architectures and low molar mass dispersity can be achieved. Among them, the RAFT process is preferentially used to obtain structurally well-defined associating model systems because several works showed that polymerization of *n*-butyl acrylate via this technique is well-controlled. In order to incorporate the terpyridine ligand within poly(*n*-butyl acrylate) macromolecules, a pre-modification strategy is followed because it is more versatile and it offers a better control over the position and the number of incorporated functional moieties.

2.1.2 RAFT polymerization

Reported by the pioneering work of Rizzardo, Moad and Thang in 1998, RAFT has emerged as one of the most powerful polymerization techniques in the field of reversible deactivation radical polymerization (RDRP).[21] The robust and versatile nature of RAFT allows the synthesis of complex polymeric architectures such as copolymers, star, branched or hyper-branched polymers. Similar to other controlled radical polymerizations, RAFT relies on the equilibrium between active and dormant chains which is achieved by a

degenerative transfer.[22] Its mechanism is illustrated in Figure 2.3. Since the overall number of radicals during the activation-deactivation process remains the same in degenerative transfer system, an external radical initiator is required to generate radicals and to proceed to the initiation step.

Initiation:

a) Radical source ⟶ I•

b) I• + M ⟶ P$_n$•

Pre-equilibrium:

c) P$_n$• + **1** ⇌ **2** ⇌ **3** + R• **4**

Re-initiation:

d) R• + M ⟶ P$_m$•

Main equilibrium:

e) P$_m$• + **3** ⇌ **5** ⇌ **6** + P$_n$•

Termination:

f) I• R• P$_n$• P$_m$• ⟶ Termination

Figure 2.3 Reversible addition-fragmentation chain transfer (RAFT) polymerization mechanism where a) and b) correspond to the initiation step, c) is the pre-equilibrium phase, d) the re-initiation, e) the main equilibrium and f) the termination step.

After the initiation step where the external initiator fragments into radicals, the latter start to polymerize monomers to form P$_n$• radicals. Then the propagating P$_n$• radical species add to the RAFT agent (chain transfer agent, CTA) to form the radical intermediate 2. The latter fragments to form a thiocarbonylthio-containing CTA 3 and a new radical R•. The radical R• may react with 3 or polymerizes the monomers to form a new propagating radical P$_m$•. Once all CTA is consumed, the main equilibrium of activation-deactivation is established between active propagating chains P$_n$•/P$_m$• and dormant

species 3/6. The overall process consists in the monomer insertion between the R- and the Z−C(=S)S- groups of a CTA, which forms the R-derivative and Z-derivative end-groups of the resulting polymeric chains. While the chains formed via RAFT polymerization always bear the Z−C(=S)S- group, the resulting products are with and without the R-derivative moiety. It corresponds respectively to the fractions of living and dead polymer chains. By living chains, it means that they can be subjected to further extension via subsequent monomer addition and still bear the R-derivative group.

A key parameter in RAFT polymerization, is the use of radical initiators which directly impacts the polymerization rate and the fraction of living chains. Indeed, the number of chains that does not contain the R-derivative group corresponds to the number of initially added initiators that have fragmented during the polymerization reaction. Consequently, the fraction of dead chains can be controlled by adjusting the number of radical initiators introduced to the reaction with respect to the RAFT agent. More precisely, because the amount of CTA is usually much higher than the amount of radical initiators, the fraction of dormant thiocarbonylthio-containing chains is higher than the fraction of chains initiated by the radical initiators. Hence, most chains are living after the polymerization. Additionally, one must note the possible presence of byproducts of the polymerization which are the chains initiated by the radical initiators ($P_n^{\bullet}$) and those initiated by the CTA R-group ($P_m^{\bullet}$). However, by properly setting polymerization conditions, the formation of targeted polymer chains can be achieved with low yield of byproducts and dead chains. If the reaction reaches full conversion, termination reactions can occur by disproportionation or recombination to form dead chains.

RAFT polymerization is an attractive technique because of its ability to polymerize a wide range of monomers such as styrenics, dienes, vinyl esters, (meth)acrylates or (meth)acrylamides.[23–28] This versatility in monomers with RAFT arises from the reactivity of the CTA which can be finely tuned according to the monomer of interest. To ensure an effective RAFT polymerization, the C=S bond of the CTA has to be more reactive than the C=C bond of the monomer. This can

be achieved by meticulously selecting the Z- and R-groups of the RAFT agent. The Z-group ensures the reactivity of the C=S bond toward radical addition and dictates the stability of the formed intermediate radical during the polymerization. The R-group has to be a good leaving group to form a relatively stable radical. It has to be reactive enough so that it can rapidly re-initiate propagation to ensure that all chains are initiated at the same time to obtain low molar mass dispersity. Depending on the monomer, general guidelines for the selection of Z- and R-groups are reported in the literature.[29,30]

From an experimental point of view, RAFT polymerization also has the advantages to be carried out under different conditions such as a wide range of polymerization solvents, including water, under biologically friendly conditions and at various temperatures ranging from -15°C up to 180°C.[31–36] Hence, the RAFT process will be used in this thesis to synthesize the entangled polymers. The rest of this chapter is organized as follows. In section 2.2 the experimental procedures to synthesize and characterize the associating polymeric models are summarized. Section 2.3 presents the additional UV/visible characterization to qualitatively and quantitatively confirm the success of incorporating terpyridine moieties within polymers. The elaboration of metallo-supramolecular bulk polymers is described in section 2.4. The conclusions are drawn in section 2.5 and the experimental parts are detailed in section 2.6.

2.2 Incorporation of terpyridine ligands into entangled polymers

2.2.1 Synthesis of modified chain transfer agents

2.2.1.1 RAFT chain transfer agents

The first stage is to synthesize different chain transfer agents in which the Z- and R-groups are meticulously selected with respect to the *n*-butyl acrylate monomer. Well-controlled polymerization reactions can thus be conducted to elaborate well-defined and low dispersity

polymers. While the R- group is fixed as a methylpropionic acid $((CH_3)_2$-C-COOH) to ensure end functionality, the Z-moiety varies between one CTA to another depending on the architecture and on the functionality number of the targeted associating polymers. Hence, by carefully defining the R- and Z-groups of the RAFT agent as illustrated in Figure 2.4, one can gain control over the structural and functionality parameters of the polymeric precursors.
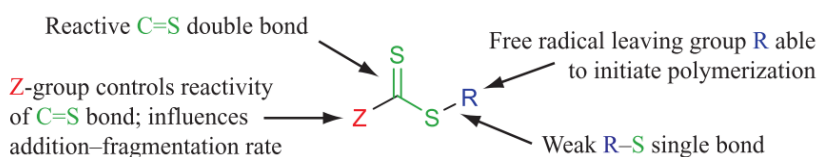

Figure 2.4 Chemical structure of the general RAFT agent.[37]

To control the polymerization of *n*-butyl acrylate with different topologies, trithiocarbonates (TTC) based chain transfer agents are used to synthesize polymers with various architectures. TTCs are the most popular among the CTAs for polymerization of acrylate monomers since they can balance between high propagation activity and stability towards side reactions such as hydrolysis. Furthermore they can be easily obtained from simple synthetic routes. For instance, a very versatile TTC-CTA is the commercially available 2-(Dodecylthiocarbonothioylthio)-2-methylpropionic acid (DDMAT). The latter bears a carboxylic acid function that can be coupled with terpyridine derivatives. In the scope of using the same strategy to obtain other RAFT agents bearing the same carboxylic acid function but with different topologies, 2-(2-Carboxyethylsulfanylthiocarbonylsulfanyl)-2-methylpropionic acid (CBMAT) and pentaerythritoltetrakis-(2-(2-Carboxyethylsulfanylthio-carbonylsulfanyl)-2-methylpropionic acid) (PTMAT) have been synthesized in this thesis in order to obtain bifunctional and tetra-functional polymers respectively.

The synthesis of DDMAT, as illustrated in Figure 2.5, is conducted following a procedure described by Lai et al.[38] First, equimolar amounts of alkyl mercaptan and carbon disulfide are

reacted in presence of hydroxide ions, followed by an alkylation with chloroform and acetone in a phase transfer catalyzed (PTC) reaction. After acidification, the product is isolated in low yield from the side products, and purified by recrystallization in a non-polar solvent. The purity and the functionality of the synthesized CTA is checked by ^{1}H nuclear magnetic resonance (NMR) analysis. Using the same synthetic route, CBMAT is synthesized according to another procedure elaborated by Wang et al. as illustrated in Figure 2.6.[39]
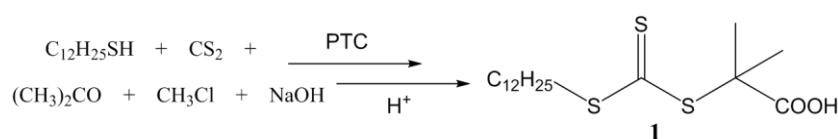

Figure 2.5 Synthesis of mono-functional DDMAT chain transfer agent.
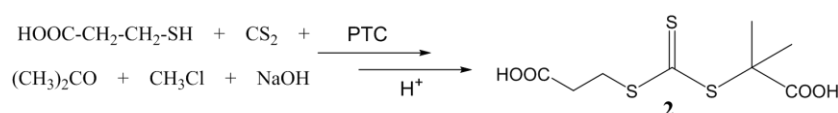

Figure 2.6 Synthesis of bi-functional CBMAT chain transfer agent.

The elaboration of the tetra-functional TTC is inspired by the procedure described by Mayadunne and Whittaker *et al*. with some modifications.[40,41] The method used (for the synthesis of RAFT agents having trithiocarbonate groups) is quite simple and requires inexpensive commercially available reagents. Figure 2.7 illustrates the one-pot procedure to obtain tetra-functional TTC with a relatively good yield. Although one-pot, the key point of this procedure is the dropwise sequential addition of carbon disulfide and 2-bromo-2-methylpropionic acid to ensure that all four arms bear trithiocarbonate moieties and carboxylic acid groups as shown in Figure 2.7.
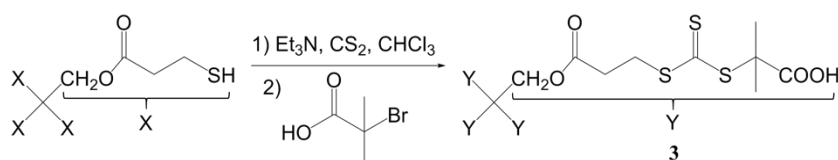

Figure 2.7 Synthesis of tetra-functional PTMAT chain transfer agent.

2.2.1.2 Amino-terpyridine derivative

An amine functionalized terpyridine derivative is synthesized according to a procedure described by Piogé et al.[42] The amine group is then used for coupling reaction with the carboxylic acid moieties of the different TTC-CTAs. 5-amino pentanol is reacted with chloro-terpyridine under basic conditions in dimethyl sulfoxide to yield the desired product as shown in Figure 2.8. Its structure is evidenced by ^{1}H NMR analysis. The efficiency of the reaction is confirmed by a marked downfield shift of the NMR signal of protons initially adjacent to the hydroxyl group, after addition of 5-amino pentanol onto chloro-terpyridine.
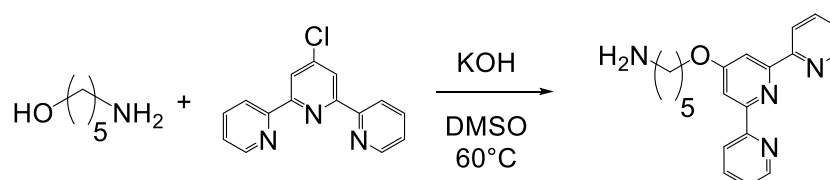

Figure 2.8 Synthesis of the amino-terpyridine (NH$_2$-Tpy) derivative.

2.2.1.3 Terpyridine modified CTAs

Once all the RAFT agents are obtained along with the amino-tepyridine derivative, the final step of the pre-modification approach can be performed. It consists in performing the same coupling reaction between the CTAs bearing the carboxylic acid functions at the termini and the amine moiety from the NH$_2$-Tpy to yield ligand-functionalized chain transfer agents. The formation of amide, from the corresponding carboxylic acid by condensation with the primary amine, is mediated by the presence of carbodiimide, following a standard methodology of peptide coupling synthesis as summarized in Figure 2.9. The coupling is achieved after activation of carboxyl group with 1-hydroxybenzotriazole/N-(3-dimethyl-aminopropyl)-N'-ethylcarbodiimide hydrochloride salt (HOBT/EDCI), in a mixture of dimethylformamide (DMF) and dichloromethane (DCM) as solvent. This reaction is catalytic in HOBT but stoichiometric in EDCI, which is converted to the corresponding derived urea.
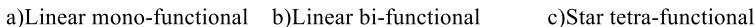
1' R = $C_{12}H_{25}$----   **2'** R =   **3'** R =

a)Linear mono-functional   b)Linear bi-functional   c)Star tetra-functional

Figure 2.9 Peptide coupling toward terpyridine functionalized CTAs.

The characterization of terpyridine-functionalized CTAs is carried out using mass spectrometry and NMR spectroscopy. As illustrated in Figure 2.10, the presence of a peak at a chemical shift around 6.60 ppm in ^{1}H-NMR, which corresponds to the amide proton, along with the downfield shift of the peak of adjacent aliphatic protons, from 2.75 ppm to 3.25 ppm after coupling reaction, prove the reaction efficiency. Similar observations are noted for all modified CTAs.
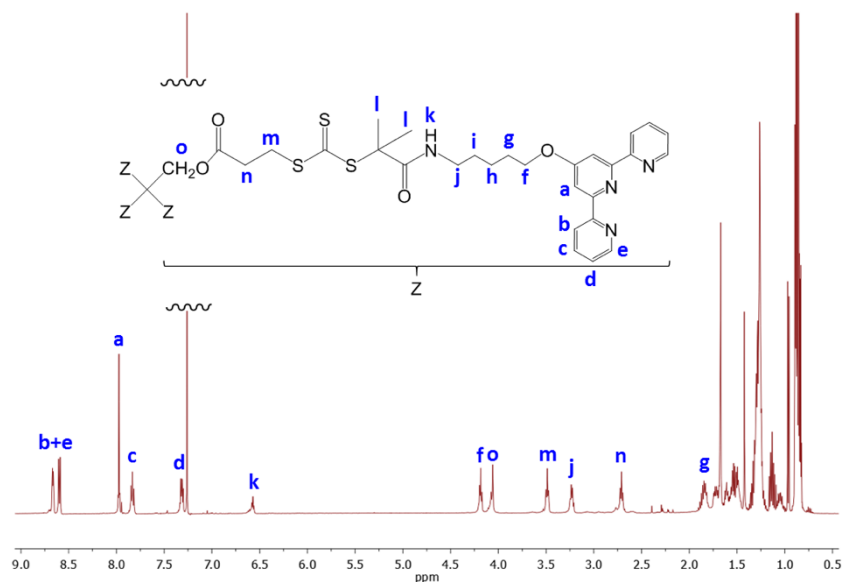

Figure 2.10 ^{1}H-NMR spectrum (500 MHz, CDCl₃-*d*, ppm) of tetra-functional PTMAT-tpy₄ chain transfer agent.

2.2.2 Synthesis of terpyridine modified monomer

2.2.2.1 Hydroxyl-terpyridine derivative

While the modified chain transfer agents are synthesized to incorporate M-L interactions at the extremities, another synthetic route is elaborated to have stickers along the polymer backbone. To ensure a decent reactivity among monomers, the idea is to design an acrylic monomer containing terpyridine moiety that can be polymerized via RAFT process afterwards. To do so, a hydroxyl functionalized terpyridine derivative is elaborated according to a procedure described by Jochum et al.[43] Similarly to the amine derivative protocol, the 1,3-propanediol is reacted with chloro-terpyridine under basic conditions in DMSO, to yield the desired product as shown in Figure 2.11. Its structure is identified by ^{1}H-NMR analysis. The efficiency of the reaction is confirmed by a marked downfield shift of the NMR signal of protons initially adjacent to the hydroxyl group, after addition of 1,3-propanediol onto chloro-terpyridine.

Figure 2.11 Synthesis of the hydroxyl-terpyridine (HO-Tpy) derivative.

2.2.2.2 Terpyridine modified acrylate

The hydroxyl group is then used for nucleophilic substitution reaction with the commercially available acryloyl chloride under basic conditions in DCM to obtain the desired terpyridine acrylate (TPA) monomer as shown in Figure 2.12. Its structure is identified by ^{1}H NMR analysis. The efficiency of the reaction is confirmed by a marked downfield shift of the NMR signal of protons initially adjacent to the hydroxyl group, after addition of HO-Tpy onto acryloyl chloride.
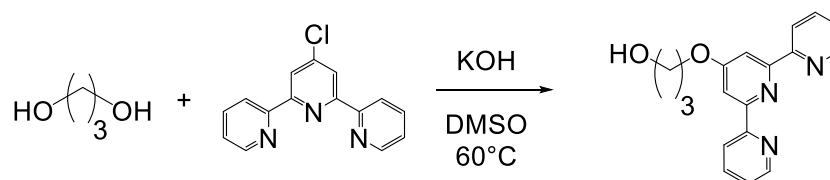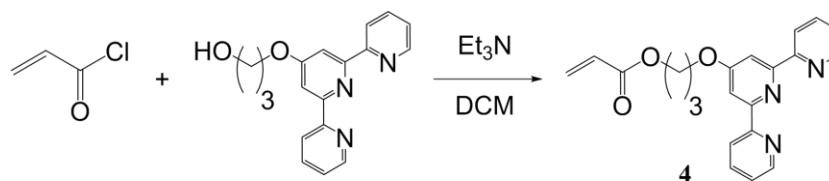
Figure 2.12 Synthesis of the terpyridine modified acrylate (TPA).

To summarize, three RAFT chain transfer agents and monomer are synthesized. All of them contain terpyridine ligand which can form metal-ligand complexes in presence of metal ions. These terpyridine modified CTAs and monomer will be tested to polymerize or to copolymerize *n*BA via RAFT process.

2.2.3 Synthesis of telechelic P*n*BA polymers

The next step is to synthesize associating polymers with the terpyridine modified CTAs and monomer by RAFT technique. As mentioned before, *n*-butyl acrylate is the monomer used in this project and the polymerization reaction conditions are defined by taking into account major parameters such as reasonable reaction duration but also well-controlled reaction towards molar mass and dispersity to elaborate well-defined associating model systems. To develop reaction conditions for each reaction, the influence of three stoichiometric ratios between monomer (M), CTA and initiator (I) is considered and finely tailored to achieve a better control over the RAFT polymerization.[30]

Since the amount of CTA determines the number of formed chains, the relative [M]/[CTA] ratio theoretically determines the number average degree of polymerization (DP_n) obtained in the absence of termination or chain transfer reactions. As mentioned in section 2.1.2, the [CTA]/[I] ratio influences the functionality at polymer chain ends. It also determines the fraction of dormant thiocarbonylthio-containing chains and of dead chains. Finally the [M]/[I] ratio impacts the rate of polymerization. Hence, the ratio between monomer/CTA/initiator is adjusted to control the polymerization of the monomer in a reasonable duration and the functionality of chain ends. By considering these parameters, a series of linear and star poly(*n*-butyl

acrylate)s end-functionalized with terpyridine ligand are elaborated accordingly.

2.2.3.1 Linear mono-functionalized PnBA-tpy

Inspired by the works of Piogé et al. and Wang et. al., the terpyridine-modified DDMAT is selected as RAFT agent for the polymerization of nBA and the reaction is conducted under bulk conditions as illustrated in Figure 2.13.[42,44] Indeed, nBA monomer can also act as a good solvent for all reagents including the growing polymer.
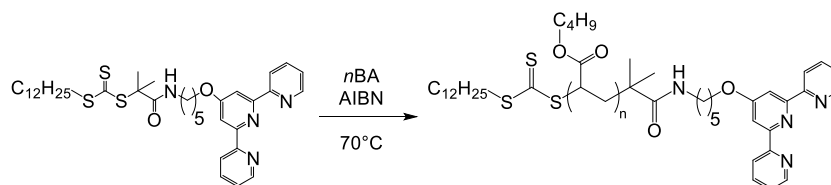

Figure 2.13 Synthesis of the linear mono-functional terpyridine end-functionalized PnBA-tpy homopolymer.

As mentioned in section 2.1.2, radical species must be added into the reaction mixture to initiate the polymerization. In this respect, commercially available 2,2'-azobis(isobutyronitrile) (AIBN) is used as source of radicals. By thermally decomposing, it generates two equivalents of propagating radicals to activate the initiation step of the polymerization. During the initiation step, a fast balance pre-equilibrium is established between initiating radical species via degenerative transfer. As a result, the homo-polymerization of poly(n-butyl acrylate) is partially initiated by propagating radicals generated by the homolytic cleavage of AIBN, and partially initiated by the R-group originated from transfer reaction to the DDMAT-tpy. To ensure high degree of chain-end functionalization, a minimum amount of AIBN initiator is used with respect to chain transfer agent ($[CTA]_0$:$[AIBN]_0$ ratio of 10:1). This amount is however sufficient to initiate the polymerization process and to ensure acceptable polymerization kinetics at 70°C.

Depending on the targeted DP_n, the initial $[nBA]_0:[CTA]_0=[I]_0$ ratio varies accordingly which allows the preparation of different homopolymers with different molar masses. Even though RAFT technique ensures a relative good control over the polymerization reaction at high monomer conversion rate ($p > 90\%$), a precaution is taken to set the highest p at 80% to ensure the maximum chain-end functionalization and to prevent side reactions such as chain termination.[21,45] In practice, this conversion rate is determined by ^{1}H-NMR analysis of the crude reaction mixture, from the ratio between the peak area of vinyl protons of unreacted nBA monomers to that of the characteristic alkyl protons of growing PnBA. According to Figure 2.14, the conversion rate is defined as follows:

$$p = \frac{Polymer\ integral}{Polymer\ integral + Monomer\ integral} = \frac{I_{c\prime}}{I_c + I_{c\prime}} \qquad (2.1)$$
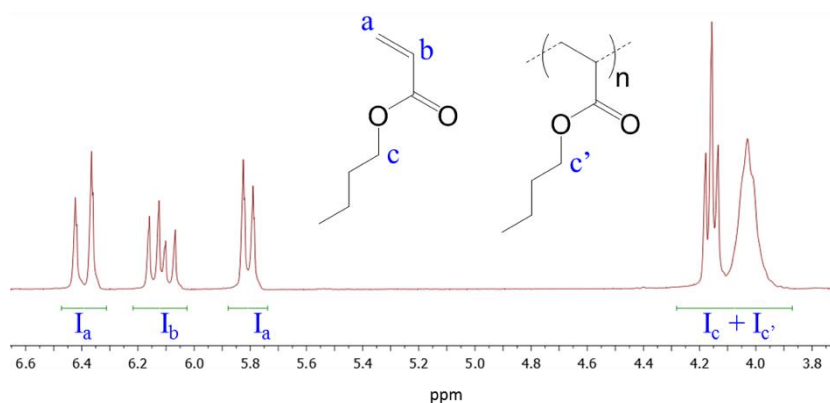
Figure 2.14 ^{1}H-NMR spectrum (300 MHz, CDCl3-*d*, ppm) of a linear mono-functional PnBA-tpy polymerization crude mixture.

Note that the DP of the synthesized polymer can be evaluated from the monomer conversion and the ratio of engaged monomers to the total number of chains produced. Since the number of initiator-derived chains is low in comparison to CTA-derived chains, the contribution of propagating radicals generated by the decomposition of AIBN is generally neglected with respect to propagating radicals originated from CTA. Hence, the expression for the theoretical degree of polymerization can be defined as follows:

$$DP_n = p.\frac{[n\text{BA}]_0}{[\text{CTA}]_0 + [\text{AIBN}]_0} \approx p.\frac{[n\text{BA}]_0}{[\text{CTA}]_0}$$

(2.2)

From equation 2.2, the theoretical molar mass ($M_{n,th}$) of the linear PnBA-tpy homopolymers can be expressed as:

$$M_{n,th} = DP_n.M_{n\text{BA}} + M_{\text{CTA}}$$ (2.3)

Where $M_{n\text{BA}}$ and M_{CTA} are respectively the molar masses of the n-butyl acrylate monomer and of the RAFT chain transfer agent.

Next step is to purify the crude product by double precipitation of the crude reaction mixture in a solvent that is selective for the unreacted monomer, and subsequent drying of the polymer. Once the linear mono-functional PnBA-tpy is purified, its molar mass can be determined by chain end titration via ^{1}H-NMR analysis. The latter can provide a quantitative checking of the terpyridine content into the polymeric system as illustrated in Figure 2.15. Additionally, the molar mass dispersity, i.e. Đ, of synthesized PnBA-tpy is determined by size exclusion chromatography (SEC) analysis using standard polystyrene samples. From SEC analysis illustrated in Figure 2.16, a mono-modal peak with a narrow dispersity (Đ < 1.3) and a symmetrical distribution is obtained which testify a decent control over the polymerization reaction. Note that the hydrodynamic volume of poly(n-butyl acrylate) is different from the polystyrene one, consequently the molar mass determined by SEC cannot be considered as an exact value but rather an indicative one.

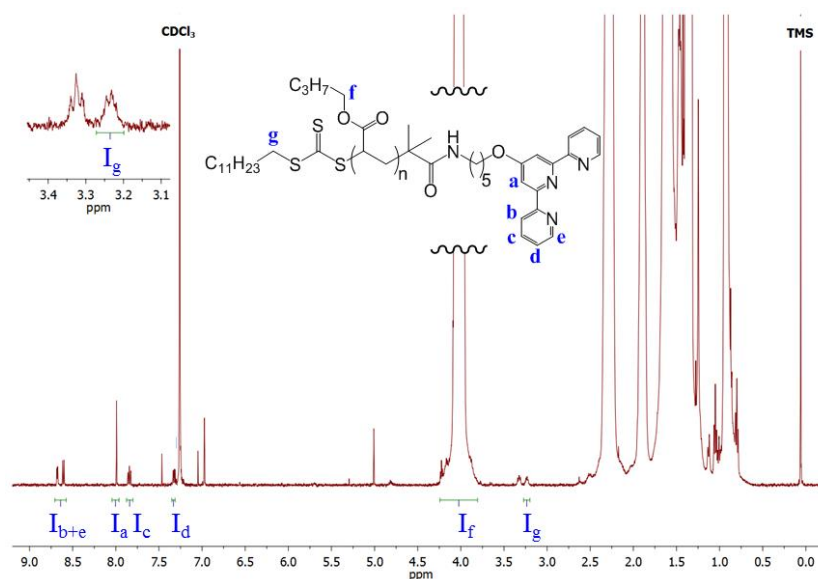**Figure 2.15** ^{1}H-NMR spectrum (500 MHz, CHCl₃-*d*, ppm) of the linear mono-functional P*n*BA-tpy.
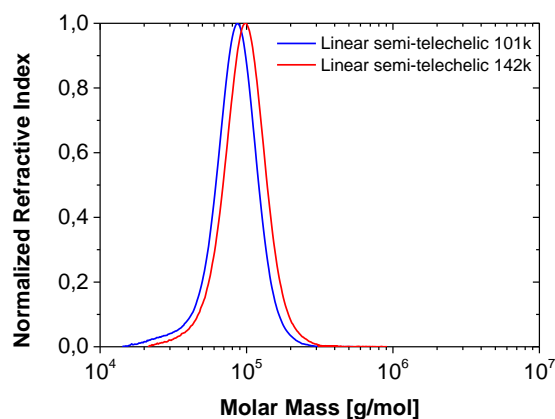

Figure 2.16 Molar mass distribution of linear mono-functional P*n*BA-tpy of 101 kg/mol (blue peak) and of 142 kg/mol (red peak).

By varying the initial [*n*BA]₀:[CTA]₀ ratio, linear mono-functional P*n*BA-tpy with different chain lengths are synthesized and are reported in Table 2.1.

Sample	DP_n (NMR) PnBA	M_n (NMR) (g/mol)	Đ (SEC)	T_g (DSC) (°C)
Mono-PnBA$_{101k}$-tpy	788 ± 15	101 000	1.14	-52
Mono-PnBA$_{142k}$-tpy	1108 ± 20	142 000	1.14	-53

Table 2.1 Characteristics of linear mono-functional PnBA-tpy homopolymers synthesized via RAFT using DDMAT-tpy.

2.2.3.2 Linear bi-functionalized PnBA-tpy$_2$

Under identical reaction conditions, a set of linear telechelic PnBA-tpy$_2$ is synthesized using the CBMAT-tpy$_2$ chain transfer agent as illustrated in Figure 2.17. The same thermal initiator as source of primary radicals with the same $[TTC]_0:[AIBN]_0$ ratio of 10:1 is engaged so that almost the entirety of the polymer is functionalized with terpyridine ligand at the end.
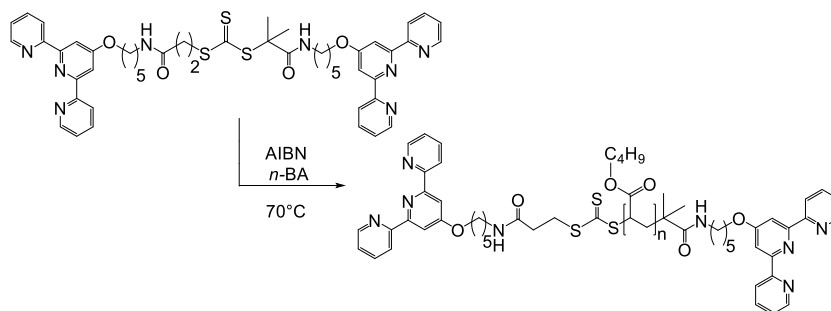
Figure 2.17 Synthesis of the linear telechelic terpyridine end-functionalized PnBA-tpy$_2$ homopolymer.

The composition of the obtained linear telechelic PnBA-tpy$_2$ is determined by ^{1}H-NMR analysis, which further attests the presence of tpy ligand as illustrated in Figure 2.18. The ratios between peak areas of terpyridine protons and aliphatic protons adjacent to the trithiocarbonate group are in good agreement with a nearly quantitative

incorporation of the ligand. In parallel, SEC analysis on linear telechelic PnBA-tpy2 reveals narrow and symmetrical molar mass distributions. In addition, low dispersities (Đ < 1.3) are obtained for all synthesized associating polymers attesting the decent control over the polymerization process. As shown in Figure 2.19, the increase in molar masses with polymerization is evidenced by the shift of the SEC traces to low elution times, i.e. to high molar masses. Note that the molar masses determined by SEC cannot be considered as an exact value but rather an indicative one due to hydrodynamic volume differences between polystyrene and poly(n-butyl acrylate).
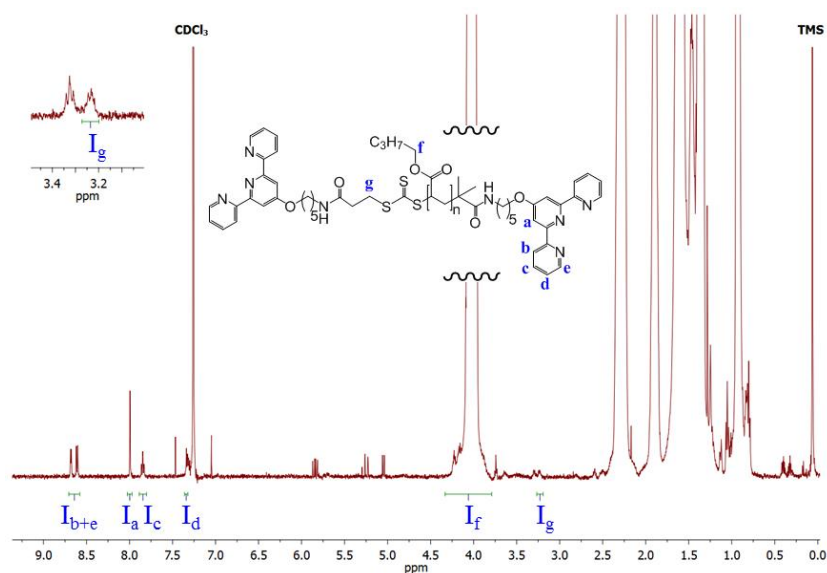
Figure 2.18 ^{1}H-NMR spectrum (500 MHz, CDCl$_3$-*d*, ppm) of the linear bi-functional PnBA-tpy$_2$.
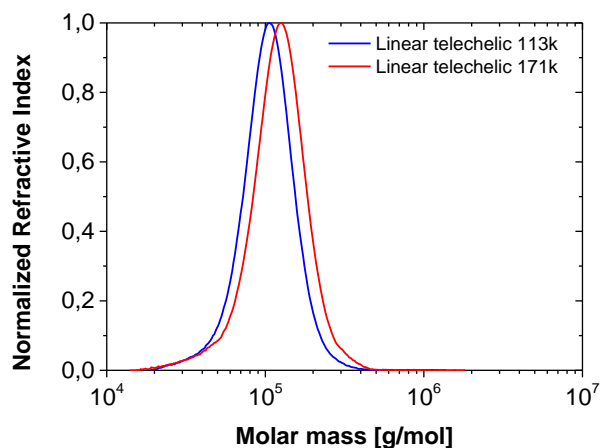
Figure 2.19 Molar mass distribution of linear bi-functional PnBA-tpy$_2$ of 113 kg/mol (blue peak) and of 171 kg/mol (red peak).

Two linear telechelic PnBA-tpy$_2$ with varying molar masses have been synthesized and are reported in Table 2.2.

Sample	DP$_n$ (NMR PnBA)	M$_n$ (NMR) (g/mol)	Đ (SEC)	T$_g$ (DSC) (°C)
Bi-PnBA$_{113k}$-tpy$_2$	875 ± 15	113 000	1.13	-50
Bi-PnBA$_{171k}$-tpy$_2$	1327 ± 20	171 000	1.18	-51

Table 2.2 Characteristics of linear bi-functional PnBA-tpy$_2$ homopolymers synthesized via RAFT using CBMAT-tpy$_2$.

2.2.3.3 Star tetra-functionalized PnBA-tpy$_4$

The use of a tetra-functional transfer agent remains a domain not fully explored. Herein, the divergent approach consists in exploiting a tetra-functional initiator as the core in which polymer chains grow from the initiating sites to produce four-arm star tetra-functional polymers as shown in Figure 2.20.
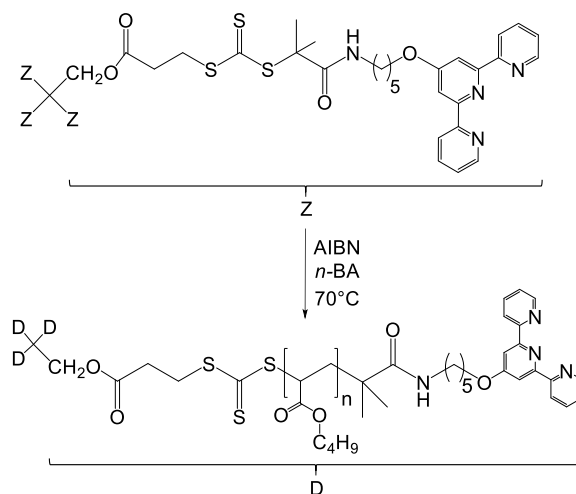
Figure 2.20 Synthesis of the four-arm star telechelic terpyridine end-functionalized P*n*BA-tpy4 homopolymer.

During the initiation process, the fragmentation of tetra-functional TTC leads to the formation of a tertiary radical detached from the core. The generated radicals add monomers to initiate polymerization resulting in a linear propagation of chains away from the star core. Thanks to the degenerative transfer (RAFT) process between the propagating radical on the growing chains and the arms of the star polymer, the growth of star polymer arms is well controlled. Hence, this allows the synthesis of well-defined star polymers with low molar mass dispersity and without any unwanted star-star coupling.[46] The absolute molar masses are determined by ^{1}H-NMR analysis of the purified telechelic 4-arm star P*n*BA-tpy4 homopolymers via end-group titration. Precisely, the calculated number average degrees of polymerization of chains are in good agreement from the ratio between the peak areas of the aliphatic ester proton of P*n*BA at 4.00 ppm, of the terpyridine protons at 8.70, 8.60 or 8.00 ppm and that of the aliphatic protons adjacent to the trithiocarbonate group at 3.25 ppm as shown in Figure 2.21.
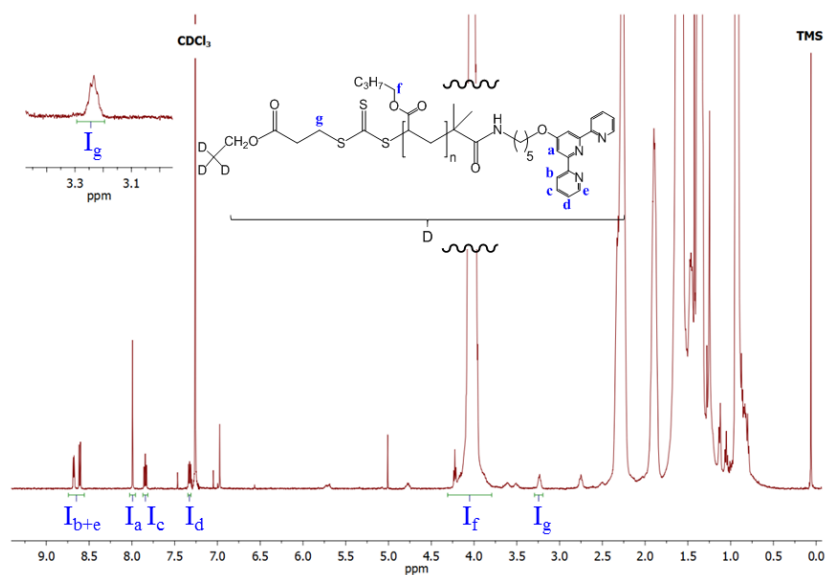
Figure 2.21 ^{1}H-NMR spectrum (500 MHz, CDCl$_3$-d, ppm) of the telechelic four-arm star PnBA-tpy$_4$.

Size exclusion chromatography analysis is performed on telechelic four-arm star PnBA-tpy$_4$ and results reveal narrow mono-modal peak with low dispersities (Đ < 1.3) as illustrated in Figure 2.22.
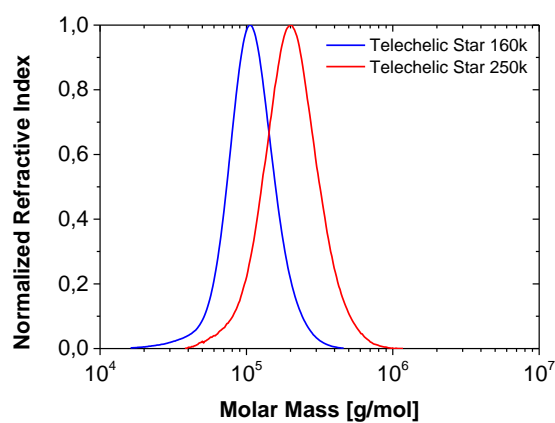
Figure 2.22 Molar mass distribution of two telechelic four-arm star PnBA-tpy$_4$ of 160 kg/mol (blue peak) and of 250 kg/mol (red peak).

Two telechelic four-arm star PnBA-tpy$_4$ have been synthesized with different chain lengths and are reported in Table 2.3.

Sample	M_n (NMR) (g/mol)	M_a (NMR) (g/mol)	Đ (SEC)	T_g (DSC) (°C)
4-arm star PnBA$_{160k}$-tpy$_4$	160 000	40 000	1.25	-51
4-arm star PnBA$_{250k}$-tpy$_4$	250 000	62 500	1.20	-52

Table 2.3 Characteristics of telechelic four-arm star PnBA-tpy$_4$ homopolymers synthesized via RAFT using PTMAT-tpy$_4$. M_n is the molar mass of the whole star macromolecule and M_a is the molar mass of a single star arm.

One way to verify that all arms of the star polymer have grown to similar lengths is to cleave the arms and characterize the resulting linear polymer via SEC analysis. As the trithiocarbonate link can be cleaved with strong nucleophiles, the two star samples are treated separately with piperidine as illustrated in Figure 2.23.
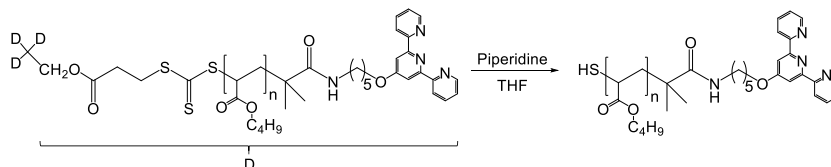
Figure 2.23 Cleavage of arms for four-arm star telechelic terpyridine end-functionalized PnBA-tpy$_4$ homopolymers.

As shown in Figure 2.24, SEC results still reveal a symmetrical mono-modal peak with low dispersity (Đ < 1.3). The narrow Đ before and after cleavage in each experiment clearly establishes that all arms of the telechelic four-arm star PnBA-tpy$_4$ have grown to similar molar masses, attesting that well-defined associating star polymers have been successfully obtained.
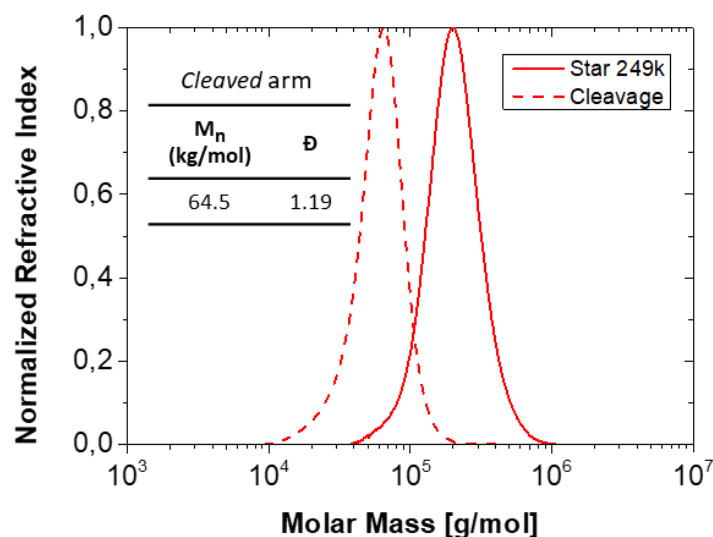
Figure 2.24 Molar mass distribution of telechelic four-arm star P*n*BA-tpy4 with a molar mass of 249 kg/mol before and after treatment with piperidine inducing cleavage.

Besides model systems based on semi-telechelic and telechelic P*n*BA polymer end-functionalized with terpyridine ligand, another set of associating model system is designed. The latter consists on P*n*BA polymer with terpyridine ligand randomly incorporated along the polymeric chain to form the so called linear sticky chain.

2.2.4 Synthesis of P*n*BA-*co*-PTPA random copolymers

Initially, the DDMAT has been selected as RAFT agent for the copolymerization of *n*BA and TPA monomers and the reaction has been conducted under bulk conditions. However, it was observed that the solubility of the TPA monomer decreases with increasing its amount within the polymer chain. Inspired by the work of Jackson et al., the polymerization reaction has been then conducted in solution to overcome this solubility issue.[47] Indeed, by using chlorobenzene as solvent, a good solubilization of all reagents including the monomers and the growing polymer has been noted (Figure 2.25). The concentration of each species in chlorobenzene has been optimized to

control the polymerization of the different monomers in a reasonable time.
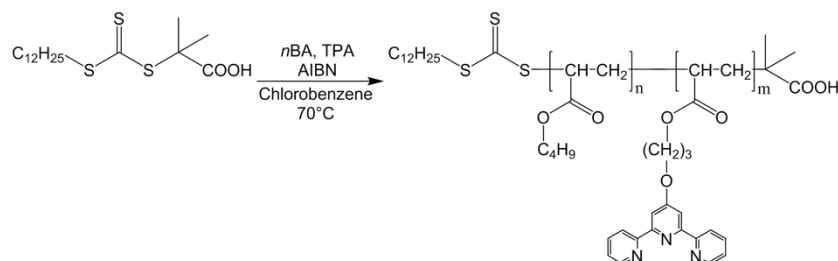
Figure 2.25 Synthesis of the linear random P*n*BA-*co*-PTPA copolymer.

The absolute molar masses are determined by ^{1}H-NMR analysis of the purified linear sticky P*n*BA-*co*-PTPA copolymers via end-group titration. Precisely, the calculated number average degrees of polymerization of chains are in good agreement with the ratio between the peak areas of the aliphatic ester proton of P*n*BA at 4.00 ppm, of the terpyridine protons at 8.70, 8.60 or 8.00 ppm and that of the aliphatic protons adjacent to the trithiocarbonate group at 3.32 ppm as shown in Figure 2.26.
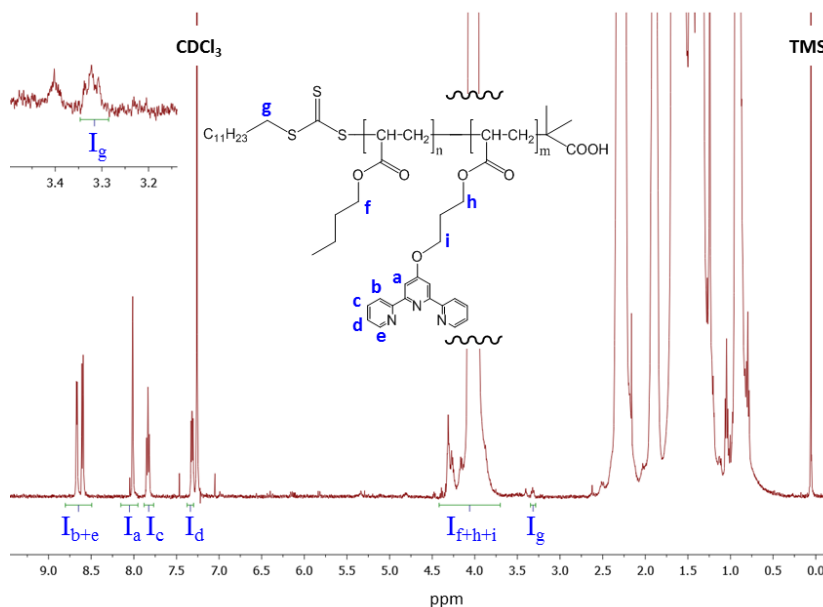
Figure 2.26 ^{1}H-NMR spectrum (500 MHz, CDCl$_3$-*d*, ppm) of the linear sticky P*n*BA-*co*-PTPA copolymer.

The SEC analysis on the linear P*n*BA-*co*-PTPA copolymers reveals narrow symmetrical mono-modal peaks with low dispersities (Đ < 1.3) attesting the decent control over the polymerization process as illustrated in Figure 2.27.
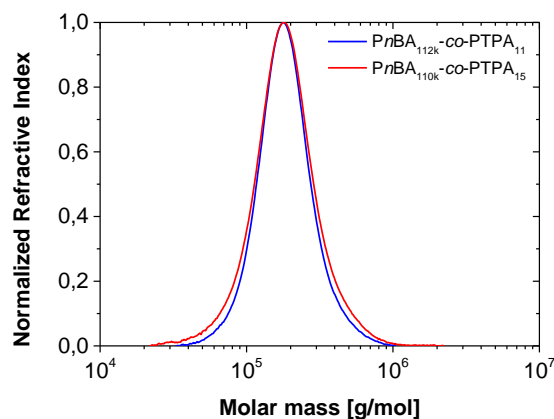
Figure 2.27 Molar mass distribution of linear sticky P*n*BA-*co*-PTPA copolymers of 112 kg/mol with 11 tpy units (blue peak) and of 110 kg/mol with 15 tpy units (red peak).

Table 2.4 summarizes the different linear sticky P*n*BA-*co*-PTPA copolymers which have been synthesized with different chain lengths and different amounts of incorporated terpyridine ligand.

Sample	DP_n (NMR) P*n*BA	DP_n (NMR) PTPA	M_n (NMR) (g/mol)	Đ (SEC)	T_g (DSC) (°C)
P*n*BA$_{840}$-*co*-PTA$_{11}$	840 ± 15	11 ± 3	112 000	1.22	-51
P*n*BA$_{814}$-*co*-PTA$_{15}$	814 ± 15	15 ± 3	110 000	1.29	-50

Table 2.4 Characteristics of linear sticky P*n*BA-*co*-PTPA copolymers synthesized via RAFT using DDMAT.

Once all associating polymers have been synthesized, additional composition analyses have been conducted besides NMR and SEC characterizations. For instance, given the relative precision of ^{1}H-NMR in the determination of the amount of incorporated terpyridine moiety, the quantitative determination of tpy group has been further addressed by ultra-violet (UV) visible titration in the following section.

2.3   UV/Vis spectroscopy titration of terpyridine content

As mentioned above, the RAFT technique requires a radical source to initiate the chain growth process. Depending on the amount of added initiator, this may decrease the end functionality of (semi-) telechelic associating polymers because part of the chains are directly initiated by the primary radicals originated from the initiator. So there is a fraction of polymer chains without terpyridine ligand at their extremity. Hence, experimental quantification of the chain-end functionality is essential. Note that this possible issue does not concern linear sticky copolymers because the tpy moieties are randomly incorporated along the polymer chains. However, it is still interesting to quantify the number of terpyridine groups incorporated within the copolymers.

Even though ^{1}H-NMR analysis displays relatively decent precision in the quantitative determination of terpyridine groups, the degree of functionalization of synthesized (semi-)telechelic polymers and sticky copolymers has been further evaluated by UV-visible titration with metal cations. This additional analysis allows us to cross-check that the terpyridine ligands are indeed present and located at the extremities of polymer chains or along the polymer backbone. Given the fact that the terpyridine moiety can form stable coordination complexes with various transition metal ions, it seems interesting to study the bis(terpyridine)-iron(II) complex because it gives rise to a strong absorption in the visible region.[48–50]

In practice, the different associating polymers are dissolved in tetrahydrofuran (THF) at a given concentration ranging between 0.005mg/µL and 0.01mg/µL, and titrated by stepwise addition of iron(II) chloride dissolved in THF and stabilized against oxidation by the presence of 0.03mg/µL ascorbic acid. Indeed, the latter prevents the oxidation of iron(II) into iron(III) ions by lowering the oxidation potential of the medium. Results from UV-Vis spectroscopy experiments are illustrated in Figure 2.28 where the formation of bis(terpyridine)-Fe(II) complexes is evidenced by the strong metal-to-ligand charge-transfer band located at the wavelength (λ) of 555nm. Due to the presence of bis(terpyridine)-Fe(II) complexes, a characteristic pinkish to purple color of the polymeric solution is observed. The electronic transitions associated to these absorption bands are originated from the charge transfer of a primarily metal-localized electron from the 3d orbital into the lowest unoccupied molecular orbital of the terpyridine.[51,52]
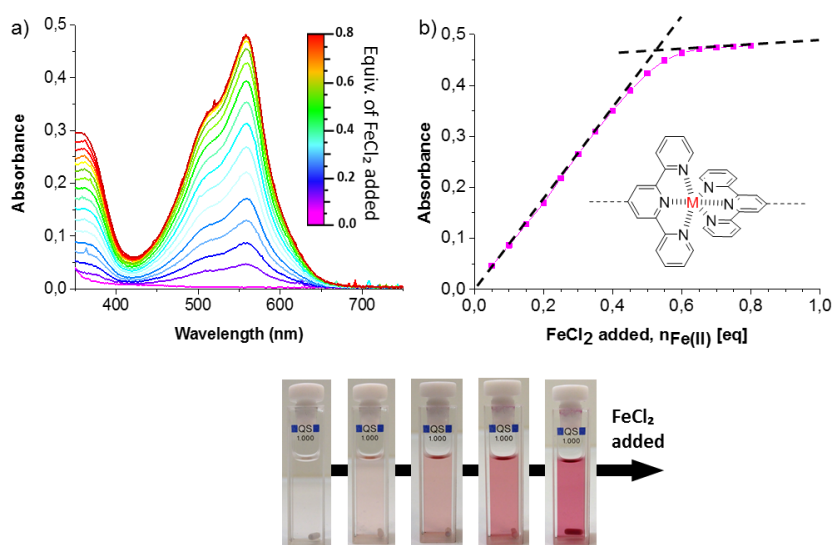
Figure 2.28 UV-Vis titration of terpyridine end-groups in a telechelic four-arm star PnBA-tpy$_4$ polymer by Fe(II). a) Evolution of absorbance at λ = 555nm during the stepwise addition of Fe(II)Cl$_2$. b) Evolution of absorbance as a function of added Fe(II)Cl$_2$ equivalents.

124

Using the molar masses calculated from ^{1}H-NMR analysis for all synthesized associating polymers, the maximum absorbance (ε_{max}) is reached close to the theoretical stoichiometric condition where full complexation of all terpyridine units is achieved. The calculated equivalence points for all systems indicate around 97±3% of functionality for (semi-)telechelic polymers, suggesting that almost the entirety of the chains is end-functionalized with the terpyridine group. Similarly for linear sticky copolymers, UV-Vis experiments allow to quantify the number of stickers incorporated within the polymer backbone. The obtained degrees of functionalization are consistent with the results obtained from ^{1}H-NMR analyses, certifying the success of incorporating terpyridine within polymeric chains with high efficiency at different locations and with different functionalities via RAFT polymerization combined with a pre-modification approach. The next step is to prepare the entangled metallo-supramolecular bulk polymers under similar conditions with few adjustments.

2.4   Elaboration of metallo-supramolecular bulk polymers (MSBPs)

2.4.1 Formation of terpyridine bis-complexes

As mentioned before, terpyridine is well-known to form stable coordination complexes with various transition metal ions. Precisely, the first row of *d*-block metals is used to form complexes for which theories of bonding are most successful. Crystal field theory can be used to explain M-L complexes where a first row metal cation is surrounded by six ligands placed on the Cartesian axes as illustrated in Figure 2.29.
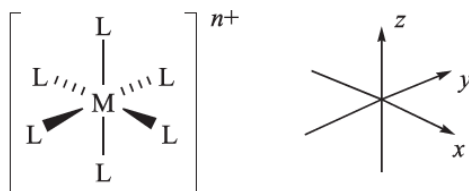
Figure 2.29 The six M-L vectors of an octahedral complex $[ML_6]^{n+}$.

Considering the terpyridine ligands are arranged in an octahedral geometry around the metal, the electrons in the d_z^2 and $d_{x^2-y^2}$ orbitals directly point at the ligands and therefore experience higher repulsion energy. Whereas the d_{xy}, d_{yz} and d_{xz} orbitals point between the ligands and thus experience less repulsion. Consequently, this leads to a splitting of the d orbitals in an octahedral crystal field. Depending on the metal cation and the ligand field, this splitting can be large or small resulting in higher or lower stabilization effects. Each orbital can host two electrons at maximum and a certain amount of energy is required to pair these electrons in the orbitals. In the case of lower crystal field splitting, promoting the electrons to the higher orbital needs less energy than pairing them. Thus the complex is considered high spin. On the opposite, for higher crystal field, pairing the electrons is favored and therefore the complex is low spin as illustrated in Figure 2.30.
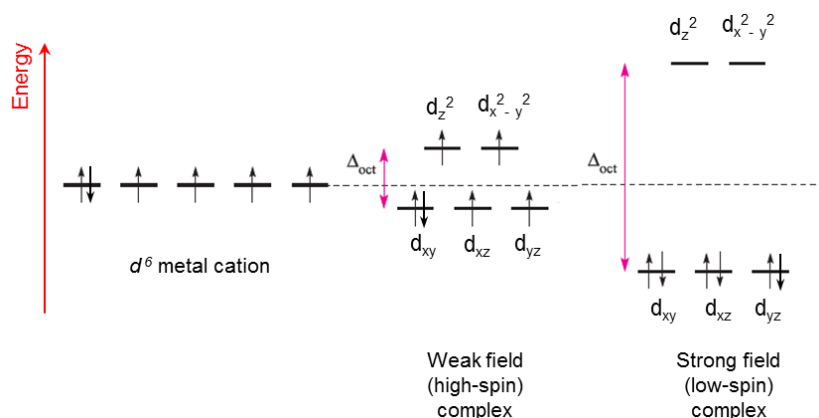
Figure 2.30 The occupation of the 3d orbitals in a weak and strong field such as Fe(II) d^6 complexes.[53]

In general, the preferences for low-spin or high spin in 3d octahedral complexes are defined as follows:

$$\Delta_{oct} < P \text{ for high-spin} \qquad (2.4)$$

$$\Delta_{oct} > P \text{ for low-spin} \qquad (2.5)$$

Where Δ_{oct} is the energy separation between $d_z{}^2$, $d_x{}^2$-$d_y{}^2$ orbitals and d_{xy}, d_{yz}, d_{xz} orbitals. *P* corresponds to the electron-pairing energy. The use of terpyridine ligand mainly leads a strong crystal field splitting, meaning that most of the complexes are in a low spin configuration.

Combining the crystal field theory with the molecular orbital theory to *d*-block octahedral metal complexes, the construction of a molecular orbital energy diagram can be established as illustrated in Figure 2.31. The combinations of the metal and ligand orbitals create six bonding and six anti-bonding molecular orbitals where the metal $2d_{xy}$, d_{yz} and d_{xz} orbitals are non-bonding. In an octahedral complex based on σ-bonds, the 12 electrons originated from the terpyridine ligand occupy the a_{1g}, t_{1u} and e_g orbitals while the valence electrons of the metal ion occupy the t_{2g} and $e_g{}^*$ orbitals.
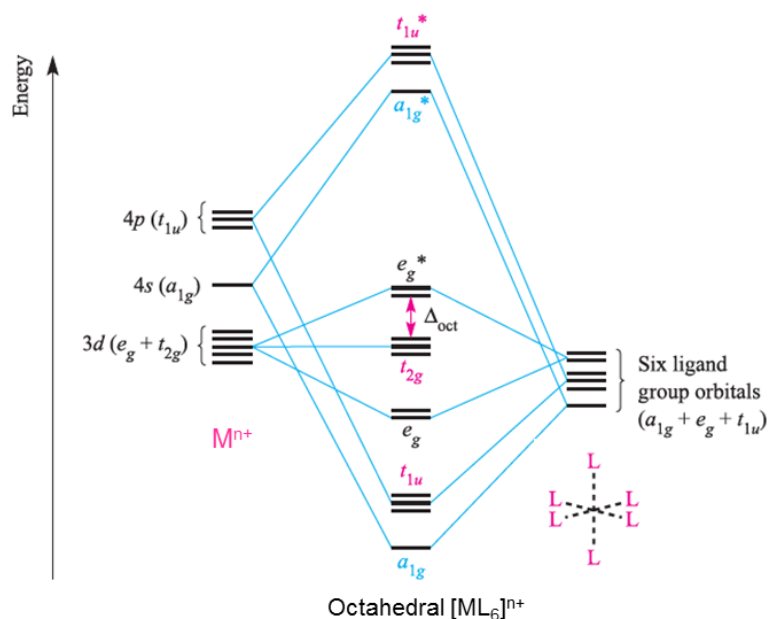
Figure 2.31 Molecular orbital diagram for the formation of $[ML_6]^{n+}$ where only σ-interactions are involved in the M-L coordination.[53]

Now that a better understanding on the M-L complexes is established, the next step is to prepare the MSBPs from previously synthesized polymeric precursors with a careful selection of first row 3*d*-block metal cations.

2.4.2 Selection of metal ions towards MSPBs

The synthesized model systems to form entangled metallo-supramolecular bulk polymers are based on (semi-)telechelic linear or star P*n*BA polymers end-capped with terpyridine ligand and on linear sticky P*n*BA-co-PTPA copolymers. These polymers have a glass transition below room temperature which allows to study them in bulk over a broad range of temperatures. These building blocks are then used to elaborate metallo-supramolecular polymeric assemblies by adding different transition metal ions which are complementary to the associating groups as explained in section 2.4.1. Among available metal ions, the first row of *d*-block metal cations is used in this project because relatively stable bis(terpyridine) complexes with controlled dissociation and association rates over a large window can be achieved. For this purpose, the Ni(II), Co(II), Cu(II) and Zn(II) cations with chloride (Cl⁻) as counter-ion are used in this project. While the chloride anion has a negligible coordinativity effect compared to terpyridine groups, two tpy ligands are coordinated to one metal ion. The ions are carefully selected based on the formation (k_f) and dissociation (k_{dis}) rates of their bis(terpyridine)-metal complexes, which are directly related to the strength and lability of the stickers. The usual sequence of stability, i.e. the binding constant, is $Zn^{2+} < Cu^{2+} < Co^{2+} < Ni^{2+}$ for terpyridine bis-complexes and their values are reported in Table 2.5.[49,54,55]

Ion	K_1 (M^{-1})	$k_{f,1}$ $(M^{-1}s^{-1})$	$k_{dis,1}$ (s^{-1})	K_2 (M^{-1})	$k_{f,2}$ $(M^{-1}s^{-1})$	$k_{dis,2}$ (s^{-1})	$\beta=K_1.K_2$ (M^{-2})
Ni(II)	$10^{10.7}$	$10^{3.1}$	$10^{-7.6}$	$10^{11.1}$	$10^{5.3}$	$10^{-5.8}$	$10^{21.8}$
Fe(II)	$10^{7.1}$	$10^{4.9}$	$10^{-2.2}$	$10^{13.8}$	$10^{7.0}$	$10^{-6.8}$	$10^{20.9}$
Co(II)	$10^{8.4}$	$10^{4.4}$	$10^{-4.0}$	$10^{9.9}$	$10^{6.7}$	$10^{-3.2}$	$10^{18.3}$
Cu(II)	10^{12}	$10^{7.3}$	-	$>10^{6}$	-	-	$>10^{18}$
Zn(II)	$10^{6.0}$	$10^{6.1}$	$10^{0.1}$	$10^{5.2}$	-	-	$10^{11.2}$

Table 2.5 Thermodynamic and knetic equilibrium parameters for the formation and dissociation of terpyridine mono- and bis-complexes with different transition metal ions in water at 25°C.[49,54,55]

Note that, the values reported in Table 2.5 correspond to the thermodynamic and knetic equilibrium parameters in solution. It is expected that these values have different order of magnitude in bulk but with the same usual sequence of binding constants as the solution one.

In practice, the metal ions are first dissolved in a good solvent. Then they are added to a concentrated polymeric solution to enhance the formation of metal-ligand complexes. The solvent is finally evaporated to obtain the desired metallo-supramolecular bulk materials as illustrated in Figure 2.32. The formation of M-L complexes provides effective bridges between associating chains. The latter enable the formation of associating networks with different rheological properties ranging from viscoelastic fluids to soft elastic solids and may respond to external stimuli conditions. Note that during sample preparation, high polymeric concentrations, e.g. 400-500g/L are fixed to favor the formation of inter-associations and avoid as much as possible the intra-associations.
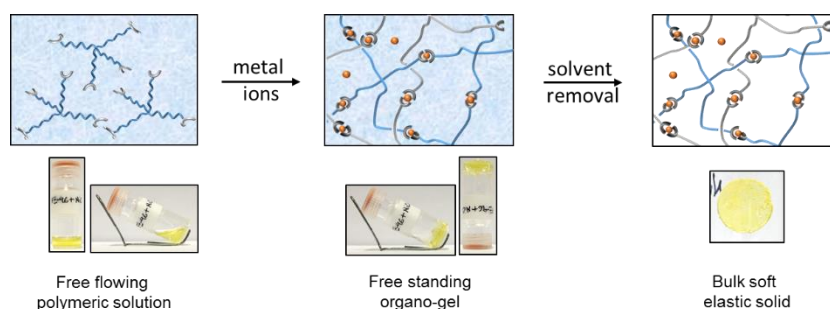
Figure 2.32 Preparation of metallo-supramolecular bulk polymers using telechelic four-arm star PnBA$_{160k}$-tpy$_4$ with nickel(II) chloride.

As illustrated in Figure 2.32, the formation of MSBPs can be evidenced by the inverted-tube test where the initially free flowing polymeric solutions turn into free-standing organo-gels upon the addition of metal ions. Additionally, the formation of M-L complexes between associating polymer chains is accompanied by the change in color and sometimes by the change in the color intensity because d-block metal complexes absorb light in the visible region. This color change is originating from the addition of the metal ions, which gives green color

with copper(II), orange color with cobalt(II), yellow with nickel(II) and no color change with zinc(II) as shown in Figure 2.33.
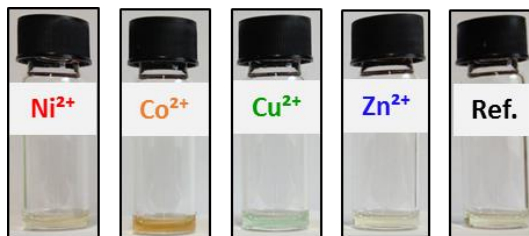
Figure 2.33 Pictures of metallo-supramolecular bulk polymers from linear semi-telechelic PnBA$_{110k}$-tpy upon the addition of different transition metal ions.

2.5   Conclusions

In this chapter, the efficiency of using a pre-modification approach combined with RAFT process is demonstrated. On the one hand, different terpyridine modified chain transfer agents are used for the RAFT polymerization of n-butyl acrylate monomer, leading to well-defined linear (semi-)telechelic and four-arm star telechelic associating polymers end-capped with terpyridine. On the other hand, terpyridine modified acrylic monomer is synthesized; then copolymerized with nBA via the RAFT technique to give linear sticky copolymers in which terpyridine moieties are randomly located within the polymer chain.

A set of associating supramolecular polymeric precursors is synthesized with relatively low molar mass distributions (Đ < 1.3). The high functionality of these well-defined associating poly(n-butyl acrylate)s is qualitatively and quantitatively ascertained by ^{1}H-NMR analysis and UV-visible titration. Furthermore they are exploited to elaborate entangled metallo-supramolecular bulk polymers in presence of the first row d-block metal cations. Once all MSBPs are obtained, the next stage is to systematically investigate their linear viscoelastic properties to demonstrate that their rheological features can be finely tailored.

2.6   Experimental part

2.6.1 Materials

All chemicals were purchased from Aldrich, Fluka, or Acros. *n*-Butyl Acrylate (*n*Ba) was freshly purified on an AlOx-filtration column to remove inhibitor immediately prior to use. 2,2-Azobis-(isobutyronitrile) (AIBN, 98% pure, Fluka) was recrystallized twice from methanol prior to use.

2.6.2 Instrumentation

^{1}H-NMR spectra were recorded on 300 or 500 MHz Avance Bruker spectrometers at 25 °C. Chemical shifts are given in ppm downfield from tetramethylsilane. Size exclusion chromatography (SEC) was carried out on a system composed of two PSS Gram columns (100 Å and 1000 Å) connected to a Waters 410 differential refractometer and a Waters UV detector, with *N,N*-dimethylformamide + 2.5 mM NH_4PF_6 as eluent (35 °C, 1 mL min^{-1}). Polystyrene standards were used for calibration. UV-visible spectra are recorded on a Varian Cary 50 Conc. spectrophotometer equipped with a Varian Cary thermostat. The measurements are performed using a 1 cm quartz cell at room temperature. Differential scanning calorimetry (DSC) measurement was performed on a Mettler Toledo 822 calorimeter. The sample was placed in an aluminum capsule (40 mL). The DSC instrument was calibrated using an Indium standard. The sample was initially heated from 30°C to 120°C with a heating rate of at 10°C/min and under nitrogen atmosphere to erase the thermal history of the material. Then, a cooling process was performed from 120°C to -80°C with the same rate. At last the sample was again heated from -80°C to 30°C at 10°C/min under a nitrogen atmosphere. The latter measurement was used to determine glass transition temperature (T_g). T_g were determined using Richardson method.

2.6.3 Synthesis of precursors

2.6.3.1 DDMAT

1-dodecanethiol (4.8 mL, 20 mmol), aliquat 336 – tricaprylylmethylammonium chloride – (0.36 mL, 0.8 mmol) and acetone (12 mL) are introduced in a 100 mL bicol. The mixture is left to stir at 10°C, under argon atmosphere, during 5 minutes. An aqueous solution (50 wt %) of NaOH (1.1 mL, 13.8 mmol) is then slowly added (10 minutes), under argon atmosphere. The solution is stirred at 10°C, during 15 min. Carbon disulfide (1.2 mL, 20 mmol), dissolved in 2.5 mL of acetone, is then slowly added (20 minutes) under argon atmosphere. The solution is left to stir at 10°C during 10 minutes. The chloroform (2.4 mL, 30 mmol) is next added. An aqueous solution (50 wt %) of NaOH (5.3 mL, 66.3 mmol) is then slowly added (25 minutes). Additional acetone (± 2.5 mL) can be added to ensure homogeneity as well as efficient stirring. The solution is finally left to stir during at least 10 hours, at 10°C and under argon atmosphere. The reaction mixture is diluted in 30 mL of water and carefully concentrated under low pressure to remove the acetone. An aqueous solution (37 wt %) of HCl is then added to reach pH 3. The solid is filtrated and dissolved in 100 mL of isopropanol. The insoluble S,S-bis(1-dodecyl)-trithiocarbonate side product is filtrated, washed with 30 mL of isopropanol. The remaining solution is subsequently concentrated under vacuum. The obtained red solid is finally crystallized from 15 mL n-hexane. The yellow solid is subsequently filtrated, washed several times with cooled n-hexane, and dried overnight in oven at 40°C under vacuum (yield = 27%).

^{1}H-NMR (300 MHz, CHCl$_3$-d, ppm): 3.27 (t, 2H, CH$_2$-C$\underline{H}_2$-S), 1.71 (s, 6H, -C(C$\underline{H}_3$)$_2$), 1.66 (q, 2H C$\underline{H}_2$-CH$_2$-S), 1.41–1.23 (m, 18H, CH$_3$-(C$\underline{H}_2$)$_9$-CH$_2$-CH$_2$-S), 0.90 (t, 3H, C$\underline{H}_3$-(CH$_2$)$_9$-CH$_2$-CH$_2$-S).

^{13}C-NMR (300 MHz, CHCl$_3$-d, ppm): 220.8 ($\underline{C}$=S), 178.9 ($\underline{C}$OOH), 55.6 (S-$\underline{C}$(CH$_3$)$_2$), 37.1 (CH$_2$-$\underline{C}$H$_2$-S), 31.9 ($\underline{C}$H$_2$-CH$_2$-S), 29.7 (CH$_3$-CH$_2$-$\underline{C}$H$_2$), 29.6–29.4 (CH$_3$-(CH$_2$)$_3$-($\underline{C}$H$_2$)$_4$-$\underline{C}$H$_2$), 29.1–29.0 (CH$_3$-(CH$_2$)$_2$-$\underline{C}$H$_2$-(CH$_2$)$_4$-$\underline{C}$H$_2$), 27.8 ($\underline{C}$H$_2$-CH$_2$-CH$_2$-S), 25.2 (C($\underline{C}$H$_3$)$_2$), 22.7 (CH$_3$-$\underline{C}$H$_2$-CH$_2$-), 14.2 ($\underline{C}$H$_3$-CH$_2$-CH$_2$).

2.6.3.2 CBMAT

3-Mercaptopropionic acid (2 mL, 23 mmol), acetone (13.8 mL) and the aliquat 336 – tricaprylylmethylammonium chloride – (0.08 mL, 0.9 mmol) are added to a round-bottom flask equipped with a magnetic stir bar. The mixture is left to stir at 10°C, under argon atmosphere, during 5 min. An aqueous solution (97 wt %) of NaOH (1.80 mL, 24 mmol) is then slowly added (10 min), under argon atmosphere. The solution is stirred for 30 min prior to the dropwise addition of carbon disulfide (1.38 mL, 23 mmol). The resulting yellow solution is stirred at room temperature overnight. Chloroform (2.75 mL, 34.4 mmol) and acetone (2.9 mL) were then added followed by the dropwise addition of 97 wt % NaOH solution (10 mL, 115 mmol). The mixture is stirred at room temperature overnight. The mixture is acidified with concentrated hydrochloric acid, and the resulting yellow precipitate is isolated by filtration with a Buchner funnel and flask. The precipitated is washed with distilled/deionized water. The product is then dried in vacuum at 40°C overnight to obtain a yellow powder (yield = 45%).

^{1}H-NMR (300 MHz, CHCl$_3$-d, ppm): 12.7 (s, 2H, COO$\underline{H}$), 3.43 (t, 2H, C$\underline{H}_2$-S), 2.62 (t, 2H, C$\underline{H}_2$-COOH), 1.59 (s, 6H, C(C$\underline{H}_3$)$_2$).

^{13}C-NMR (300 MHz, CHCl$_3$-d, ppm): 222.1 ($\underline{C}$=S), 173.6 ($\underline{C}$(CH$_3$)$_2\underline{C}$OOH), 173.0 ($\underline{C}$OOH-$\underline{C}$H$_2$,),), 57.1 (S-$\underline{C}$(CH$_3$)$_2$COOH), 35.0 (COOH-$\underline{C}$H$_2$), 32.0 ($\underline{C}$H$_2$-S), 25.5 (C($\underline{C}$H$_3$)$_2$).

2.6.3.3 PTMAT

Triethylamine (2.92 mL, 21.00 mmol) in 5 mL of CHCl$_3$ is added dropwise to a stirred solution of pentaerythritol tetrakis (3-mercaptopropionate) (95%) (0.40 mL, 1.05 mmol) and carbon disulfide (1.26 mL, 21.00 mmol) in CHCl$_3$ (7.5 mL) at room temperature. The solution gradually turned deep yellow during the addition and is stirred for 1 hour. 2-Bromo-2-methylpropanoic acid (98%) (1.75 g, 10.50 mmol) dissolved in 5 mL of CHCl$_3$ is then added dropwise, and the solution was stirred for 2 hours. The mixture is washed three times with an aqueous solution of HCl (0.2 M) and once with water. The reaction mixture is concentrated, dissolved in a minimum amount of CHCl$_3$ and precipitated in a ten fold-excess of *n*-hexane to afford a yellow powder which is further dried under vacuum at 40°C (yield = 76%).

^{1}H-NMR (300 MHz, CHCl$_3$-d, ppm): 4.12 (s, 8H, C-C$\underline{H}_2$-O), 3.53 (t, 8H, S-C$\underline{H}_2$-CH$_2$), 2.77 (t, 8H, S-CH$_2$-C$\underline{H}_2$), 1.71 (s, 24H, ((C$\underline{H}_3$)$_2$-C).

^{13}C-NMR (300 MHz, CHCl$_3$-d, ppm): 222.2 ($\underline{C}$=S), 178.3 ($\underline{C}$OOH), 176.26 (O-$\underline{C}$=O), 66.2 (C-$\underline{C}$H$_2$-O), 57.25 (S-$\underline{C}$(CH$_3$)$_2$), 42.4 (O-CH$_2$-$\underline{C}$-CH$_2$-O), 34.8 (CH$_2$-$\underline{C}$H$_2$-S), 32.9 ($\underline{C}$H$_2$-CH$_2$-S), 25.2 (C($\underline{C}$H$_3$)$_2$).

2.6.3.4 Amino-terpyridine (Tpy-NH$_2$)

5-Amino-1-pentanol (848 mg, 8.22 mmol) is dissolved in a suspension of potassium hydroxide (1.552 g, 27.65mmol) in dry DSMO (13.2 mL) and stirred at 60°C for 1 hour under argon atmosphere. 4-chloro-2,2':6',2"-terpyridine (2 g, 7.47 mmol) are then added and the reaction mixture is stirred overnight at 60°C. After cooling down to room temperature, the reaction mixture is poured into a 50-times excess of cold distilled water. The yellow precipitate is filtered, subsequently washed with distilled water (2×500 mL) and diethyl ether (2×500mL), and dried under vacuum at 40°C (yield = 64%).
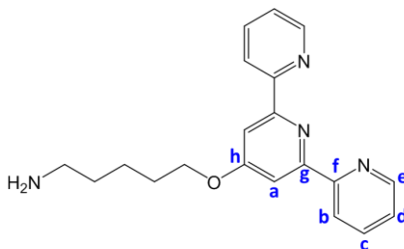
^{1}H-NMR (500 MHz, CHCl$_3$-d, ppm): 8.67 (dd, 2H, H$_{aromatic, e}$), 8.56 (dd, 2H, H$_{aromatic, b}$), 7.96 (s, 2H, $\underline{H}_a$), 7.82 (dt, 2H, $\underline{H}_c$), 7.33 (ddd, 2H, H$_d$), 4.24 (t, 2H, C$\underline{H}_2$-O), 2.75 (t, 2H, C$\underline{H}_2$-NH$_2$), 1.88 (q, 2H, C$\underline{H}_2$-CH$_2$-O), 1.63 (s, 2H, CH$_2$-N$\underline{H}_2$), 1.56 (q, 2H, C$\underline{H}_2$-CH$_2$-CH$_2$-O), 1.54 (q, 2H, C$\underline{H}_2$-CH$_2$-NH$_2$).

^{13}C-NMR (500 MHz, CHCl$_3$-d, ppm): 167.3 ($\underline{C}_h$), 157.1 ($\underline{C}_f$), 156.2 (C$_h$), 149.3 (C$_e$), 136.8 (C$_c$), 123.8 (C$_b$), 121.4 (C$_d$), 107.4 (C$_a$), 68.0 ($\underline{C}$H2-O), 42.1 ($\underline{C}$H$_2$-NH$_2$), 33.3 ($\underline{C}$H$_2$-CH$_2$-NH$_2$), 28.9 ($\underline{C}$H$_2$-CH$_2$-O), 23.4 ($\underline{C}$H$_2$-CH$_2$-CH$_2$-O).

2.6.3.5 DDMAT-tpy

Hydroxybenzotriazole hydrate (206 mg, 1.36 mmol) and 1-(3-dimethyl-aminopropyl)-3-ethyl carbodiimide hydrochloride (262 mg,

1.36 mmol) are dissolved in a DCM (5 mL) / DMF (0.7 mL) mixture at 0°C. Afterwards, DDMAT (415 mg, 1.14 mmol) is added and the solution is stirred for 1 hour. Tpy-NH$_2$ (380 mg, 1.14 mmol) is added and the reaction mixture is stirred for 24 hours. Then, the mixture is diluted with DCM (100mL) and consecutively washed with 3×100 mL of sodium carbonate aqueous solution (100 g/L), 3×100 mL of citric acid aqueous solution (100 g/L), and 3×100 mL of distilled water. The organic phase is finally separated, dried over magnesium sulfate, filtered and concentrated under low pressure to give a yellow solid which is further dried under vacuum at 40°C (yield = 83%).

^{1}H-NMR (500 MHz, CHCl$_3$-*d*, ppm): 8.68 (dd, 2H, H$_{aromatic, e}$), 8.58 (dd, 2H, H$_{aromatic, b}$), 8.01 (s, 2H, H$_{aromatic, a}$), 7.84 (dt, 2H, H$_{aromatic, c}$), 7.33 (ddd, 2H, H$_{aromatic, d}$), 6.51 (br, 1H, N$\underline{H}$-CH$_2$), 4.18 (t, 2H, O-C$\underline{H}_2$-CH$_2$), 3.29 (q, 2H, S-C$\underline{H}_2$-CH$_2$), 3.23 (t, 2H, CH$_2$-C$\underline{H}_2$-NH), 1.88 (q, 2H, S-CH$_2$-C$\underline{H}_2$), 1.73 (s, 2H, O-CH$_2$-C$\underline{H}_2$), 1.69–1.26 (m, 28H, CH$_3$-(C$\underline{H}_2$)$_9$-CH$_2$, (C$\underline{H}_2$)$_2$-CH$_2$-NH and (C$\underline{H}_3$)$_2$-C), 0.90 (t, 3H, CH$_2$–C$\underline{H}_3$).

2.6.3.6 CBMAT-tpy$_2$

Hydroxybenzotriazole hydrate (271 mg, 1.8 mmol) and 1-(3-dimethyl-aminopropyl)-3-ethyl carbodiimide hydrochloride (344 mg, 1.8 mmol) are dissolved in a DCM (5 mL) / DMF (0.7 mL) mixture at 0°C. Afterwards, DBMAT (183 mg, 0.7 mmol) is added and the solution is stirred for 1 hour. Tpy-NH$_2$ (500 mg, 1.5 mmol) is added and the reaction mixture is stirred for 24 hours. Then, the mixture is diluted with DCM (100mL) and consecutively washed with 3×100 mL of sodium carbonate aqueous solution (100 g/L), 3×100 mL of citric acid aqueous solution (100 g/L), and 3×100 mL of distilled water. The organic phase is finally separated, dried over magnesium sulfate, filtered and concentrated under low pressure to give a yellow solid which is further dried under vacuum at 40°C (yield = 79%).

^{1}H-NMR (500 MHz, CHCl$_3$-*d*, ppm): 8.67 (dd, 4H, H$_{aromatic, e}$), 8.58 (dd, 4H, H$_{aromatic, b}$), 7.97 (s, 4H, H$_{aromatic, a}$), 7.82 (dt, 4H, H$_{aromatic, c}$), 7.31 (ddd, 4H, H$_{aromatic, d}$), 6.52 (t, 2H, N$\underline{H}$-CH$_2$), 4.19 (t, 4H O-C$\underline{H}_2$-CH$_2$), 3.57 (t, 2H, S-C$\underline{H}_2$-CH$_2$), 3.23 (m, 4H, CH$_2$-C$\underline{H}_2$-NH), 2.77 (t, 2H, S-CH$_2$-C$\underline{H}_2$), 1.84 (m, 4H, O-CH$_2$-C$\underline{H}_2$), 1.70-1.40 (m, 14H, C$\underline{H}_2$-C$\underline{H}_2$-CH$_2$-NH and C$\underline{H}_3$).

135

2.6.3.7 PTMAT-tpy₄

Hydroxybenzotriazole hydrate (220 mg, 1.46 mmol) and 1-(3-dimethyl-aminopropyl)-3-ethyl carbodiimide hydrochloride (280 mg, 1.46 mmol) are dissolved in a DCM (5 mL) / DMF (0.7 mL) mixture at 0°C. Afterwards, PTMAT (346 mg, 0.3 mmol) is added and the solution is stirred for 1 hour. Tpy-NH$_2$ (407 mg, 1.22 mmol) is added and the reaction mixture is stirred for 24 hours. Then, the mixture is diluted with DCM (100mL) and consecutively washed with 3×100 mL of sodium carbonate aqueous solution (100 g/L), 3×100 mL of citric acid aqueous solution (100 g/L), and 3×100 mL of distilled water. The organic phase is finally separated, dried over magnesium sulfate, filtered and concentrated under low pressure to give a yellow solid which is further dried under vacuum at 40°C (yield = 89%).

^{1}H-NMR (500 MHz, CHCl$_3$-*d*, ppm): 8.67 (dd, 8H, H$_{aromatic, e}$), 8.58 (dd, 8H, H$_{aromatic, b}$), 8.00 (s, 8H, H$_{aromatic, a}$), 7.86 (dt, 8H, H$_{aromatic, c}$), 7.34 (ddd, 8H, H$_{aromatic, d}$), 6.59 (t, 4H, N$\underline{H}$-CH$_2$), 4.21 (t, 8H, O-C$\underline{H}_2$-CH$_2$), 4.06 (s, 8H, O-C$\underline{H}_2$-C), 3.49 (t, 8H, S-C$\underline{H}_2$-CH$_2$), 3.23 (m, 8H, CH$_2$-C$\underline{H}_2$-NH), 2.71 (t, 8H, S-CH$_2$-C$\underline{H}_2$), 1.84 (m, 8H, O-CH$_2$-C$\underline{H}_2$), 1.67 (s, 24H, C$\underline{H}_3$), 1.56 (m, 8H, CH$_2$-C$\underline{H}_2$-CH$_2$-NH), 1.49 (m, 8H, C$\underline{H}_2$-CH$_2$-CH$_2$-NH).

2.6.3.8 Hydroxyl-terpyridine (Tpy-OH)

1,3-propanediol (7.1 g, 93.4 mmol) and 30 mL of dry DMSO are placed in a flask equipped with a magnetic stirrer under an argon atmosphere. Dry potassium hydroxide pellets 85% (5.24 g, 93.4 mmol,) are added and the mixture is stirred for 1 hour at 60°C. 4-chloro-2,2':6',2''-terpyridine (5 g, 18.7 mmol) is then added. The reaction is continued for 2 days at 60°C under an argon atmosphere. The mixture is cooled down to ambient temperature and poured onto an ice-water mixture, where the product started to precipitate. The pH is then adjusted to 6 using dilute hydrochloric acid. The precipitated product is filtered, washed with cold water and dried in a vacuum oven at 40°C (yield = 72%).

^{1}H-NMR (500 MHz, CHCl$_3$-*d*, ppm): 8.61 (dd, 2H, , H$_{aromatic, e}$), 8.54 (dd, 2H, , H$_{aromatic, b}$), 7.95 (s, 2H, , H$_{aromatic, a}$), 7.78 (dt, 2H, , H$_{aromatic, c}$),

7.26 (ddd, 2H, , $H_{aromatic, d}$), 4.33 (t, 2H, C$\underline{H}_2$-O), 3.88 (t, 2H, C$\underline{H}_2$-OH), 2.05 (q, 2H, C$\underline{H}_2$-CH$_2$-O).

2.6.3.9 Terpyridine acrylate (TPA)

Tpy-OH (5.2 g, 16.9 mmol) is dissolved 150 mL of dry DCM. Triethylamine (4.1 mL, 28.8 mmol) is then added and the reaction mixture is stirred for 1 hour. Acryloyl chloride (2.34 mL, 28.8 mmol) is added dropwise under stirring at 0°C using an ice bath. After 2 hours, the cooling bath is removed and stirring of the reaction mixture is continued overnight. The solution is diluted with 150 mL of DCM, transferred to a separation funnel and then washed twice with a sodium carbonate (5% w/v) solution and once with pure water. The organic layer was isolated and dried over sodium sulfate. The solvent was removed in vacuum at 40°C. The residue is filtrated through column chromatography using neutral aluminum oxide and hexane:ethyl acetate (1 3 v/v) as eluent. After evaporation of the solvent, the solid is crystallized from hexane:ethyl acetate (7 : 1 v/v) to obtain white fluffy solid (yield = 65%).
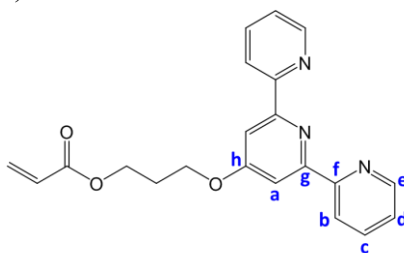
^{1}H-NMR (500 MHz, CHCl$_3$-*d*, ppm): 8.61 (dd, 2H, , $H_{aromatic, e}$), 8.54 (dd, 2H, , $H_{aromatic, b}$), 7.95 (s, 2H, , $H_{aromatic, a}$), 7.77 (dt, 2H, , $H_{aromatic, c}$), 7.25 (ddd, 2H, , $H_{aromatic, d}$), 6.37 (d, 1H, C$\underline{H}_2$=CH), 6.12 (dd, 1H, CH$_2$=C$\underline{H}$), 5.49 (d, 1H, C$\underline{H}_2$=CH), 4.31 (t, 2H, C$\underline{H}_2$-O), 4.27 (t, 2H, C$\underline{H}_2$-O-CO), 2.17 (q, 2H, C$\underline{H}_2$-CH$_2$-O).

^{13}C-NMR (500 MHz, CHCl$_3$-*d*, ppm): 167.3 (C=O), 167.0 (C$_h$), 156.9 (C$_g$), 155.9 (C$_f$), 148.9 (C$_e$), 137.0 (C$_c$), 136.2 ($\underline{C}$H$_2$=CH), 125.7 (CH$_2$=$\underline{C}$H), 123.9 (C$_d$), 121.5 (C$_b$), 107.5 (C$_a$), 64.7 ($\underline{C}$H$_2$-O), 61.3 ($\underline{C}$H$_2$-O-CO), 28.5 (CH$_2$-$\underline{C}$H$_2$-CH$_2$).

2.6.4 Synthesis of associating polymers

2.6.4.1 Homopolymerization

A typical procedure for the homopolymerization of *n*BA under bulk condition at 70°C using mono-functional TTC-tpy as RAFT agent is provided below. AIBN (1 mg, 6.09 µmol), DDMAT-tpy (42 mg, 0.06 mmol) and *n*BA (10.1 mL, 70 mmol) are introduced into a 25 mL round-bottom Schlenk tube. After degassing the solution using four freeze-pump-thaw cycles, the reaction mixture is sealed, purged with argon and then immersed in a preheated oil bath at 70°C. The polymerization is stopped by immediate exposure to air and cooling with liquid nitrogen. The crude product is dissolved in a minimum amount of acetone and purified by precipitation (two times) into cold distilled water:methanol (50:50 v/v). A yellow tacky soft solid is recovered and dried in a vacuum oven at 40°C. The purified mono-functional polymer is analyzed using a combination of size exclusion chromatography and NMR spectroscopy.

Linear semi-telechelic PnBA$_{101k}$-tpy.

^{1}H-NMR (500 MHz, CHCl$_3$-*d*, ppm): 8.66 (dd, 2H, H$_{aromatic, e}$) 8.58 (dd, 2H, H$_{aromatic, b}$), 7.97 (s, 2H, H$_{aromatic, a}$), 7.82 (dt, 2H, H$_{aromatic, c}$), 7.31 (ddd, 2H, H$_{aromatic, d}$), 4.02 (m, 1574H, O-C$\underline{H_2}$-CH$_2$, PnBA$_{101k}$), 3.23 (m, 2H, CH$_2$-C$\underline{H_2}$-NH), 2.26-0.93 (m, 8400H, P*n*BA$_{backbone\ aliphatics}$ and TTC-tpy, $_{aliphatics}$). M$_n$ (^{1}H-NMR) = 101 000 g/mol, Đ (SEC) = 1.14, yield = 68%.

The same procedure is used for the other RAFT agents to obtain linear telechelic and four-arm star telechelic poly(*n*-butyl acrylate)s functionalized with terpyridine ligand at chain extremities.

Linear telechelic PnBA$_{113k}$-tpy$_2$.

^{1}H-NMR (500 MHz, CHCl$_3$-*d*, ppm): 8.67 (dd, 4H, H$_{aromatic, e}$), 8.58 (dd, 4H, H$_{aromatic, b}$), 7.97 (s, 4H, H$_{aromatic, a}$), 7.82 (dt, 4H, H$_{aromatic, c}$), 7.31 (ddd, 4H, H$_{aromatic, d}$), 4.03 (m, 1776H, O-C$\underline{H_2}$-CH$_2$, PnBA$_{113}$-), 3.23 (m, 2H, CH$_2$-C$\underline{H_2}$-NH), 2.26-0.93 (m, 9180H, P*n*BA$_{backbone\ aliphatics}$ and TTC-tpy$_2$, $_{aliphatics}$). M$_n$ (^{1}H-NMR) = 113 000 g/mol, Đ (SEC) = 1.13, yield = 64%.

Telechelic four-arm star PnBA$_{160k}$-tpy$_4$.

^{1}H-NMR (500 MHz, CHCl$_3$-*d*, ppm): 8.67 (dd, 8H, H$_{aromatic, e}$), 8.58 (dd, 8H, H$_{aromatic, b}$), 8.00 (s, 8H, H$_{aromatic, a}$), 7.86 (dt, 8H, H$_{aromatic, c}$), 7.34 (ddd, 8H, H$_{aromatic, d}$), 4.01 (m, 2486H, O-C$\underline{H}_2$-CH$_2$, PnBA$_{160}$-), 3.23 (m, 8H, CH$_2$-C$\underline{H}_2$-NH), 2.27-0.93 (m, 13 220H, PnBA$_{backbone\ aliphatics}$ and TTC-tpy$_{4,\ aliphatics}$). M$_n$ (^{1}H-NMR) = 160 000 g.mol^{-1}, Đ (SEC) = 1.25, yield = 72%.

2.6.4.2 Copolymerization

A typical procedure for the copolymerization of *n*BA and TPA in solution at 70°C using DDMAT as RAFT agent is provided below. AIBN (1 mg, 6.09 μmol), DDMAT (22 mg, 0.06 mmol), *n*BA (10.1 mL, 70 mmol), TPA (470 mg, 1.30 mmol) and 15 mL chlorobenzene are introduced into a 50 mL round-bottom Schlenk tube. After degassing the solution using four freeze-pump-thaw cycles, the reaction mixture is sealed, purged with argon and then immersed in a preheated oil bath at 70°C. The polymerization is stopped by immediate exposure to air and cooling with liquid nitrogen. The crude product is dissolved in a minimum amount of acetone and purified by precipitation (two times) into cold distilled water:methanol (50:50 v/v). A yellow tacky soft solid is recovered and dried in a vacuum oven at 40°C. The purified copolymer is analyzed using a combination of size exclusion chromatography and NMR spectroscopy.

^{1}H-NMR (500 MHz, CHCl$_3$-*d*, ppm): 8.66 (dd, 22H, H$_{aromatic, e}$), 8.61 (dd, 22H, H$_{aromatic, b}$), 7.97 (s, 22H, H$_{aromatic, a}$), 7.84 (dt, 22H, H$_{aromatic, c}$), 7.32 (ddd, 22H, H$_{aromatic, d}$), 4.31 (m, 44H, O-C$\underline{H}_2$-CH$_2$-C$\underline{H}_2$-O, PTPA), 4.03 (m, 3504H, O-C$\underline{H}_2$-CH$_2$, PnBA$_{112}$-), 3.23 (m, 2H, CH$_2$-C$\underline{H}_2$-NH), 2.26-0.93 (m, 18 026H, PnBA$_{backbone\ aliphatics}$, PTPA$_{,\ backbone\ aliphatics}$ and PTPA O-CH$_2$-C$\underline{H}_2$-CH$_2$-O). M$_n$ (^{1}H-NMR) = 112 000 g/mol with 11 incorporated terpyridine units, Đ (SEC) = 1.22, yield = 69%.

2.6.4.3 Summary of polymeric precursors

Sample	M_n (NMR) (g/mol)	Conversion p (NMR)	$M_{n,th}$ (NMR) (g/mol)	Đ (SEC)
Mono-PnBA$_{101k}$-tpy	101 000	0.68	100 700	1.14
Mono-PnBA$_{142k}$-tpy	142 000	0.72	140 500	1.14
Bi-PnBA$_{113k}$-tpy$_2$	113 000	0.64	111 300	1.13
Bi-PnBA$_{171k}$-tpy$_2$	171 000	0.82	169 400	1.18
Star PnBA$_{160k}$-tpy$_4$	160 000	0.72	158 600	1.25
Star PnBA$_{250k}$-tpy$_4$	250 000	0.60	248 900	1.20
PnBA$_{840}$-co-PTA$_{11}$	112 000	0.69	110 700	1.22
PnBA$_{814}$-co-PTA$_{15}$	110 000	0.63	107 800	1.29

Table 2.6 Summary of poly(n-butyl acrylate) precursors synthesized via RAFT polymerization.

2.6.5 Arm cleavage of star polymers

In a 10 mL round bottom flask, 4-arm star PnBA-tpy$_4$ (150 mg) is dissolved in 6 mL of THF and is stirred under air for 20 min. Then piperidine (~200 µL) is added and the solution is left to stir for 10 hours at room temperature. After 10 hours, the volatiles are removed under reduced pressure and the crude residue is dried under vacuum at 40°C overnight. After drying, the crude product is analyzed by SEC.

2.6.6 Sample Preparation

Samples are prepared by dissolving a given amount of associating polymeric precursors in acetone. The sealed reaction vessels are mixed for 30 min via vortex at room temperature to obtain concentrated polymeric solutions with a concentration ranging between 400-500g.L^{-1}. The metallo-polymers are then readily obtained by adding 0.5 stoichiometric equivalents of transition metal ions (with respect to the terpyridine content) dissolved in acetone or methanol. The reaction vessels are mixed via vortex for 30 min, then left to rest for 1 hour at room temperature to ensure total complexation of the metal. The solvent is evaporated under reduced pressure at 40°C then the sample is dried under vacuum at 40°C for 24 hours to obtain metallo-supramolecular bulk polymers.

2.6.7 UV-Vis titration of terpyridine content

Terpyridine-functionalized polymers are dissolved in 2 mL of THF at a concentration between 0.005mg/µL and 0.01mg/µL. The polymeric solution is then titrated by stepwise addition of a THF solution of iron(II) chloride at stabilized against oxidation by the presence of 0.03 mg/µL ascorbic acid. After every addition, a UV-vis spectrum is recorded after 2 min. The absorption value of the maximum of the metal to ligand charge transfer (MLCT) at 555 nm is used to obtain the UV-vis titration curve.

Bibliography

(1)   Schubert, U. S.; Hien, O.; Eschbaumer, C. Functionalized Polymers with Metal Complexing Segments: A Simple and High-Yield Entry towards 2,2′:6′,2″-Terpyridine-Based Oligomers. *Macromol. Rapid Commun.* **2000**, *21*, 1156–1161.

(2)   Heller, M.; Schubert, U. S. Optically Active Supramolecular Poly (l - Lactide) s End-Capped with Terpyridine. *Macromol. Rapid Commun.* **2001**, *22*, 1358–1363.

(3)   Lohmeijer, B. G. G.; Schubert, U. S. Supramolecular Engineering with Macromolecules: An Alternative Concept for Block Copolymers. *Angew. Chemie - Int. Ed.* **2002**, *41*, 3825–3829.

(4)   Gohy, J. F.; Lohmeijer, B. G. G.; Varshney, S. K.; Décamps, B.; Leroy, E.; Boileau, S.; Schubert, U. S. Stimuli-Responsive Aqueous Micelles from an ABC Metallo-Supramolecular Triblock Copolymer. *Macromolecules* **2002**, *35*, 9748–9755.

(5)   Gohy, J. F.; Lohmeijer, B. G. G.; Schubert, U. S. Reversible Metallo-Supramolecular Block Copolymer Micelles Containing a Soft Core. *Macromol. Rapid Commun.* **2002**, *23*, 555–560.

(6)   Gohy, J. F.; Lohmeijer, B. G. G.; Varshney, S. K.; Schubert, U. S. Covalent vs Metallo-Supramolecular Block Copolymer Micelles. *Macromolecules* **2002**, *35*, 7427–7435.

(7)   Chiper, M.; Meier, M. A. R.; Wouters, D.; Hoeppener, S.; Fustin, C.; Gohy, J.; Schubert, U. S.; Uni, V.; Lou, D.; Pasteur, P. L.; et al. Supramolecular Self-Assembled Ni (II), Fe (II), and Co (II) ABA Triblock Copolymers. *Macromolecules* **2008**, *41*, 2771–2777.

(8)   Guillet, P.; Fustin, C.-A.; Mugemana, C.; Ott, C.; Schubert, U. S.; Gohy, J.-F. Tuning Block Copolymer Micelles by Metal–ligand Interactions. *Soft Matter* **2008**, *4*, 2278.

(9)   Gohy, J. F. Metallo-Supramolecular Block Copolymer Micelles. *Coord. Chem. Rev.* **2009**, *253*, 2214–2225.

(10)   Guillet, P.; Fustin, C.-A.; Wouters, D.; Hoeppener, S.; Schubert, U. S.; Gohy, J.-F. Amphiphilic Brushes from Metallo-Supramolecular Block Copolymers. *Soft Matter* **2009**, *5*, 1460.

(11)   Guillet, P.; Mugemana, C.; Stadler, F. J.; Schubert, U. S.; Fustin, C.-A.; Bailly, C.; Gohy, J.-F. Connecting Micelles by Metallo-Supramolecular Interactions: Towards Stimuli Responsive Hierarchical Materials. *Soft Matter* **2009**, *5*, 3409.

(12)   Morgan, G. T.; Burstall, F. H. Dehydrogenation of Pyridine by Anhydrous Ferric Chloride. *J. Chem. Soc.* **1932**, *0*, 20–30.

(13)   Vellis, P. D. .; Mikroyannidis, J. A. .; Lo, C.-N. .; Hsu, C.-H. . Synthesis of Terpyridine Ligands and Their Complexation with Zn21 and Ru21 for Optoelectronic Applications. *J. Polym. Sci. Part A Polym. Chem.* **2008**, *46*, 7702–7712.

(14)   Wang, P.; Li, Z.; Lv, G. C.; Zhou, H. P.; Hou, C.; Sun, W. Y.; Tian, Y. P. Zinc(II) Complex with Teirpyridine Derivative Ligand as "on-off" Type Fluorescent Probe for Cobalt(II) and Nickel(II) Ions. *Inorg.*

Chem. Commun. **2012**, *18*, 87–91.

(15) McWhinnie, W. R.; Miller, J. D. The Chemistry of Complexes Containing 2,2′-Bipyridyl, 1, 10-Phenanthroline, or 2,2′,6′,2″-Terpyridyl as Ligands. *Adv. Inorg. Chem. Radiochem.* **1970**, *12*, 135–215.

(16) Constable, E. C. The Coordination Chemistry of 2,2′:6′,2″-Terpyridine and Higher Oligopyridines. *Adv. Inorg. Chem.* **1986**, *30*, 69–121.

(17) Cargill Thompson, A. M. W. The Synthesis of 2,2′:6′,2″-Terpyridine Ligands — Versatile Building Blocks for Supramolecular Chemistry. *Coord. Chem. Rev.* **1997**, *160*, 1–52.

(18) Schubert, U. S.; Eschbaumer, C.; An, Q. R.; Salditt, T. Terpyridine Metal Complexes as Building Blocks for Supramolecular Assemblies and Polymers: Thermal Stabilities and Thin Film Preparation. *J. Incl. Phenom. Macrocycl. Chem.* **1999**, *35*, 35–43.

(19) Mark, J. E. *Physical Properties of Polymers Handbook*, Second Edi.; Springer-Verlag: New York, 2007.

(20) Ellis, B.; Smith, R. *Polymers: A Property Database*, Second Edi.; CRC Press: New York, 2008.

(21) Chiefari, J.; Chong, Y. K.; Ercole, F.; Krstina, J.; Jeffery, J.; Le, T. P. T.; Mayadunne, R. T. A.; Meijs, G. F.; Moad, C. L.; Moad, G.; et al. Living Free-Radical Polymerization by Reversible Addition - Fragmentation Chain Transfer: The RAFT Process. *Macromolecules* **1998**, *31*, 5559–5562.

(22) Moad, G.; Rizzardo, E.; Thang, S. H. Radical Addition-Fragmentation Chemistry in Polymer Synthesis. *Polymer (Guildf).* **2008**, *49*, 1079–1131.

(23) Yang, C.; Cheng, Y. L. RAFT Synthesis of Poly(N-Isopropylacrylamide) and Poly(Methacrylic Acid) Homopolymers and Block Copolymers: Kinetics and Characterization. *J. Appl. Polym. Sci.* **2006**, *102*, 1191–1201.

(24) Arita, T.; Buback, M.; Vana, P. Cumyl Dithiobenzoate Mediated RAFT Polymerization of Styrene at High Temperatures. *Macromolecules* **2005**, *38*, 7935–7943.

(25) Perrier, S.; Barner-Kowollik, C.; Quinn, J. F.; Vana, P.; Davis, T. P. Origin of Inhibition Effects in the Reversible Addition Fragmentation Chain Transfer (RAFT) Polymerization of Methyl Acrylate. *Macromolecules* **2002**, *35*, 8300–8306.

(26) Stenzel, M. H.; Cummins, L.; Roberts, G. E.; Davis, T. P.; Vana, P.; Barner-Kowollik, C. Xanthate Mediated Living Polymerization of Vinyl Acetate: A Systematic Variation in MADIX/RAFT Agent Structure. *Macromol. Chem. Phys.* **2003**, *204*, 1160–1168.

(27) Fijten, M. W. M.; Paulus, R. M.; Schubert, U. S. Systematic Parallel Investigation of RAFT Polymerizations for Eight Different (Meth)Acrylates: A Basis for the Designed Synthesis of Block and Random Copolymers. *J. Polym. Sci. Part A Polym. Chem.* **2005**, *43*, 3831–3839.

(28) Chernikova, E.; Morozov, A.; Leonova, E.; Garina, E.; Golubev, V.; Bui, C.; Charleux, B. Controlled Free-Radical Polymerization of n -

Butyl Acrylate by Reversible Addition - Fragmentation Chain Transfer in the Presence of Tert -Butyl Dithiobenzoate . A Kinetic Study. *Macromolecules* **2004**, *37*, 6329–6339.

(29)   Keddie, D. J.; Moad, G.; Rizzardo, E.; Thang, S. H. RAFT Agent Design and Synthesis. *Macromolecules* **2012**, *45*, 5321–5342.

(30)   Keddie, D. J. A Guide to the Synthesis of Block Copolymers Using Reversible-Addition Fragmentation Chain Transfer (RAFT) Polymerization. *Chem. Soc. Rev.* **2014**, *43*, 496–505.

(31)   Li, H.; Li, M.; Yu, X.; Bapat, A. P.; Sumerlin, B. S. Block Copolymer Conjugates Prepared by Sequentially Grafting from Proteins via RAFT. *Polym. Chem.* **2011**, *2*, 1531.

(32)   Li, M.; Li, H.; De, P.; Sumerlin, B. S. Thermoresponsive Block Copolymer-Protein Conjugates Prepared by Grafting-from via RAFT Polymerization. *Macromol. Rapid Commun.* **2011**, *32*, 354–359.

(33)   Sun, X.-L. .; He, W.-D. .; Li, J. .; Li, L.-Y. .; Zhang, B.-Y. .; Pan, T.-T. . RAFT Cryopolymerizations of N,N-Dimethylacrylamide and N-Isopropylacrylamide in Moderately Frozen Aqueous Solution. *J. Polym. Sci. Part A Polym. Chem.* **2009**, *47*, 6863–6872.

(34)   Sun, X. L.; He, W. D.; Pan, T. T.; Ding, Z. L.; Zhang, Y. J. RAFT Cryopolymerizations of Acrylamides and Acrylates in Dioxane at -5 °C. *Polymer (Guildf).* **2010**, *51*, 110–114.

(35)   Sumerlin, B. S. Proteins as Initiators of Controlled Radical Polymerization: Graftingfrom via ATRP and RAFT. *ACS Macro Lett.* **2012**, *1*, 141–145.

(36)   Paulus, R. M.; Becer, C. R.; Hoogenboom, R.; Schubert, U. S. High Temperature Initiator-Free RAFT Polymerization of Methyl Methacrylate in a Microwave Reactor. *Aust. J. Chem.* **2009**, *62*, 254–259.

(37)   Ran, R.; Chen, Z.; Wang, X. L. Substituent Effects on Trithiocarbonates-Mediated Polymerization of Styrene. *J. Appl. Polym. Sci.* **2009**, *111*, 2011–2017.

(38)   Lai, J. T.; Filla, D.; Shea, R. Functional Polymers from Novel Carboxyl-Terminated Trithiocarbonates as Highly Efficient RAFT Agents. *Macromolecules* **2002**, *35*, 6754–6756.

(39)   Wang, R.; Mccormick, C. L.; Lowe, A. B. Synthesis and Evaluation of New Dicarboxylic Acid Functional Trithiocarbonates : RAFT Synthesis of Telechelic Poly (n-Butyl Acrylate) s Trithiocarbonates : RAFT Synthesis of Telechelic Poly (n-Butyl Acrylate) S. *Macromolecules* **2005**, *38*, 9518–9525.

(40)   Mayadunne, R. T. a; Jeffery, J.; Moad, G.; Rizzardo, E. Living Free Radical Polymerization with Reversible Addition-Fragmentation Chain Transfer (RAFT Polymerization): Approaches to Star Polymers. *Macromolecules* **2003**, *36*, 1505–1513.

(41)   Whittaker, M. R.; Monteiro, M. J. Synthesis and Aggregation Behavior of Four-Arm Star Amphiphilic Block Copolymers in Water. *Langmuir* **2006**, *22*, 9746–9752.

(42)   Piogé, S.; Fustin, C. A.; Gohy, J. F. Temperature-Responsive Aqueous Micelles from Terpyridine End-Capped Poly(N-

Isopropylacrylamide)-Block-Polystyrene Diblock Copolymers. *Macromol. Rapid Commun.* **2012**, *33*, 534–539.

(43) Jochum, F. D.; Brassinne, J.; Fustin, C.-A.; Gohy, J.-F. Metallo-Supramolecular Hydrogels Based on Copolymers Bearing Terpyridine Side-Chain Ligands. *Soft Matter* **2013**, *9*, 2314.

(44) Wang, R.; Mccormick, C. L.; Lowe, A. B. Synthesis and Evaluation of New Dicarboxylic Acid Functional Trithiocarbonates : RAFT Synthesis of Telechelic Poly (n-Butyl Acrylate)S. *Macromolecules* **2005**, *38*, 9518–9525.

(45) Rizzardo, E.; Chen, M.; Chong, B.; Moad, G.; Skidmore, M.; Thang, S. H. RAFT Polymerization: Adding to the Picture. *Macromol. Symp.* **2007**, *248*, 104–116.

(46) Mayadunne, R. T. A.; Jeffery, J.; Moad, G.; Rizzardo, E. Living Free Radical Polymerization with Reversible Addition−Fragmentation Chain Transfer (RAFT Polymerization): Approaches to Star Polymers. *Macromolecules* **2003**, *36*, 1505–1513.

(47) Jackson, A. C.; Beyer, F. L.; Price, S. C.; Rinderspacher, B. C.; Lambeth, R. H. Role of Metal-Ligand Bond Strength and Phase Separation on the Mechanical Properties of Metallopolymer Films. *Macromolecules* **2013**, *46*, 5416–5422.

(48) Schubert, U. S.; Hofmeier, H.; Newkome, G. R. *Modern Terpyridine Chemistry*; Wiley-VCH: Weinheim, 2006.

(49) Holyer, R. H.; Hubbard, C. D.; Kettle, S. F. a; Wilkins, R. G. The Kinetics of Replacement Reactions of Complexes of the Transition Metals with 2,2',2"-Terpyridine. *Inorg. Chem.* **1966**, *5*, 622–625.

(50) Hogg, R.; Wilkins, R. G. Exchange Studies of Certain Chelate Compounds of the Transitional Metals. Part VIII. 2,2′,2″-Terpyridine Complexes. *J. Chem. Soc.* **1962**, 341–350.

(51) Harzmann, G. D.; Neuburger, M.; Mayor, M. 4,4″-Disubstituted Terpyridines and Their Homoleptic FeIIcomplexes. *Eur. J. Inorg. Chem.* **2013**, *2013*, 3334–3347.

(52) Chiper, M.; Hoogenboom, R.; Schubert, U. S. New Terpyridine Macroligands as Potential Synthons for Supramolecular Assemblies. *Eur. Polym. J.* **2010**, *46*, 260–269.

(53) Housecroft, C. E.; Sharpe, A. G. *Inorganic Chemistry*, Fourth Edi.; Pearson: Edinburgh, 2012.

(54) Cali, R.; Rizzarelli, E.; Sammartano, S.; Siracusa, G.; Press, A.; Interscience, W.; Gupta, S. K.; Kapoor, R. N.; Wilkinson, G.; Knifton, J. F.; et al. Thermodynamics of 2,2′,2″-Terpyridinecopper(II) Complexes in Aqueous Solution. *Transit. Met. Chem.* **1979**, *4*, 328–332.

(55) Dobrawa, R.; Ballester, P.; Saha-Möller, C. R.; Würthner, F. Thermodynamics of 2,2′:6′,2″-Terpyridine-Metal Ion Complexation. *ACS Symp. Ser.* **2006**, *928*, 43–62.

Chapter 3

Linear rheology of entangled bulk polymers functionalized with metal-ligand interactions

Abstract

This Chapter studies the linear viscoelastic properties of a series of relatively low dispersity poly(*n*-butyl acrylate) chains end-functionalized with 2,2';6',2"-terpyridine, able to self-associate by metal-ligand coordination. Depending on the architecture and functionality of the chains, the polymers self-assemble into different metallo-supramolecular bulk structures once metal ions are added. Linear building blocks (mono-functional or bi-functional) form longer chains while four-arm stars or linear sticky copolymers form transient networks. The properties of the obtained materials can be fine tuned depending on the length of the polymer chains and the type of metal. In this respect, enhanced control is gained over the dynamics of this class of metallo-supramolecular assemblies. Hence, they are extremely interesting for specific applications such as adhesives or mechano-sensors.

3.1 Introduction

3.1.1 Supramolecular polymeric materials

The advent of supramolecular chemistry in the last decades has provided powerful tools to form adaptable materials based on the ability of molecules to self-assemble. It relies on (macro)molecules able to adapt their properties and structures in response to external stimuli.[1] However, most of these self-assembled materials are studied in solution because commonly used polymers have a glass transition above room temperature. If the material is an amorphous flexible polymer with a glass transition below the ambient temperature, it can be investigated without solvent in the melt state as a soft material.[2]

While several works are reported in Chapter 1 on supramolecular bulk systems based on metal-ligand interactions, progress in associating polymers for the formation of bulk materials can be highlighted with other supramolecular interactions as well. For instance Guan's works on polystyrene-*b*-poly(*n*-butyl acrylate) (PS-*b*-P*n*BA) diblock copolymers end-capped with ureidopyrimidinone (UPy) at one extremity. Upy-Upy hydrogen bonds lead to the elaboration of PS-*b*-P*n*BA-*b*-PS triblock bulk copolymers.[3] Rozes reported a material based on *n*BA copolymerized with a sulfonate acrylamide-functionalized butyltin oxo-cluster macrocation. Ionic interactions occur between the macrocation and sulfonate groups forming supramolecular crosslinks which provide elastomeric properties to the resulting bulk material.[4] Schubert described histidine-based monomers copolymerized with either butyl methacrylate (BMA) or lauryl methacrylate (LMA). The polymers are crosslinked through metal-ligand coordination by adding zinc(II) ions to the polymer solution and a film is formed by solvent casting.[5] Colquhoun and Hayes reported supramolecular bulk materials crosslinked by π-π stacking. Using divalent or trivalent pyrenyl end-functionalized poly(ethylene oxide) polymers mixed with a copolymer that contains naphthalene-diimide chain-folding and 2,2'-(ethylenedioxy) bis(ethylamine) linker.[6,7]

However, most of these works are essentially focused on healing properties of the resulting materials at the expense of fundamentally understanding their mechanical features which are linked to self-healing. Rheological properties and dynamics of these systems have not been deeply studied and a deeper understanding on topological effect within bulk materials is unfortunately not provided.

3.1.2 Systematic mechanical investigations

By functionalizing flexible polymer chains with associating units, or so also called "stickers", reversible networks of polymers are obtained, which constitute an interesting class of soft materials because of the richness in their rheological behavior.[8] Several chemical motifs can be used as stickers which brings the classification of associating polymers depending on the nature of the associations.[9] Among those, metal-ligand interactions are particularly interesting because of their high directionality and the large range of binding strength achievable according to the metal-ligand combination.[10] The same polymers can also be classified according to the number and the position of the associating moieties. Generally, they are localized either at the center[11], at the end[12] or as pendant groups[13] of the macromolecular chains.

In order to better understand the complex rheological properties of such soft materials, where large-scale supramolecular structures are combined with bond energy of stickers and entanglements, it is essential to work with model systems where different parameters such as polymer molar mass, location of the associating units on the chain, and the number of stickers are well-defined. In this direction, the objective of this chapter is to study the dynamics of well-defined linear and star telechelic polymers containing stickers at chains extremities. While they constitute one of the most studied classes of associating polymers[14], the specificity of the systems proposed here is that they are based on entangled building blocks. Consequently, their rheological behavior is expected to depend on both entanglement and stickers dynamics. Furthermore, we would like to vary their composition parameters in a systematical way, in order to identify their exact contribution in the viscoelastic response.

These samples can be prepared by controlled radical polymerization and further used as precursors to form different supramolecular structures. Specifically, the presence of associating groups at the chain-end allows their use as cross-linkers or chain extenders.[15,16] Following these aspects, a more comprehensive study is carried out on the rheological properties of polymer chains with a glass transition temperature (T_g) below ambient temperature and end-functionalized with associating moieties. In this respect, PnBA is selected as a matrix whose glass transition is generally reported around -55 °C.[17] The tridentate terpyridine ligand (tpy) is used as sticker which forms coordinative interactions once metal ions are added.[18]

3.2 Materials and experimental

3.2.1 Materials

In this chapter, a series of terpyridine functionalized PnBA with low dispersity Đ is synthesized via RAFT polymerization using ligand-modified chain transfer agents and or ligand-functionalized monomer as explained in Chapter 2. Molecular weights are targeted above the average molar mass between entanglements of pure PnBA (M_e = 18 kg.mol^{-1}) as reported in Table 3.1.[19]

Samples	$M_{n, system}$[a] (kg/mol)	Đ[b]	Z=M_n/M_e [c]
Linear Mono-PnBA$_{101k}$-tpy	101	1.14	5.6
Linear Bi-PnBA$_{113k}$-tpy$_2$	142	1.14	7.8
4-arm star PnBA$_{160k}$-tpy$_4$	160	1.25	2.2/arm
Linear PnBA$_{110k}$-co-PTA$_{15}$	110	1.29	6.1

Table 3.1. Structural parameters of PnBA polymers functionalized with terpyridine ligand. [a] Molar mass determined by ^{1}H-NMR. [b] Dispersity determined by SEC. [c] Number of entanglements calculated using M_e = 18 000 g/mol.

Details on the model systems are schematically reported in Figure 3.1. These building blocks are then used to elaborate metallo-supramolecular polymeric assemblies by adding different transition metal ions which are complementary to the associating groups or the so called "stickers".
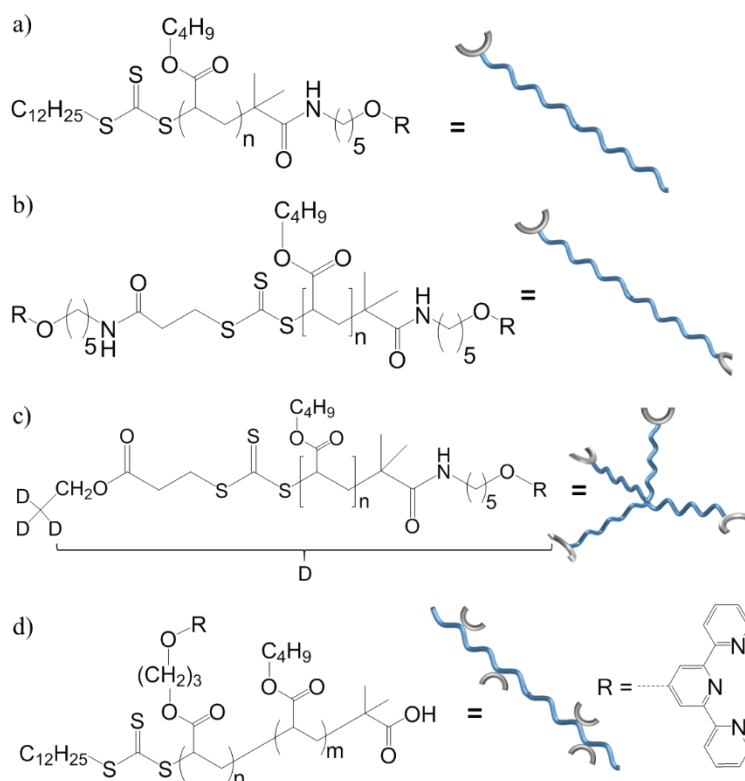

Figure 3.1. Chemical structures of a) Linear mono-functional P*n*BA end-functionalized with terpyridine (P*n*BA-tpy) b) Linear telechelic P*n*BA-tpy$_2$ c) Telechelic 4-arm star P*n*BA-tpy$_4$ and d) Linear sticky P*n*BA-*co*-PTPA.

3.2.2 Experimental

To investigate the linear viscoelastic properties of associating polymers, shear rheological experiments were performed in the linear regime on an Ares (TA Instruments) rheometer equipped with a

air/nitrogen convection oven that ensure an accurate temperature control (± 0.1°C). Dynamic meachanical measurements were carried out at given temperatures, using stainless steel 8 mm plate−plate geometries. The gap was adjusted between 400 and 500 μm so that the geometry was completely filled. The sample was equilibrated in the rheometer at 130°C for 30 min. Normal forces were checked to be relaxed prior any measurement. Dynamic frequency sweeps were performed at a deformation amplitude of 3% over a temperature range of -20°C to 80°C and a frequency range of $10^2 – 10^{-3}$ rad/s. All dynamic measurements were performed within the linear viscoelastic region, which was determined from dynamic strain sweep experiments. At each temperature, the equilibration was checked with dynamic time sweep measurements up to 1 hour. The collected data were shifted along the frequency axis using the time-temperature superposition (TTS), yielding master curves that were constructed at the same reference temperature $T_{ref} = 0°C$.

3.3 Linear telechelic associative PnBA

3.3.1 Linear mono-functional PnBA-tpy

The linear rheological properties of these systems are investigated within a large range of temperatures (from 80°C to -20°C). The properties of these materials reflect the role of both macromolecular structures and coordinative interactions. They are fine-tuned by varying either the structure, the length of the chain or the type of transition metal ion used to trigger the complexation with the ligand. The choice of metal ion allows controlling the rate at which each physical cross-linker associates or dissociates respectively from each other. To do so, metal ions are dissolved in a good solvent then they are added to a concentrated polymeric solution to enhance the formation of metal-ligand complexes and solvent is finally evaporated to obtain the desired metallo-supramolecular bulk materials.

As a first test, different samples based on linear mono-functional PnBA building blocks are prepared in order to investigate the influence of first row transition metal ions on the rheological

properties of metallo-supramolecular bulk polymers. Figure 3.2 shows the linear rheological behavior at 25°C of the precursor alone or mixed with different transition metal ions which are Ni(II), Co(II), Cu(II) and Zn(II). The ions are carefully selected based on the formation (k_f) and dissociation (k_{dis}) rates of their bis-complexes with terpyridine, which are directly related to the strength and lability of the stickers. The usual sequence of stability is $Zn^{2+} < Cu^{2+} < Co^{2+} < Ni^{2+}$ for terpyridine bis-complexes.[20]
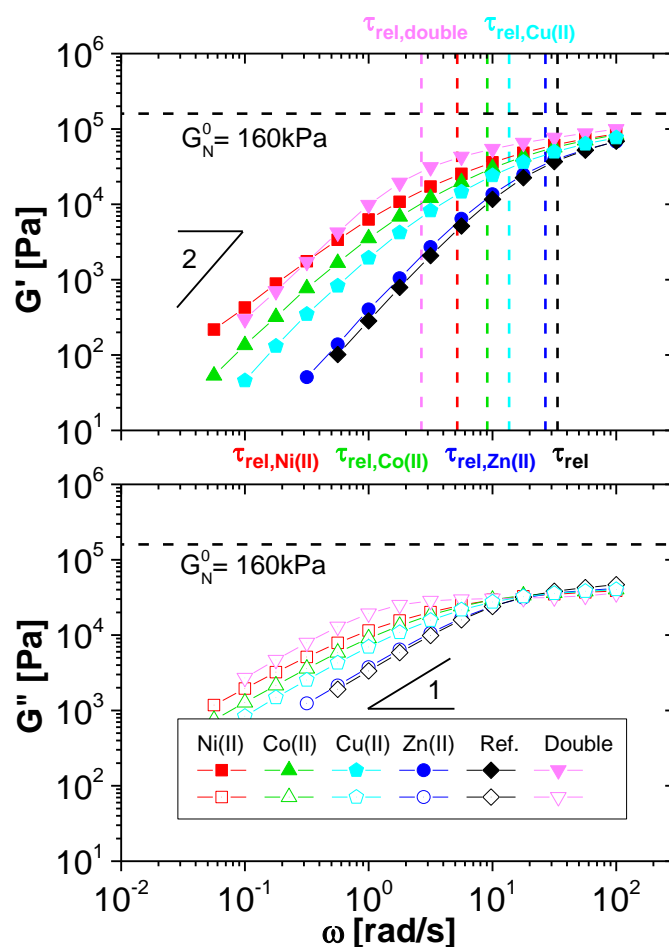

Figure 3.2 Linear rheology curves at 25°C of linear mono-functional P*n*BA-tpy (melts) with different transition metal ions. The diamonds correspond to the reference polymer without metal ions and the inverse triangles to simple linear P*n*BA 205 kg/mol without any tpy unit

153

referred as double. Terminal relaxation times are probed within the measurement range that are $\tau_{rel} = 29$ ms, $\tau_{rel,Zn(II)} = 43$ ms, $\tau_{rel,Cu(II)} = 73$ ms, $\tau_{rel,Co(II)} = 107$ ms, $\tau_{rel,Ni(II)} = 191$ ms and $\tau_{rel,Double} = 365$ ms.

Oscillatory frequency sweeps have been performed in the linear regime at 25 °C. As the oscillation frequency (ω) is decreased, the reference polymer, which does not have active sticker, quickly reaches its terminal relaxation regime and flows like a viscous liquid. Containing around 5.9 entanglements per chain, this polymer is relaxing by reptation and contour length fluctuations (CLF), combined with constraint release (CR), as it is well-described by tube models.[21,22] In the terminal regime, the storage and loss moduli, G'(ω) and G''(ω), respectively exhibit scaling with ω^2 and ω^1 as expected from Maxwell prediction. The cross-over frequency between these curves is used to determine the terminal relaxation time ($\tau_{rel} = 1/\omega_{rel.}$) which is around 29 ms at 25°C. In presence of active stickers, different behaviors are observed for metallo-supramolecular polymers. In the case of Zn(II) ions, the resulting system shows a rheological signature extremely close to the polymer reference with a $\tau_{rel,Zn(II)} = 43$ ms. The reason why linear mono-functional zinc metallo-supramolecular polymer behaves nearly like the reference one is linked to the bis-terpyridine complexes lability. In fact, when metal-ligand coordination is formed with Zn(II) ions, the resulting reversible interactions are very labile.[23] Therefore, the stickers constantly switch between the associated and dissociated states at a rate that exceed the relaxation frequency of the pristine polymer. Hence the presence of stickers with zinc ions does not sustantially affect the relaxation of the polymer, which mainly relaxes as a single chain through primitive path fluctuation near the chain ends combined with reptation of the inner part of the chain.[24]

On the other hand, in presence of Cu(II), Co(II) or Ni(II) ions the cross-over between G' and G'' is shifted from high to intermediate frequencies. Consequently, the terminal relaxation time increases for these systems, precisely $\tau_{rel,Cu(II)} = 73$ ms, $\tau_{rel,Co(II)} = 107$ ms and $\tau_{rel,Ni(II)} = 191$ ms. Thus, in presence of less labile ions, the metal-ligand bridges are stronger and associating units have a direct impact on the relaxation of the supramolecular polymer. In presence of copper or cobalt ions, more stable metal-ligand complexes are formed and the

resulting metallo-supramolecular polymers do not relax anymore as a single chain but rather as two polymer chains attached together with an active sticker at the center (referred to as double polymer chain). These double chains can relax either by reptation, or by dissociation of their metal-ligand complexes followed by the reptation of the dissociated chains. It is expected that the relative importance of these two relaxation processes depends on the time needed for the reptation of the double polymer chain, compared to the time needed for the complex to dissociate and therefore, depends on the metal ions used to create the complexes. In Figure 3.2, it is observed that the terminal relaxation time of the telechelic PnBA chains in the presence of cobalt ions is closer to the terminal time of a reference linear PnBA with a molar mass of M_n = 205 kg/mol than to the terminal relaxation time of the single chain.
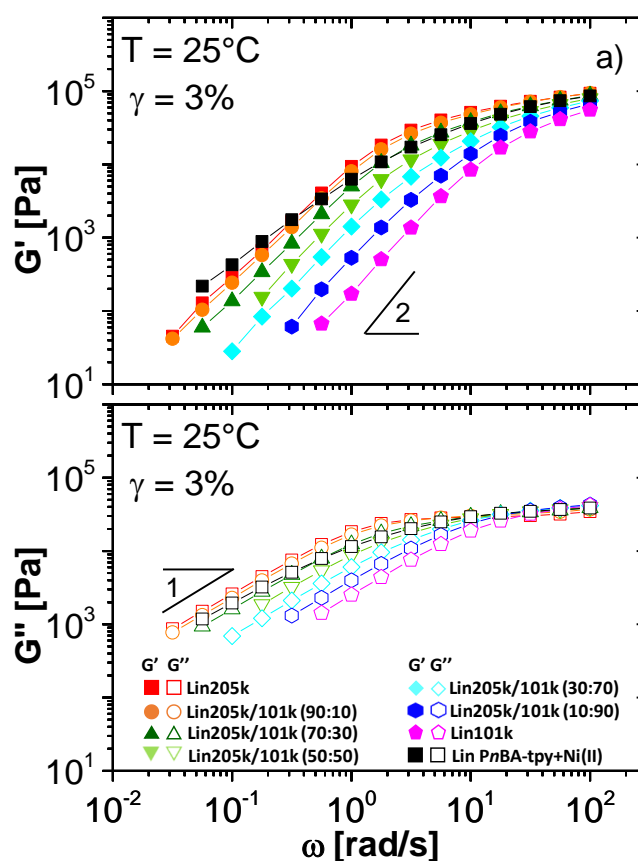

Figure 3.3 a) Comparison of linear poly(n-butyl acrylate)s and poly(n-butyl acrylate) blends at T = 25°C with linear PnBA-tpy+Ni(II).
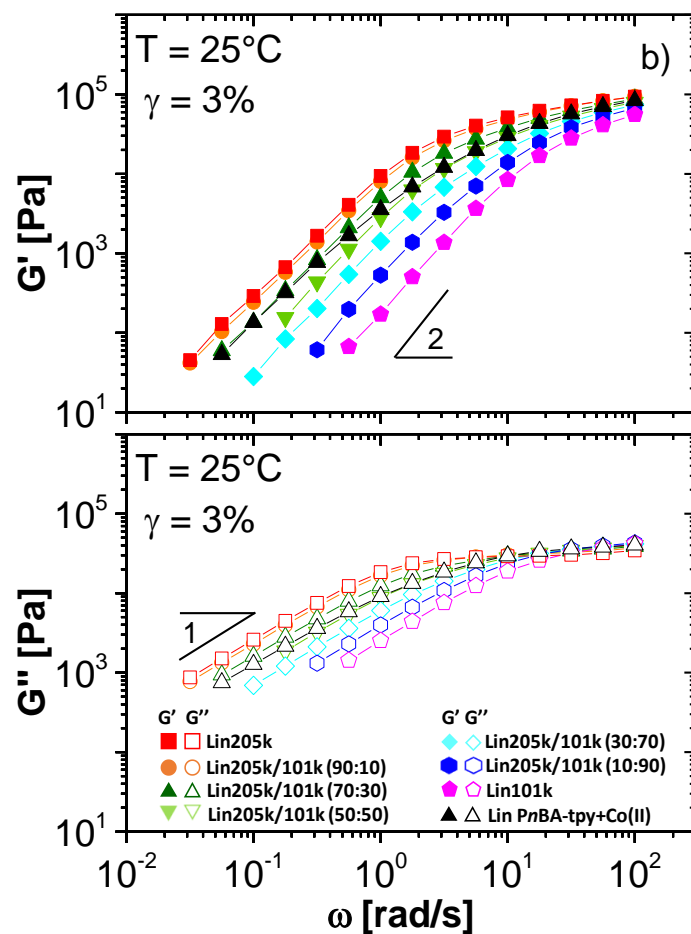
Figure 3.3 b) Comparison of linear poly(*n*-butyl acrylate)s and poly(*n*-butyl acrylate) blends at T = 25°C with linear P*n*BA-tpy+Co(II).
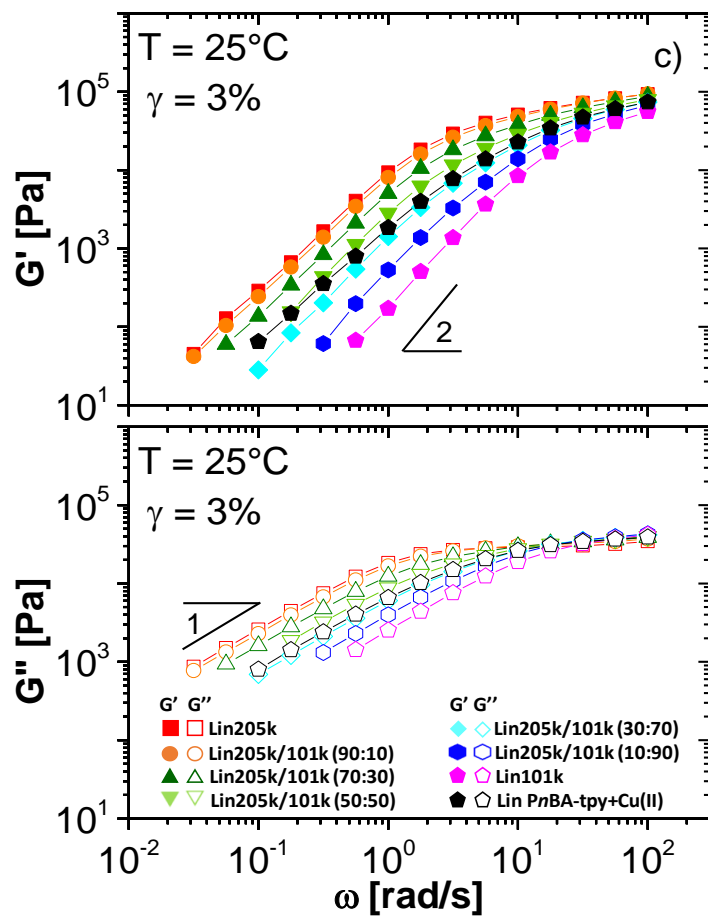
Figure 3.3 c) Comparison of linear poly(*n*-butyl acrylate)s and poly(*n*-butyl acrylate) blends at T = 25°C with linear P*n*BA-tpy+Cu(II).

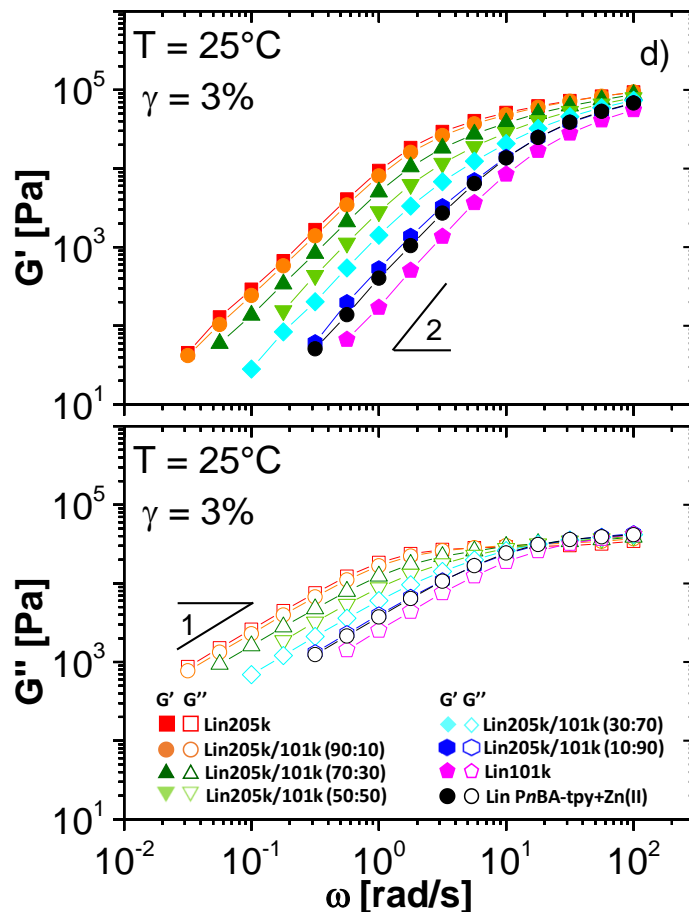**Figure 3.3** d) Comparison of linear poly(*n*-butyl acrylate)s and poly(*n*-butyl acrylate) blends at T = 25°C with linear P*n*BA-tpy+Zn(II).

Therefore, we expect that the sample contains a large amount of double polymer chains (with an average number molar mass estimated to 202 kg/mol). However, one can also observe that despite similar dispersity, the relaxation time spectrum of the supramolecular chains is broader than the reference linear P*n*BA. Same behavior is found with copper ions and nickel ions. This can be easily understood by the probable presence of metallo-supramolecular chains with functionalized end-groups in their non-associated state, which relax as single chains while the majority of the chains are associated and have longer relaxation times. In order to investigate experimentally if the lifetimes of the complexes are long enough to ensure that the reptation

of these double linear chains takes place before their dissociation, Figure 3.3 compares the viscoelastic response of the different mono-functional P*n*BA polymers to the storage and loss moduli of binary blends composed of (non-supramolecular) linear P*n*BA-tpy polymers of molar mass 101 kg/mol and 205 kg/mol, in different proportions.

From this figure, it is clear that only the supramolecular polymer with zinc-ligand complexes behaves similarly to a binary blend of single and double linear chains (see Figure 3.3.d). Its storage and loss moduli are very similar to the covalent blend composed of 10 wt% of P*n*BA chains with M_n = 205 kg/mol, i.e. largely dominated by the relaxation of the single chains. With cobalt or copper as metal ions, larger distribution of relaxation time is found, which does not fit the behavior of any of the blends. At high frequencies, where it is expected that most of the associated chains do not have time to dissociate, the level of the storage modulus corresponds to an association probability of around 70 wt% for the linear sample P*n*BA-tpy+Co(II) and around 50 wt% in the linear sample P*n*BA-tpy+Cu(II). However, at intermediate frequencies (i.e. around 3 rad/s), it is observed that their storage modulus is lower than the one of the corresponding blends (containing 70 wt% or 50 wt% of P*n*BA of 205 kg/mol), indicating that a fraction of the double chains found a way to relax faster. While a more detailed analysis is needed in order to accurately describe the relaxation of these double chains, this faster relaxation can be attributed to their relaxation by dissociation followed by the reptation of the single chains. This suggests that the dissociation dynamics of the complexes already takes place at relatively short times, which is consistent with the thermo-rheological complexity shown by these samples at intermediate frequency as shown in Figure 3.4. Linear rheology of this linear mono-functional precursor and its resulting metallo-supramolecular bulk polymers (MSBPs) is investigated over a range of temperatures (from −20 to 60°C). Master curves are constructed by setting the reference temperature at 0°C for all bulk materials, and by applying the time−temperature superposition (TTS) principle, based on the reference polymer without metal ions. For the references, i.e. precursors without any metal ion, superposition of the viscoelastic moduli fits well. MSBPs data cannot be reduced into a well-fitted master curves. However, since part of the associated chains has a terminal relaxation time similar to

the one of the double linear chains, this also suggests that the dissociation times of the complexes can be quite long and therefore, are distributed over a long range of times.
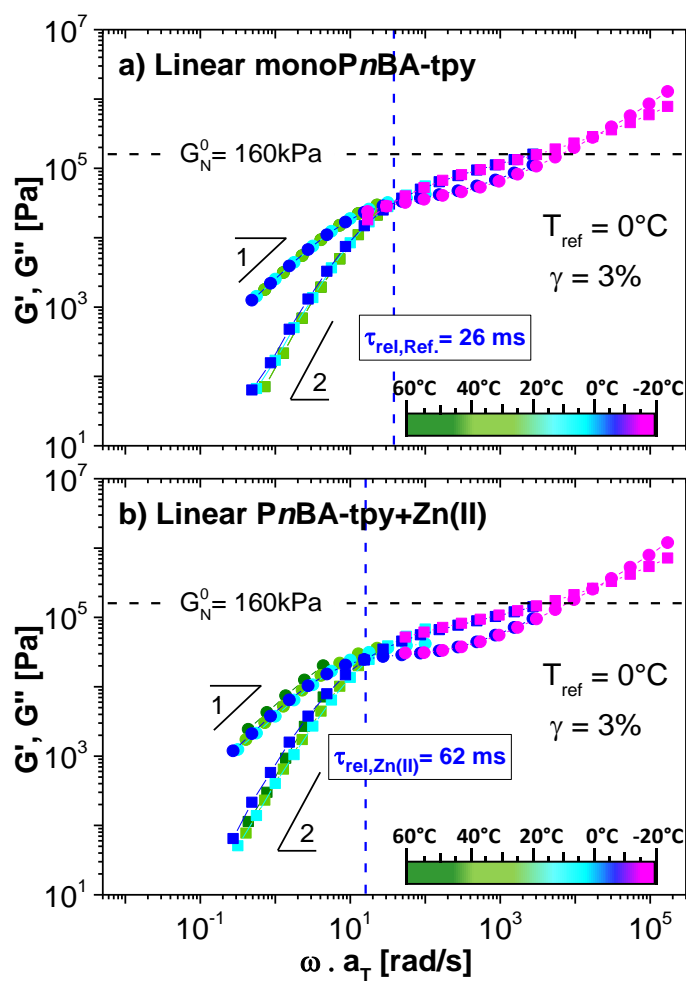

Figure 3.4 G' (■) and G'' (●) Master curves for linear mono-functional a) PnBA-tpy (reference) and b) PnBA-tpy+Zn(II) at T_{ref} = 0 °C. The color of experimental curves indicates the temperature at which frequency sweeps in linear regime are performed.

Figure 3.4 G' (■) and G'' (●) Master curves for linear mono-functional c) P*n*BA-tpy+Cu(II) and d) P*n*BA-tpy+Co(II) at $T_{ref} = 0$ °C. The color of experimental curves indicates the temperature at which frequency sweeps in linear regime are performed.

Figure 3.4 G' (■) and G'' (●) Master curves for linear mono-functional e) P*n*BA-tpy+Ni(II) at T_{ref} = 0 °C. The color of experimental curves indicates the temperatu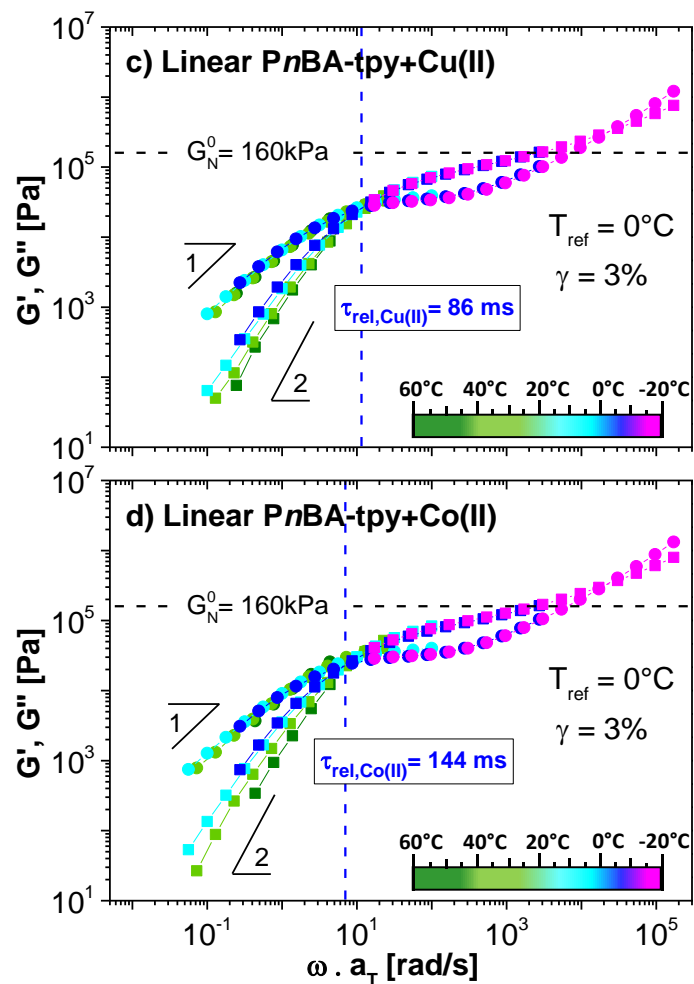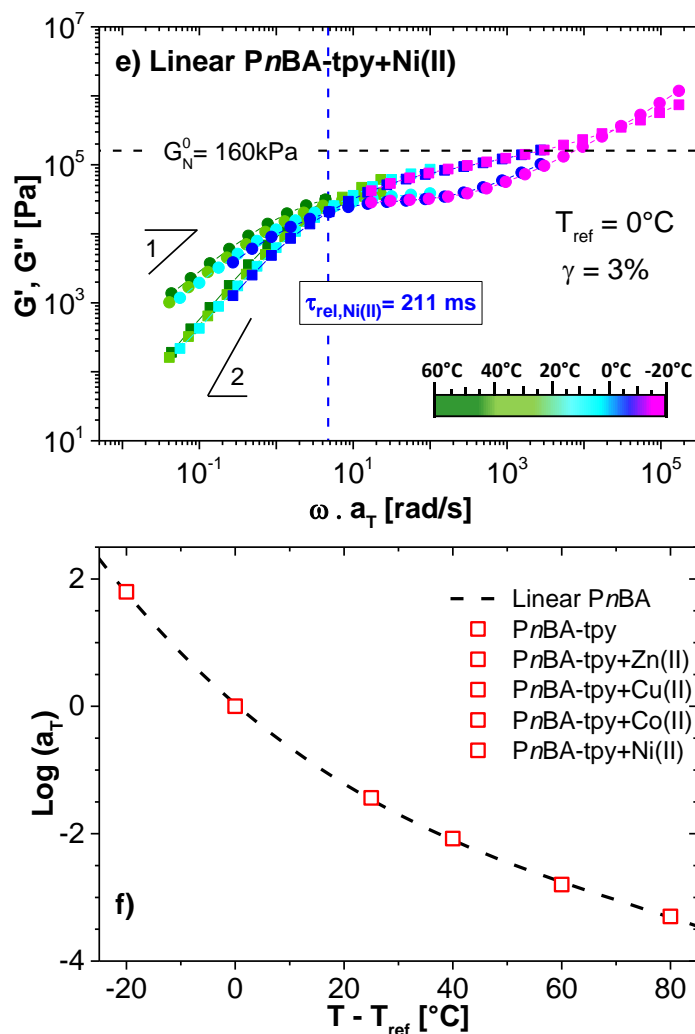re at which frequency sweeps in linear regime are performed. f) Horizontal shift factors (a_T) of the linear mono-functional P*n*BA-tpy (i.e. Reference). The same shift factors are used for P*n*BA-tpy with different metal ions at T_{ref} = 0°C.

The same discussion can be applied to Ni(II) coordination to explain the delayed relaxation. However, at low frequency, the Maxwell mode is not obtained and the shape of its storage modulus differs from the one obtained with cobalt or copper ions: as observed in

Figure 3.2, while G"(ω) displays a slope close to 1 , G'(ω) exhibits a slope of 1.2 rather than 2, which means the polymeric system has not completely relaxed yet. Furthermore, it is observed that part of the supramolecular chains relaxes slower than a reference linear PnBA with M_n = 205 kg/mol. This suggests the possibility of other interactions within the system such as cluster formation between associating units.[25-26] Hence, instead of simply having a coupling of chains to create double chains, there might be formation of aggregates toward the creation of star-like assemblies, which tend to relax differently from double length linear chains since these assemblies cannot reptate.[27] We attribute this possible formation of aggregates to the difference in polarity between the charged terpyridine metal ion complexes and the rather apolar PnBA polymer matrix. This could favor a clustering of the charged complexes.

Thus, the association of linear terpyridine mono-functionalized PnBA chains with different transition metal ions allows shifting the terminal relaxation time of the pristine polymer (τ_{rel}) to lower frequencies. However, since the metal-ligand associations can only lead to the creation of double chains, which have a short relaxation time compared to the association lifetime, the chains relaxation is limited by the relatively fast relaxation of the stable assemblies and their viscoelastic properties are close to a Maxwell behavior. In order to obtain more complex viscoelastic behavior, linear bi-functional PnBA-tpy$_2$ should be considered, as proposed in the next section.

3.3.2 Linear bi-functional PnBA-tpy$_2$

In order to obtain longer assemblies, a terpyridine function is now grafted at each end of a linear polymer chain. Figure 3.5 shows the linear rheological behavior at 25°C of bi-functional PnBA-tpy$_2$, either alone or mixed with the same transition metal ions than for the mono-functional PnBA-tpy chains. At 25°C the reference polymer, *i.e.* bi-functional polymer without metal ions, relaxes easily as it contains only 6.7 entanglements. The terminal relaxation zone is reached with τ_{rel} = 45 ms and the latter is going through reptation combined with CLF and CR mechanisms. However, when metal ions are added, the polymer

163

with active stickers behaves quite differently. Even with zinc ions, the bi-functionalized metallo-supramolecular bulk material has a longer terminal relaxation time, $\tau_{rel,Zn(II)}$ = 134 ms. Although zinc is considered as a labile ion (meaning that zinc bis-terpyridine complex lifetime is short), associating units which keep switching between free and attached states clearly affect the rheological properties over half a decade before going through the flow regime. This result differs from the one observed for mono-functional supramolecular polymers, for which adding Zn ions had only little effect. This difference can be attributed to the larger association probability (or average lifetime) of the bi-functional chains since they can connect via their two extremities and since the proportion of ions in the sample is nearly twice more important.
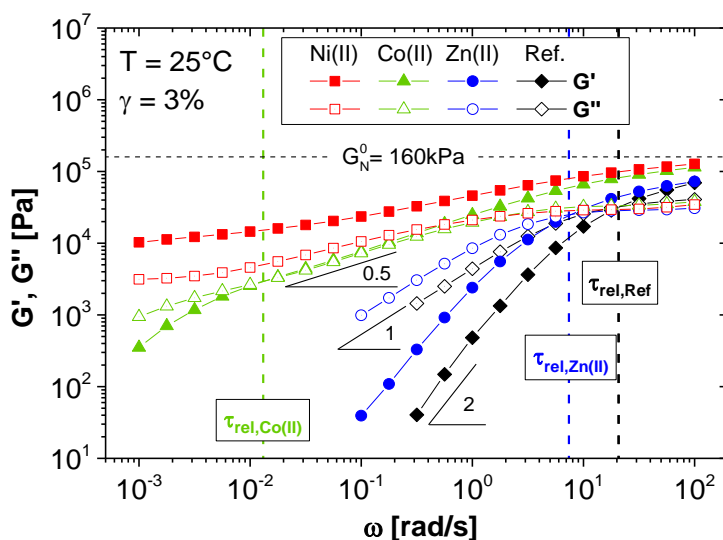

Figure 3.5 Linear rheology curves at 25°C of linear bi-functional P*n*BA-tpy₂ (melts) with different transition metal ions. The reference corresponds to a polymer without metal ions. The storage modulus G' is represented by filled symbols, the loss modulus G" by empty symbols. Terminal relaxation times are τ_{rel} = 45 ms, $\tau_{rel,Zn(II)}$ = 134 ms and $\tau_{rel,Co(II)}$ = 80 s.

Supramolecular effects are emphasized when Co(II) and Ni(II) are used to form bis-terpyridine complexes, as shown in Figure 3.5. At high frequency, the end of the rubbery plateau is observed. At lower

frequency, the sample relaxation is not described by a Maxwell mode anymore. The moduli of the sample containing cobalt ions display a dissipative regime with $G' \sim G'' \sim \omega^{0.5}$ over nearly two decades, which is similar to relaxation by a Rouse process and could come from a Constraint Release Rouse process of a very slow relaxing architecture blended to much more mobile chains.[19] However, without further analysis, one cannot exclude that this ω-dependence comes from the relaxation of specific mixtures of chains with different lengths. Then at long time scale, the apparent onset of terminal process is observed, with a G' and G'' cross-over corresponding to $\tau_{rel,Co(II)} = 80$ s. The broad spectrum of relaxation times observed with this sample can be attributed to the different chain structures which are created from the association of the bi-functional P*n*BA-tpy$_2$ chains through metal-ligand complexes as illustrated in Figure 3.6.
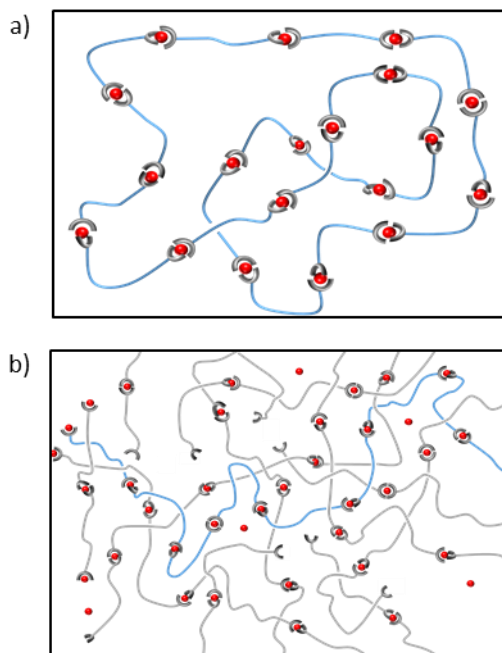

Figure 3.6. a) Idealistic schematic view of an entangled super long supramolecular polymer loop from linear bi-functional polymers end-functionalized with a sticker at each extremity. b) Schematic view of different associating configurations from linear associating bi-

functional polymers resulting in a large distribution in supramolecular polymer sizes.

Indeed, when the stoichiometric amount of metal ions is added to PnBA-tpy$_2$ polymer, the idealistic case of the formation of a single super long entangled supramolecular chain loop as represented in Figure 3.6.a is never reached. Bi-functional associating polymers rather self-assemble into several configurations. Supramolecular chains with high dispersity in length are created, each of them having their own relaxation time. For the PnBA-tpy$_2$ polymer in presence of Co^{2+} ions, a large part of the assemblies relaxes similarly to the reptation of double chains while the longest relaxation time of the supramolecular polymer corresponds to the reptation time of an assembly containing around seven precursors.

Furthermore, loops of different sizes can also be formed, leading to assemblies which do not contain dangling ends. Indeed, the two extremities of a given chain can associate and create entangled loop from one precursor. Larger loops including several precursors could also be formed. Entanglements between two polymer loops can only be released after the dissociation of a supramolecular bond and opening of the loop, followed by the relaxation by reptation of the assembly. Therefore, if the sample contains long-lifetime stickers, their relaxation time can be much longer than the relaxation time of a linear supramolecular assembly with similar molar mass. While the creation of supramolecular loops is not highly probable, only few of them are needed to explain the long relaxation time observed in Figure 3.5 with cobalt ions. Indeed, by assuming that these slowly relaxing chains could only relax by constraint release process and by approximating their contribution to the storage modulus to 3 kPa, we can estimate the proportion of slowly relaxing chains to around 13 wt% (since the corresponding level of the storage modulus should be a factor φ^2 lower than the rubbery plateau, with φ being the proportion of chains not relaxed at time t_{3k} such that G'(ω=1/ t_{3k} = 0.01 rad/s) = 3kPa), including both long assemblies and polymer loops. This dispersity, both in size and in shape, results in a large distribution of τ_{rel} which is emphasized through a dissipative regime at intermediate frequency.[28] The formation of loops is one of the possibilities to interpret the obtained results.

However, highlighting the presence of loops remains a challenge and this explanation cannot be confirmed. It must be noted that another possible origin of the long relaxation times is the presence of a few aggregates of complexes, as it was observed for the PnBA-tpy+Ni(II) polymer. Indeed, the metal-ligand complexes can phase separate from the polymer matrix due to the polar moieties of terpyridine complexes. Hence, they can form aggregates composed of a few stacks of metal-ligand complexes and immersed in the PnBA matrix. However, such aggregates were not detected in the rheology of PnBA-tpy+Co(II) polymer. Also, SAXS measurements on this sample did not show any trace of cluster.

Besides dispersity, one needs to account for the associating probability of the supramolecular units located at the extremities of each polymer chain, the stickers switching between the free and associated states with time. It is therefore important to consider the probability for each sticker to be attached again once detached,[29] which can differ in function of the sample composition.[30] Indeed, the times during which the stickers remain associated (τ_{ass}) or free (τ_{free}) can change from orders of magnitude depending on the probability for a sticker to quickly find a close neighboring associating unit or not. It must be noted that the dissociation of a sticker, which immediately re-associates with the same sticker before losing initial entanglements should not counted as effective dissociation since the chains do not have the possibility to relax. It is expected that this dissociation process of the stickers will promote faster relaxation of highly entangled polymer assemblies[31,32], since these last ones become shorter and therefore, more mobile. In Figure 3.5, we attribute the onset of the terminal relaxation of the PnBA-tpy$_2$ chains with cobalt ions to the starting of an effective dissociation time of the stickers, which allows the relaxation of the remaining oriented fraction of the polymer.

While with cobalt ions the onset of the terminal relaxation is reached, as expressed by the modulus cross-over, it is not achieved in presence of nickel ions, within the frequency range of measurement. As stipulated above, this observation can be related to the fact that Ni(II) bis-terpyridine complexes are more stable (or less labile) than those with cobalt or zinc ions.[20,23] Furthermore, the possible presence of few

aggregates, as highlighted with the mono-functional PnBA chains, can reduce the proportion of linear self-assemblies, able to relax by reptation at intermediate frequencies. As shown in Figure 3.5, a transition from the plateau modulus (estimated at 160 kPa for PnBA chains) at high frequencies to a second, low frequency, plateau (of around 10 kPa) at long time scale is observed. By assuming that these slowly relaxing chains could only relax by constraint release process, the second plateau level should be a factor φ^2 lower than the rubbery plateau with φ being the proportion of chains not relaxed, which corresponds to 25 wt% of the polymer which cannot disentangle as fast as the majority of the chains. The first relaxation, from the rubbery plateau to the second plateau, can be attributed to the relaxation of the different self-assembled supramolecular linear chains composed of few (2-3) precursors by reptation and fluctuations processes. On the other hand, the relaxation of the second plateau, is most probably due to the fact that part of the chains (such as polymer loops, molecular segments trapped between two aggregates or extremely long assembly composed of 12 precursors) are not able to relax before the dissociation of the stickers.[20] Their relaxation is expected to be governed by stickers dynamics, which, in case of nickel ions, is becoming very slow.

Furthermore, linear rheology of these polymers was investigated over a range of temperatures (from −20 to 60°C). Master curves were constructed by setting the reference temperature at 0°C for all bulk materials, and by applying the time−temperature superposition (TTS) principle, based on the reference polymer without metal ions. For the latter polymer, superposition of the viscoelastic moduli works well, as shown in Figure 3.7.a. Their shift factors (a_T) values were found to be similar to the factors measured for pure linear poly(n-butyl acrylate) without any terpyridine ligand attached to the extremity as shown in Figure 3.7.c. The resulting master curve shows clear viscoelastic properties of PnBA-tpy$_2$ over few decades and WLF relation is applied to determine C_1 = 7.63 and C_2 = 103.8 K for the reference polymer. These values are consistent with earlier reports on similar polymers such as poly(ethyl methacrylate) or poly(n-butyl methacrylate).[33,34] The same shift factors are then used for the entangled MSBPs (see Figure 3.7.b). When stickers are active for linear entangled metallo-supramolecular bulk polymers the superposition fails to fit properly:

P*n*BA-tpy$_2$+Co(II) frequency sweeps in linear regime at different temperature cannot be reduced to a well-defined master curve. Hence MSBPs tend to be thermo-rheologically complex since rheological properties do not only depend on the dynamics of macromolecular chains but also on the stickers dynamics, i.e. metal-ligand coordination. Increasing temperature leads to shorter lifetime of the stickers.
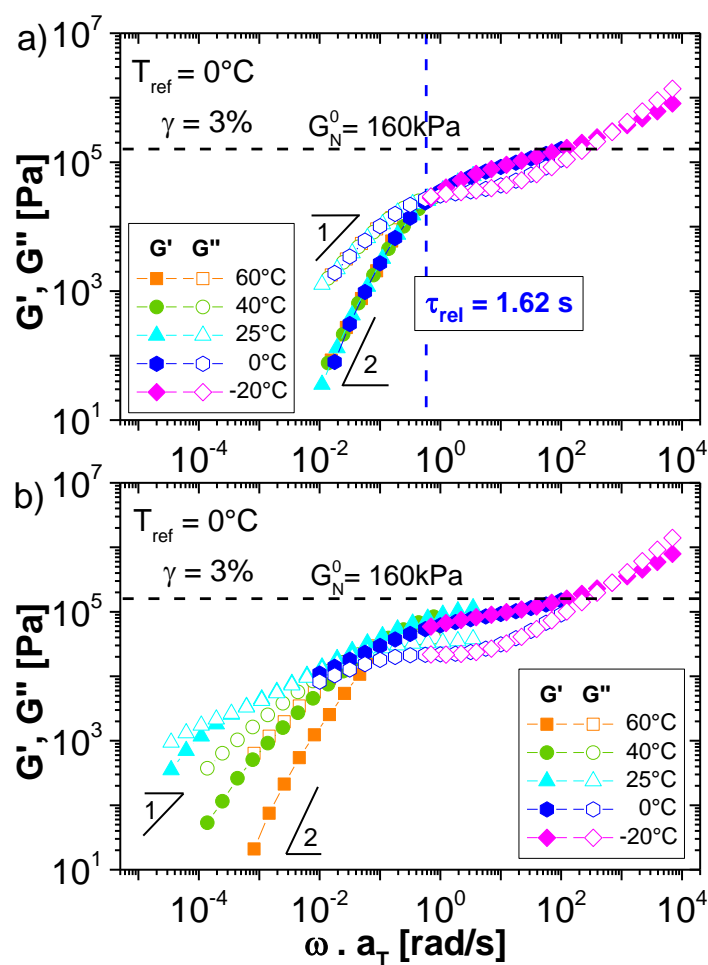

Figure 3.7 G' and G'' Master curves for a) entangled linear P*n*BA-tpy$_2$ (reference) with τ_{rel} = 1.62 s and b) linear entangled P*n*BA-tpy$_2$+Co(II) at T_{ref} = 0°C. The color of experimental curves indicates the temperature at which frequency sweeps in linear regime are performed.
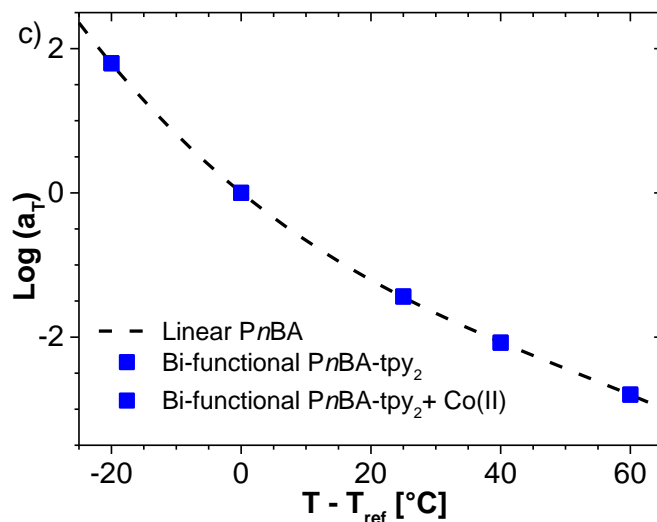
Figure 3.7 c) Horizontal shift factors of Linear P*n*BA (dash line), P*n*BA-tpy$_2$ and P*n*BA-tpy$_2$+Co(II) (symbols) at with T_{ref} = 0°C. The same shift factors are used for P*n*BA-tpy$_2$ with Zn(II) and Ni(II) ions.

Consequently, the probability of a sticker randomly selected to be associated is smaller. Therefore, at a specific time, the supramolecular self-assemblies are, from a statistical point of view, have shorter association lifetime than at lower temperature and relax faster, as observed by the shifting towards higher frequency of the G'-G'' cross-over. But the largest effect of temperature is observed at low frequencies, where it is clear that the influence of temperature is too important to be attributed to changes in chain mobility only. This can be explained by the fact that terminal relaxation corresponds to the relaxation of the longest assemblies, the size of which depends on the lifetime of the stickers. It also depends on the polymer fraction which requires first the dissociation of the stickers in order to be able to relax (such as the polymer loops) and thus, which strongly depends on the sticker lifetime. With increasing temperature, the survival probability of the slow-relaxing assemblies strongly decreases and the second relaxation peak becomes hardly visible. The same trend was observed with the linear P*n*BA-tpy$_2$+Zn(II) and the linear P*n*BA-tpy$_2$+Ni(II) materials as shown in Figure 3.8.
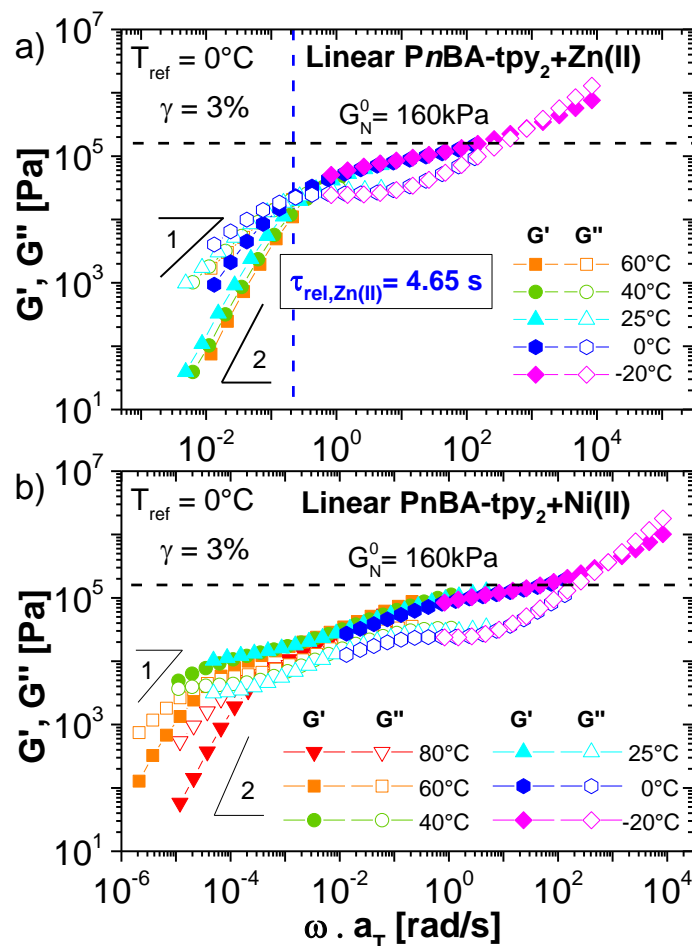
Figure 3.8 G' and G'' Master curves for linear bi-functional a) P*n*BA-tpy$_2$ + Zn(II) with $\tau_{rel,Zn(II)}$ = 4.65 s and b) P*n*BA-tpy$_2$ + Ni(II) at T$_{ref}$ = 0°C using the same shift factors reported above for P*n*BA-tpy$_2$+Co(II). The color of experimental curves indicates the temperature at which frequency sweeps in linear regime are performed.

Thus, by functionalizing each extremity of linear P*n*BA with a terpyridine ligand unit, we have shown that the resulting materials behave differently than mono-functionalized ones, and their dynamics is affected by the nature of transition metal ions. Contribution of associating moieties is underlined and can be distinguished from usual predictions. Their complex viscoelastic behavior seems to come from the combination of two contributions: the reptation of the linear

supramolecular molecular assemblies made of several precursors and the dissociation followed by the relaxation of more complex architectures (such as polymer loops). In order to prevent the possible relaxation of the polymer assemblies before the dissociation of their stickers, polymer topologies containing more than two associating functionalities (f > 2) should be used. This is the topic of the next section.

3.4 Associative PnBAs towards transient networks

3.4.1 Star telechelic associative PnBA-tpy$_4$

To explore the effect of polymer topology on linear viscoelastic properties, four-arm star polymers functionalized with stickers at each chain end are elaborated. Figure 3.9 shows the linear rheological properties at 25°C of tetra-functional PnBA-tpy$_4$ alone and mixed with transition metal ions, added in stoichiometric amount.
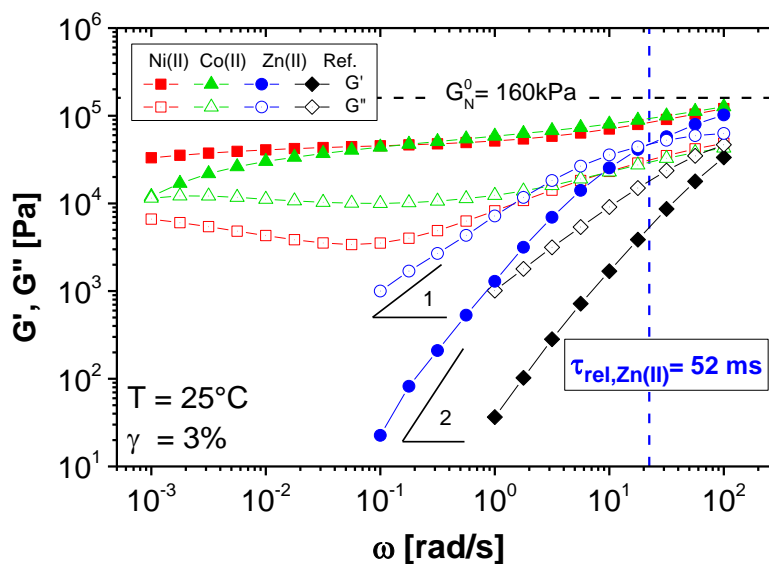

Figure 3.9 Linear rheology curves at 25°C of four-arm star PnBA-tpy$_4$ (melts) with different transition metal ions. The diamonds correspond

to the reference polymer without metal ions. The storage modulus G' is represented by filled symbols, the loss modulus G" by unfilled symbols.

The reference polymer (see Table 3.1) is already in its terminal regime at high frequency and terminal cross-over time is not probed at 25°C. Despite the fact that the star polymer has the same chemical nature and the same molar mass as the investigated linear polymers, the presence of branching point speeds-up the relaxation process. This is due to the fact that the present star polymers have a much shorter end-to-end distance compared to the linear polymers, and contain only few entanglements (2.2) per arm, see Figure 3.10.
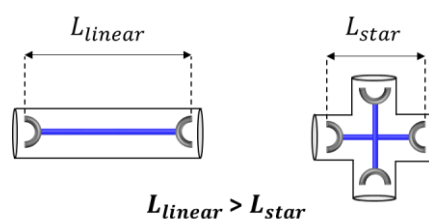

Figure 3.10 Schemic illustration of the molecular length. L is the maximum distance from one edge of the fully extended polymer to the most distant other edge. For the same molar mass a linear polymer has a longer L than a star one.

Therefore, the star polymer can easily relax by contour length fluctuation process,[21,22] and the slowing down of their relaxation due to the suppression of reptation process is largely compensated by the speeding-up of their fluctuations due to the shorter arms.[35,36] Once transition metal ions are added, the resulting polymeric systems behave differently from one ion to the other. In case of Zn(II), the metallo-supramolecular polymer shows the same tendency as the reference material except that the flowing regime is deferred. This delay can now be related to the fact that the stickers at the extremity of the star arms must firstly dissociate in order to allow the arms to relax through fluctuations. Contrary to the mono- or bi-functional linear chains, star arms cannot relax when stickers are attached. Since zinc ions are labile, associating units have only a slight effect on the polymer material properties, and a relaxation time of $\tau_{rel,Zn(II)} = 52$ ms is measured from the modulus cross-over before reaching the terminal relaxation zone. This time, which is longer than the relaxation time of an unassociated

arm, can be seen as a measure of the sticker lifetime. Interestingly, one can observe that the self-assemblies created from the mono-functional P*n*BA-tpy chains relax before this lifetime. While one cannot exclude that the latter have shorter sticker lifetime, it is likely that the difference observed is due to the fact that the chains do not need to dissociate in order to relax, as discussed earlier. On the other hand, the lifetime of the linear assemblies created from bi-functional P*n*BA-tpy$_2$ chains is very similar to the one of the telechelic star chains.

With less labile complexes such as those formed by terpyridines and Co(II) ions, the self-assembled material shows a rubbery plateau spreading over at least four frequency decades. Compared to the reference, this stability in both elastic and viscous moduli suggests the formation of a polymeric network when stable metal ions are added, and confirms the very long lifetime of the related stickers. However, the obtained networks are not idealistic as illustrated in Figure 3.11.a and may contain defects. Indeed, the storage modulus G' decreases slightly from high to intermediate frequencies ($\omega = 100 - 1$ rad/s), meaning that part of the resulting systems is relaxing much faster than expected. This proportion of relaxed polymers might come from the presence of dangling chains, *i.e.* arms that could not form bis-terpyridine complexes and/or from the formation of an intra-loop between two arms of the same star polymer as depicted in Figure 3.11.b.[8]

Dangling ends can be generated either by steric hindrance within the network after addition of metal ions, either by the possible presence of non-functionalized arms during the synthesis or even by a slight difference in stoichiometry among ligand and metal during sample preparation. Hence, this portion of dangling arms and loops can relax easily and does not participate to the polymer network.[37] Then, at low frequency, the cross-over between G', G" is observed, presumably followed by a flow regime. In that sense, the dissociation of metal-ligand complexes is probed, followed by a fluctuation process from chain end to the core to relax the system.[36,38] The large value found for the sticker lifetime also confirms the assumption proposed in the previous section, according to which linear supramolecular assemblies rather relax by reptation than by dissociation, and breaking of the

complexes is only needed for the relaxation of more complex architectures such as polymer loops.
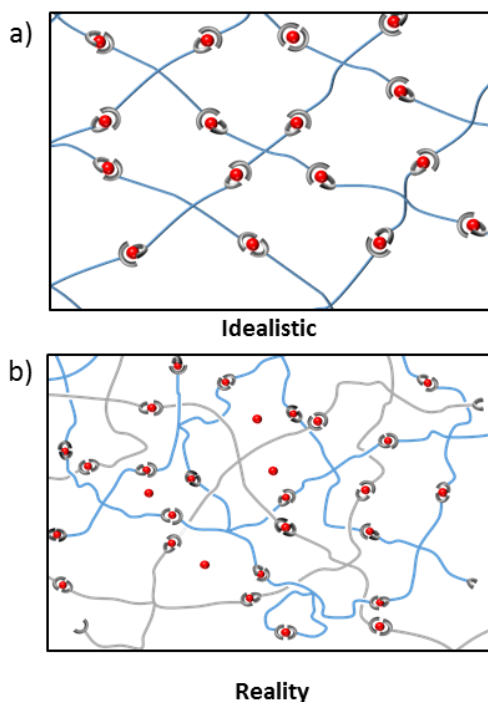

Figure 3.11 Schematic view of ideal and real supramolecular networks obtained from telechelic 4-arm star precursor, highlighting respectively a regular mesh and the presence of dangling chains and loops.

In the presence of much more stable complexes such as those formed by terpyridines and Ni(II) ions, the effect of stickers is even more pronounced with a rubbery plateau spreading over at least five frequency decades. Like four-arm PnBAtpy4+Co(II), a slight decrease in storage modulus at high frequency is still observed. This certifies the existence of dangling chains and/or loops within metallo-supramolecular polymeric networks when cobalt and nickel ions are added. They contribute to the fast relaxation of the materials, independently from one metal ion to another. Then a pronounced plateau modulus of around 40 kPa is obtained and the terminal zone is not reached within the measured frequency range. Despite the presence of dangling ends and loops, the network structure obtained with Ni(II) is stable over a relatively long timescale compared to networks formed with cobalt or zinc. This observation can be related to the fact that stable

nickel bis-terpyridine complexes do not open within the timescale of the measurement. In turn, associated arms cannot relax their tip by arm fluctuations, unless the stickers dissociate.[39] Hence, this shows that transient polymeric networks can be obtained once metal ions are added to four-arm star PnBA-tpy$_4$. As expected, delays in the relaxation times are observed with τ_{rel} shifting to low frequency with zinc, cobalt and presumably nickel ions, even if a terminal relaxation is not probed yet for the latter.

Since there is a higher sticker content in the associating star polymer where on average four hydrophilic terpyridine moieties are incorporated within the hydrophobic molten polymeric matrix, one can suspect the possible formation of aggregates or clusters. In practice, wide-angle X-ray scattering (WAXS) analysis has been performed on 4-arm star PnBA-tpy$_4$ in the presence of transition metal cations (Zn^{2+}, Cu^{2+}, Co^{2+} and Ni^{2+}) and results are shown in Figure 3.12.
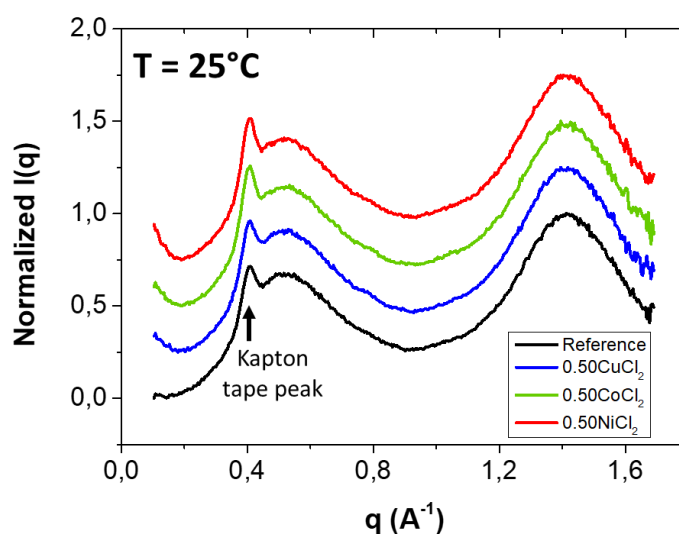
Figure 3.12 Wide angle X-ray scattering of telechelic 4-arm star PnBA-tpy$_4$ with different transition metal ions at 25°C. Only the polymer amorphous halo is probed without any trace of aggregates at nanoscale.

Results from SAXS data display a sharp peak corresponding to the characteristic peak of the Kapton® tape which is used to trap the sample within the sample holder during the measurements. Besides this peak, only the amorphous halo of the poly(n-butyl acrylate) is observed,

suggesting the absence of clusters or aggregates within these metallo-supramolecular bulk polymers.

To conclude, upon self-assembly, the telechelic four-arm star precursors can form stable model transient networks with specific dynamics, which depends on the stickers. These networks are created from the combination of covalent cross-linking nodes originated from the polymer cores, along with dynamic physical bridges, coming from M-L complexes and formed at star arm extremities. In the next section, the possible cumulative effect of stickers positioned along the same polymer backbone is studied, allowing us to show the large versatility of their viscoelastic response. After addition of metal ions, a transient network is formed, only based on physical cross-links.

3.4.2 Linear sticky P*n*BA-*co*-PTPA random copolymer

To investigate the cumulative effect of stickers over the linear viscoelastic properties, a linear sticky P*n*BA-*co*-PTPA copolymer with 15 terpyridine side groups randomly incorporated along the polymer chain has been prepared. Figure 3.13 shows the linear mechanical response at 25°C of this linear sticky copolymer with and without adding zinc(II) or copper(II) cations in stoichiometric amounts. The labile Zn(II) cation and less labile Cu(II) ion have been purposely selected for the shorter lifetime of their supramolecular bonds, which leads to the formation of reversible dynamic networks within the experimental time window. Indeed using M-L interactions with these ions does not lead to the formation of a permanent network or so called frozen network where the moduli G' and G" are frequency independent over a large range.

At 25°C, the reference polymer, i.e. the linear sticky copolymer with no added metal ions relaxes as a conventional linear polymer with 6.1 entanglements. The terminal relaxation time is reached where G' ~ ω^2, G" ~ ω with $\tau_{rel} = 0.58$ s and the latter is relaxing through reptation combined with CLF and CR mechanisms. In presence of labile zinc ions, the resulting linear sticky chains display a rheological trend similar to the one of the reference system but with a longer relaxation

time $\tau_{rel,\ Zn(II)}$ = 8.55 s. This delay is related to the fact that the stickers along the polymer chains have to dissociate in order to allow the trapped segments to relax through reptation process. Furthermore, the fraction of dangling ends (i.e. the molecular segments located between a chain extremity and a first sticker) is relatively low. Therefore, only a small fraction of the polymer chains can relax at short time, before the dissociation of the stickers. This is confirmed by the high value of the storage modulus, close to the rubbery plateau, found at high frequency. So unlike the linear (semi-)telechelic precursors, the stickers along the polymer chains need to dissociate to let the sticky polymer chain to relax. Moreover, the retardation effect of M-L complexes with zinc ions is more pronounced than in the case of mono-functional chains, most probably due to the fact that more than four stickers are incorporated within the polymer, thus enhancing the sticker cumulative effect. Indeed, similarly to the branches in a comb polymer, these stickers act as extra friction points in the reptation of the backbone.
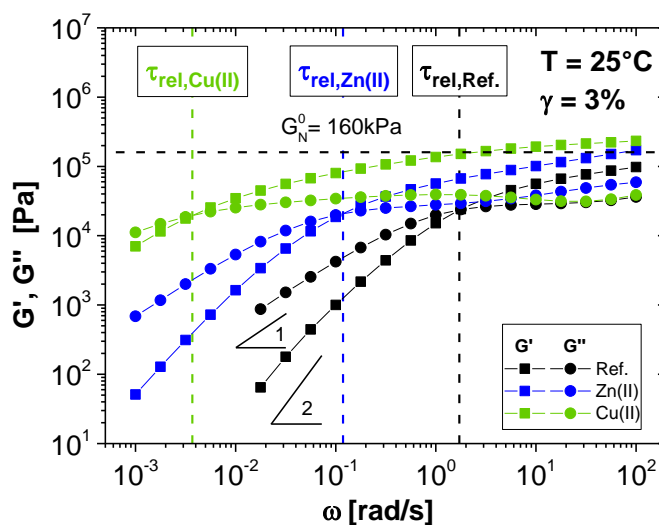
Figure 3.13 Linear rheology curves at 25°C of linear sticky PnBA$_{110k}$-co-PTPA$_{15}$ with zinc(II) ions (circles) and copper (II) ions (pentagons). The diamonds correspond to the reference polymer without metal ions. The storage modulus G' is represented by filled symbols, the loss modulus G" by unfilled symbols. Terminal relaxation times are $\tau_{rel,Ref.}$ = 0.58 s, $\tau_{rel,Zn(II)}$.= 8.55 s and $\tau_{rel,Cu(II)}$ = 270 s.

With intermediately stable bis(terpyridine)-metal complexes such as those formed with copper(II) ions, the self-assembled polymeric network displays a rubbery plateau extending over four frequency decades. Similarly to the telechelic star system, this plateau modulus indicates the formation of a transient network when less labile ions are added. Then the G',G" cross-over is reached with a terminal relaxation time $\tau_{rel, Cu(II)}$ = 270 s. The cross-over frequency decreases with increasing the stability of the metal ions as mentioned earlier.

While most of the chain segments are expected to participate to the entangled network with the telechelic star precursors, it was found that with stoichiometric amount of ions, only a fraction of the arms, around 60 wt%, are effectively trapped into the network (see Chapter 4). In the case of the transient networks originated from linear sticky chains, dangling chain ends or loops could also be present, as illustrated in Figure 3.14.
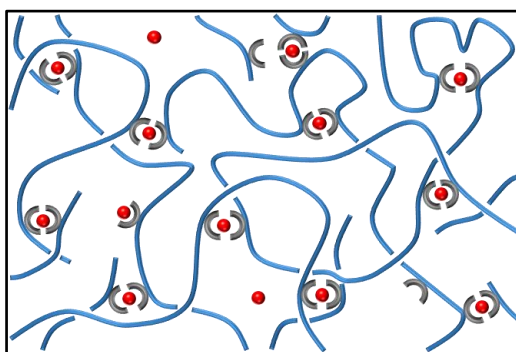

Figure 3.14 Schematic view of the transient network obtained from the linear sticky copolymer, highlighting the presence of network defects such as dangling chains and polymeric loops.
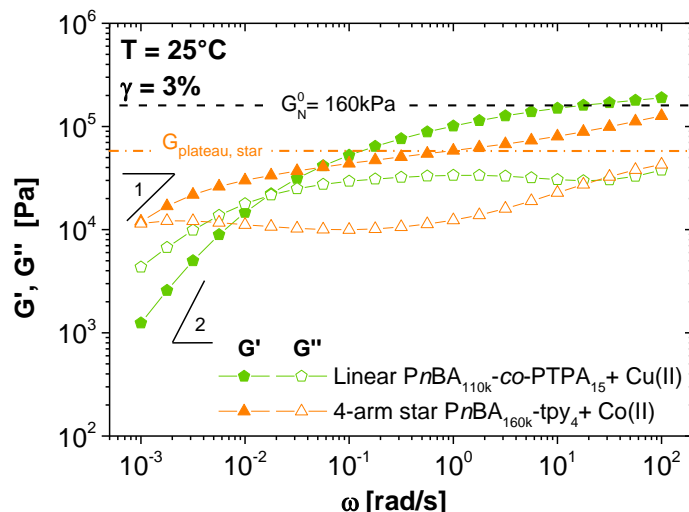
179

Figure 3.15 Linear rheology curves at 25°C of linear sticky PnBA$_{110k}$-*co*-PTPA$_{15}$ + copper (II) ions (pentagons) and 4-arm star PnBA-tpy$_4$ + cobalt(II) ions (triangles). The storage modulus G' is represented by filled symbols, the loss modulus G" by unfilled symbols.

However, it seems that the fraction of dangling ends has less effect on the rheological properties. Indeed, this can be verified when transient networks respectively originating from 4-arm star polymers and from linear sticky copolymers are compared as illustrated in Figure 3.15. The comparison clearly shows that the MSBN obtained from the linear sticky copolymer has a pseudo network modulus (223 kPa) much higher than that of the 4-arm star precursor (5.70 kPa). This can be partially attributed to the larger proportion of metal ions present in the sample (1 per chain of 15 kg/mol rather than 1 per arm of 40 kg/mol). It can also be attributed to the fact that for a free sticker located in the middle of a chain, it has no effect on the trapped chain segment if this free sticker, e.g. sticker B or C represented in Figure 3.16, is located between two other associated stickers. Furthermore, it is observed that the plateau modulus of the associated sticky chains is slightly larger than the entanglement plateau modulus. This indicates that the cross-linking density has increased, including both the entanglements and the sticky groups. This affords more elastically effective chains compared to the telechelic star system or entangled non-functionalized linear chains. Thus, a transient network can be obtained with Cu(II) over a

relatively long timescale by increasing the cross-linking density within the MSBN.

As already mentioned, trapped chain segments between two active stickers cannot relax by reptation unless the stickers dissociate. Depending on the location of associating units and on the position (or generation) of trapped segments within the linear sticky copolymers, the reptation process may vary accordingly where a dependency of one sticker dissociation with respect to another one can play a key-role as suggested by Hawke et al.[19]
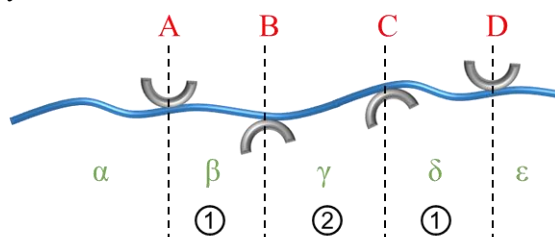

Figure 3.16 Schematic representation of different generations of trapped segments between active stickers. The metal ions and the associations with other polymer chains are not drawn for clarity.

As illustrated in Figure 3.16, one can easily imagine that dangling chain ends (segments α or ε) can easily relax through fluctuations. While the stickers A and D must dissociate to respectively let the first generation of trapped segments β and δ relax, the second generation of trapped segment γ requires that A and B or C and D stickers dissociate in order to allow its relaxation through 'sticky CLF'. Since the probability that two (or more) consecutive stickers are free simultaneously is very small, such CLF process is expected to be much slower than the relaxation of the reference sample. As the number of generation increases, the complete relaxation of its corresponding trapped segments through this process becomes more and more dependent on the sticker dissociation dynamics. On the other, the chain can also relax through reptative motion, at the rhythm of the association/dissociation of the stickers, in a similar way as defined by the sticky reptation model.[40] But these reptation modes are also very slow since each sticker adds extra friction to the chain diffusion. The relative importance of these two relaxation mechanisms should depend on the number and density of stickers along the chain as well as on the

length of the chain. This slow dynamics dominated by the sticker association/dissociation explains why a stable transient network can be obtained once copper metal ions are added to the linear sticky PnBA-co-PTPA copolymer bearing 15 tpy moieties.

Then, linear rheology of these polymers was investigated over a range of temperatures (from −20 to 100°C). Master curves were constructed by setting the reference temperature at 0°C for all bulk materials, and by applying the time−temperature superposition (TTS) principle with the same shift factors reported in Figure 3.7, based on the reference polymer without metal ions. For this polymer, superposition of the viscoelastic moduli fits well, as illustrated in Figure 3.17. Whereas for transient networks, curves cannot be reduced into a well-fitted master curve, highlighting once again the thermo-rheological complexity of these associating polymers.
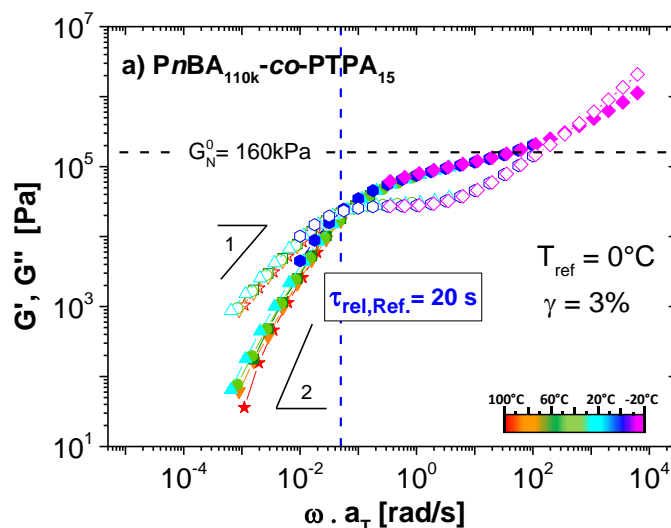

Figure 3.17 G' (■) and G'' (●) Master curves for linear sticky a) PnBA-co-PTPA (reference) at T_{ref} = 0°C. The color of experimental curves indicates the temperature at which frequency sweeps in linear regime are performed.

182
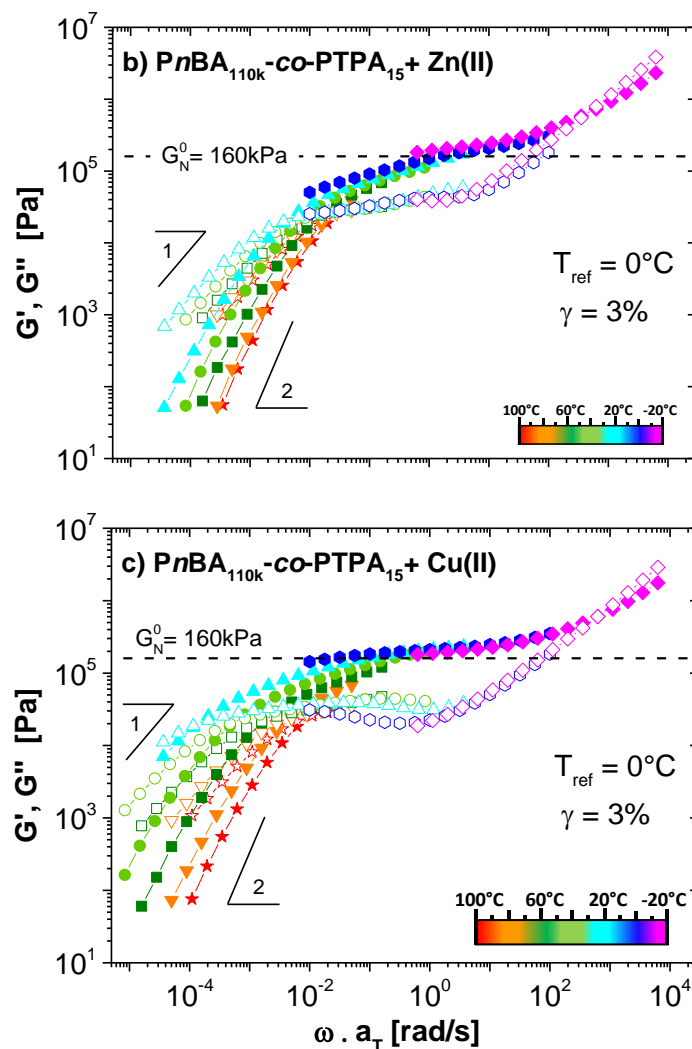
Figure 3.17 G' (■) and G'' (●) Master curves for linear sticky b) P*n*BA-*co*-PTPA + Zn(II) and c) P*n*BA-*co*-PTPA + Cu(II) at T_{ref} = 0°C. The color of experimental curves indicates the temperature at which frequency sweeps in linear regime are performed.

Interestingly, the comparison of the linear sticky precursor with the linear telechelic system (Figure 3.18) in absence of metal ions, shows that the former displays a longer relaxation time (τ_{rel} = 0.58 s) with respect to the linear telechelic system (τ_{rel} = 45 ms). Since both samples have almost the same molar mass and almost the same number

of entanglements (110 kg/mol with 6.1 entanglements for linear sticky and 113 kg/mol with 6.7 entanglements for linear bi-functional), one should expect that they display similar rheological trend but it is not the case.
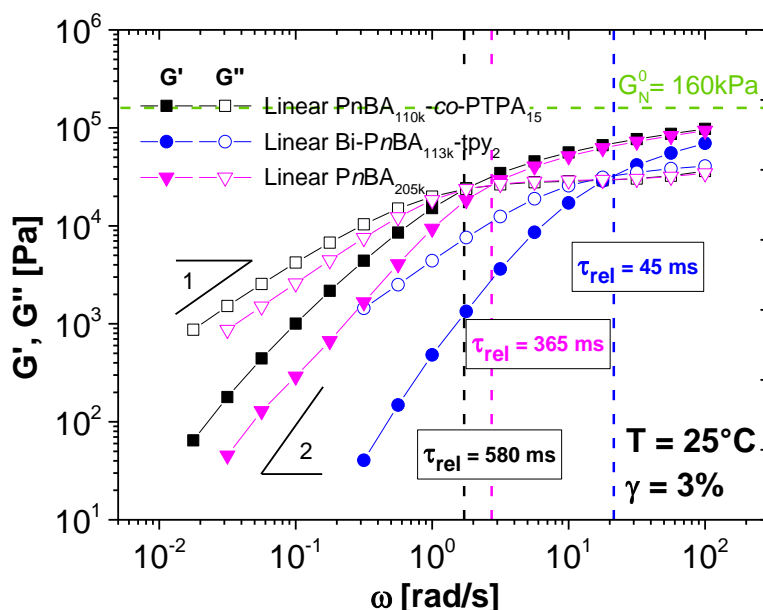
Figure 3.18 Comparison of linear poly(*n*-butyl acrylate)s, and linear sticky poly(*n*-butyl acrylate)-*co*-poly(terpyridine acrylate) random copolymer at T = 25°C.

From Figure 3.18, it appears that the reference linear sticky P*n*BA-*co*-PTPA behaves similarly to a classical linear P*n*BA with a molar mass of 205 kg/mol from high to intermediate frequency ($\omega = 100 - 3$ rad/s). Then in this intermediate frequency range, we can observe that the moduli of the sticky copolymer are higher than the moduli of the linear P*n*BA, indicating that a fraction of the linear sticky chains relaxes slowly. This slow relaxation at low frequency can be attributed to a possible formation of aggregates of clusters because a higher content of sticker (~ 5 wt%) is present within the polymeric matrix. However, the absence of aggregate is further confirmed by WAXS and SAXS measurements as illustrated in Figure 3.19. Similarly to the telechelic star component, only a peak belonging to the Kapton® is observed along with the polymer amorphous halo.

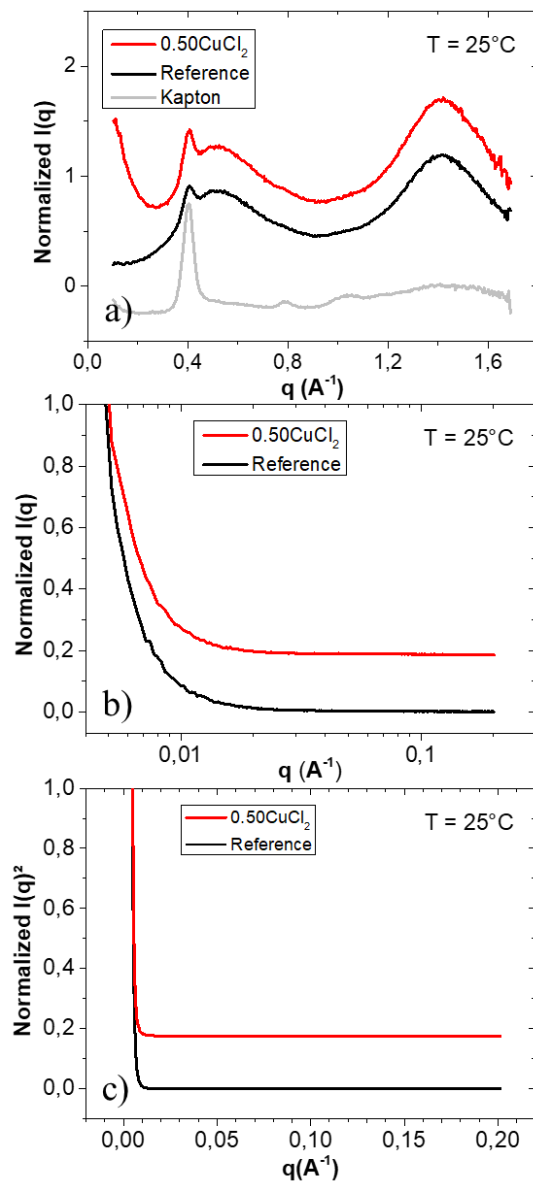**Figure 3.19** a) Wide, b) and c) Small angle X-ray scattering of linear sticky P*n*BA-*co*-PTPA with and without copper(II) ions. Only the polymer amorphous halo is probed without any trace of aggregates at nanoscale.

From WAXS data, one may suggest that the onset of a peak belonging to the aggregates might be probed when the lowest scattering vector (q ~ 0.2 Å^{-1}) is reached. This is why additional SAXS measurement has been performed on the same sample and the results clearly reveal the absence of any peak, suggesting that there is no formation of clusters within the linear sticky copolymer. Hence from X-ray scattering analysis, the slow relaxation of the linear sticky copolymer cannot be attributed to the formation of aggregates. Another plausible explanation for this slow relaxation could be the π-π stacking interactions between electron deficient aromatic rings of the terpyridine ligand. As suggested by Huang et al., terpyridine molecules can indeed form different π-stacking patterns as illustrated in Figure 3.20.[41]
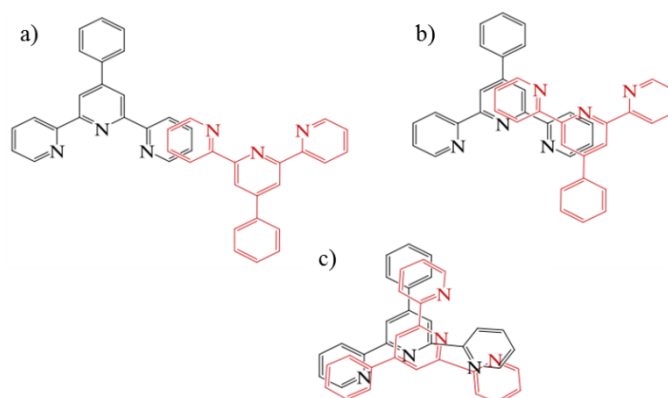
Figure 3.20 Different π-stacking configurations within the 2,2':6',2"-terpyridine ligands showing that π-π interactions may lead to stable structure.[41]

Since ~ 5 wt% of terpyridine ligand are incorporated corresponding to 15 stickers randomly attached on the polymer chain, these stickers may display π-π stacking interactions. Hence, those interactions can lead to the formation of extended polymeric structures in absence of metal ions. This can explain why the linear sticky copolymer does not have the same behavior as the linear telechelic sample, even though they have the similar molecular weight. Instead, the linear sticky sample rather behaves as a linear polymer with a higher molar mass of 205 kg/mol and it has a slower relaxation process at low frequency which is probably due to π-π interactions.

3.5   Conclusions

Well-defined structures and well-controlled molar mass poly(*n*-butyl acrylate)s functionalized with the terpyridine ligand at chain extremities or along the polymer chain were obtained and exploited to elaborate entangled metallo-supramolecular bulk polymers (MSBPs) in presence of metal ions. Their linear viscoelastic properties were then characterized in presence of different transition metal ions: Zn(II), Cu(II), Co(II) and Ni(II). By varying the topology of polymeric building blocks, self-assembled materials with different structures were achieved. In the case of linear mono-functional P*n*BA-tpy, chain length extension occurred when metal ions were added. The chains mainly relaxed as relatively stable assemblies and their viscoelasticity was close to Maxwell predictions. Hence, τ_{rel} was often shifted to low frequency. On the other hand, stickers effect was even more emphasized with linear telechelic P*n*BA-tpy$_2$ system. Their complex viscoelastic behavior came from the combination of the reptation of the linear supramolecular molecular assemblies and the dissociation of stickers followed by the relaxation of more complex architectures such as polymer loops resulting in the presence of a second plateau modulus and an increase in modulus (G', G"). By controlling the number of chain ends, stickers' contribution on the system properties was clearly distinguished from usual predictions. Four-arm star polymers self-assembled into transient polymeric networks in presence of metal ions. Networks were established by the combination of covalent cross-linking nodes, which came from the polymer cores, along with dynamic physical bridges, which originated from metal-ligand complexes formed at star arm extremities. When metal-ligand complexes were relatively stable, a rubbery plateau was obtained over frequency decades due to an increase in cross-linking density confirming the very long lifetime of stickers. The star arm extremities must, first, dissociate, in order to allow the arms to relax through fluctuations. Hence, the resulting entangled bulk materials were able to behave as soft solids over a large frequency range. Last but not least, linear sticky precursors can also lead to elaboration of transient networks based only on physical cross-links. The latter showed that the possible network defects have little influence on the elastic plateau of these samples, being

compensated by the increased number of incorporated stickers within the polymer, and their larger cumulative effect. Consequently, the resulting reversible network has a higher cross-linking density where most of the chains participate to the elasticity of the network upon addition of metal ions. Moreover, the different generations of trapped segments along the chain force the chains to move and disentangle and the rhythm of their dissociation/association dynamics. These two parameters allowed the formation of a transient metallo-supramolecular network over a large frequency range by using less stable metal ions.

This study provides a better understanding of rheological properties of entangled MSBPs. Incorporation of terminal active stickers on polymers shows that viscoelastic properties can be finely tailored by varying polymer topologies, the position of the sticker within the polymeric matrix as well as the type of metal ion. Self-assembled supramolecular linear chains relax rather by reptation than by stickers dissociation, whereas breaking of metal-ligand complexes is first required for associating star systems, linear sticky copolymers or for polymer loops in order to relax. Hence, a toolkit of associating soft materials has been successfully established and it can be transposed towards potential applications with unique features such as healing[42,43] or shape-memory[44] materials, where a precise control over the molecular structure and properties is necessary. In fact, depending on the desired viscoelastic properties for a material, one can simply select one of the polymeric precursor and one type of transition metal ions. For example, the architecture of a four-arm star precursor mixed with cobalt or nickel ions can be used to form soft elastic solids. Table 3.2 summarizes the viscoelastic parameters of metallo-supramolecular bulk polymers at 25°C. Note that the influence of temperature on the viscoelastic properties of MSBPs is also investigated. Therefore, one can also select the polymeric precursor and the metal ion of interests as function of the temperature as well.

	System	$Z=M_n/M_e$	Metal ion	G' at ω = 10rad/s	G'' at ω = 10rad/s	τ_{rel}	Modulus at G'=G''	Material state
L	Mono PnBA-tpy	5.6	-	8.42×10^3 Pa	1.89×10^3 Pa	29ms	3.46×10^4 Pa	VF
I	Mono PnBA-tpy	5.6	Zn^{2+}	1.36×10^4 Pa	2.43×10^4 Pa	43ms	3.46×10^4 Pa	VF
	Mono PnBA-tpy	5.6	Cu^{2+}	2.27×10^4 Pa	2.63×10^4 Pa	73ms	2.89×10^4 Pa	VF
	Mono PnBA-tpy	5.6	Co^{2+}	3.03×10^4 Pa	2.95×10^4 Pa	107ms	2.90×10^4 Pa	VF
	Mono PnBA-tpy	5.6	Ni^{2+}	3.60×10^4 Pa	2.94×10^4 Pa	191ms	2.41×10^4 Pa	VF
N	Bi-PnBAtpy$_2$	7.8	-	1.71×10^4 Pa	2.57×10^4 Pa	45ms	3.17×10^4 Pa	VF
E	Bi-PnBAtpy$_2$	7.8	Zn^{2+}	3.03×10^4 Pa	2.67×10^4 Pa	134ms	2.53×10^4 Pa	VF
A	Bi-PnBAtpy$_2$	7.8	Co^{2+}	6.63×10^4 Pa	3.23×10^4 Pa	80s	3.059×10^3 Pa	VM
R	Bi-PnBAtpy$_2$	7.8	Ni^{2+}	8.55×10^4 Pa	2.88×10^4 Pa	-	-	ES
	PnBA-co-PTA$_{15}$	6.1	-	5.60×10^4 Pa	2.85×10^4 Pa	580ms	2.37×10^4 Pa	VM
	PnBA-co-PTA$_{15}$	6.1	Zn^{2+}	10.09×10^4 Pa	3.82×10^4 Pa	8.55s	2.07×10^4 Pa	VM
	PnBA-co-PTA$_{15}$	6.1	Cu^{2+}	19.28×10^4 Pa	3.32×10^4 Pa	270s	1.93×10^4 Pa	ES
S	Star PnBA-tpy$_4$	2.2/arm	-	1.63×10^3 Pa	8.66×10^3 Pa	<30ms	-	VF
T	Star PnBA-tpy$_4$	2.2/arm	Zn^{2+}	2.24×10^4 Pa	2.98×10^4 Pa	52ms	3.63×10^4 Pa	VF
A	Star PnBA-tpy$_4$	2.2/arm	Co^{2+}	8.02×10^4 Pa	2.28×10^4 Pa	-	-	ES
R	Star PnBA-tpy$_4$	2.2/arm	Ni^{2+}	7.05×10^4 Pa	2.31×10^4 Pa	-	-	ES

Table 3.2 Experimental linear viscoelastic parameters of metallo-supramolecular bulk polymers with different transition metal ions at 25°C.

189

Bibliography

(1)   Brassinne, J.; Zhuge, F.; Fustin, C.-A.; Gohy, J.-F. Precise Control over the Rheological Behavior of Associating Stimuli-Responsive Block Copolymer Gels. *Gels* **2015**, *1*, 235–255.

(2)   Callies, X.; Véchambre, C.; Fonteneau, C.; Pensec, S.; Chenal, J.-M.; Chazeau, L.; Bouteiller, L.; Ducouret, G.; Creton, C. Linear Rheology of Supramolecular Polymers Center-Functionalized with Strong Stickers. *Macromolecules* **2015**, *48*, 7320–7326.

(3)   Hentschel, J.; Kushner, A. M.; Ziller, J.; Guan, Z. Self-Healing Supramolecular Block Copolymers. *Angew. Chemie - Int. Ed.* **2012**, *51*, 10561–10565.

(4)   Potier, F.; Guinault, A.; Delalande, S.; Sanchez, C.; Ribot, F.; Rozes, L. Nano-Building Block Based-Hybrid Organic–inorganic Copolymers with Self-Healing Properties. *Polym. Chem.* **2014**, *5*, 4474–4479.

(5)   Enke, M.; Bode, S.; Vitz, J.; Schacher, F. H.; Harrington, M. J.; Hager, M. D.; Schubert, U. S. Self-Healing Response in Supramolecular Polymers Based on Reversible Zinc-Histidine Interactions. *Polymer (Guildf).* **2015**, *69*, 274–282.

(6)   Hart, L. R.; Nguyen, N. A.; Harries, J. L.; Mackay, M. E.; Colquhoun, H. M.; Hayes, W. Perylene as an Electron-Rich Moiety in Healable, Complementary ??-?? Stacked, Supramolecular Polymer Systems. *Polymer (Guildf).* **2014**, *69*, 293–300.

(7)   Hart, L. R.; Hunter, J. H.; Nguyen, N. A.; Harries, J. L.; Greenland, B. W.; Mackay, M. E.; Colquhoun, H. M.; Hayes, W. Multivalency in Healable Supramolecular Polymers: The Effect of Supramolecular Cross-Link Density on the Mechanical Properties and Healing of Non-Covalent Polymer Networks. *Polym. Chem.* **2014**, *5*, 3680–3688.

(8)   Seiffert, S.; Sprakel, J. Physical Chemistry of Supramolecular Polymer Networks. *Chem. Soc. Rev.* **2012**, *41*, 909–930.

(9)   Brassinne, J.; Gohy, J.-F.; Fustin, C.-A. Controlling the Cross-Linking Density of Supramolecular Hydrogels Formed by Heterotelechelic Associating Copolymers. *Macromolecules* **2014**, *47*, 4514–4524.

(10)   Steed, J. W.; Atwood, J. L. *Supramolecular Chemistry.*, 2nd ed.; Wiley, 2009; Vol. 260.

(11)   Ressouche, E.; Pensec, S.; Isare, B.; Ducouret, G.; Bouteiller, L. Rational Design of Urea-Based Two-Component Organogelators. *ACS Macro Lett.* **2016**, *5*, 244–247.

(12)   Balkenende, D. W. R.; Coulibaly, S.; Balog, S.; Simon, Y. C.; Fiore, G. L.; Weder, C. Mechanochemistry with Metallosupramolecular Polymers. *J. Am. Chem. Soc.* **2014**, *136*, 10493–10498.

(13)   Seiffert, S. Effect of Supramolecular Interchain Sticking on the Low-Frequency Relaxation of Transient Polymer Networks. *Macromol. Rapid Commun.* **2016**, *37*, 257–264.

(14)   Yan, T.; Schröter, K.; Herbst, F.; Binder, W. H.; Thurn-Albrecht, T. Nanostructure and Rheology of Hydrogen-Bonding Telechelic

Polymers in the Melt: From Micellar Liquids and Solids to Supramolecular Gels. *Macromolecules* **2014**, *47*, 2122–2130.

(15)   Schmatloch, S.; Schubert, U. S. Engineering with Metallo-Supramolecular Polymers: Linear Coordination Polymers and Networks. *Macromol. Symp.* **2003**, *199*, 483–497.

(16)   Wang, R.; Geven, M.; Dijkstra, P. J.; Martens, P.; Karperien, M. Hydrogels by Supramolecular Crosslinking of Terpyridine End Group Functionalized 8-Arm Poly(Ethylene Glycol). *Soft Matter* **2014**, *10*, 7328–7336.

(17)   Mark, J. E. *Physical Properties of Polymers Handbook*, 2nd ed.; Springer: New York, 2007.

(18)   Constable, E. C. 2,2':6',2''-Terpyridines: From Chemical Obscurity To Common Supramolecular Motifs. *Chem. Soc. Rev.* **2007**, *36*, 246–253.

(19)   Hawke, L. G. D.; Ahmadi, M.; Gondansaz, H.; van Ruymbeke, E. Viscoelastic Properties of Linear Associating Poly(n-Butyl Acrylate) Chains. *J. Rheol. (N. Y. N. Y).* **2016**, *60*, 297–310.

(20)   Holyer, R. H.; Hubbard, C. D.; Kettle, S. F. a; Wilkins, R. G. The Kinetics of Replacement Reactions of Complexes of the Transition Metals with 2,2',2"-Terpyridine. *Inorg. Chem.* **1966**, *5*, 622–625.

(21)   Taylor, P.; Mcleish, T. C. B. Tube Theory of Entangled Polymer Dynamics. *Adv. Phys.* **2002**, *51*, 1379–1527.

(22)   Doi, M.; Edwards, S. F. *The Theory of Polymer Dynamics*; Oxford University Press, 1986.

(23)   Dobrawa, R.; Würthner, F. Metallosupramolecular Approach toward Functional Coordination Polymers. *J. Polym. Sci. Part A Polym. Chem.* **2005**, *43*, 4981–4995.

(24)   Watanabe, H. Viscoelasticity and Dynamics of Entangled Polymers. *Prog. Polym. Sci.* **1999**, *24*, 1253–1403.

(25)   Vlassopoulos, D.; Pitsikalis, M.; Hadjichristidis, N. Linear Dynamics of End-Functionalized Polymer Melts: Linear Chains, Stars, and Blends. *Macromolecules* **2000**, *33*, 9740–9746.

(26)   Wang, Z.; Fan, W.; Tong, R.; Lu, X.; Xia, H. Thermal-Healable and Shape Memory Metallosupramolecular Poly(n-Butyl Acrylate-Co-Methyl Methacrylate) Materials. *RSC Adv.* **2014**, *4*, 25486.

(27)   van Ruymbeke, E.; Vlassopoulos, D.; Mierzwa, M.; Pakula, T.; Charalabidis, D.; Pitsikalis, M.; Hadjichristidis, N. Rheology and Structure of Entangled Telechelic Linear and Star Polyisoprene Melts. *Macromolecules* **2010**, *43*, 4401–4411.

(28)   Hackelbusch, S.; Rossow, T.; Assenbergh, P. van.; Seiffert, S. Chain Dynamics in Supramolecular Polymer Networks. *Macromolecules* **2013**, *46*, 6273–6286.

(29)   Kwon, Y.; Matsumiya, Y.; Watanabe, H. Viscoelastic and Orientational Relaxation of Linear and Ring Rouse Chains Undergoing Reversible End-Association and Dissociation. *Macromolecules* **2016**, *49*, 3593–3607.

(30)   Watanabe, H.; Matsumiya, Y.; Masubuchi, Y.; Urakawa, O.; Inoue, T. Viscoelastic Relaxation of Rouse Chains Undergoing Head-to-Head

Association and Dissociation: Motional Coupling through Chemical Equilibrium. *Macromolecules* **2015**, *48*, 3014–3030.

(31) Cates, M. E. Reptation of Living Polymers: Dynamics of Entangled Polymers in the Presence of Reversible Chain-Scission Reactions. *Macromolecules* **1987**, *20*, 2289–2296.

(32) Read, D. J.; Jagannathan, K.; Sukumaran, S. K.; Auhl, D. W. A Full-Chain Constitutive Model for Bidisperse Blends of Linear Polymers. *J. Rheol. (N. Y. N. Y)*. **2012**, *56*, 823–873.

(33) Ferry, J. D.; Child, W. C. J.; Zand, R.; Stem, D. M.; Wiuiams, M. L.; Landel, R. F. Dynamic Mechanical Properties of Polyethyl Methacrylate. *J. Colloid Sci.* **1957**, *12*, 53–67.

(34) Child, W. C. J.; Ferry, J. D. Dynamic Mechanical Properties of Poly-n-Butyl Methacrylate. *J. Colloid Sci.* **1957**, *12*, 327–341.

(35) Dealy, J. M.; Larson, R. G. *Structure and Rheology of Molten Polymers*; Hanser, 2006.

(36) Fetters, L. J.; Kiss, A. D.; Pearson, D. S.; Quack, G. F.; Vitus, F. J. Rheological Behavior of Star-Shaped Polymers. *Macromolecules* **1993**, *26*, 647–654.

(37) Xu, D.; Hawk, J. L.; Loveless, D. M.; Jeon, S. L.; Craig, S. L. Mechanism of Shear Thickening in Reversibly Cross-Linked Supramolecular Polymer Networks. *Macromolecules* **2010**, *43*, 3556–3565.

(38) McLeish, T. C. B.; Milner, S. T. *Entangled Dynamics and Melt Flow of Branched Polymers*; Springer, 1999.

(39) Xu, D.; Craig, S. L. Scaling Laws in Supramolecular Polymer Networks. *Macromolecules* **2011**, *44*, 5465–5472.

(40) Rubinstein, M.; Semenov, A. N. Dynamics of Entangled Solutions of Associating Polymers. *Macromolecules* **2001**, *34*, 1058–1068.

(41) Huang, T. H.; Zhang, M. H.; Gao, C. Y.; Wang, L. T. Synthesis, Structures and Characterization of Metal Complexes Containing 4′-Phenyl-2,2′:6′,2″-Terpyridine Ligands with Extended ΠΠ Interactions. *Inorganica Chim. Acta* **2013**, *408*, 91–95.

(42) Bode, S.; Bose, R. K.; Matthes, S.; Ehrhardt, M.; Seifert, A.; Schacher, F. H.; Paulus, R. M.; Stumpf, S.; Sandmann, B.; Vitz, J.; et al. Self-Healing Metallopolymers Based on Cadmium Bis(Terpyridine) Complex Containing Polymer Networks. *Polym. Chem.* **2013**, *4*, 4966–4973.

(43) Burnworth, M.; Tang, L.; Kumpfer, J. R.; Duncan, A. J.; Beyer, F. L.; Fiore, G. L.; Rowan, S. J.; Weder, C. Optically Healable Supramolecular Polymers. *Nature* **2011**, *472*, 334–337.

(44) Kumpfer, J. R.; Rowan, S. J. Thermo-, Photo-, and Chemo-Responsive Shape-Memory Properties from Photo-Cross-Linked Metallo-Supramolecular Polymers. *J. Am. Chem. Soc.* **2011**, *133*, 12866–12874.

Chapter 4

Decoding the linear viscoelastic properties of MSBPs

Abstract

This Chapter focuses on the linear viscoelastic properties of entangled telechelic bulk metallo-supramolecular polymers. The latter are based on linear and star poly(*n*-butyl acrylate)s functionalized with a terpyridine ligand at each chain extremity, in presence of transition metal ion of varying nature. The systems are investigated both experimentally and theoretically using small amplitude oscillatory shear (SAOS) and a modified version of the tube-based time marching algorithm (TMA) respectively. The experimental data reveal that sample relaxation depends on both disentanglement and association dynamics, with the respective importance of these two processes depending on the nature of the metal ion and on the temperature. A good description of the data is achieved using the modified TMA model, provided that dissociation events of metal-ligand complexes occur via ligand exchange. The model contains two fitting parameters, i.e. the fraction of unassociated stickers and the longest time needed in order to ensure that all the chains were dissociated at least once. This latter time is found to be independent of the chain architecture and is well described by an Arrhenius equation, which allows to derive the related activation energy. This work provides the necessary framework to explore other metallo-supramolecular networks, built from different chain architectures, and exploit the large richness of their dynamics.

4.1 Introduction

4.1.1 Supramolecular polymers

Supramolecular polymers based on reversible physical associations form an interesting class of materials because of the richness in their tailorable properties compared to their non-associating counterparts. Noncovalent bonds such as $\pi-\pi$ stacking[1], hydrogen bonding[2], ionic interactions[3,4] or metal$-$ligand complexes[5] are sensitive to stimuli such as pH, irradiation, temperature or mechanical forces and their reversibility provides unique features such as healing[6,7], mechano-sensitive and shape-memory properties.[8,9] Supramolecular polymers have potential applications in various domains where a precise control over the molecular structure and properties is necessary such as drug delivery[10], tissue engineering[11], coatings[12], adhesives[13] and shock absorbers[14]. Regardless of the final application, the possible industrial exploitation of the transient nature hinges on the rheological behavior and resulting processability. In this respect, the design of adaptable materials of supramolecular polymers is dependent on our fundamental understanding of their structure and dynamics in the melt state. The latter are not only determined by the association/dissociation events of the transient interactions but they are also governed by the internal dynamics of the building blocks (entanglements). Therefore, the influence of these two processes on the rheological properties and how they interact need to be addressed and understood.

4.1.2 Theoretical models for associating polymers

Theoretical models on associating polymers have been mostly focused on static properties, in particular the sol$-$gel transition, the aggregation of associating groups or the flower-like micelles bridged by flexible polymer chains.[15–18] Semenov and Rubinstein have developed a sticky Rouse model for unentangled polymers with many pairwise associating units per chain and considering that a sticker goes through many association and dissociation events with its old partner

before finding a new sticker partner to associate with.[19] The sticky reptation model has been established to extend this idea to entangled associating polymers with many regularly spaced stickers in which polymer chains go through sticky Rouse motion along the confined tube to relax the stress.[20] Bedrov et al. performed standard molecular dynamic simulations of unentangled telechelic polymer solutions where associating groups are able to aggregate and form interlinked micellar clusters.[21] The stress relaxation in these systems was described as a two-step mechanism. First, a decay due to the translational motion or positional rearrangement of the end-groups inside their aggregates, and second by the fast hopping diffusion of end-groups between one micellar cluster into another one, which is then followed by the terminal relaxation due to cluster disintegration. Wang et al. studied the dynamics and rheology of unentangled telechelic polymer networks in which stickers with finite functionality are able to form interconnected clusters.[22] Their predictions revealed that the stress relaxation of such systems is governed by the partner exchange process rather than the single sticker hopping mechanism. The partner (ligand) exchange process offers the stickers the possibility to bind to another partner in a new cluster without breaking all the sticky bonds formed in the initial cluster.

In the aforementioned studies, the simulations are essentially focused on unentangled associating systems or supramolecular polymers in solution. Furthermore, the polymeric spacers in between the stickers are relatively short and the content of stickers is relatively high. Hence, in this type of systems, the attention focuses on the aggregate/cluster formation. On the contrary, when the spacers between stickers are long enough, the amount of incorporated associating moieties becomes minor compared to the polymer matrix, and the sticker density becomes negligible compared to the density of entanglements. As a result, aggregation and/or cluster formation is less pronounced and the associated domains can be seen as physical cross-linking points for the entangled chains. Theoretical models to explain the rheological properties and dynamics of such entangled telechelic systems are scarce.[23,24] One of the objectives of this work is to provide such a theoretical contribution, based on model polymers. In particular, this requires using telechelic chains characterized by pair-wise

supramolecular interactions, in order to avoid the formation of large, ill-defined aggregates. It also requires selecting a polymer which can be studied under a large range of temperatures in order to have access to its full dynamics and to have many possibilities to vary the association strength of the reversible bonds.

Here, we report on the investigation of the linear viscoelastic properties of entangled telechelic polymers based on linear and star poly(*n*-butyl acrylate) P*n*BA that we synthesized and functionalized with a terpyridine (tpy) ligand (a pairwise sticker) at each chain extremity. Once transition metal ions are added, metal-ligand coordination occurs to form bis-terpyridine complexes which play the role of transient junctions between the polymer chains.[25] Depending on the architecture of the polymer, rheological data show that the effect of stickers is the retardation of terminal relaxation by several orders of magnitude. Since the reference samples have a large molar mass and only contain the ligands at their extremities, the weight proportion of terpyridine in the samples is very low, ranging from 0.3 to 0.8 wt%. Therefore, for all samples, the level of the plateau modulus stays governed by the entanglements density. Another consequence of this low density of ligands is the fact that we do not expect the formation of aggregates or large clusters of terpyridine due to phase separation, as it was observed for example in the work of Jackson et al.[26] The absence of aggregate was further confirmed by WAXS measurement.

A refined version of the time marching algorithm (TMA) is developed to describe the experimental rheological properties. Model predictions are compared to systematic experimental data obtained from small angle oscillatory shear (SAOS) measurements and results are presented herein. The rest of this chapter is organized as follows. In section 4.2 the experimental procedures to synthesize and characterize the associating polymeric models are summarized. Section 4.3.1 presents the assumptions made and the additional parameters applied to TMA. The refined TMA for entangled sticky polymers is described in section 4.3.2. Model predictions on the dynamic and rheological properties of entangled telechelic polymers are presented and discussed in section 4.4. The conclusions are drawn in section 4.5.

4.2 Materials and experimental

4.2.1 Materials

The synthesis of the linear (M_n = 101 kg/mol and M_n = 142 kg/mol) and four-arm star (M_n = 160 kg/mol and M_n = 249 kg/mol) poly(n-butyl acrylate)s end-functionalized with terpyridine ligand (PnBA-tpy$_x$) was achieved by reversible addition-fragmentation chain-transfer (RAFT) polymerization in bulk condition as explained in Chapter 2. Details on the precursor samples are given in Table 4.1.

a) Linear mono-functional PnBA-tpy

b) Four-arm telechelic star PnBA-tpy$_4$
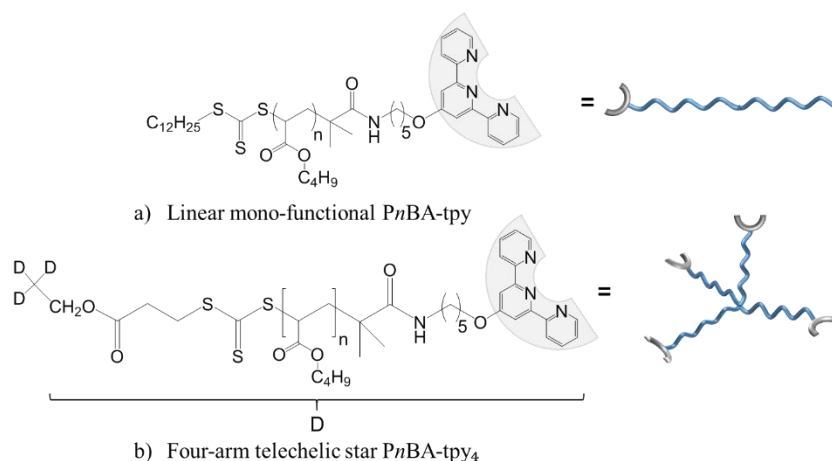
Samples	$M_{n, system}$[a] (kg/mol)	$M_{n, arm}$[b] (kg/mol)	$Z=M_n/M_e$[c]	Đ[d]
Lin100k	101	/	5.6	1.14
Lin140k	142	/	7.8	1.14
Star160k	160	40	2.2 per arm	1.25
Star250k	249	62	3.4 per arm	1.20

Table 4.1 Structural parameters of PnBA polymers functionalized with terpyridine ligand at chain extremity. [a,b] Molar mass of whole system determined by ^{1}H-NMR. [c] Number of entanglements calculated using

M_e = 18 kg/mol. [d] Molar mass dispersity of the polymers determined by SEC, polystyrene standards were used for calibration.

4.2.2 Sample nomenclature

All samples are prepared at stoichiometric conditions to promote the formation of complexes made by one metal ion coordinated by two terpyridine ligands. Terpyridine moieties and trithiocarbonate functions are thermodynamically stable (during and after measurement) within the temperature range of the investigation. A list of samples is reported in Table 4.2.

Annotation	Description
Lin100k+Zn	Linear Mono- PnBA$_{788}$-tpy + 0.5 eq. ZnCl$_2$
Lin100k+Cu	Linear Mono- PnBA$_{788}$-tpy + 0.5 eq. CuCl$_2$
Lin100k+Co	Linear Mono- PnBA$_{788}$-tpy + 0.5 eq. CoCl$_2$
Lin140k+Zn	Linear Mono- PnBA$_{1108}$-tpy + 0.5 eq. ZnCl$_2$
Lin140k+Cu	Linear Mono- PnBA$_{1108}$-tpy + 0.5 eq. CuCl$_2$
Lin140k+Co	Linear Mono- PnBA$_{1108}$-tpy + 0.5 eq. CoCl$_2$
Star160k+Zn	4-arm star star PnBA$_{1248}$-tpy$_4$ + 0.5 eq. ZnCl$_2$
Star160k+Cu	4-arm star star PnBA$_{1248}$-tpy$_4$ + 0.5 eq. CuCl$_2$
Star160k+Co	4-arm star PnBA$_{1248}$-tpy$_4$ + 0.5 eq. CoCl$_2$
Star250k+Zn	4-arm star PnBA$_{1943}$-tpy$_4$ + 0.5 eq. ZnCl$_2$
Star250k+Cu	4-arm star PnBA$_{1943}$-tpy$_4$ + 0.5 eq. CuCl$_2$
Star250k+Co	4-arm star PnBA$_{1943}$-tpy$_4$ + 0.5 eq. CoCl$_2$

Table 4.2 List of sample annotations and their descriptions.

The glass transition temperatures of the reference samples and of the supramolecular polymers were measured by DSC. No specific change

of T_g was observed with the sample architecture or with the addition of the metal ions. Values ranging from -53°C to -51°C were found.

4.2.3 Rheological characterization

For the reference samples (i.e. precursor materials without metal ions), master curves were built at a reference temperature of 25°C, following a WLF equation with the constant $C_1 = 7.63$ and $C_2 = 103.8K$.[27] Vertical shift was applied in order to compensate for the density effect. The vertical shift factors, b(T), can be expressed as *b(T)=(ρ(T$_{ref}$).T$_{ref}$)/ (ρ(T).T)*, where *ρ(T)* is the density (g/cm^3) of the material at temperature *T* (K), and the reference temperature *T$_{ref.}$ = 298 K*. In the case of poly(*n*-butyl acrylate), the temperature dependence of the density is given by $\rho(T) = 1.2571 - 6.89 \ 10^{-4} \ T$.[28,29] Then, the same shift factors were used to shift the viscoelastic data of the supramolecular polymers. In such a way, only the influence of temperature on the segmental dynamics is taken into account, which allows us to isolate its influence on the dynamics of the supramolecular bonds. Since the association dynamics of the stickers also depends on T, it is expected that the supramolecular polymers exhibit complex rheological behavior.

4.3 Modelling the viscoelastic properties of slightly entangled sticky polymers.

4.3.1 Experimental observations and assumptions behind the model

In this section the basic assumptions behind the modified time marching algorithm (TMA) model, which is developed in Section 4.3.2, are detailed. As explained below, these assumptions are supported by experimental observations.

Since a good understanding of the molecular dynamics of the precursor samples is helpful in building a molecular picture for the supramolecular systems, we will first discuss the modelling of the

rheological observations of the parent materials, which has been achieved by the use of the original TMA.[23,30] The latter is a tube based model that incorporates all the reorientation processes in the linear flow regime, namely reptation, contour length fluctuations (CLF), and constraint release (CR). It requires the use of three molecular parameters, which are topology independent, namely the entanglement plateau modulus, G_N^0, the entanglement relaxation time, τ_e, and the molecular weight between entanglements M_e. The model predictions presented in Figure 1 have been obtained using the following values: $G_N^0 = 160\ kPa,\ \tau_e = 2.3\ 10^{-4}\ s,\ M_e = 18\ kg/mol$, consistently with previous work.[31] Moreover, the number average molecular weights and dispersity have been optimized as followed: $M_n = 38.5$ kg/mol per arm and $Ð = 1.04$ for the Star160k, $M_n = 66$ kg/mol per arm and $Ð = 1.08$ for the Star250k, $M_n = 101$ kg/mol and $Ð = 1.08$ for the Lin100k, and $M_n = 138$ kg/mol and $Ð = 1.08$ for the Lin140k. These molar masses are within the 8% of variation with the experimental values, while the optimized $Ð$ are systematically slightly smaller than the experimental values.

Figure 4.1 compares the theoretical (lines) and the experimental (symbols) response and phase angle of the reference telechelic star and mono-functional linear polymers. It demonstrates that chains are slightly entangled, since all samples exhibit a short plateau region and have relatively short terminal relaxation times. At the reference temperature T = 25°C, the values of the terminal times, τ_{rel}, are $\simeq 0.01$ s for samples Star160k and Lin100k, and $\simeq 0.1$ s for samples Star250k and Lin140k. Moreover, the comparison reveals that linear chains are short enough to relax their orientation, mainly by means of CLF as the star chains do. For example, the Lin140k sample, which contains around 7.8 entanglements, has very similar τ_{rel} to the Star250k sample. The fact that both linear and star chains are slightly entangled will be taken into account in assumption A2 below.
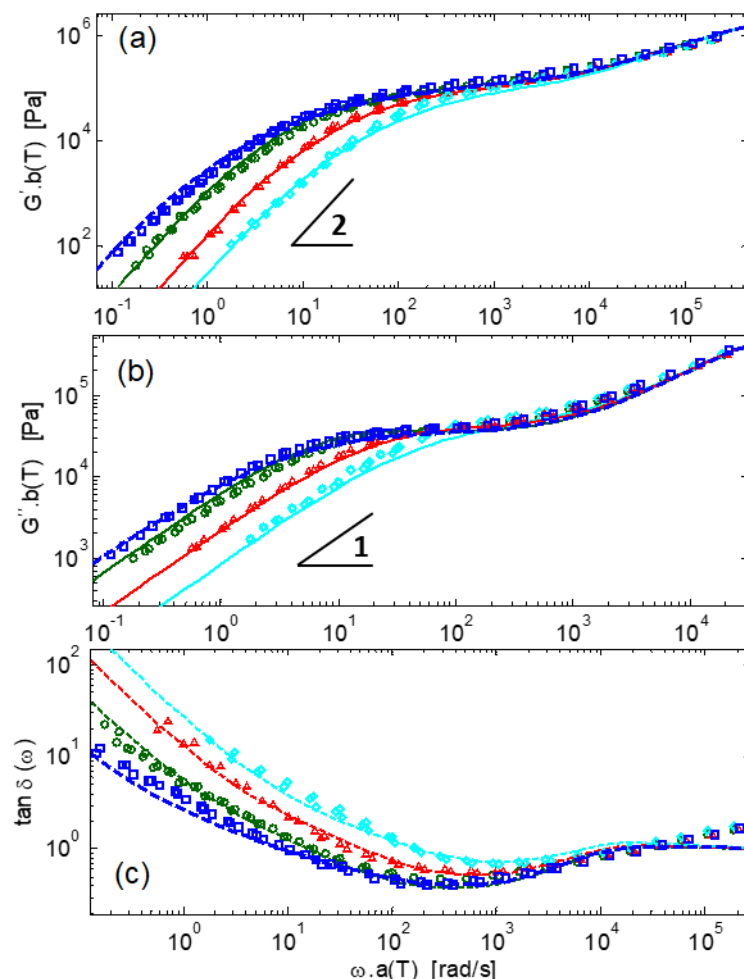
Figure 4.1 Storage modulus (a), loss modulus (b) and tan δ curves of the reference star and linear polymers (cyan ◊: Star160k, red Δ: Lin100k, green o: Lin140k, blue □: Star250k). Symbols are experimental data and lines are model predictions. Master curves have been built at 25°C.

In Figure 4.2, the black symbols show the viscoelastic response of the Star160k+Cu supramolecular sample with a stoichiometric amount (0.5 Eq.) of Cu ions as well as with an excess of ions (1 Eq.). Despite the fact that the sample comprises metal-ligand interactions the value of the (apparent) plateau modulus stays close to the value of the entanglement plateau, i.e. 160 kPa, of the precursor poly(*n*-butyl acrylate) chain.[31] This observation is typical for melts of associating

chains in which the number of active functional groups per chain is lower than the number of entanglements per chain.[32,33] Hence, rather than reinforcing the plateau modulus, the main effect of the stickers (while active/associated) is to delay chain disentanglement, i.e. the terminal relaxation.
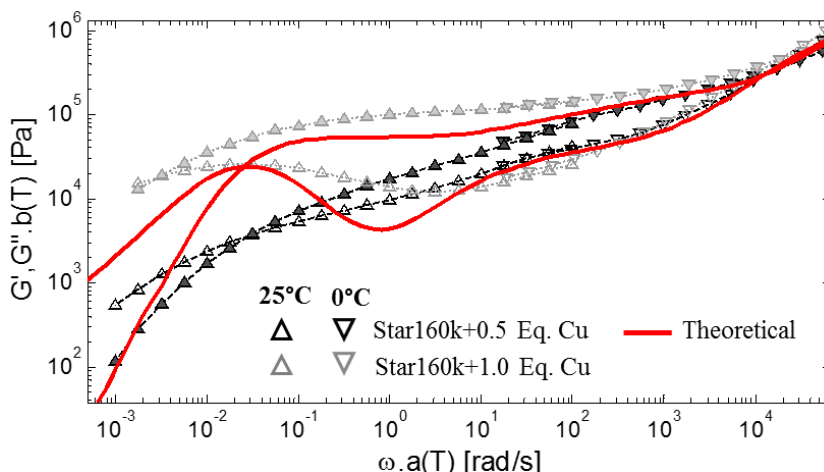

Figure 4.2 Experimental storage (filled symbols) and loss (open symbols) moduli of Star160k+Cu containing 0.5 Eq. of Cu ions (black symbols), or 1 Eq. of ions (grey symbols). The data have been measured at 25°C (Δ) and 0°C (∇) and shifted to the reference temperature of 25°C. The continuous red curves in panel are the theoretical viscoelastic response of sample Star160k with 0.5 Eq. of Cu ions, assuming that 45 wt% of arms are unassociated and considering an association time, τ_{ass}, equal to 60 s.

From the same curves of sample Star160k containing 0.5 Eq. of Cu ions, it is evident that at intermediate frequency, the storage modulus undergoes a gradual decrease. The corresponding frequency range is comparable to the one of the relaxation of the reference polymer (see Figure 4.1). This suggests that part of the ligands is initially dissociated, i.e. they do not form transient interactions with metal ions, and have time to relax. Thus, despite the fact that the metal ions have been added in a stoichiometric amount in order to fulfill all the complexes, a large fraction of star arms are free and do not participate to the supramolecular network. This difficulty to create metal-ligand complexes is attributed to the low density of metal ions present in the

202

sample, which reduces the probability of a chain end to meet a free ion and another free end in its surrounding. In order to reduce the amount of free dangling arms, the Cu ions must be added in excess, as it is illustrated by the grey curves, which were obtained by adding 1 Eq. of Cu ions. In this last case, a longer and higher plateau is observed in the storage modulus curve. Thus, since a stoichiometric amount of metal ions has been added to the different supramolecular samples studied in this work (see Table 4.2), we expect the proportion of dangling arms to be larger than the proportion obtained if we only account for their association/dissociation probability and equilibrium state.

Figure 4.2 also reveals the presence of polymer fractions (arms) having relaxation times much longer than the reference sample. This is because disentanglement of such fractions is prevented as long as their extremities are involved in metal-ligand complexes. Consideration of the two aforementioned experimental facts allows us to make the following assumption:

Assumption A1. Initially, i.e. at time $t = 0$, there are two different populations of ligands: the associated ones and the dissociated (or free) ones. Hereafter, these two populations will be referred to as population A and population F, respectively. For a schematic representation of the system at $t = 0$ see Figure 4.3. The same applies to the system made of mono-functional linear chains. Roughly speaking, the weight fractions of the two populations are similar.
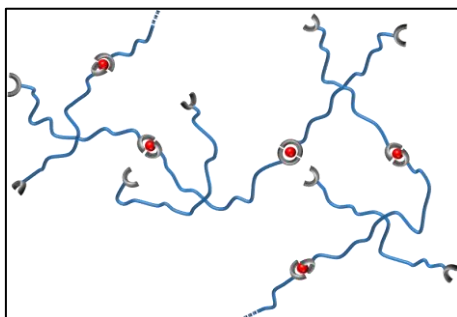

Figure 4.3 Schematic representation of telechelic star polymers with the presence of two different ligand (sticker) populations.

As explained above (c.f. discussion of Figure 4.1) the star arms are slightly entangled, therefore they renew orientation relatively fast. By utilizing this fact we can safely consider the following:

Assumption A2. The star arms that belong to population F will fully relax by CLF before they associate. In other words, we assume that the fluctuation time for a full retraction is shorter than the average time a sticker spends in the dissociated state. Similarly, it is considered that a star arm which is initially associated and which dissociates at any time t will have enough time to fully disentangle before its sticker associates again.

The solid lines in Figure 4.2 correspond to model prediction found when (1) the weight fraction of free arms at time $t = 0$, i.e. of population F, is 45 wt%, and (2) all stickers of population A have a single association lifetime, τ_{ass}. The latter is defined by the inverse of the G'/G" crossover frequency, therefore it is much longer that the terminal relaxation time of the precursor material. To avoid possible confusion, we stress that the model predictions here do not correspond to the original version of the TMA for non-associating chains, but to a special case of the modified TMA for associating chains, which is presented below. Comparison of the model predictions and the data demonstrates two points. First, in the frequency range 10^4 - 10^1 rad/s, the slow decrease of the moduli is well captured by the fast relaxation of the free arms that are bearing a ligand of population F. In other words, the arms that are ended by a free ligand. Second, the terminal response cannot be reproduced by assuming a unique association lifetime τ_{ass} for all the ligands of population A. Such an assumption results in a Maxwell-like terminal relaxation characterized by a single exponential decrease of the form $exp(-t/\tau_{ass})$, which is clearly not the case for the experimental data, which show large relaxation time spectrum. This result was not expected since all the metal-ligand complexes are of same nature, and therefore should have a similar bonding energy and association time. In order to explain this departure from a Maxwell-like behavior, we consider that a chain end never dissociates by itself, but rather dissociates thanks to a process of ligand exchange around the ions. It is similar to the mechanism suggested by Wang et al. to describe the dynamics in supramolecular polymer networks formed by

associating telechelic chains.[22] There, it was demonstrated that, in the case of unentangled telechelic polymers, the energy related to sticker (ligand) exchanges is much lower than the energy cost to dissociate a sticker from an ion through hopping process, without replacing it by another one. Thus, the necessary time for a sticker to dissociate by ligand exchange is expected to be much shorter than the dissociation time of a sticker unable to benefit from the presence of free dangling arms in its surrounding. This is in agreement with the results of Figure 4.2 where it is observed that the star arms are relaxing much slower when the proportion of dangling arms is reduced. Therefore we adopt the ligand exchange mechanism in our systems containing a stoichiometric amount of metal ions. This leads to the following assumption regarding our modified TMA model:

Assumption A3. The association/dissociation events are achieved via ligand exchanges between free and associated populations (see panels a and b of Figure 4.4 for a schematic representation). Nevertheless, we anticipate that most of the ligand exchanges are inefficient in allowing new arms to relax. In other words, it is likely that ligand exchange occurs among arms that have been already relaxed and therefore, such event cannot further contribute to the polymer relaxation. For example, consider the case illustrated in panel c of Figure 4.4 (red dotted circle): here, the ligand exchange takes place between a ligand of population F and a ligand that initially belonged to population A but had the possibility to fully relax in a previous step (see panel b).
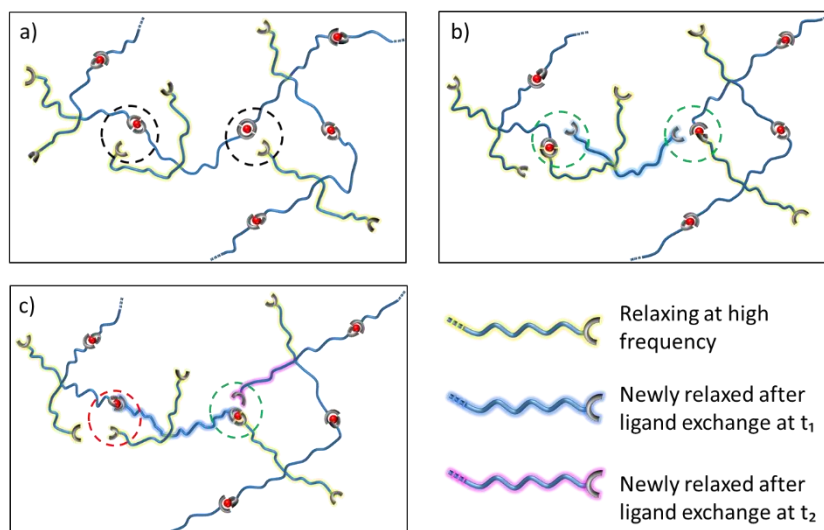
Figure 4.4 Schematic representation of ligand exchange mechanism in telechelic star polymers a) at t = 0, b) at t = t_1 and c) at t = $t_2 > t_1$.

In this respect, it seems realistic to consider that the number of these inefficient exchanges increases with time since the fraction of relaxed material increases with time as well. Moreover, some stickers could be trapped around a specific metal ion, meaning that they dissociate and associate again with the same ion, cancelling in this manner their dissociation step. Such stickers do not have the possibility to easily find another ligand in the surrounding. In either case, it is expected that the probability for new arms to relax is becoming extremely low through time. In consequence, the time needed for the stickers initially associated to dissociate for the first time exhibits very broad polydispersity, which explains the strong deviation from a Maxwell-like terminal relaxation behavior. To quantify this polydispersity in the model we will make the following assumption:

Assumption A4. Since a ligand exchange taking place when a fraction *1/n* of the arms are unrelaxed is approximately *n* times less efficient than an initial exchange, herein we assume that the times needed for the associated stickers to dissociate for the first time (and thus, to start contributing to the polymer relaxation) are equally distributed on a log time scale. It should be stressed that this time distribution does not represent the distribution of times after which a sticker will dissociate,

but it rather represents the distribution of times after which a sticker attached to an unrelaxed arm will dissociate. Somehow, it represents the distribution of the *effective* association times. As shown in Figure 4.5, we consider these times to be distributed between $\tau_{exchange}$ and τ_{final}. The first time represents the minimum waiting time needed to observe the dissociation of some arms. It can be seen as the 'internal clock' of the supramolecular bond dynamics, which dictates the rhythm at which the ligand exchanges are observed. The second time, τ_{final}, corresponds to the longest effective association time of the stickers. Notice that $\tau_{exchange}$ must be rather small since before this time none of the associated ligands can dissociate. Therefore, a large value would lead to the appearance of a second plateau in the storage modulus at intermediate frequency as observed in Figure 4.2, with single, long association time. Herein, we consider a constant value for $\tau_{exchange}$, which governs the onset of the ligand exchange process (see discussion below for explanation of this choice). Thus, the parameter τ_{final} is the only parameter which must be defined in order to determine the distribution of effective association times of the stickers. While considered as a fit parameter in the model, it will be shown in Section 4.4 that this relaxation time has a physical meaning and follows an exponential dependence with activation energy.

This way of determining the *effective* association time distribution allows us to simply account for the fact that the majority of the arms are dissociating at short times (i.e. after few $\tau_{exchange}$), while allowing some of them to have very long association times.
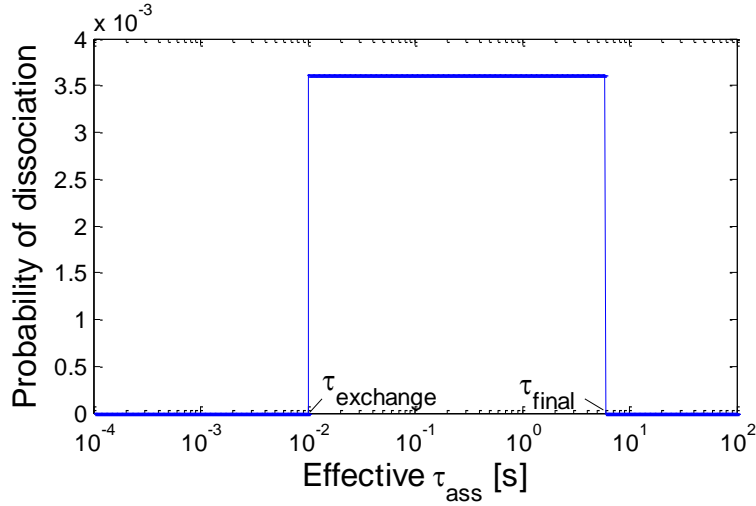
207

Figure 4.5 Example of distribution of *effective* association times taken in the model, assuming that $\tau_{exchange} = 0.01$ s and $\tau_{final} = 6$ s. This distribution represents the probability for an associated sticker to detach for the first time at the corresponding effective association time.

The influence of $\tau_{exchange}$ and τ_{final} is shown in Figure 6. In this example, we consider that the proportion of associated arms, $p_{ass,}$ is equal to 60 wt%. A detailed discussion concerning p_{ass} follows further down in this section. The predictions shown in Figure 6 are based on the model described in Section 4.3.2.
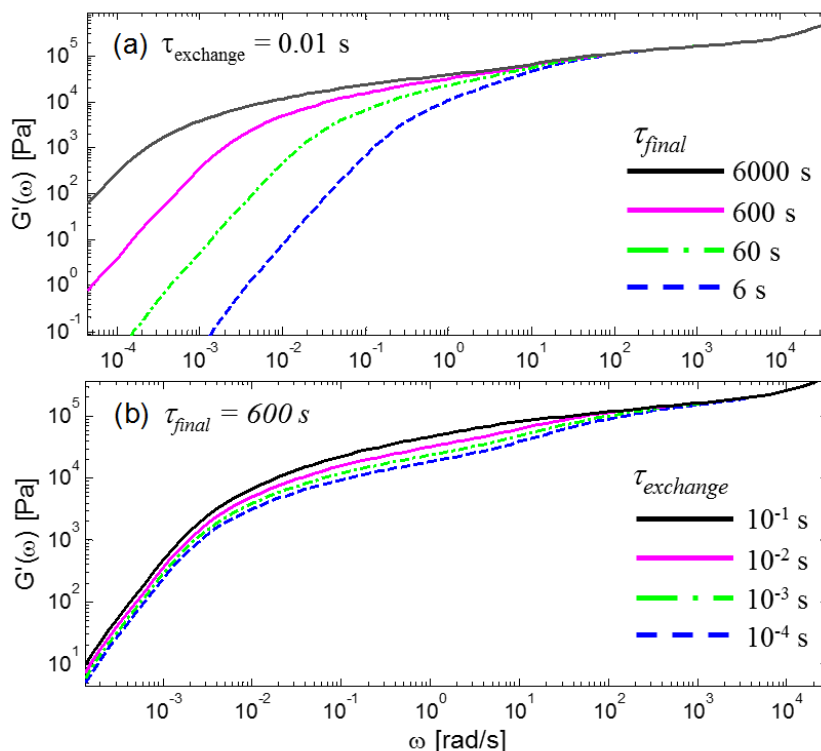
Figure 4.6 Influence of $\tau_{exchange}$ and τ_{final}. (a) The value of $\tau_{exchange}$ is fixed to 0.01 s and the value of τ_{final} is equal to 6 s (--), 60 s (-·), 600 s (—) or 6000 s (—); (b) The value of τ_{final} is fixed to 600 s and the value of $\tau_{exchange}$ is equal to 10^{-4} s (--), 10^{-3} s (-·), 10^{-2} s (—) or 10^{-1} s (—).

While it is clear that the predictions are strongly sensitive to the value of τ_{final}, the results obtained for different values of $\tau_{exchange}$ are similar when this parameter is becoming short. Generally, one can estimate $\tau_{exchange}$ by looking at the experimental data, in particular at the frequency at which the storage modulus starts to decrease faster than expected if we consider that the star arms cannot exchange their ligands. It was found that it should be around 0.01 s. Based on Figure 4.6.b, we do not expect a large influence of this parameter, therefore we consider it as a constant, i.e. $\tau_{exchange} = 0.01$ s for all the samples at T = 25°C. In a way, this time can be seen as the 'clock' of the supramolecular dynamics, i.e. which fixes the rhythm at which we are observing the

ligand exchanges, while the ratio $(1/\tau_{final})$ is related to the amount of exchanges observed at each time step.

Thus, the model contains only two unknown parameters: the longest association time of the stickers, τ_{final}, and the proportion of associated arms p_{ass}. It must be noted that the longest association time, τ_{final}, cannot be determined from the G'-G" crossover at low frequency. Indeed, as discussed in Section 4.4, the terminal relaxation time of these samples includes both dissociation dynamics and disentanglement dynamics. Therefore, its value is expected to be larger than τ_{final}. We now turn our attention to the latter parameter, i.e. p_{ass}, for which we make the following assumption:

Assumption A5. The average fraction of associated arms, p_{ass}, is constant through time (the arms of population A initially). This means that each time an arm becomes free, another one becomes associated, in agreement with the idea of ligand exchanges. Note however that the arm that becomes associated might have already relaxed through a previous ligand exchange event.

The parameter p_{ass}, is fixed from the experimental data, by determining the proportion of arms which are able to relax at short times, *i.e.* at high frequency. Since the predictions are quite sensitive to this parameter, its value can be fixed with an accuracy of around 5%. Usually, values around 50 wt% are found, which are quite low. This means that the average time during which a freshly/newly dissociated sticker will stay free is quite long. This also means that at each time step ($\tau_{exchange}$), only few of the free stickers are able to create an exchange of ligands. As already mentioned, this can be understood by considering the low density of stickers and the slow diffusion process of the chains, leading to the presence of dangling arms which do not find a metal-ligand complex in their surroundings. The presence of a small fraction of non-functionalized arms must also be envisaged. It must be noted that in case of an entangled telechelic polymer, the fact that two arms of a same star can associate and create a polymer loop is not expected to enhance the proportion of fast relaxing polymers. Indeed, in order to disentangle, polymer loops must also dissociate. The values of p_{ass} and τ_{final} are discussed in Section 4.4. In the next section, we assume that

they are known, and present the model we developed in order to account for the sticker dynamics.

All assumptions described above are applied to linear mono-functional polymers as well. Nevertheless, in the case of the mono-functional chains, the terminal relaxation times are limited by the possible reptation of the whole self-assembly, which is composed of two linear chains associated through metallo-supramolecular bonds at the center as depicted in Figure 4.7.
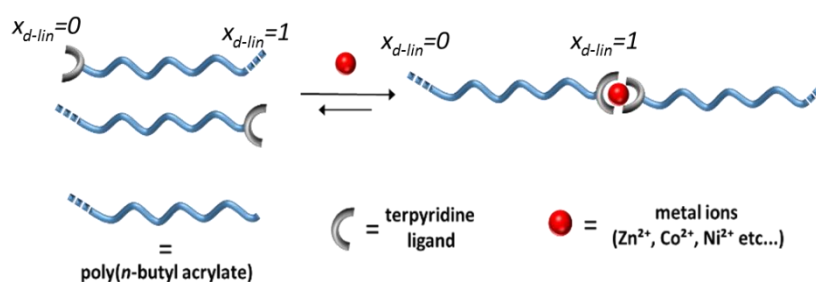

Figure 4.7 Self-assembly of associating linear semi-telechelic polymers.

4.3.2 Modified TMA model

Based on the assumptions presented in Section 4.3.1., we can now extend our TMA model to the specific case of slightly telechelic entangled chains. A specificity of the systems studied in this work is the fact that the relaxation time of a free arm is shorter than the time during which a sticker stays free. Therefore, the model is based on the idea that once an arm is dissociated, it has enough time to relax (see assumptions A2 and A5). In case of very long and well entangled polymers, this would not be the case anymore. So one should also consider the situation in which an arm is able to fully relax only after several dissociation/association blinking events.

4.3.2.1 TMA model

We first briefly describe the main equations behind the TMA model[34], as it is used for describing the viscoelastic properties of the reference samples and serves as the starting point of our modified model. A more detailed explanation can be found in the literature.[30,35]

It must be noted that in TMA, linear chains are considered as 2-arm stars, which are able to relax by reptation.

In this model, the relaxation modulus as a function of time, $G(t)$, accounts for both the high frequency Rouse process, $G_R(t)$, and the disentanglement modulus $G_d(t)$[36]:

$$G(t) = G_{\mathrm{R}}(t) + G_{\mathrm{d}}(t) \tag{4.1}$$

with

$$G_{\mathrm{R}}(t) = \sum_k \frac{\upsilon_k \rho RT}{M_{arm,k}} \left\{ \frac{1}{4} \sum_{p=1}^{Z_k} \exp\left(-\frac{p^2 t}{\tau_{\mathrm{R}}(M_{arm,k})} \right) + \sum_{p=Z_k+1}^{n} \exp\left(-\frac{2p^2 t}{\tau_{\mathrm{R}}(M_{arm,k})} \right) \right\} \tag{4.2}$$

In Equation 4.2, υ_k and $\tau_R(M_{arm,k})$ represent the weight fraction and the Rouse time of an arm of chain k, respectively. Z_k represents the number of entanglements in an arm of chain k; the parameter ρ is the monomeric density, R is the gas constant and T is the temperature.

The disentanglement modulus and the plateau modulus G_{N}^0 are defined as:

$$G_{\mathrm{d}}(t) = G_{\mathrm{N}}^0 \varphi'(t) \{\phi(t)\}^\alpha \tag{4.3}$$

$$G_{\mathrm{N}}^0 = \frac{4}{5} \frac{\rho RT}{M_e} \tag{4.4}$$

with $\varphi'(t)$, being the unrelaxed fraction of initial tube segments and α, the dynamic dilution exponent, which is fixed here to 1.[37] Constraint Release mechanisms (CR) are taken into account by the dilation factor $\phi(t)$, which defines the diameter a of the dilated tube ($a = a_0 \cdot \phi(t)^{-\alpha/2}$, with a_0, the initial tube diameter). As long as the polymer relaxation occurs gradually, the dilation factor $\phi(t)$ is equal to the unrelaxed fraction of initial tube segments, $\varphi'(t)$.[35] This last parameter can be determined by looking at all molecular segments $x_{arm,k}$, from $x_{arm,k} = 0$ at the extremity of an arm to $x_{arm,k} = 1$ at the middle, of all arms (in proportion υ_k), and by determining if they are still moving in their initial

tube or not, i.e. if they are not yet relaxed through reptation or contour length fluctuations mechanisms:

$$\varphi'(t) = \sum_k \upsilon_k \int_0^1 p_{fluc}(x_{arm,k}t) \ p_{rept}(x_{arm,k}t) \ dx_{arm,k} \tag{4.5}$$

In this equation, the survival probability related to the reptation process, $p_{rept}(x_{arm,k},t)$ is either fixed to 1 in case of a star molecule (since it cannot reptate), either determined, based on the Doi and Edwards equation in case of a linear chain[38]:

$$p_{rept}(x_{arm,k},t) = \sum_{p \ odd} \frac{4}{p\pi} \sin\left(\frac{p\pi x_{arm,k}}{2}\right) \exp\left(\frac{-p^2 t}{\tau_{rept}(2M_{arm,k})}\right) \tag{4.6}$$

In such a case, since linear chains of molar mass M_k are described as 2-arm stars which are able to reptate, they contain two arms of molar mass $M_{arm,k} = M_k/2$, and their corresponding reptation time is described as:

$$\tau_{rept}(M_k = 2 M_{arm,k}) = 3 \tau_e \left(\frac{2 M_{arm,k}}{M_e}\right)^3 \tag{4.7}$$

On the other hand, the survival probability related to the fluctuations process, $p_{fluc}(x_{arm,k},t)$, is considered as equal to $exp(-t/\tau_{fluc}(x_{arm,k}))$, in which the fluctuation time is determined by taking into account both the early fluctuations of the chain ends, and the deeper, activated, retraction of the arms:

$$\tau_{early,arm}(x_{arm,k}) = \frac{9\pi^3}{16} \tau_e \left(\frac{M_{arm}}{M_e}\right)^4 x_{arm,k}^4 \tag{4.8.a}$$

$$\tau_{activated}(x_{arm,k}) = \ln \ \tau_{activated}(x_{arm,k} - \delta x_{arm}) + 3\left(\frac{M_{arm}}{M_e}\right) x_{arm,k} \ \phi(x_{arm,k})^\alpha \cdot (\delta x_{arm}) \tag{4.8.b}$$

$$\tau_{fluc,arm}(x_i) = \tau_{early,arm}(x_{tr}) \ \exp\left(\frac{\tau_{activated,arm}(x_i)}{\tau_{activated,arm}(x_{tr})}\right) \tag{4.8.c}$$

In Equation 4.8.b, it is considered that the molecular segment located just before the segment $x_{arm,k}$ is positioned at $(x_{arm,k} - \delta x_{arm})$. The

function $\phi(x_{arm,k})$ represents the polymer fraction which is not yet relaxed at the time the segment $x_{arm,k}$ of the arm is relaxing.[39] Note that in case of monodisperse sample, we would have $\phi(x_{arm,k}) = \phi(x_{arm}) = [1-x_{arm}]$. In Equation 4.8.c, the position x_{tr} represents the position of the arm segment at which the potential is equal to kT, i.e. at which the transition between early fluctuations and deep retraction is taking place.

4.3.2.2 Telechelic star molecules

In order to predict the linear viscoelastic properties of the telechelic star molecules, we start from the fact, that at time $t = 0$ there are two different populations of arms: A fraction p_{ass} of arms which are associated (and belong to population A), and a fraction ($1-p_{ass}$) of dissociated arms (which belong to population F). Following assumptions A1 and A2, the free arms will be able to relax before becoming associated. Their fluctuation times are determined, based on Equations 4.8. It must be noted that in this case, the parameter $\phi(x_{arm,k})$ in Equation 4.8.b must be determined by accounting for the fact that part of the arms cannot relax. Thus, in case of monodisperse stars, we would have $\phi(x_{arm,k}) = \phi(x_{arm}) = [p_{ass}+(1-p_{ass}).(1-x_{arm})]$.

On the other hand, the associated arms have first to dissociate, before being able to fluctuate and relax. Since the storage modulus is mainly dominated by the entanglements and since the arms forming intra-associations are also entangled, it is expected that these last arms contribute to the sample relaxation in a similar way as the arms inter-connected. As described in Section 4.3.1., a distribution of effective associated times, ($\tau_{eff,ass,j}$, $\upsilon_{eff,ass,j}$) must be considered in order to account for the time decreasing probability to detach an unrelaxed arm through exchange of ligand and thus, to correctly describe the relaxation of these telechelic systems. Therefore the survival probability of a specific segment $x_{arm,k}$ of an arm of mass M_k is described as:

$$p_{fluc}(x_{arm,k},t) = \sum_j \upsilon_{eff,ass,j} \exp\left(\frac{-\max\left(0,\left(t-\tau_{eff,ass,j}\right)\right)}{\tau_{fluc}(x_{arm,k})}\right) \qquad (4.9)$$

By adding the condition according to which $\left(t-\tau_{eff,ass,j}\right)$ is always positive, this equation can also be used at time shorter than the effective

association time $\tau_{eff,ass,j}$. Indeed, in such a case, the survival probability of the associated arms is simply equal to 1. Then, by using Equation 4.9 in Equation 4.5, the unrelaxed fraction of initial tube segments at time t is determined, which allows us to calculate the relaxation modulus $G(t)$ based on Equation 4.3.

4.3.2.3 Mono-functional linear chains

Mono-functional linear chains can only be associated at one extremity, on which a terpyridine ligand is attached. Therefore, chains can only relax either as simple (dissociated) chain, or as double (associated) chains. Since the average times during which a chain stays associated or free are rather long, and since the reptation time of a double chains (i.e. a pair of associated single chains) is only around 8 times slower than the single chains, it is expected that most of the molecules do not have time to change their association status before being fully relaxed.[25] However, there is a small fraction of the double chain, which will relax by dissociation followed by the reptation of the single chains, especially when a weaker metal ion is used. Therefore, it is important to account for the possibility of the chain extremity to dissociate.

To this end, the same approach as proposed for the star polymers is followed. However, there are specific points which must be included in the model. The first point is the fact that the length of the relaxing chain can vary, from single to double. Therefore, it is important to define a common coordinate system to localize a specific molecular segment. Here, as illustrated in the cartoon in Figure 4.7, we take the double chain as reference chain, with ($x_{d-lin} = 0$) at one of its extremity, to ($x_{d-lin} = 1$) for its middle segment. This means that in the case the chains are dissociated and relaxing as single chains, since the reference system stays the one of the double chains, one needs to consider that these double (unassociated) chains are able to relax from their middle in order to keep consistency between the two statuses. Indeed, if the double chain is dissociated, its middle segment is becoming an extremity of the single chain, i.e. its relaxation time, $\tau_{rel}(x_{d-lin}=1)$ is shorter than the relaxation of the middle segment of the single chain, $\tau_{rel}(x_{d-lin}=0.5)$. A second specificity of the mono-functional chains is the fact they can always relax, as double or single chains.

215

Therefore, if a chain k is associated at time $t = 0$, it belongs to the population A and the survival probability of one of its molecular segment $x_{d\text{-}lin,\,k}$ at time t can be described as:

$$p(x_{d-lin,k}, t, A) = \sum_j \upsilon_{eff,ass,j} \cdot \exp\left(\frac{-\min(t, \tau_{eff,ass,j})}{\tau_{rel}(x_{d-lin,k}, 2M_w)}\right) \cdot \exp\left(\frac{-\max(0, (t - \tau_{eff,ass,j}))}{\tau_{rel}(x_{d-lin,k}, M_w)}\right)$$

$$(4.10)$$

In this Equation, we use the relaxation times, τ_{rel}, rather than the corresponding reptation and fluctuations times in order to keep the model simple. Thus, approximating the survival probability $p_{rept}(x,t)$ by a single exponential, $exp\left(\frac{-t}{\tau_{rept}}\right)$, rather than using Equation 4.6. Note that the error in this approximation is negligible. As long as the double chain stays associated, the relaxation time $\tau_{rel}(x_{d\text{-}lin,k},\ 2M_w)$ of its molecular segment $x_{d\text{-}lin,k}$, is then described as:

$$\tau_{rel}\left(x_{d-lin,k}, 2M_w\right) = \left(\frac{1}{\tau_{rept}(x_{d-lin,k}, 2M_w)} + \frac{1}{\tau_{fluc}(x_{d-lin,k}, 2M_w)}\right)^{-1} \qquad (4.11)$$

with the reptation time and fluctuation time determined as for a covalent double chain (see Equations 4.7 and 4.8) relaxing in a blend composed by a fraction p_{ass} of double chains and $(1\text{-}p_{ass})$ of single chains.

Same expressions can be used for the single chains relaxation, but this requires first determining the corresponding reptation and fluctuations time in the usual coordinate system of a single chain, i.e. from $(x_{s\text{-}lin} = 0)$ at the extremity of the single chain, to $(x_{s\text{-}lin} = 1)$ at the middle, and then by transposing the results in the reference coordinate systems, $x_{d\text{-}lin}$, based on the double chains:

$$\tau_{rel}\left(x_{d-lin,k}, M_w\right) = \tau_{rel}\left(x_{s-lin,k} = 2 \cdot \min\{x_{d-lin,k},\ (1 - x_{d-lin,k})\}, M_w\right)$$

$$(4.12)$$

In order to illustrate Equation 4.10, the evolution through time of the survival probability $p(x_{d-lin,k}, t,\ A)$ is shown in Figure 4.8, for single chains of molar mass M_n of 101 kg/mol, i.e. with a relaxation time of 0.15 s, while the relaxation time of the double chain is equal to 1.22 s. In this example, the distribution of effective association times has been built by considering either $\tau_{final} = 1$ s in Figure 4.8.a or $\tau_{final} = 100$ s in

216

Figure 4.8.b (while $\tau_{exchange}$ has a fixed value, equal to 0.01 s). By considering $\tau_{final} = 1\ s$, which is slightly shorter than the reptation time of the double chain, part of chain relaxes thanks to the dissociation of the ligand followed by the relaxation of the single chains (see Figure 4.8.a). On the other hand, we observe that the chains characterized by a longer effective association time, $\tau_{final} = 100\ s$, will basically relax as a binary blends composed of single and double chains (see Figure 4.8.b).
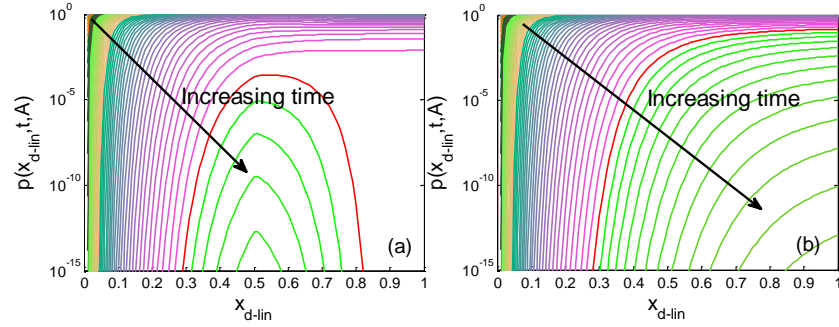
Figure 4.8 Survival probabilities $p(x_{d-lin}, t,\ A)$ of the molecular segments of mono-functional monodisperse linear chains associated at time $t = 0$, from $x_{d-lin} = 0$ at the extremity of the double chain to $x_{d-lin} = 1$ at the middle. The corresponding single chains have a molar mass M_n of 101 kg/mol (i.e. a relaxation time of 0.15 s, while the relaxation time of the double chains is 1.22 s), and $p_{ass} = 0.5$. The distribution of effective association times is built by considering either $\tau_{final} = 1\ s$ (a), or $\tau_{final} = 100\ s$ (b).

On the other hand, we assume that the chains which are not associated at time $t = 0$ (thus, which belong to the population F) have time to fully relax before their association. Therefore, their relaxation time can be determined as described in Equation 4.12, following assumptions A1 and A2:

$$p(x_{d-lin,k}, t, F) = \exp\left(\frac{-t}{\tau_{rel}(x_{d-lin,k},\ M_w)} \right) \tag{4.13}$$

Finally, the survival fraction of initial tube segments at time t, $\varphi'(t)$, is determined, based on Equations 4.10 and 4.13:

$$\varphi'(t) = p_{ass} \sum_k \upsilon_k \int_0^1 p(x_{d-lin,k}, t, \ A) \ dx_{d-lin,k} \ + (1 - p_{ass}) \sum_k \upsilon_k \int_0^1 p(x_{d-lin,k}, t, \ F) \ dx_{d-lin,k}$$

$$(4.14)$$

Together with Equations 4.1 to 4.4, we can determine the relaxation modulus $G(t)$ of these samples, and compare the theoretical results to the experimental data (see Section 4.4). As already mentioned, this model contains two unknown parameters, p_{ass} and τ_{final}. They will be first considered as fit parameters. Then we will analyze their value in order to understand how they are varying.

4.4 Results and discussion

Generally, the dynamics of these associating polymers are affected by both the disentanglement process of polymer chains and the dissociation process of the stickers. Depending on the architecture of the macromolecules, the temperature and the strength of metal-ligand complexes, one process is dominant compared to the other one. Below, we will examine each case systematically, starting from the influence of the temperature.

4.4.1 Influence of the temperature

Figure 4.9 presents the experimental data of the telechelic Star160k+Cu and Star250k+Cu samples at different temperatures. As shown in Figure 4.9.a, at high temperature (T = 60°C), the stickers are weak and consequently the relaxation process is mainly governed by the disentanglement mechanism of contour length fluctuations, which are longer for the Star250k+Cu material since it has arms longer than the other star polymer (see Table 4.1).

At lower temperatures, however, the sticker lifetime becomes longer than the fluctuation time of the arms, therefore the process of sticker dissociation dominates the terminal relaxation of the star systems (c.f. Figure 4.9.b and 4.9.c). Thus, similar terminal times are observed for the two telechelic star samples, despite their difference in arm lengths. As it will be seen below the longest effective association time is identical for both star polymers. However, the influence of the

218

arm length is noticeable at intermediate frequencies, where we observe that the star arms which are not associated are able to relax. This influence is highlighted in Figure 4.9.d which represents the tan δ curves of these samples. This is consistent with Assumption 1, according to which part of the arms are free and can relax at short times.
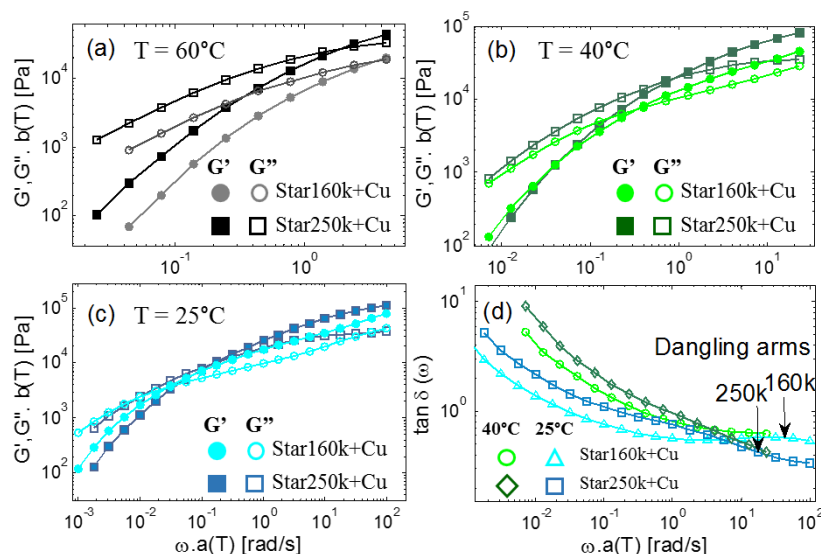

Figure 4.9 Storage (filled symbols) and loss (open symbols) moduli of the telechelic Star160k+Cu (o) and Star250k+Cu (□), at (a) T = 60°C, (b) T = 40°C and (c) T = 25°C; (d) tan δ curves of Star160k+Cu at 40°C (o) and 25°C (Δ), and of Star250k+Cu at 40°C (◊) and 25°C (□).The data have been shifted to a reference temperature of 25°C, based on the shift factors determined for the reference samples.

Figures 4.10 and 4.11 compare the predictions of our modified TMA model (lines) with the experimental data (symbols), for these two star polymers, in the presence of a stoichiometric amount of copper ions at several temperatures. From those Figures it is evident that the model captures well the viscoelastic behavior of the samples. Concerning the two model parameters, namely the longest (effective) association time, τ_{final}, and the fraction of associated arms, p_{ass}, we find that identical values can be used for both systems, i.e. independently from the chain length. Furthermore, we notice that p_{ass}, is temperature independent, whereas τ_{final} varies with temperature, from 5 s at high temperature (T

= 60°C) to 5000 s at low temperature (T = 0°C). We anticipate these values to follow an exponential decrease with temperature (see the analysis of this parameter below). The fact that p_{ass} is temperature independent whereas τ_{final} is temperature dependent confirms our hypothesis that these two parameters are not directly related, as suggested in Section 4.3.1, due to the presence of dangling arms, which could not find any partner in their surroundings to associate. Also, if the fraction of associated stickers was only dependent on the association and dissociation kinetics of the stickers, we would expect p_{ass} to decrease with T, which is not observed here. This is again attributed to the dominant effect of the dangling arms unable to find a free ion, which does not seem to be affected by the temperature.

In Figure 4.11, it is observed that at high temperature, T = 80°C, the sample mostly relaxes as the reference sample (see Figure 4.1.a), i.e. with a negligible effect of the supramolecular association. On the other hand, the influence of associated sticker is clear at low temperature.
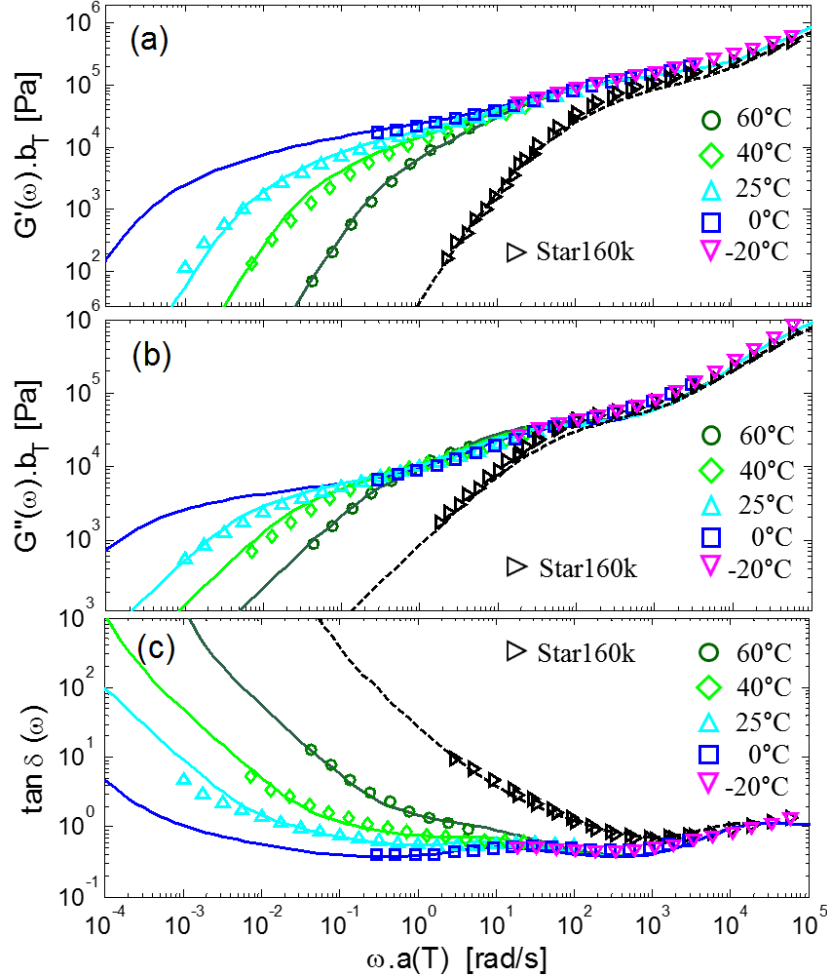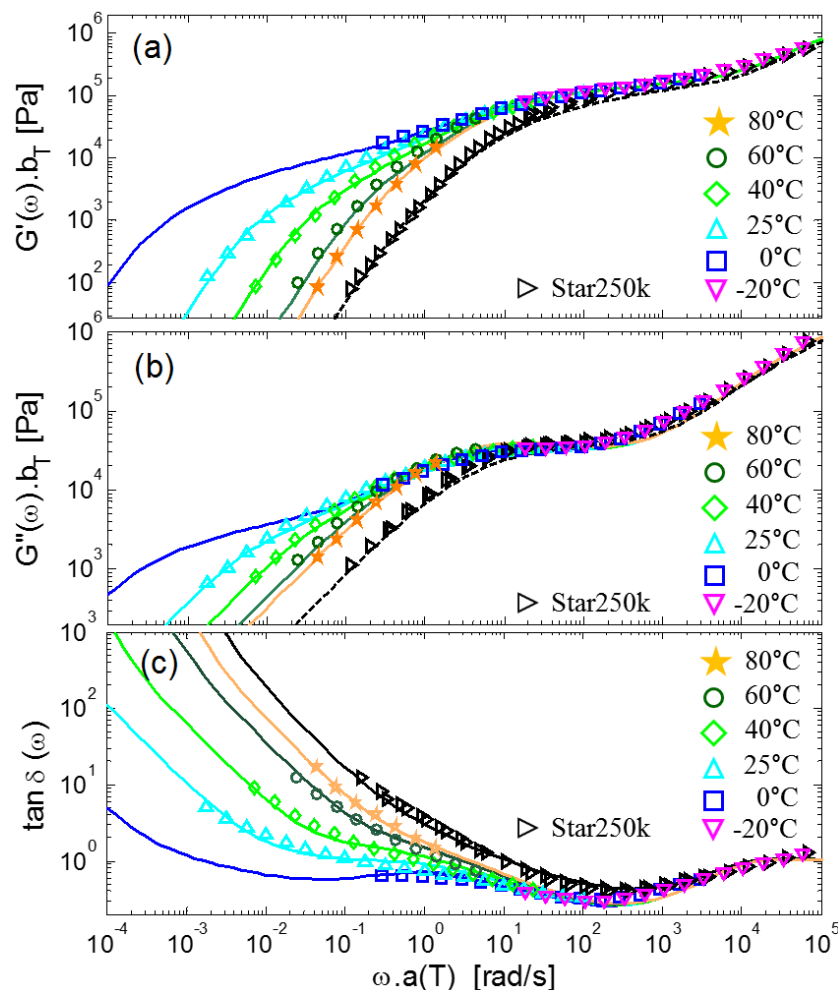
Figure 4.10 (a) Storage modulus, (b) Loss modulus and (c) tan δ curves of the reference sample Star160k (black, ▷) and of the telechelic Star160k+Cu measured at temperature T = 60°C (dark green, o), 40°C (green, ◊), 25°C (cyan, Δ), 0°C (blue, □) and -20°C (magenta, ∇). The experimental data (symbols) have been shifted to a reference temperature of 25°C, based on the shift factors determined for the reference samples. The theoretical curves (continuous and dashed curves) have been obtained by fixing p_{ass} = 0.45 and τ_{final} = 5 s at 60°C, 50 s at 40°C, 250 s at 25°C and 5000 s at 0°C.

Figure 4.11 (a) Storage modulus, (b) Loss modulus and (c) tan δ curves of the reference sample Star250k (black, ▷) and of the telechelic Star250k+Cu measured at temperature T = 80°C (orange, ★), T = 60°C (dark green, o), 40°C (green, ◊), 25°C (cyan, Δ), 0°C (blue, □) and -20°C (magenta, ∇). The experimental data (symbols) have been shifted to a reference temperature of 25°C, based on the shift factors determined for the reference samples. The theoretical curves (continuous and dashed curves) have been obtained by fixing p_{ass} = 0.45 and τ_{final} = 1 s at 80°C, 5 s at 60°C, 50 s at 40°C, 250 s at 25°C and 5000 s at 0°C.

4.4.2 Influence of the chain architecture

In this section we discuss the influence of the chain topology on the viscoelastic response. For this reason we compare the response of star and linear molecules associating via copper complexes. Figure 12 shows such a comparison for Lin100k+Cu and Star160k+Cu (see Table 4.2). One has to keep in mind that the arm molecular weight of the stars (40 kg/mol) is smaller than half the molecular weight of the linear chains, which leads to a faster relaxation of the reference star sample. However, the situation is inverted once the ions are added to the polymer. From Figure 4.12 it is evident that the polymers based on the mono-functional linear chains relax much faster than the telechelic star molecules. This behavior suggests that, contrary to star polymers, there is an upper limit in the terminal relaxation time of the linear chains. In theory, this upper limit would correspond to the relaxation time of the double linear chain, i.e. two mono-functional chains linked together through transient bonds. In other words, even if some of the transient associations have an effective lifetime that is much longer than the terminal time of the precursor, the sticker effect will not translate to further retardation of the terminal relaxation since the supramolecular chains can reptate as doubled linear chains.

To examine this behavior further, we plot together in Figure 4.13 the experimental data for samples Lin100k+Cu and Lin140k+Cu at several temperatures. We observe that data nearly overlap, despite the large difference observed in the viscoelastic response of their reference samples. This indicates that the relaxation of the supramolecular chains is dominated by the association dynamics. We also see that the sample Lin100k+Cu is relaxing significantly slower than the reference sample (green, $\triangleright$), but faster than the corresponding double chains. It is indeed relaxing similarly to the reference sample Lin140k. We therefore expect that the effective association times of the stickers are localized between the relaxation time of the single chains and the relaxation time of the double chains. On the other hand, the influence of the stickers on sample (Lin140k+Cu) is very weak. Again, this suggests that the lifetimes of the stickers are quite short compared to the relaxation time of sample Lin140k, and thus the dominating effect in this case is the disentanglement of the chain.
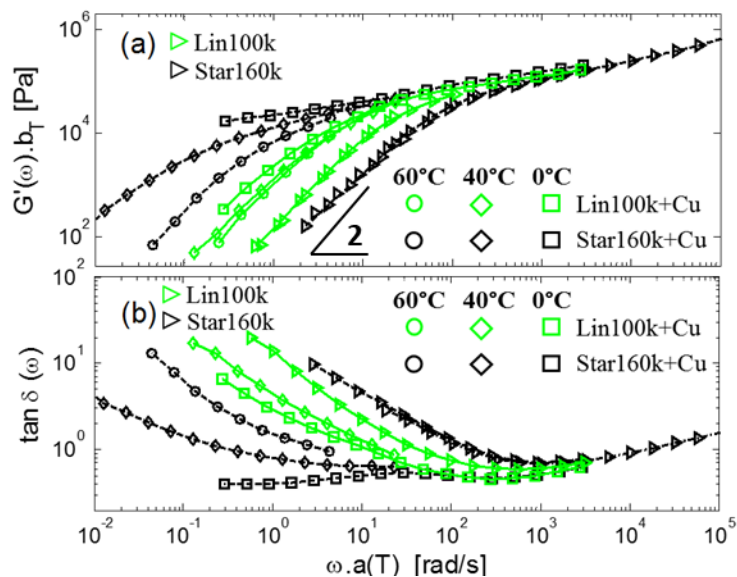
Figure 4.12 Storage modulus (a) and tan δ curves (b) of the reference samples Lin100k (green, ▷) and Star160k (black, ▷), and of the supramolecular samples Lin100k+Cu (green) and Star160k+Cu (black), measured at T = 60°C (o), 40°C (◊) and 0°C (□). The data have been shifted to a reference temperature of 25°C, based on the shift factors determined for the reference samples.
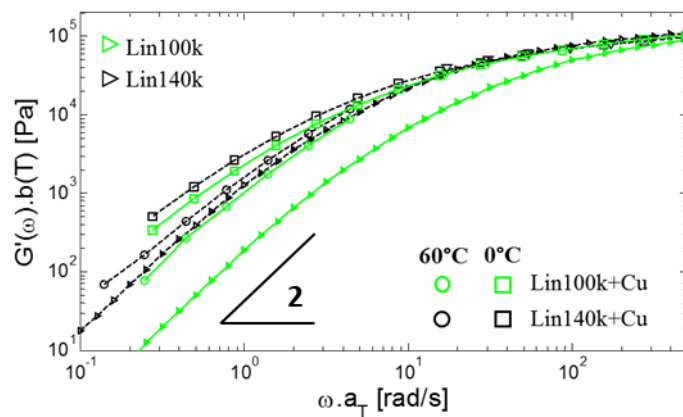

Figure 4.13 Storage modulus of the reference samples Lin100k (green, ▷) and Lin140k (black, ▷), and of the supramolecular samples Lin100k+Cu (green) and Lin140k+Cu (black), measured at T = 60°C

(o) and 0°C (□). The data have been shifted to a reference temperature of 25°C, based on the shift factors determined for the reference samples.

We now move on to provide a quantitative account using our modified tube model. Figure 4.14 compares model predictions and data. Solid lines refer to model predictions when ligand exchange is considered while dashed lines are the corresponding predictions when sticker dissociation/ association events are disregarded. In the latter case the single and double chains present at time $t = 0$ stay in the same state during the whole frequency range, meaning that they are not allowed to dissociate or associate. This allows us to evaluate the influence of chain dissociation, going from double chains to single chains. Figures 4.14.a and 4.14.c reveal that at high T the model compares better with the data when ligand exchange is accounted for. Nevertheless, the ligand exchange effect is not as important as in the case of telechelic star molecules in which it is clearly visible. The influence of ligand exchange also explains why a well fitted master-curve cannot be constructed with the data of the star complexes at different temperatures. There, the sample relaxation depends on the longest association time τ_{final}, which strongly varies with the temperature, in a different way as the Rouse time of an entanglement segment, τ_e. This is further discussed in the next section.

Interestingly, same values of the longest relaxation time, τ_{final}, have been used for all these samples, i.e. for the two linear and the two star polymers, suggesting that the average effective lifetime of an associated bond does not depend on the chain architecture, but is only a function of the temperature. On the other hand, the fraction of associated arms, p_{ass}, is found to be identical for the two telechelic stars ($p_{ass} = 0.45$), while it differs for the mono-functional linear chains ($p_{ass} = 0.65$ for Lin100k and $p_{ass} = 0.25$ for Lin140k). This can be understood by the fact that these samples have different density of ions and different chain mobility which should affect the ability to create efficient bis-terpyridine complexes. The low fraction of associated chains of sample (Lin140k+Cu), with an effective association time τ_{final} of 5 s at 60°C also explains the small influence of the stickers found in Figure 4.13 for this sample.
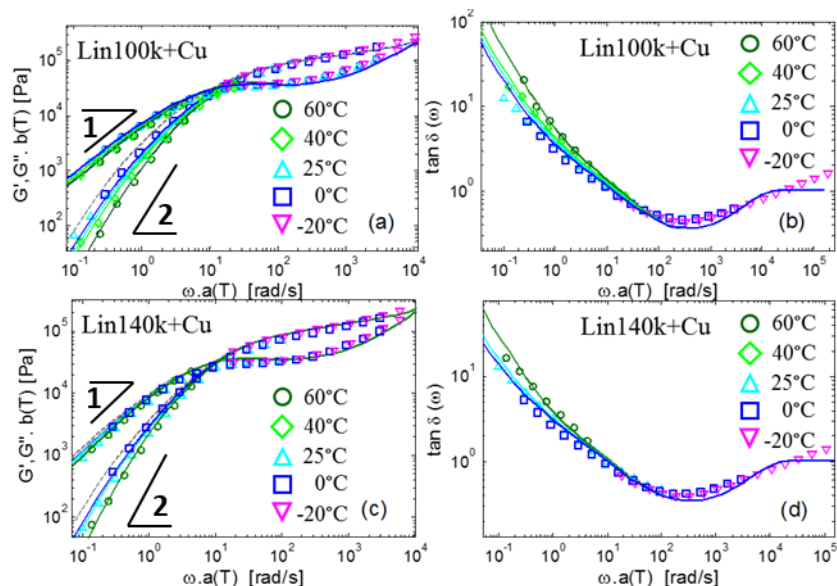
225

Figure. 4.14 Storage modulus, Loss modulus and tan δ curves of the mono-functional sample Lin100k+Cu (Panels a and b, respectively) and Lin140k+Cu (Panels c and d, respectively). The experimental data have been measured at temperature T = 60°C (dark green, o), 40°C (green, ◊), 25°C (cyan, Δ), 0°C (blue, □) and -20°C (magenta, ∇). The experimental data (symbols) have been shifted to a reference temperature of 25°C, based on the shift factors determined for the reference samples. The theoretical curves (continuous and dashed curves) have been obtained by fixing p_{ass} = 0.65 for Lin100k+Cu and 0.25 for Lin140k+Cu, and using the same values of τ_{final} = 5 s at 60°C, 50 s at 40°C, 250 s at 25°C and 5000 s at 0°C. The dashed lines represent the predicted moduli if we exclude any sticker dissociation or association.

4.4.3 Influence of the ion nature

While in Sections 4.4.1 and 4.4.2, the viscoelastic properties of the telechelic molecules in presence of copper ions have been analyzed, we now vary the nature of the ions. An extreme case is found with the star systems associated with zinc ions, which leads to weaker bonds compared to the copper ions.[40] Results obtained with the two star polymers are shown in Figure 4.15. Despite the fact that these samples

have similar effective association time, τ_{final} (see below) and that the associated arms cannot relax before the dissociation of their stickers, it is observed that the two samples have very different terminal times, contrary to the results found with copper (see Figure 4.9).
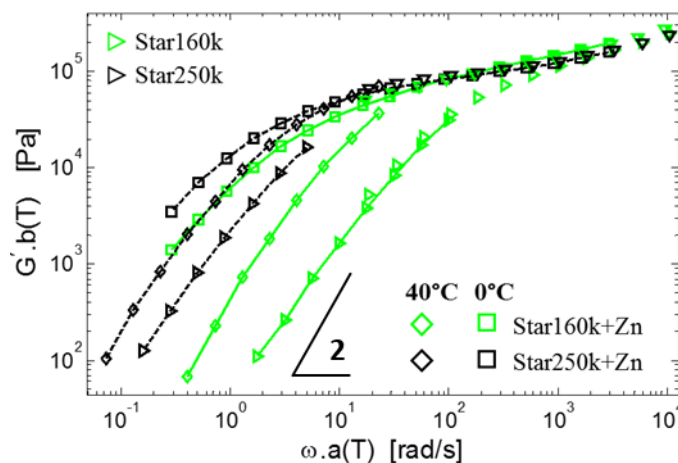

Figure 4.15 Storage modulus of the reference samples Star160k (green, $\triangleright$), Star250k (black, $\triangleright$), of the supramolecular samples Star160k+Zn (green) and Star250k+Zn (black), measured at T = 40°C ($\lozenge$) and 0°C ($\square$). The data have been shifted to a reference temperature of 25°C, based on the shift factors determined for the reference samples.

This can be explained by the fact that, in the specific case of Star250k+Zn, the lifetime of the metallo-supramolecular bonds is relatively short, in comparison to the relaxation time of Star250k by CLF and arm retraction mechanism. Therefore, their terminal relaxation stays dominated by the disentanglement time and is found to be only slightly longer than the terminal relaxation time of the reference sample (black, $\triangleright$) due to slight effect of zinc bis-terpyridine complexes. On the other hand, the terminal relaxation time of the Star160k+Zn is clearly longer compared to the relaxation of the Star160k reference. This indicates that the relaxation of this shorter sample is dominated by the dissociation time, as it is found with the other ions. In this case, the dissociation time is significantly longer than the relaxation time of the corresponding reference sample. From this example, it is expected that the dissociation time for zinc bis-terpyridine complex is around 1 s.

Figure 4.16 below presents a summary of the data based on telechelic samples with zinc ions. Again, same values of the parameter τ_{final} could be used, independently from the chain architecture. Furthermore, the parameter p_{ass} was also found to be the same for these four different sets of associating samples. The low values of the association times are consistent with the fact that the zinc complexes are very labile as discussed earlier.
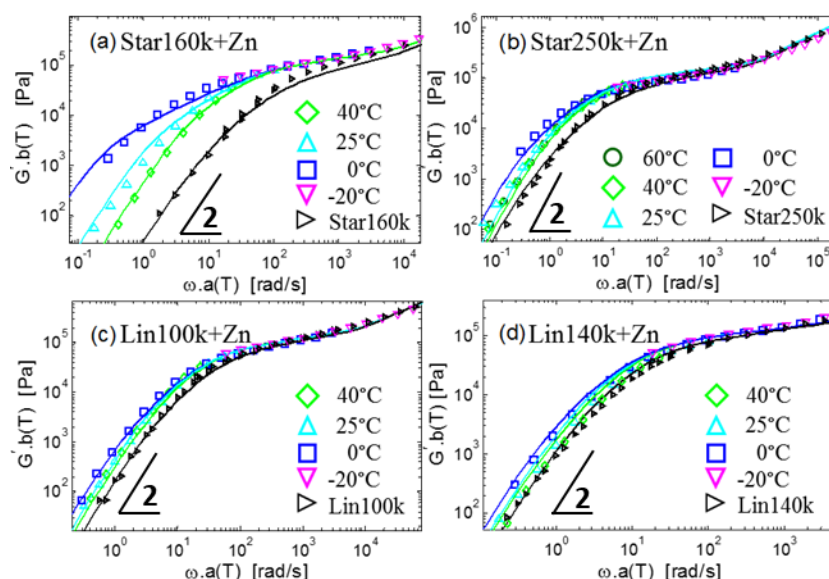

Figure 4.16 Storage modulus of samples Star160k+Zn (a), Star250k+Zn (b), Lin100k+Zn (c) and Lin140k+Zn (d), and their corresponding reference samples (black, $\triangleright$). The experimental data have been measured at temperature T = 60°C (dark green, o), 40°C (green, ◊), 25°C (cyan, Δ), 0°C (blue, □) and -20°C (magenta, ∇). The experimental data (symbols) have been shifted to a reference temperature of 25°C, based on the shift factors determined for the reference samples. The theoretical curves have been obtained by fixing p_{ass} = 0.4 for all the samples, as well as τ_{final} = 0.07 s at 60°C, 0.3 s at 40°C, 1 s at 25°C and 6 s at 0°C.

We also see in Figure 4.16 that temperature has only a small effect on the terminal relaxation time, compared to the samples with copper ions. This is due to the fact that the contribution of the disentanglement time

to the total relaxation time of the molecules (see Equations 4.9 and 4.10) becomes important. Therefore, since this part does not depend on temperature, the data being shifted in the same way as the reference sample, the difference between the different terminal relaxation times is reduced.

On the other hand, if a stronger metal ion is used such as cobalt ions, the thermo-rheological complexity of the sample is enhanced. This is shown in the Figure 4.17 for the telechelic Star250k+Co as well as the two mono-functional linear chains Lin100k+Co and Lin140k+Co. Here again, same values of the association time could be used for all these samples. However, a larger discrepancy is observed between the experimental and the theoretical data, especially in the low frequency window of the tan δ curves. In particular, it is observed that a small fraction of sample Lin140k+Co relaxes slower than the predicted relaxation of linear chains with twice the molecular weight of Lin140k, i.e. 280 kg/mol (see the dashed curves on Figure 4.17.f). As discussed earlier in Chapter 3, this could be due to the presence of few small aggregates (not detectable by WAXS measurement).
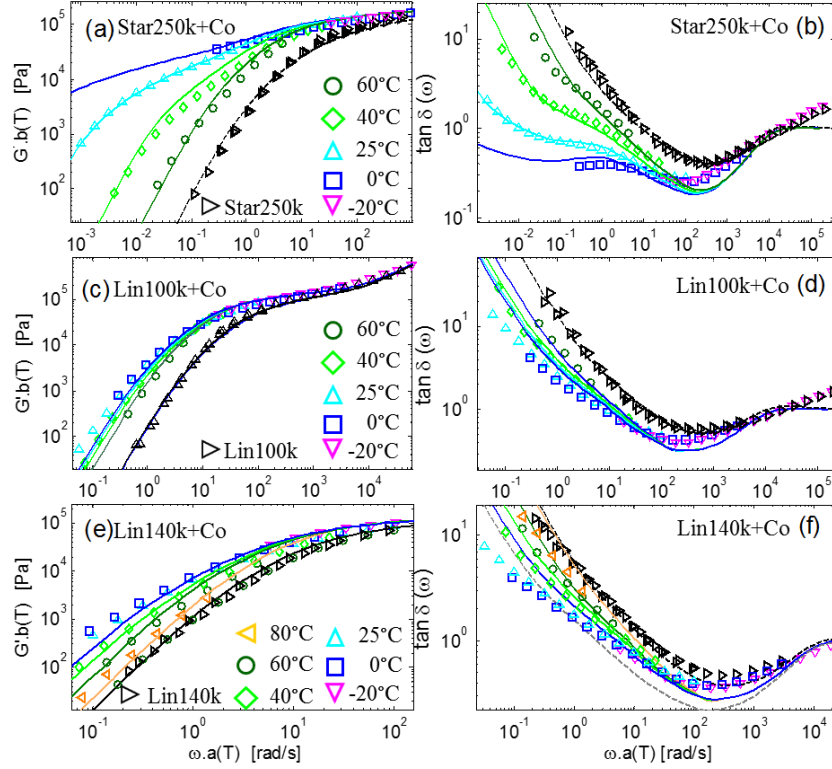
Figure 4.17 Storage modulus and tanδ curve of samples Star250k+Co (a, b), Lin100k+Co (c, d) and Lin140k+Co (e, f), and their corresponding reference samples (black, ▷). The experimental data have been measured at temperature T = 80°C (orange ◁), 60°C (dark green, o), 40°C (green, ◊), 25°C (cyan, Δ), 0°C (blue, □) and -20°C (magenta, ∇). The experimental data (symbols) have been shifted to a reference temperature of 25°C, based on the shift factors determined for the reference samples. The theoretical curves have been obtained by fixing p_{ass} = 0.65 with the Star250k and Lin140k, and p_{ass} = 0.85 with the Lin100k. For all samples, τ_{final} = 0.4 s at 80°C, 7 s at 60°C, 70 s at 40°C, 1200 s at 25°C and $4 \cdot 10^4$ s at 0°C.

4.4.4 Value of the effective association time τ_{final}

Since the theoretical curves have been obtained by determining the longest effective association time τ_{final} by best fitting procedure, it is interesting to analyze how this parameter depends on temperature for the different ion complexes. The influence of temperature on the local dynamics of the molecules has been taken into account by shifting the experimental data following the WLF equation determined for the reference sample. Therefore, the variation of τ_{final} is only related to the supramolecular dynamics of the reversible bonds. Results are shown in Figure 4.18 and we observe that all sets of data fall into a line, when plotted in a semi-log graph as a function of the inverse temperature. This is consistent with Arrhenius dependence, which is known to well describe the temperature dependence of most of the associative systems:

$$\tau_{final}(T) = \tau_{final}(T = 25\,^{\circ}C)\, exp\left(\frac{E_a}{RT}\right) \tag{4.15}$$
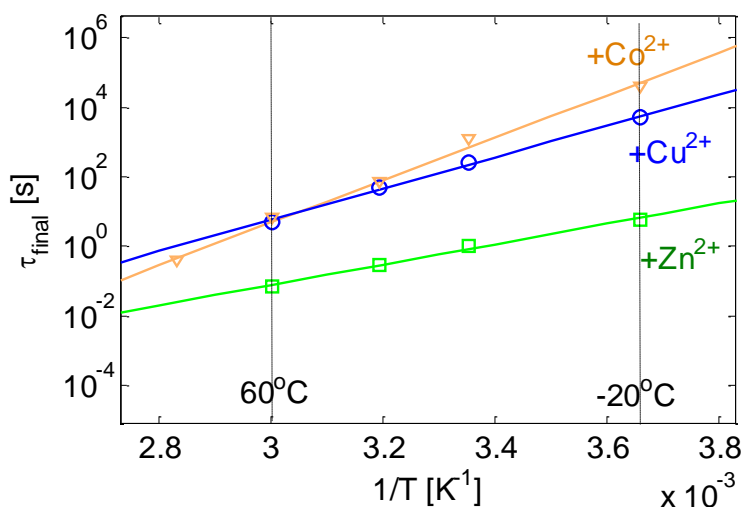

Figure 4.18 τ_{final} versus inverse temperature for the systems based on Cu ions (blue o) or Zn ions (green □) and Co ions (orange ∇).

This figure clearly shows that the influence of temperature on the dynamics of the reversible bonds follows an Arrhenius equation,

while its influence on the local mobility of the molecules is well described by a WLF equation. These two different dependences allow us to explain the thermo-rheological complexity of the samples. While at high frequency, the relaxation moduli are only governed by the local mobility of the molecules and thus follow a WLF equation, the moduli are governed by both dynamics at low frequency. It is also important to note that the experimental terminal relaxation time does not correspond to τ_{final}, but is influenced by both τ_{final} and the disentanglement time of the molecules. Since these two times vary differently with temperature, their relative importance is also a function of T (as shown and discussed with Figure 4.9).

From Equation 4.15, we can determine the activation energy E_a of the complexes with the different ions. It is found that $E_a = 168$ kJ/mol for Co^{2+}, 125 kJ/mol for Cu^{2+}, and 81 kJ/mol for Zn^{2+}. These relatively high values, especially with cobalt, are consistent with the fact that metal-ligand associations are quite strong associations.[41] Since the effective association time τ_{final}, and thus the activation energy was found not to depend on the chain architecture, one should be able to determine these values for other polymers based on the same terpyridine-ion complexes. Thus, if τ_{final} can be determined in advance, the only unknown parameter of the model is the average fraction of associated stickers, p_{ass}. However, it is important to remind that these results are valid as long as the samples contain a stoichiometric amount of metal ions, and that association/dissociation events are achieved via ligand exchanges, as mentioned in assumption A3. If an excess of ions is considered, the fraction of free dangling ends will be strongly reduced and longer association times will be found.

4.5   Conclusions

In this chapter, we investigated the linear viscoelastic behavior of entangled telechelic star PnBA and mono-functional linear PnBA which are able to associate through metal-ligand interactions. Terpyridine was used as ligand and several ions of different lability (Co^{2+}, Cu^{2+} and Zn^{2+}) were added to the samples, in stoichiometric amount. Based on the experimental data, we could show that the

relaxation of the samples depends on both disentanglement and association dynamics. By playing with temperature, we could vary the respective importance of these two processes and analyze their impact on the terminal relaxation time of the samples. It was found that the latter mostly depends on the slower process. By looking at sample relaxation in the intermediate range of frequencies, we also pointed out the presence of a large amount of unassociated stickers in the samples.

Based on these observations, we developed a modified version of our tube-based TMA model, in order to account for the dynamics of the stickers. In particular, inspired by the recent work of Wang et al.[22], we considered dissociation of a metal-ligand complex to take place via ligand exchange. The model contains two unknown parameters, i.e. p_{ass}, the fraction of associated stickers, and τ_{final}, the longest time needed to ensure that all the chains were dissociated at least once. We could determine these two parameters by best-fitting procedure and obtain a very good description of the experimental curves. It was found that τ_{final} is not dependent on the chain architecture and is well described by an Arrhenius equation. The corresponding activation energy could be determined, which let the model with only one undetermined parameter. Thus, with this work, we have now the necessary framework to explore other metallo-supramolecular networks, based on different architectures. In particular, we would like to study the viscoelastic behavior of blends of two kinds of telechelic polymers as well as blends of telechelic and covalent molecules, and to be able to control the modulus of these samples.

Bibliography

(1) Burattini, S.; Greenland, B. W.; Merino, D. H.; Weng, W.; Seppala, J.; Colquhoun, H. M.; Hayes, W.; MacKay, M. E.; Hamley, I. W.; Rowan, S. J. *J. Am. Chem. Soc.* **2010**, *132*, 12051–12058.

(2) Lewis, C. L.; Stewart, K.; Anthamatten, M. *Macromolecules* **2014**, *47*, 729–740.

(3) Chen, Q.; Tudryn, G. J.; Colby, R. H. *J. Rheol.* **2013**, *57*, 1441–1462.

(4) Chen, Q.; Masser, H.; Shiau, H. S.; Liang, S.; Runt, J.; Painter, P. C.; Colby, R. H. *Macromolecules* **2014**, *47*, 3635–3644.

(5) Winter, A.; Schubert, U. S. *Chem. Soc. Rev.* **2016**, *45*, 5311–5357.

(6) Herbst, F.; Döhler, D.; Michael, P.; Binder, W. H. *Macromol. Rapid Commun.* **2013**, *34*, 203–220.

(7) Cordier, P.; Tournilhac, F.; Soulié-Ziakovic, C.; Leibler, L. *Nature* **2008**, *451*, 977–980.

(8) Hu, J.; Zhu, Y.; Huang, H.; Lu, J. *Prog. Polym. Sci.* **2012**, *37*, 1720–1763.

(9) Xie, T. *Nature* **2010**, *464*, 267–270.

(10) Bae, Y.; Fukushima, S.; Harada, A.; Kataoka, K. *Angew. Chemie Int. Ed.* **2003**, *42*, 4640–4643.

(11) Webber, M. J.; Appel, E. A.; Meijer, E. W.; Langer, R. *Nat. Mater.* **2015**, *15*, 13–26.

(12) Wei, Q.; Schlaich, C.; Prévost, S.; Schulz, A.; Böttcher, C.; Gradzielski, M.; Qi, Z.; Haag, R.; Schalley, C. A. *Adv. Mater.* **2014**, *26*, 7358–7364.

(13) Callies, X.; Véchambre, C.; Fonteneau, C.; Pensec, S.; Chenal, J.-M.; Chazeau, L.; Bouteiller, L.; Ducouret, G.; Creton, C. *Macromolecules* **2015**, *48*, 7320–7326.

(14) Cao, Y.; Li, H. *Nat. Mater.* **2007**, *6*, 109–114.

(15) Marrucci, G.; Bhargava, S.; Cooper, S. L. *Macromolecules* **1993**, *26*, 6483–6488.

(16) Indei, T.; Schieber, J. D.; Takimoto, J. *Rheol. Acta* **2012**, *51*, 1021–1039.

(17) Manassero, C.; Raos, G.; Allegra, G. *J. Macromol. Sci. Part B Phys.* **2005**, *44*, 855–871.

(18) Wilson, M.; Rabinovitch, A.; Baljon, A. R. C. *Phys. Rev. E* **2011**, *84*, 1–8.

(19) Rubinstein, M.; Semenov, A. N. *Macromolecules* **2001**, *34*, 1058–1068.

(20) Semenov, A. N.; Rubinstein, M. *Macromolecules* **2002**, *35*, 4821–4837.

(21) Bedrov, D.; Smith, G. D.; Douglas, J. F. *Europhys. Lett.* **2002**, *59*, 384–390.

(22) Amin, D.; Likhtman, A. E.; Wang, Z. *Macromolecules* **2016**, *49*, 7510–7524.

(23) van Ruymbeke, E.; Vlassopoulos, D.; Mierzwa, M.; Pakula, T.; Charalabidis, D.; Pitsikalis, M.; Hadjichristidis, N. *Macromolecules* **2010**, *43*, 4401–4411.

(24) Boudara, V. A. H.; Read, D. J. *J. Rheol.* **2017**, *61*, 339–362.

(25) Zhuge, F.; Brassinne, J.; Fustin, C.-A.; van Ruymbeke, E.; Gohy, J.-F. *Macromolecules* **2017**.

(26) Jackson, A. C.; Beyer, F. L.; Price, S. C.; Rinderspacher, B. C.; Lambeth, R. H. *Macromolecules* **2013**, *46*, 5416–5422.

(27) Ferry, J. D. *Viscoelastic Properties of Polymers*, 3rd Editio.; Wiley, Ed.; Wiley: New York, 1980.

(28) Ruymbeke, E. Van; Muliawan, E. B.; Vlassopoulos, D.; Gao, H.; Matyjaszewski, K. *Eur. Polym. J.* **2011**, *47*, 746–751.

(29) Walsh, D.; Zoller, P. *Standard Pressure-Volume-Temperature Data for Polymers*; Press, C., Ed.; Press, CRC: New York, 1995.

(30) Shchetnikava, V.; Slot, J. J. M.; van Ruymbeke, E. *Macromolecules* **2014**, *47*, 3350–3361.

(31) Hawke, L. G. D.; Ahmadi, M.; Gondansaz, H.; van Ruymbeke, E. *J. Rheol.* **2016**, *60*, 297–310.

(32) Tierney, N. K.; Register, R. A. *Macromolecules* **2003**, *36*, 1170–1177.

(33) Chen, Q.; Zhang, Z.; Colby, R. H. *J. Rheol.* **2016**, *60*, 1031–1040.

(34) van Ruymbeke, E.; Vlassopoulos, D.; Kapnistos, M.; Liu, C. Y.; Bailly, C. *Macromolecules* **2010**, *43*, 525–531.

(35) Ebrahimi, T.; Taghipour, H.; Grießl, D.; Mehrkhodavandi, P.; Hatzikiriakos, S. G.; van Ruymbeke, E. *Macromolecules* **2017**, *50*, 2535–2546.

(36) Taylor, P.; Mcleish, T. C. B. *Adv. Phys.* **2002**, *51*, 1379–1527.

(37) van Ruymbeke, E.; Shchetnikava, V.; Matsumiya, Y.; Watanabe, H. *Macromolecules* **2014**, *47*, 7653–7665.

(38) Doi, M.; Edwards, S. F. *The Theory of Polymer Dynamics*; Oxford University Press, 1986.

(39) Milner, S. T.; McLeish, T. C. B. *Macromolecules* **1997**, *30*, 2159–2166.

(40) Holyer, R. H.; Hubbard, C. D.; Kettle, S. F. a; Wilkins, R. G. *Inorg. Chem.* **1966**, *5*, 622–625.

(41) Mendes, A. C.; Baran, E. T.; Reis, R. L.; Azevedo, H. S. *Wiley Interdiscip. Rev. Nanomedicine Nanobiotechnology* **2013**, *5*, 582–612.

Chapter 5

Nonlinear rheology of transient polymeric networks

Abstract

In this Chapter, we investigate the linear, nonlinear shear and uniaxial extensional viscoelasticity of telechelic low-disperse (below 1.3) entangled poly(*n*-butyl acrylate) chains functionalized with terpyridine ligands. Upon self-assembly, the telechelic four-arm star precursors form model networks with minimum fraction of defects. Most of the chain segments participate in the entangled network, contrary to networks originating from linear chains with metal binding ligands along their backbone, which contain a large proportion of dangling chain ends or loops. These model systems are therefore perfect to investigate how the dynamics of metallo-supramolecular bulk networks (MSBNs) is affected by both the dissociation kinetics of M-L complexes and the disentanglement process, and how these two mechanisms are coupled. The measurements are performed on a filament stretching rheometer and on a strain controlled rotational rheometer equipped with a cone-partitioned plate geometry. In extension the MSBNs show strain hardening at extension rates below their respective terminal relaxation times. Since the transient viscosity of MSBNs is measured at low strain rates, the strain hardening is attributed to the physical crosslinks which comprise M-L coordination. On the other hand, strong shear thinning behavior is observed at similar deformation rates in nonlinear shear flow. By altering the temperature, we systematically vary the relative importance of the M-L complexes, which allows us to determine their specific contribution to the network properties. Moreover, the properties of these systems can be finely tailored with varying the type or the nature of metal ions.

237

5.1 Introduction

5.1.1 Towards a complete mechanical investigations

Transient polymeric networks with dynamic cross-links are an important class of smart materials based on reversible, relatively weak and noncovalent interactions such as π-π stacking[1–3], hydrogen bonding[4,5], host-guest complexation[6–8], metal-ligand coordination[9–11] and ionic interactions.[12–14] The advent of dynamic metal-ligand (M-L) coordination has emerged as a powerful strategy for the design of various self-assembled materials with stimuli-responsive properties.[15] Among them, reversible polymeric networks obtained by functionalizing flexible polymer chains with M-L coordination are a promising avenue to engineer soft materials with tunable mechanical properties.[16] Contrary to covalently cross-linked networks, metallo-supramolecular bulk networks (MSBNs) have transient associations with relatively weak binding energy with respect to covalent counterpart[17], so that external stimuli or thermal fluctuations enhance dissociation and re-formation of M-L coordination at different timescales suitable for material engineering.[18] This reversibility provides unique properties such as healing[19,20], stimuli-responsive or shape-memory features.[21–23] Moreover, these metal-containing polymeric systems may give access to additional magnetic, redox, optical or electrochromic properties.[24,25] As finely tunable materials, MSBNs can be found in numerous applications such as optoelectronic materials[26], adhesives[27], smart coatings[28], energy conversion and storage devices.[29]

The linear rheology of associating polymeric networks bearing dynamic junctions has been the topic of several studies.[18,30–33] In general, due to the delayed diffusional motion of polymer chains, three effects are often highlighted, (i) the longer terminal relaxation times, (ii) the increase in plateau modulus and consequently, (iii) the increase of viscosity which is several orders of magnitude higher with respect to the polymer melts. Under linear deformation, these systems behave as soft elastic solids at times shorter than the lifetime of the sticky

junctions but they also exhibit viscous liquid-like behavior on longer timescales during which M-L cross-links dissociate. In absence of aggregates, the dynamic moduli of metallo-supramolecular networks is modulated by the exchange rate of physical cross-links as long as the exchange timescale is faster than that of polymer diffusion.[34]

Under large shear deformation, only limited works have been reported on the nonlinear viscoelastic properties of metallo-supramolecular networks which are more challenging. In shear, Craig et al. reported the nonlinear rheological properties of MSNs formed by reversible cross-links of semi-dilute unentangled poly(4-vinylpyridine), i.e. PVP solutions.[35] The physical junctions were based on palladium(II) or platinum(II) coordinated to the pyridine group of PVP. Under steady shear, both shear-thinning and shear thickening were observed on metallopincer-crosslinked PVP networks. Usually, systems with fast dissociation kinetics display a shear-thinning behavior which is attributed to the shear induced disentanglements of associating and dissociating network chains. Whereas for systems with slower dissociation kinetics, a shear-thickening behavior is observed, due to the network reorganization above a critical shear rate. The latter enhances shear-induced reorganization of the transient network which transforms intra-chain cross-links into inter-chain ones, resulting in a reinforced polymeric network. Later on, Craig et al. pursued their work in the semi-dilute entangled regime and results reveal various types of shear-thinning or thickening which depend on the polymeric concentration, on the cross-link density and its efficiency (rate of dissociation and association).[36] The divergent steady shear behavior was related to a competition between two different timescales: the average time during which a sticker remains associated or dissociated and the local relaxation time of a polymer chain.

In contrast, molten transient networks have been extensively studied in tensile tests with a wide selection of metal-ligand coordination as physical cross-links. For instance Guan et al. elaborated a hard/soft two-phase brush copolymer based on polystyrene as the backbone from which imidazole modified poly(n-butyl acrylate) brushes were grown.[37] The addition of zinc(II) ions was enhancing the formation of MSBNs with Zn^{2+}-imidazole interactions acting as physical cross-links which ameliorated the mechanical response toward

stretching. While numerous studies are reported in the literature on MSBNs, the majority of these works are focused on the high performances, e.g. improved strength and toughness along with the healing properties at the expense of fundamentally understanding the mechanical features of transient networks based on M-L interactions.[29,38–41] Regardless of the application, the possible industrial exploitation of transient networks hinges on their processability under large deformation and on their rheological behaviors. In this respect, the design of smart materials of supramolecular network is dependent on our fundamental understanding of their structure and dynamics in the molten state. The mechanical responses are not only governed by the association/dissociation events of the metal-ligand complexes but they are also modulated by the internal dynamics of the building blocks (entanglements). Therefore, the influence of these two processes on the rheological properties and how they interact need to be addressed and understood.
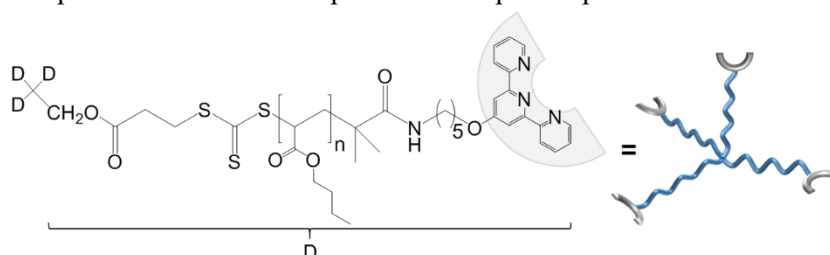
This chapter is the continuity of a systematic investigation on viscoelastic bulk properties of terpyridine containing poly(n-butyl acrylate)s dynamically cross-linked with different transition metal ions.[34] Precisely, a unique combined extensional and shear rheological experimental data set is provided on well-defined entangled telechelic star polymer as model system. The tridentate tpy ligand is used due to its ability to easily form complexes of different binding constants with a wide range of metal ions, thus allowing a decent control over the complex strength. The zinc(II), copper (II) or cobalt(II) cations are selected because of their thermodynamic stabilities and kinetics to form bis(terpyridine) complexes.[42] Moreover, they have the same charge and similar ionic radius, making them suitable for comparison. Upon addition of metal salts, dynamic MSBNs are obtained where metal-ligand complexes act as physical cross-links. Results show that the combination of M-L complexes along with polymer entanglements dictates the resistance capacity of the transient network under load. The amount of metal loading is systematically varied to control the ratio of uncoordinated stickers. These unbounded ligands play an active role on the network stress distribution and relaxation which occurs via ligand exchange mechanism.[34] Herein, the bulk rheological properties of

reversible networks are not only dependent on the dynamics of physical cross-links and building blocks but also on the presence of uncoordinated stickers. They influence the rate of ligand exchange, the stress redistribution under load and thus the transient network mechanical features under large deformation. By altering the temperature, we systematically vary the relative importance of the M-L complexes, which allows us to determine their specific contribution to the network properties. Moreover, the properties of these systems can be finely tailored by varying the type or the nature of metal ions. In section 5.2 the experimental procedures to elaborate transient networks and the methods are summarized. The obtained experimental results are explained in section 5.3 for shear rheology and in section 5.4. for uniaxial extension rheology. The conclusions are drawn in section 5.5.

5.2 Materials and methods

5.2.1 Materials

The synthesis of the telechelic four-arm star (M_n = 249 kg/mol) poly(n-butyl acrylate) end-capped with terpyridine ligand (4-arm star PnBA-tpy$_4$) was achieved by reversible addition-fragmentation chain-transfer (RAFT) polymerization in bulk condition as explained in Chapter 2.[43] Details on the precursor sample are provided in Table 5.1.

Samples	$M_{n, system}$[a]	$M_{n, arm}$[b]	Z=M_n/M_e[c]	Đ[d]	T_g[e]
	(kg/mol)	(kg/mol)			(°C)
Star250k	249	62	3.4 per arm	1.20	-52

Table 5.1 Structural parameters of telechelic 4-arm star PnBA-tpy$_4$ polymers.[a,b] Molar mass of whole system determined by ^{1}H-NMR.[c]

Number of entanglements calculated using M_e = 18 kg/mol.[d] Molar mass dispersity of the polymers determined by SEC, polystyrene standards were used for calibration. [e] Glass transition temperature measured by DSC.

5.2.2 Highlights on cone partitioned plate (CPP)

Nonlinear shear measurements were performed on an Ares (TA Instruments) rheometer equipped with a force rebalance transducer (2KFRTN1), using a home-made stainless steel cone-partitioned plate geometry designed by Vlassopoulos et al.[44-46] Pioneered by the work of Meissner et al.[47] and Schweizer et al.[48,49], the latter is built to properly fit into the ARES convection oven, ensuring an accurate temperature control (± 0.1°C). The tools have specific characteristics as depicted in Figure 5.1.

Inner parallel plate (ø = 6 mm)

Outer hollowed parallel plate (ø$_{hollow}$ = 6.2 mm, ø = 15 mm)

Polymer sample

Cone geometry
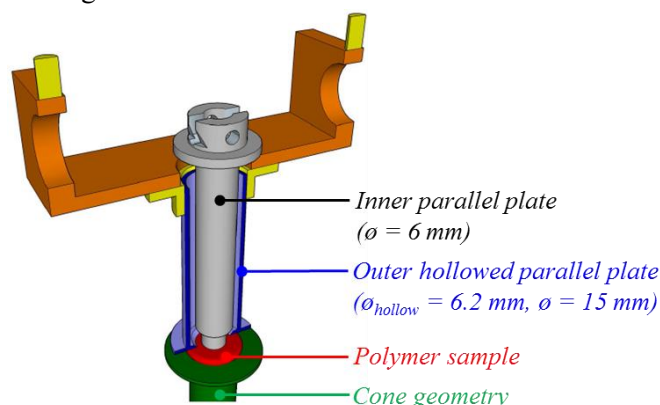
Figure 5.1 Scheme of the cone-partitioned plate setup.[46]

An inner measuring parallel plate with a diameter of 6 mm is directly connected to the transducer and an external hollowed parallel plate with an inner diameter of 6.2 mm and an outer diameter of 15 mm is used to protect the measured part of the sample. Once aligned, the gap between the two partitions is around 100 µm. A standard 50 mm diameter cone with an angle of 0.04 rad and a truncation of 58 µm was used as bottom geometry to reach high strain value as explained by Vlassopoulos et al.[45] Rheological measurements under large deformation of entangled polymeric systems are often challenging due to the presence of flow instabilities at high shear rate such as wall slip, shear banding or edge

fracture. The use of the CPP geometry can postpone the latter anomaly which allows us to collect more reliable data until the fracture that appears at the extremity of the sample propagates into the measured surface.

Dynamic meachanical measurements were carried out at given temperatures, using stainless steel 8 mm plate−plate geometries. The gap was adjusted between 400 and 500 μm so that the geometry was completely filled. The sample was equilibrated in the rheometer at 130°C for 30 min. Dynamic frequency sweeps were performed at a deformation amplitude of 3% over a temperature range of -20°C to 100°C and a frequency range of $10^2 - 10^{-3}$ rad/s. All dynamic measurements were performed within the linear viscoelastic region, which was determined from dynamic strain sweep experiments. At each temperature, the equilibration was checked with dynamic time sweep measurements up to 1 hour. The collected data were shifted along the frequency axis using the time-temperature superposition (TTS), yielding master curves that were constructed at the same reference temperature T_{ref} = 25°C. The temperatures for the nonlinear measurement were fixed in such a way that both the terminal flow and the rubbery plateau region can be observed in the frequency range from 100 to 0.1 rad/s.[44] Step-strain measurements were conducted with CPP at several shear rates ($100 - 0.1$ s^{-1}) and at different temperatures from 60°C to 40°C. Samples were equilibrated at 130°C for 30 min. Fresh samples were loaded when measurement reproducibility was beyond the experimental error.

5.2.3 Highlights on filament stretching rheometer

Nonlinear uniaxial extensional measurements were performed on a filament stretching rheometer (FSR) VADER 1000 with a force transducer of 5 Newton.[50] The device consists of a top and a bottom cylindrical stainless steel plates with a diameter of 6 mm between which the sample is sandwiched. A laser micrometer monitors the midfilament plane of the sample. The top plate moves upward, leading to a stretching of the filament and a load cell is mounted on the bottom plate as illustrated in Figure 5.2.
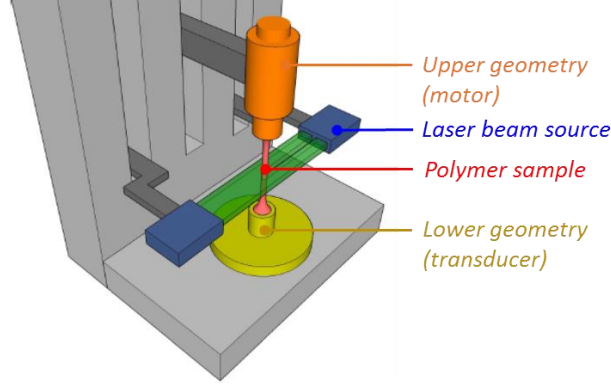
Figure 5.2 Scheme of the filament stretching rheometer VADER 1000.

The sample was molded in the instrument at 130°C. At such temperature, the MSP can flow to form a cylindrical shape with a fixed radius of $R_0 = 3.0$ mm and an initial length L_0 when the top plate was brought into contact with the sample. Once shaped, the sample was pre-stretched to a radius $R_p = 2.7 – 2.8$ mm at 130°C prior to the extensional measurements. The temperature was then decreased to the experimental temperature T and uniaxial stretching was performed under air and at constant Hencky strain rate ($\dot{\varepsilon}$). The Hencky strain (ε) and the corresponding mean extensional stress difference in the midfilament plane $<\sigma_{zz} - \sigma_{rr}>$ are defined as follows[51]:

$$\varepsilon(t) = -2 \, ln \frac{R(t)}{R_p} \qquad (5.1)$$

and

$$< \sigma_{zz} - \sigma_{rr} > = \frac{F(t) - \frac{m_f g}{2}}{\pi R^2(t)} X \frac{1}{1 + \left[\frac{R(t)}{R_0}\right]^{\frac{10}{3}} exp\left[\frac{-\Lambda_0^3}{3\Lambda_0^2}\right]} \qquad (5.2)$$

Where $R(t)$ is the midfilament radius at time t during a stretch experiment, m_f is the filament weight, g is the gravitational acceleration, F(t) is the force measured by the load cell, $\Lambda_0 = L_0/R_0$ is the initial aspect ratio of the sample and it ranged between 0.4 and 0.5. The extensional stress growth coefficient is defined as $\eta_{el}^+ = < \sigma_{zz} - \sigma_{rr} >/\dot{\varepsilon}$.

5.3   Shear rheology

5.3.1 Influence of metal ion amount on the linear viscoelasticity of MSBNs

From the systematic investigation on the linear viscoelastic of metallo-supramolecular bulk networks formed with different transitions metals, a focus is put on transient polymeric networks obtained with zinc(II), copper(II) and cobalt(II) ions because they display interesting dynamics with a decent compromise between frozen and labile networks as presented in Chapter 3. While the influence on the nature of metal ions over the linear rheology of MSBNs is highlighted, another factor such as the amount of added metal ions can also impact the mechanical properties of the resulting metal-containing system. For the following investigation, different amounts (0.50, 0.75 and 1.00 eq.) of cations were added to the polymeric precursors to form transient networks. Figure 5.3 shows the linear rheological properties at 40°C of telechelic 4-arm star PnBA-tpy$_4$ alone and mixed with different amounts of metal ions. The reference precursor without metal ion is in its terminal relaxation region. The latter is characterized by the cross-over between the storage and loss moduli, G'(ω) and G"(ω) and respectively exhibits scaling with ω^2 and ω^1 as expected from Maxwell prediction. The cross-over gives a characteristic terminal relaxation time ($\tau_{rel} = 1/\omega_{rel.}$) which is around 27 ms at 40°C for the precursor.
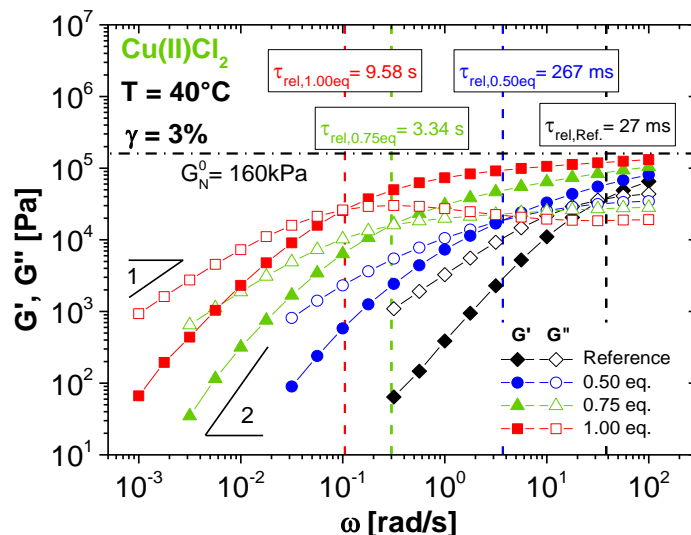
Figure 5.3 Linear rheology curves at 40°C of telechelic 4-arm star PnBA-tpy$_4$ (melts) with different amounts of copper(II) ions. The diamonds correspond to the reference polymer without metal ions. The storage modulus G' is represented by filled symbols, the loss modulus G" by unfilled symbols.

Once different amounts of copper(II) ions are added, the resulting transient polymeric systems behave differently from one mole ratio to the other. Initially, with 0.5 equivalents of Cu(II) ions (which corresponds to the stoichiometric amount of ions), the onset of the plateau modulus is probed and the terminal relaxation time $\tau_{rel, 0.5eq}$ = 267 ms is shifted to intermediate frequency. These observations certify the formation of transient MSBN upon addition of metal ions where metal-ligand complexes act as physical cross-links. As the amount of added metal ions increases, the rubbery plateau is extended over two and three decades of frequency with respectively 0.75 eq. and 1.00 eq. Their terminal relaxation times are also shifted to lower frequency with $\tau_{rel, 0.75eq}$ = 3.34 s and $\tau_{rel, 1eq}$ = 9.58 s, highlighting the formation of more stable reversible networks where the majority of the M-L cross-links dissociates at the timescale of the rheological experiment.

It must be noted that adding an excess of metal cations (0.75 or 1.00 eq.) compared to the theoretical stoichiometric ratio of 0.50 eq. gives access to higher cross-linked polymeric systems with a higher rubbery

plateau, which reaches a value close to the plateau modulus of entangled P*n*BA polymers, 160 kPa. We attribute the lower plateau level found with a lower amount of ions to the low density of metal ions in the polymeric matrix, making part of the cations unable to coordinate with terpyridine groups. Hence, at 0.50 eq. of metal ions, there is a fraction of uncoordinated chains that is not participating to the formation of the network. These dangling chains are relaxing at very short time. By adding an excess of metal ions, this fraction decreases because more transient junctions are formed and consequently the number of chains participating to the elasticity of the MSBNs increases.

The linear bulk rheological properties of MSBNs are strongly influenced by the thermodynamic stability and the kinetics of exchange of the M-L cross-links. As explained in Chapter 4, the ligand exchange mechanism is considered in presence of uncoordinated chains for the network relaxation.[34] At low content of metal ions, e.g. 0.50 eq., the M-L junctions can rapidly exchange due to the relatively high fraction of uncoordinated terpyridine end-capped chains which is estimated around 40%. Hence, this fraction has a direct impact on the mechanical properties by influencing the rate of cross-links remodeling under deformation. As the amount of metal ions is approaching 1.00 eq., almost all tpy units are coordinated to metal ions reducing the fraction of unbounded chains. The absence of uncoordinated tpy moieties further slows down the ligand exchange process which hinders the network remodeling and increases the network relaxation time. Note that, the presence of high cross-linking density also leads to higher fraction of entanglements trapped between two M-L junctions which also participate to the elasticity of the transient networks. Since the sample relaxation is governed by both the dissociation of the supramolecular bonds and the disentanglement of the chains, thermo-rheological complexity is observed at low frequency as shown in Figure 5.4, which presents the linear rheology of the telechelic 4-arm star precursor and its resulting metallo-supramolecular bulk network over a range of temperatures (from 80 to -20°C). Master curves are constructed by setting the reference temperature at 25°C for all bulk materials, and by applying the time−temperature superposition (TTS) principle, based on the reference polymer without metal ions.
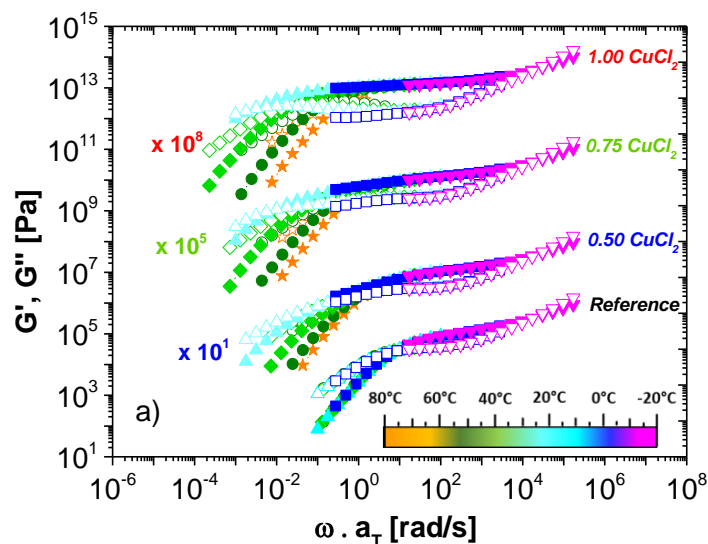
Figure 5.4 a) Master curves for the reference sample Star250k and of the Star250k + Cu(II) measured at temperature T = 80°C (orange, ★), T = 60°C (dark green, o), 40°C (green, ◊), 25°C (cyan, Δ), 0°C (blue, □) and -20°C (magenta, ∇). The experimental data have been shifted to a reference temperature of 25°C, based on the shift factors determined for the reference samples. Additionally data are vertically shifted for clarity. The storage modulus G' is represented by filled symbols, the loss modulus G" by unfilled symbols.
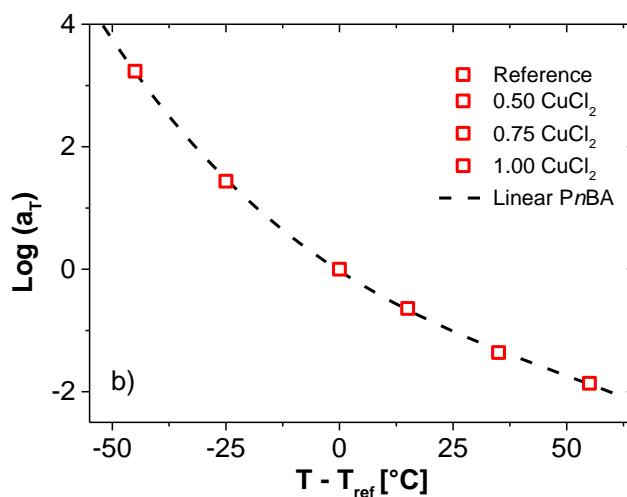
Figure 5.4 b) The same horizontal shift factors (a_T) are used for the Star250k and for the Star250k + Cu(II) with $T_{ref} = 25$°C.

To summarize, the uncoordinated terpyridine end-capped chains can impact the relaxation of the transient networks and their bulk properties. As more metal ions are added to the system, the polymeric network becomes more cross-linked, the rate of ligand exchange mechanism is reduced, and the resulting network further displays a collectively higher resistance towards flow, i.e. longer relaxation time and higher rubbery plateau. At some point, there should be a critical amount of metal ions above which the ligand exchange mechanism is becoming very slow because all stickers are associated and therefore the fraction of uncoordinated chains reaches zero. This proposed picture is supported by WAXS analysis reported in Figure 5.5, which shows that there is no formation of metal cation aggregates or clusters from the hydrophobic polymer matrix.
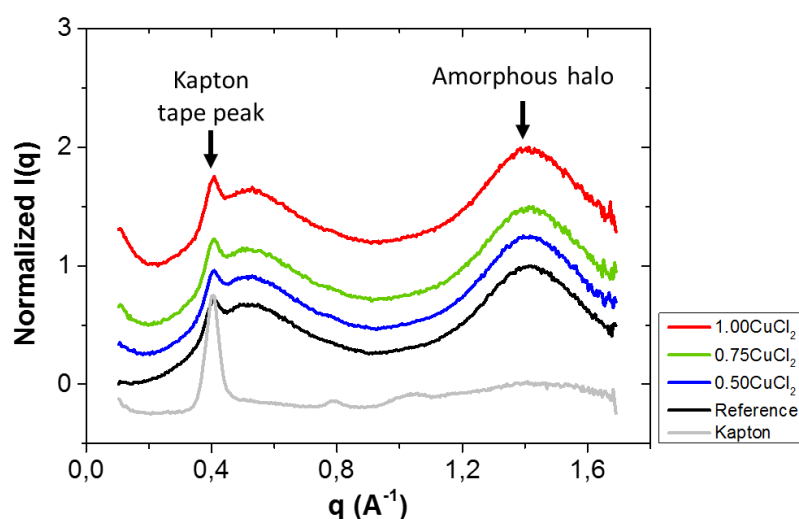
Figure 5.5 Wide angle X-ray scattering of telechelic 4-arm star PnBA-tpy$_4$ with different amounts of Cu(II)Cl$_2$. Only the polymer amorphous halo is probed without any trace of aggregates at nanoscale.

By adding different amounts of transition metal ions to form bis(terpyridine) complexes, it is possible to engineer the bulk linear viscoelastic properties of metallo-supramolecular bulk networks. Depending on the quantity of metals added, the latter directly influences the density of active M-L cross-links (i.e. the structure of the transient network) and the rate of metal-ligand exchange (i.e. the temporal

249

response towards flow). It is expected that the nonlinear viscoelastic properties of MSBNs can be tailored using the same approach.

5.3.2 Influence of metal ion amount on the nonlinear viscoelasticity of MSBNs

Start-up deformation is the most commonly applied measurement to explore nonlinear rheological responses of molten polymers. Herein, the startup shear data of a telechelic 4-arm star precursor and its resulting reversible networks with different amounts of copper(II) ions are systematically measured at 40°C by using the CPP geometry. For instance, Figure 5.6 illustrates typical transient shear viscosity results for the precursor material and the transient network obtained with 0.50 equivalents of copper(II) chloride.

The precursor material exhibits a linear response when the shear rate ($\dot{\gamma}$) is smaller than 31.62 s^{-1}, because the entanglement state of the chains is left intact. In a dimensionless form, this deformation rate corresponds to a Weissenberg number (Wi = $\dot{\gamma}.\tau_{rel}$) below unity and in this case homogeneous deformation is expected to prevail. Under the condition Wi > 1, i.e. shear rate higher than the reciprocal relaxation (fluctuations) time of the star precursor, a slight viscosity overshoot is observed. The latter corresponds to a yield point delimiting the end of an elastic deformation and the onset of an irreversible deformation.
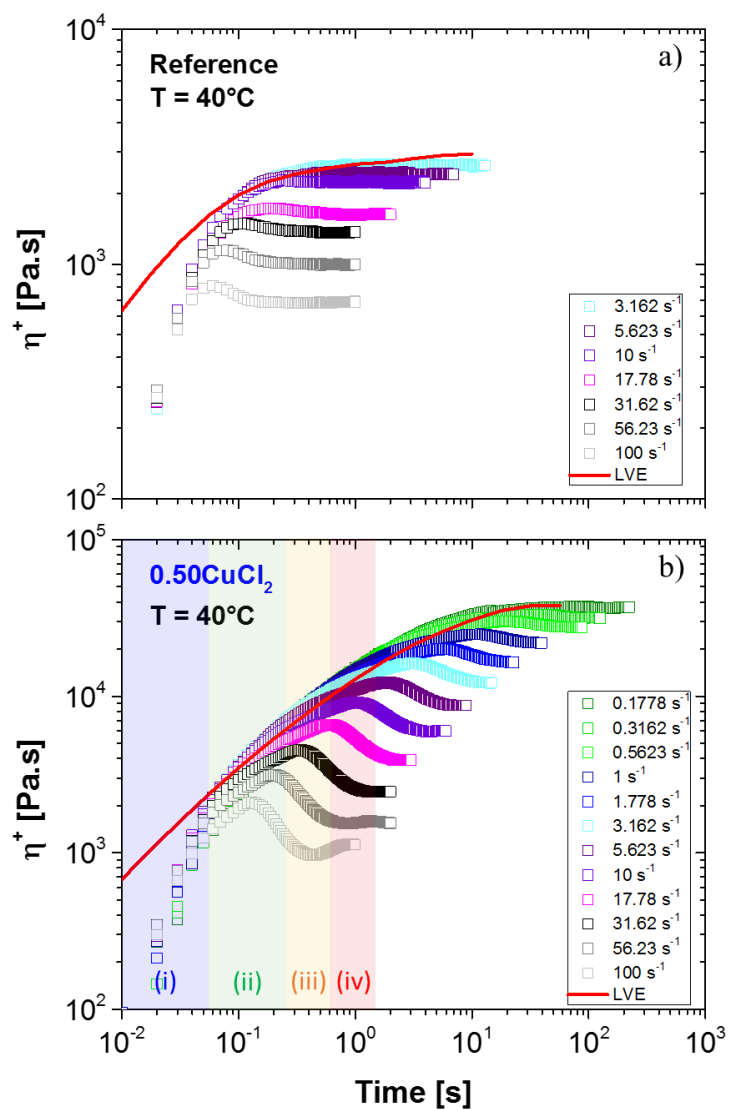
Figure 5.6 Transient shear viscosity at 40°C of a) telechelic 4-arm star P*n*BA-tpy$_4$ and b) telechelic 4-arm star P*n*BA-tpy$_4$ + 0.50eq. of Cu(II)Cl$_2$ at different shear rates ranging from 0.1 to 100 s^{-1}.
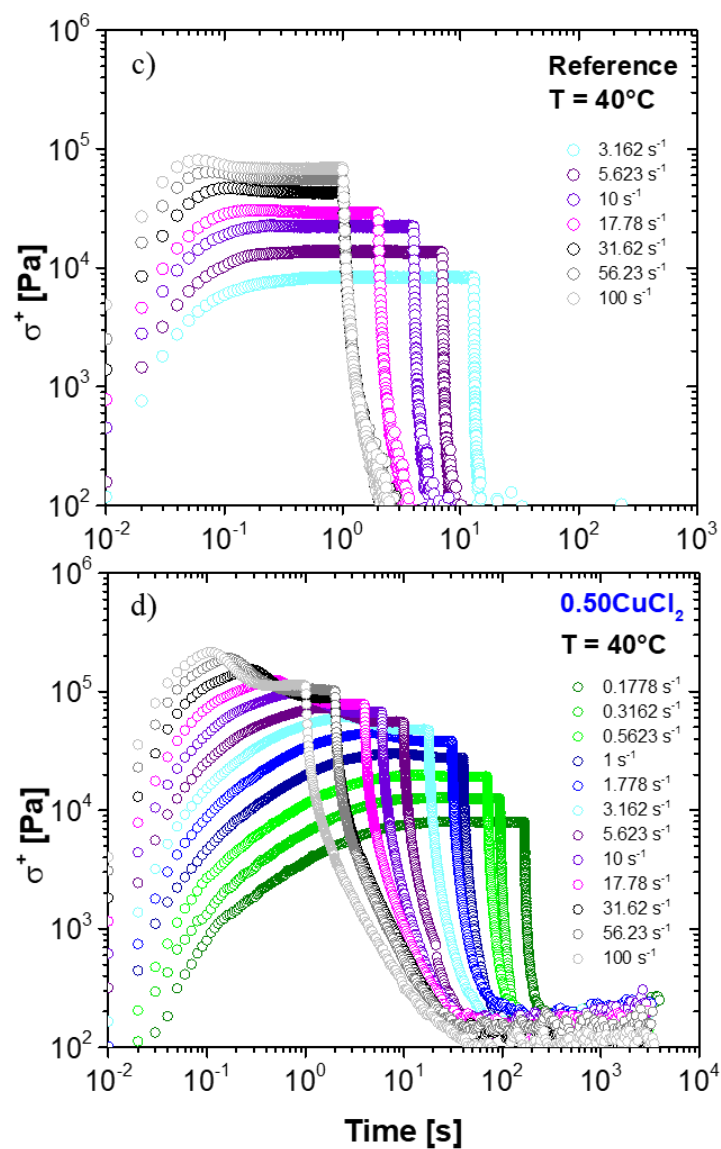
Figure 5.6 Stress relaxation upon cessation of simple shear flow at 40°C for c) telechelic 4-arm star P*n*BA-tpy4 and d) telechelic 4-arm star P*n*BA-tpy4 + 0.50eq. of Cu(II)Cl2 at different shear rates ranging from 0.1 to 100 s^{-1}.

While the precursor shows typical linear responses with a slight hump at high shear rates, the transient networks with 0.50 eq. of copper(II) clearly displays four different regions. At relatively short time the viscosity increases linearly which corresponds to the elastic deformation region (i) as mentioned above. Note that the transient viscosity does not overlap well with the linear viscoelastic envelope at relatively short times, which is probobaly due to a time resolution issue of the instrument itself. A clear overshoot region (ii) is probed when Wi is above unity. The latter is attributed to the collective orientation and stretching of the entangled transient network towards the deformation which produces yielding.[52–54] Below the yield point (or the maximum transient shear viscosity), the sample undergoes complete elastic recoil and can nearly fully recover its initial equilibrium state. The degree of elastic recovery is related to the structural integrity of the entangled MSBN. On the contrary, the recovery is impeded and cannot be fully completed when the sample is far beyond the yield point. Right after the overshoot, another region (iii) may appear, especially during high shear rate startup measurement that reveals an undershoot in the transient shear viscosity. The latter is attributed to the shear-induced motion of the chains, i.e. the tumbling motion of entangled polymers as suggested by Costanzo et al.[46] and confirmed by other studies.[55,56] Precisely, the chains initially stay aligned to the shear direction and then they suddenly flip direction by a shear-induced rotation. Finally, the steady state region (iv) is reached where the transient viscosity stays constant with increasing shear strain. In this region, the deformation is dissipative where the chains have remodeled themselves into less entangled or no longer entangled structures in their deformed states.

Similar nonlinear investigations were conducted under the same conditions, at different imposed shear rates (ranging from 0.1 to 100 s^{-1}) on dynamic reversible networks obtained with 0.75 and 1.00 eq. of $CuCl_2$ and results are reported in Figure 5.7.
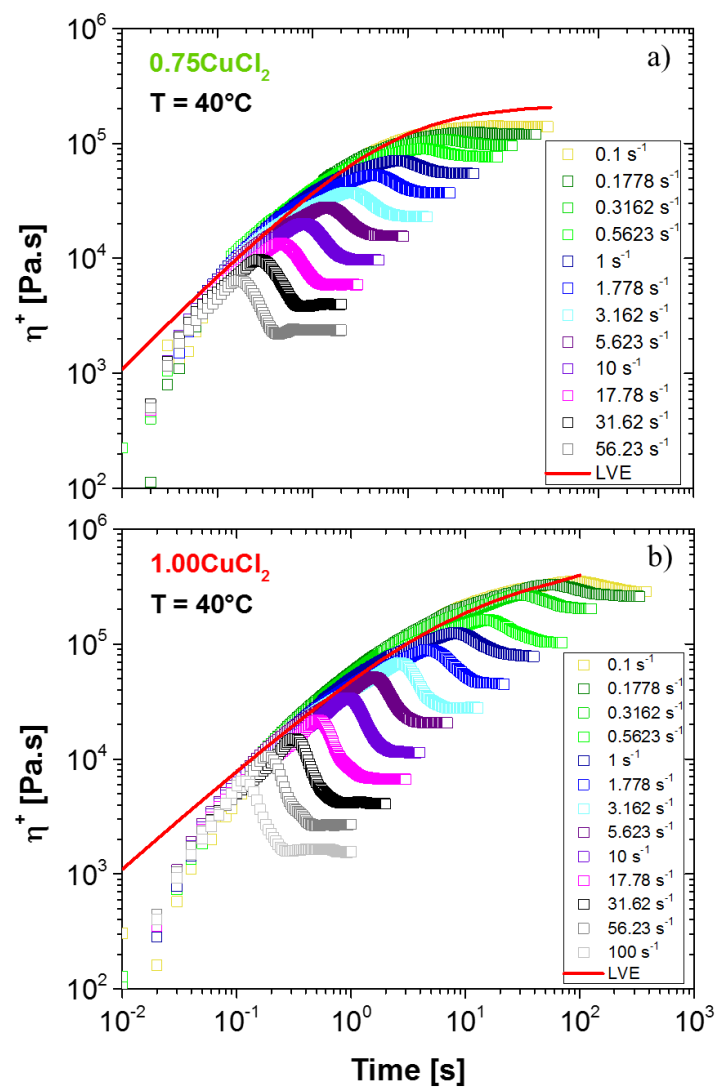
Figure 5.7 Transient shear viscosity at 40°C MSBNs obtained with a) 0.75eq. of CuCl₂ and b) 1.00eq. of CuCl₂ at different shear rates ranging from 0.1 to 100 s⁻¹.
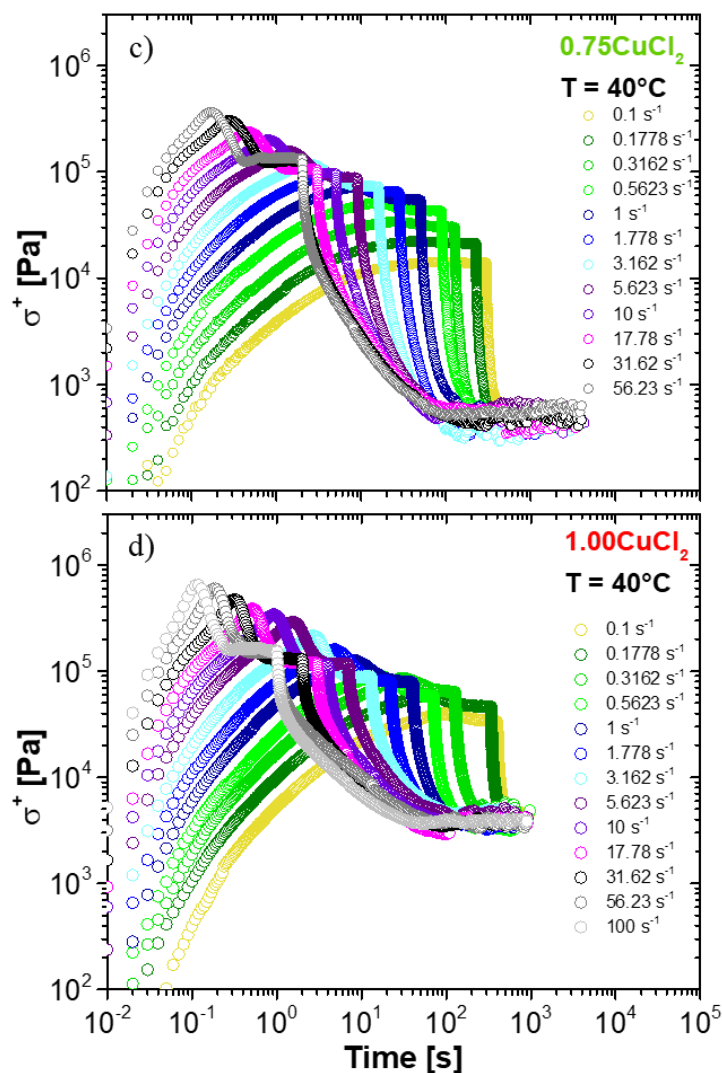
Figure 5.7 Stress relaxation upon cessation of simple shear flow at 40°C for MSBNs obtained with a) 0.75eq. of CuCl$_2$ and b) 1.00eq. of CuCl$_2$ at different shear rates ranging from 0.1 to 100 s^{-1}.

In order to compare the nonlinear data between the reference sample and the transient networks cross-linked with M-L interactions, the maximum transient shear viscosity (i.e. the yield point, η_{max}) and the steady state shear viscosity (η_{steady}) are extracted from the results. For instance, the empirical Cox-Merz rule is applied on the steady state

255

shear viscosity of the 4-arm star precursor along with the transient networks and results are shown in Figure 5.8.[57]
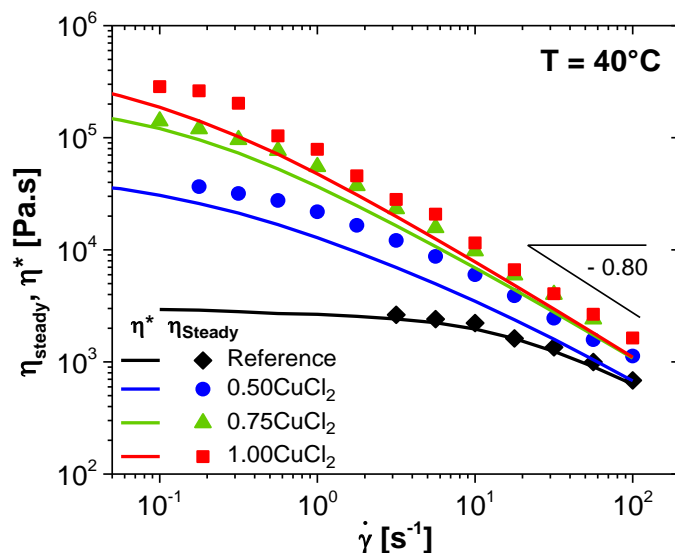
Figure 5.8 Cox-Merz rule for telechelic 4-arm star P*n*BA-tpy₄ (black, ◊), with different amounts of copper(II) ions 0.50eq. (blue, o), 0.75eq.(green, Δ) and 1.00eq.(red, □) at 40°C.

The latter consists in comparing the complex viscosity obtained from linear oscillatory shear rheology with the steady state transient shear viscosity and checking if the following rule is validated.

$$\eta(\dot{\gamma}) = \left. \eta^*(\omega) \right|_{\omega = \dot{\gamma}} \qquad (5.3)$$

While the empirical rule can be applied and is validated for the 4-arm star precursor which behaves as a classical branched polymer, it is not valid anymore for the polymeric networks with M-L cross-linking nodes. Indeed a deviation between the complex viscosity and the steady transient viscosity is clearly observed and this discrepancy is beyond the experimental margin error. Moreover, this difference in viscosities is also consistent with the thermo-rheological complexity of these MSBNs where both the entanglement/disentanglement processes of the building blocks and the association/dissociation mechanisms of the M-L complexes directly impact the resulting mechanical properties of the materials. Indeed, since the empirical rule works for the precursor, the Cox-Merz failure observed with the reversible networks can be

attributed to the formation of M-L complexes with different density. To confirm the aforementioned assumption, startup shear measurements are also performed at higher temperature (e.g. 60°C). As the temperature increases, the dynamics of M-L complexes is expected to weaken because its thermodynamic stability and kinetic exchange are altered compared to the values at 40°C. Consequently, the deviation in the Cox-Merz rule should be less pronounced for data obtained at 60°C.
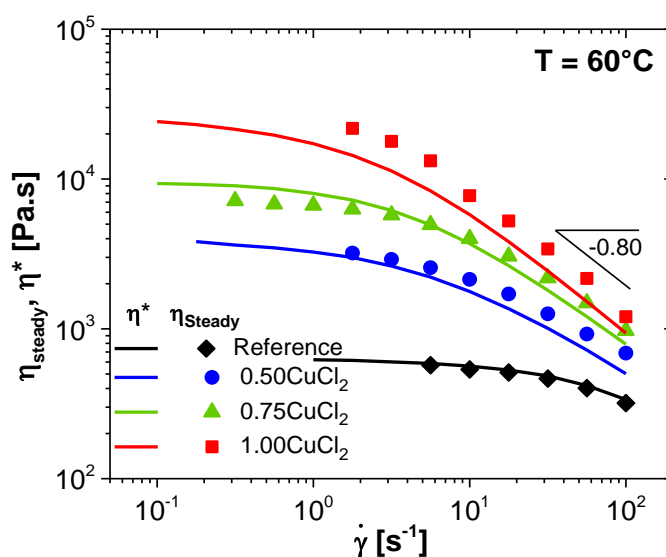

Figure 5.9 Cox-Merz rule for telechelic 4-arm star PnBA-tpy$_4$ (black, ◊), with different amounts of copper(II) ions 0.50eq. (blue, o), 0.75eq.(green, Δ) and 1.00eq.(red, □) at 60°C.

As expected, the empirical rule is still valid for the precursor material at 60°C. Interestingly, Figure 5.9 shows that the discrepancy between the complex and steady state viscosities decreases as the temperature increases. Especially for transient networks obtained with 0.50eq. and 0.75eq. of copper(II) ions, the gap becomes smaller, whereas for the polymeric network obtained 1.00eq., a clear deviation is still present. Thus, these results confirm the assumption that M-L complexes originate the failure on the empirical Cox-Merz rule.

Additionally, the steady state shear viscosities are normalized with respect to the dynamic zero shear viscosity which is given by:

$$\eta_0 = G_N^0 . \tau_{rel} \tag{5.4}$$

Where G_N^0 is the plateau modulus and τ_{rel} is the terminal relaxation time. The ratio is plotted against the Weissenberg number based on the terminal relaxation time which is defined as:

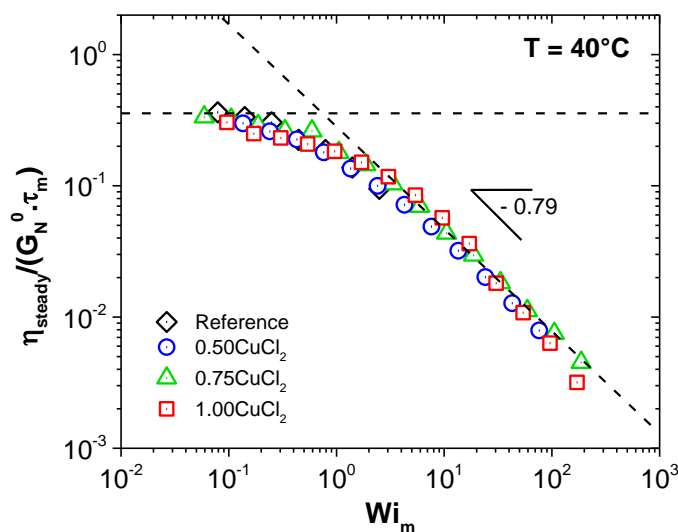$$W_i = \dot{\gamma}.\tau_{rel} \qquad (5.5)$$

Figure 5.10 Comparison of the normalized steady state shear viscosities as function of the Weissenberg number based on the terminal relaxation time for the 4-arm PnBA-tpy4 (black, ◊), with different amounts of copper(II) ions 0.50eq. (blue, o), 0.75eq.(green, Δ) and 1.00eq.(red, □) at 40°C.

From the dimensionless plot represented in Figure 5.10, it is observed that all the steady state viscosities collapse into a universal trend for all the systems with and without metal ions, displaying a shear thinning behavior. The value of the slope (e.g. -0.79) is consistent with the values reported in the literature on shear thinning polymers.[44,48,49] For example, Costanzo et al. reported similar slope value with linear entangled polystyrene melts and solutions. Snijkers et al. also found that the normalized steady shear viscosity data exhibit a slope smaller than -1 for entangled 4-arm and 8-arm star polyisoprene melts.

Besides steady state viscosity, additional information can be obtained by analyzing the maximum transient shear viscosity which is

normalized to facilitate comparisons. For instance the η_{max}/η_{steady} ratio plotted against the shear rate can indicate the capacity of a material to resist deformation as represented in Figure 5.11. Precisely, this ratio can be seen as a measure of the cohesive strength of the entangled transient network before its partial destruction in order to accommodate large deformation.
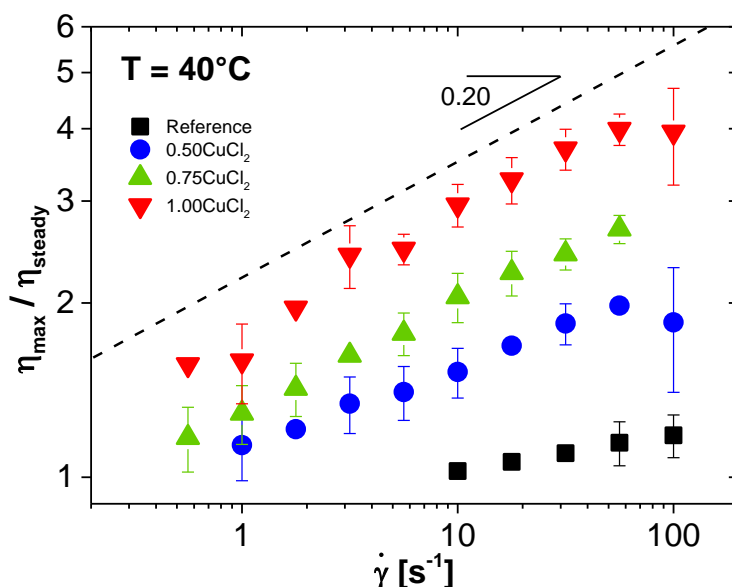

Figure 5.11 Comparison of the normalized maximum transient shear viscosity as function of the shear rate for the 4-arm PnBA-tpy4 (black, ◊), with different amounts of copper(II) ions 0.50eq. (blue, o), 0.75eq.(green, Δ) and 1.00eq.(red, □) at 40°C.

The entangled reference sample displays a viscosity ratio close to unity with an extremely small increase that is weaker than the power law slope of 0.20 at 40°C, meaning that the material does not exhibit any significant resistance towards large deformation. This slope value of 0.20 is consistent with early report on linear entangled polystyrene melts and solutions from Costanzo et al.[46] Upon addition of metal ions, this ratio starts to increase. Both the formation of a denser polymeric network through the M-L complexes and the contribution of entanglements trapped between these transient junctions enable the resulting material to have a capacity to resist deformation. As the amount of added metal ions increases, this resistance capacity increases

259

as well due to the fact that more physical cross-links with a longer lifetime are formed via M-L complexes as explained in Section 5.3.1. Consequently, more chains are participating to the elasticity of the network as illustrated in Figure 5.12, resulting in a higher collective resistance towards deformation. This is why the highest maximum viscosities are obtained when 1.00eq. of copper(II) ions is used to form a transient network. For instance at $\dot{\gamma} = 56.23$ s^{-1}, the η_{max}/η_{steady} ratio has increased by 73% with 0.50eq., by 134% with 0.75eq. and by 248% with 1.00eq. of ions compared to the reference. Note that at the highest shear rate (e.g. $\dot{\gamma} = 100$ s^{-1}), a decrease of this ratio is observed, which can be attributed to the sample breakage at high shear rate.

M-L cross-linking density ↗

Figure 5.12 Schematic view of metallo-supramolecular networks obtained from telechelic 4-arm star precursor, highlighting the influence of physical cross-linking density.

This larger resistance to flow observed with increasing the amount of metal ions can be validated by checking the stress component during startup shear measurements. Precisely, the maximum transient shear stress (σ_{max}) is extracted and plotted against the shear rate as illustrated in Figure 5.13. It is observed that when one equivalent of copper ions is used to form a transient network with higher cross-linking density, the stress needed to reach the overshoot is indeed higher than that obtained with 0.75eq. or 0.50eq., which confirms the influence of M-L junctions on the capacity of the material to withstand deformation. Furthermore, it is observed that the stress component varies linearly in a log-log scale as function of the shear rate with respectively a power law of 0.4 for MSBNs and 0.6 for the reference. To our knowledge, these values are unfortunately not reported in the literature. So no further comparison or discussion can be elaborated.
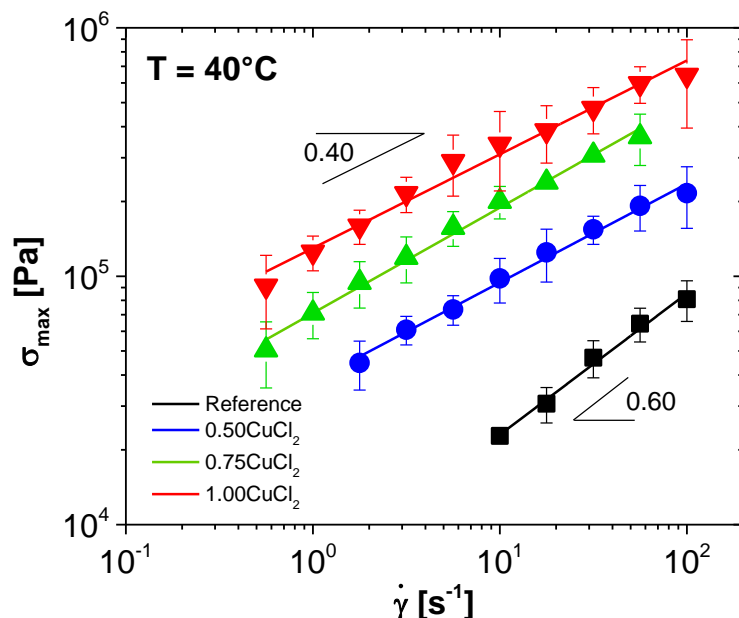
Figure 5.13 Comparison of the maximum shear stress component as function of the shear rate for the 4-arm PnBA-tpy$_4$ (black, ◊), with different amounts of copper(II) ions 0.50eq. (blue, o), 0.75eq.(green, Δ) and 1.00eq.(red, □) at 40°C.

Last but not least, the effect of temperature is investigated in nonlinear shear rheology of these systems. Precisely, the temperature is increased up to 60°C and startup measurements are performed at different shear rates. Figure 5.14 summarizes the maximum transient viscosity results obtained at higher temperature. While the η_{max}/η_{steady} ratio remains close to one for the 4-arm star precursor due to entropy elasticity, the MSBNs still exhibit a certain capacity to resist deformation but the latter has clearly decreased when compared with its behavior at 40°C. As mentioned above, this decrease is attributed to the fact that the dynamics of M-L complexes weaken with increase in temperature. More precisely, the binding strength of the bis(terpyridine) complexes decreases and kinetic exchange increases, resulting in less stable and more labile cross-linking junctions within the polymeric network. These results are consistent with the fact that M-L complexes originate from and dictate the capacity of the material to resist deformation. In fact, compared to the ratios at 40°C, the latter have only

261

increased by 20-22% for 0.50 and 0.75eq. and by 53% for 1.00eq. at a similar shear rate of 56.23 s^{-1}. Hence, besides the amount of metal ions, the ability of a transient network to withstand large deformation can also be engineered by varying the temperature. While the increase in temperature leads to more labile and less stable complexes, decreasing the temperature will result into a transient frozen network where the dynamics of the stickers and of the macromolecules can be significantly slowed down.
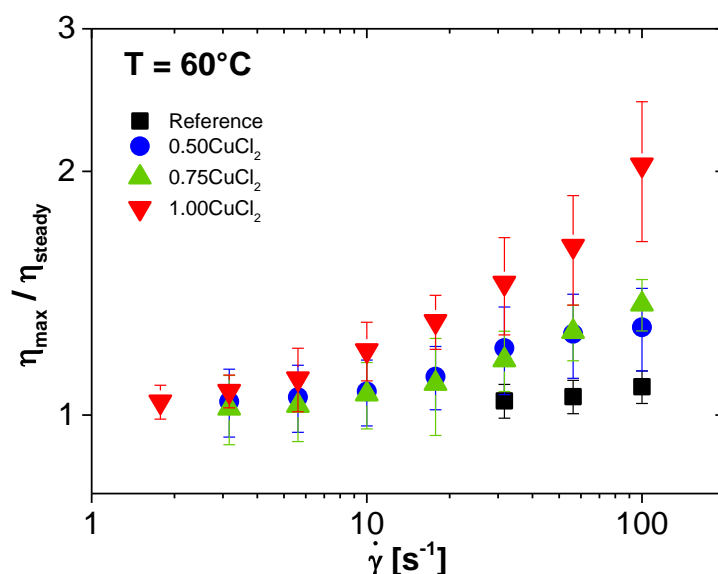

Figure 5.14 Comparison of the normalized maximum transient shear viscosity as function of the shear rate for the 4-arm P*n*BA-tpy$_4$ (black, ◊), with different amounts of copper(II) ions 0.50eq. (blue, o), 0.75eq.(green, Δ) and 1.00eq.(red, □) at 60°C.

5.4 Uniaxial extensional rheology

5.4.1 Effect of metal ion amount on the nonlinear viscoelasticity of MSBNs

It is then envisioned that the M-L mechanism can also be exploited to tune mechanical response towards tensile stress where larger deformation can be achieved. To do so, the mechanical properties

of MSBNs are investigated using the filament stretching rheometer (FSR) VADER 1000 where strong unidirectional flow can be achieved and the tumbling effect cannot occur due to the absence of any rotational component. The nonlinear uniaxial extensional responses of the MSBNs obtained with different ratios of copper(II) ions are reported in Figure 5.15.

Indeed, in absence of the tumbling effect, the extensional response at different Hencky strain rates ($\dot{\varepsilon}$) shows a strain hardening behavior for all samples stretched at 40°C. As a preliminary comparison, one can focus on the applied $\dot{\varepsilon}$ for each transient network. For instance with 0.50eq. of $CuCl_2$, the highest Hencky strain rate ($\dot{\varepsilon}$ = 3 s^{-1}) can be applied to stretch the material, whereas with 0.75eq. and 1.00eq. of metal ions, such deformation rate cannot be applied because it will generate important normal forces exceeding the highest limit of the force transducer (5 Newton). Similarly, a deformation rate of $\dot{\varepsilon}$ = 1 s^{-1} cannot be applied as well for MSBN obtained with 1.00 equivalent of copper. On the contrary, the lowest Hencky strain rate that can be applied with 0.75eq. or 1.00 eq. of cations is $\dot{\varepsilon}$ = 0.03s^{-1}. Below this rate, the mechanical response of the material is not strong enough as the transducer sensitivity limit is reached.

The limited range of elongation rates applied to a material can give preliminary insights about its mechanical behavior. Indeed, for instance the transient network obtained with 1.00eq. of copper exhibits higher collective resistance to deformation due to its high cross-linking density. As a direct consequence, the stress needed to deform the network for a given strain is more important at 1.00 eq. than for 0.75eq. or 0.50eq. This is why the upper limit of the force transducer is exceeded with deformation rate of $\dot{\varepsilon}$ = 1 s^{-1}. The same rate can be applied to the two other reversible networks with lower cross-linking densities. Note that for the reference system, the mechanical responses are very weak even at the highest shear rate, displaying extremely noisy data. Hence, no decent data have been collected for the telechelic 4-arm star polymeric precursor, indicating once more the key role of the M-L complexes. The combination of both the supramolecular junctions and the entanglements trapped in the transient network directly impacts the resistance ability of the material under load.
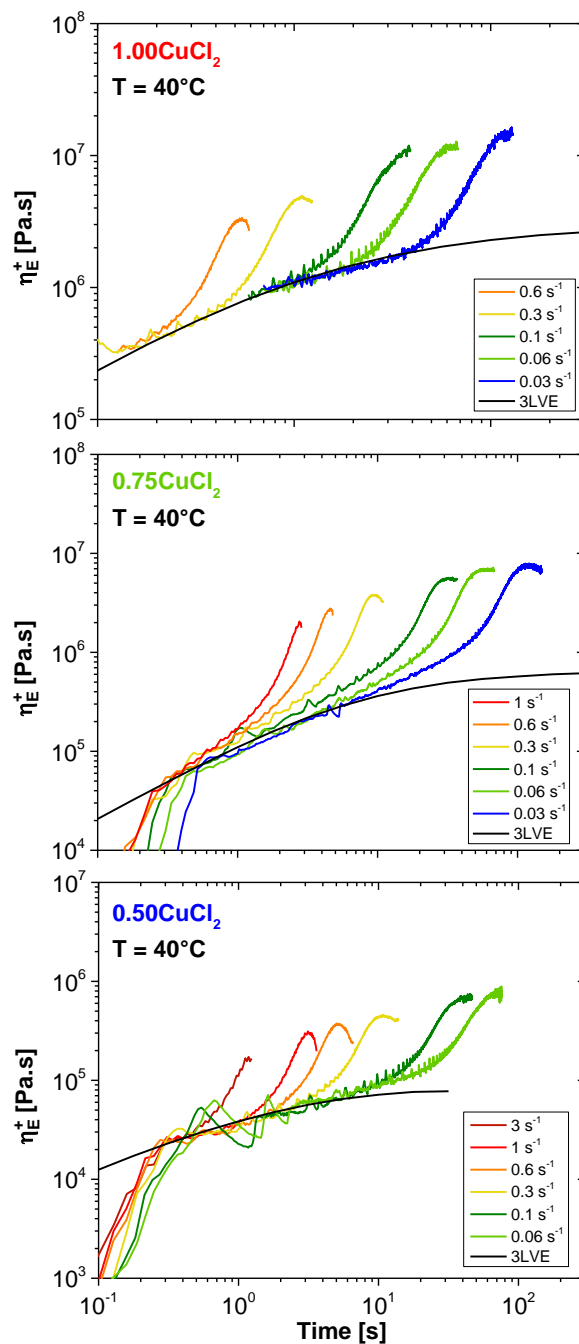
Figure 5.15 The extensional stress growth coefficient η_E^+ at different constant Hencky strain rates and at 40°C for transient networks obtained with a) 1.00eq. b) 0.75eq. and c) 0.50eq. of copper(II) ions.
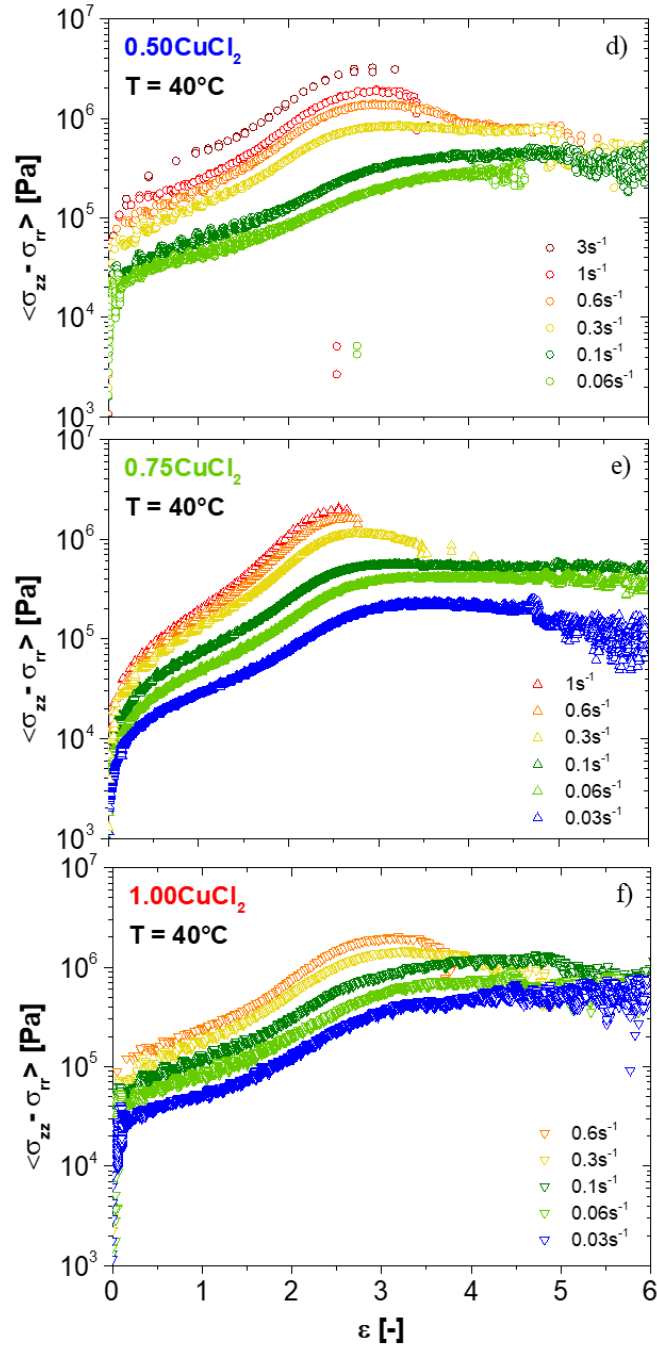
Figure 5.15 The extensional $< \sigma_{zz} - \sigma_{rr} >$ at different constant Hencky strain rates and at 40°C for transient networks obtained with d) 1.00eq. e) 0.75eq. and f) 0.50eq. of copper(II) ions.

265

From the uniaxial extension data reported in Figure 5.15, MSBNs exhibit a large strain hardening behavior, attributed to the significant chain stretch in extensional flow which cannot be obtained in shear flows. Precisely, strain hardening highlights the resistance of the reversible polymeric networks, which prevent the disentanglement process during extensional tests, until reaching the point at which the complexes cannot resist further to the chain stretch and dissociate. It is thus observed that the final collapse of the entanglement network is effectively delayed with increasing the cross-linking density. Such postponed behavior can be favorable for film blowing or fiber spinning process. In order to compare the transient extensional viscosities of the different networks, the steady elongational viscosity ($\eta_{E,se}$) parameter is extracted from different rates of deformation. They are then plotted against the deformation rate and results are reported in Figure 5.16.
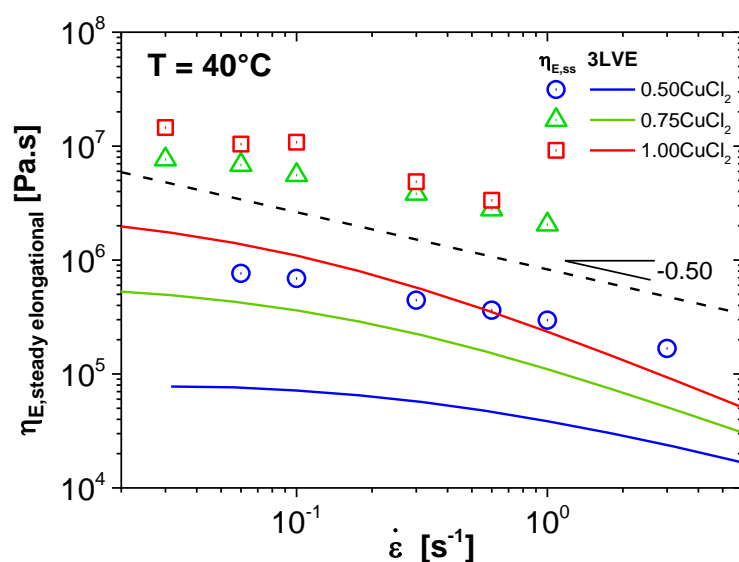

Figure 5.16 Comparison of the elongational steady stretch viscosity ($\eta_{E,se}$) and the dynamic complex viscosity (solid lines, multiplied by the Trouton ratio 3) as function of the Hencky strain rate for the 4-arm P*n*BA-tpy$_4$ with different amounts of copper(II) ions 0.50eq. (blue, o), 0.75eq.(green, Δ) and 1.00eq.(red, □) at 40°C.

It appears that this extensional hardening tendency follows a pattern in which the magnitude of the strain hardening increases when the deformation rate increases. Indeed, $\eta_{E,se}$ decreases linearly in a log-log

scale with increasing the Hencky strain rate with a slope of -0.50 for all MSBNs. This pattern is consistent with earlier reports on associating polymers that form transient networks or for slightly branched polymeric systems.[58,59] In uniaxial extension, the model MSBNs display strain hardening behavior even at Hencky strain rates below their respective reciprocal terminal relaxation times (see Table 5.2), highlighting the contribution of the physical M-L cross-links.

Samples	τ_{rel} (s)	τ_{rel}^{-1} (s^{-1})
Star250k + 0.50eq. Cu(II)	0.27	3.74
Star250k + 0.75eq. Cu(II)	3.34	0.30
Star250k + 1.00eq. Cu(II)	9.58	0.10

Figure 5.2 Terminal relaxation times of the metallo-supramolecular bulk networks formed with different ratios of Cu(II) ions. The timescales are obtained from the SAOS measurements.

Even though it is not the main objective of this chapter, it is noteworthy to mention that melt fractures are observed when the imposed Hencky strain rate is larger than the reciprocal of the terminal relaxation time of the viscoelastic transient network during uniaxial extensional tests.[60] This is why at $\dot{\varepsilon} = 3$ s^{-1} the steady stretch elongational viscosity could not be probed before the melt fracture occurs for MSBNs formed with 0.75eq. of copper(II).

As expected, the transient network obtained with 1.00eq. of metal ions exhibits the highest $\eta_{E,se}$ because more transient junctions are formed. Similarly to the shear rheology presented above, the bulk tensile mechanical features of MSBNs can also be modulated by varying the amount of added metal ions. For instance, when the metal ratio is increased from 0.50 to 0.75 equivalents of copper ions, the steady elongational viscosity is impressively augmented by a factor of 10. This result can be understood by the fact that the density and lifetime of the transient cross-links increases with increasing the amount of metal ions. Indeed, with 0.50eq. of copper ions, the proportion of dangling arms, i.e. the arms which are not participating to the transient network, has been estimated to 40% based on the linear

viscoelastic data. This means that in average, a star molecule has 2.4 connections with its neighboring molecules. On the other hand, with 0.75eq. ions, the dangling arms only represent around 20% of the sample, which corresponds to an average of 3.2 connections per molecules. Therefore, in this last case, the network connectivity is significantly increased. The formation of a larger number of transient junctions also leads to a larger contribution from the entanglements as more chains segments are trapped. In order to relax, the stickers have to dissociate first to let the chain arms relax through fluctuations.

Then, it is observed that increasing the amount of metal ion from 0.75 to 1 equivalent does not lead to another significant increase in $\eta_{E,se}$ but rather a slight gain of 2, despite the fact that the cross-linking density is increased from 80% of cross-linked arms with 0.75 eq. ions to 100% of cross-linked arms with 1.00eq. of ions. A transition from a very extensible network to a more rigid material is obtained. A possible explanation for this difference in bulk extensional properties is related to their respective ligand exchange mechanism. Indeed, from the analysis of the LVE data (see Chapters 3 and 4), we know that the ligand exchange process allows a faster relaxation of the transient network. Similarly, it is expected that the presence of free ligands enables a faster destruction/reconstruction of the complexes under extension, thus leading to a material able to withstand high deformation, as illustrated in Figure 5.17. On the other hand, a drastic reduction of uncoordinated tpy units in the bulk network (as observed with 1.00eq. of ions) would severely slow down this rate of exchange, altering the stress release within the sample. Consequently, the network cannot adapt to the deformation anymore and breaks at lower strain.
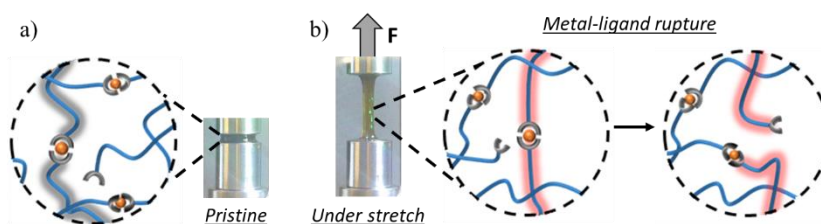

Figure 5.17 Scheme of the MSBN a) at equilibrium and b) under mechanical stress where chains are initially stretched. At a certain

critical deformation, the M-L junctions rupture to release the stress, protecting the network from any breakage of covalent bonds.

As mentioned earlier, the uncoordinated chains have an active role on the bulk mechanical properties of MSBNs. Herein, from the theoretical model explained in Chapter 4, the proportion of dangling chains (i.e. uncoordinated terpyridine ligand) is estimated to be around 40% when 0.50eq. of ions are added, 20% with the ratio of 0.75 equivalents and 0% in the case where 1.00eq. of copper chloride ions is used. Therefore, based on the above explanation, we could have expected a very large deformability of the transient network containing 0.50eq. of ions since the complexes can easily break and reform. But in average, its connectivity number of 2.4 is not sufficient to correctly form well cross-linked polymeric network. It rather gives an extremely loose and slightly cross-linked material. Under extension, the resulting system is initially stretched and exhibits strain-hardening behavior till the M-L complexes dissociate. While breaking, the stress is released and the initially connected chains are not stretched anymore and the whole system collapses due to the lack of connected star arms. In the case of the reversible network formed with 0.75eq. of Cu(II), the MSBN has in average 3.2 associated arms, allowing the formation of a relatively well cross-linked material with 20% of uncoordinated arms. So, during the M-L dissociation, the material remains sufficiently cross-linked, letting the connected arms to withstand further stretch before collapsing. Hence, the transient network exhibits a larger strain hardening compared to the one formed with 0.50eq. of copper.

Another way to explain this large strain hardening observed with 0.75eq. is the finite extensibility argument. Since the 0.75eq. sample still contains a large fraction of dangling ends (20%), the average molar mass between two cross-linking points is increased compared to the 1.00eq. network. This provides a larger "reservoir" of deformation, before reaching the maximum stretch at which the complexes break. These dangling ratios are consistent with the interpretation of the experimental extensional results, indicating that the M-L complexes along with the uncoordinated ligands do impact the kinetics of the ligand exchange. The latter ultimately influences the transient viscosity, the extensibility and the rigidity of the polymeric material.

5.4.2 Effect of metal ion type on the nonlinear viscoelasticity of MSBNs

Besides varying the amount of metal ions, the extensional properties of metallo-supramolecular bulk networks can also be engineered by changing the nature of the transition metal ions. Similarly to the linear shear rheology data, it is envisioned that nonlinear extensional viscoelastic properties can be finely tailored as well. It is established that the capacity of a network to resist large deformation is originated and dictated by the M-L complex coupled with entanglements and its ligand exchange mechanism. Then, changing the nature of the transition metal ions should directly affect the dynamics of these reversible junctions and ultimately the nonlinear extensional viscoelasticity of the material. Figure 5.18 summarizes the nonlinear extensional data of MSBN obtained by adding 0.50eq. of cobalt(II) ions instead of copper(II). While both transient networks formed with 0.50eq. of copper(II) and 0.50eq. of cobalt(II) exhibit almost similar complex viscosity in linear rheology, a significant difference between these two materials is spotted in uniaxial extensional measurements. In fact, it is observed that the transient steady stretch viscosities of MSBN with 0.50eq. of Co(II) are always higher compared to the network formed with Cu(II) ions with the same ratio. This difference can be first explained by the fact that bis(terpyridine)-cobalt complexes have a higher binding constant and are kinetically less labile than bis(terpyridine)-copper complexes.[42]
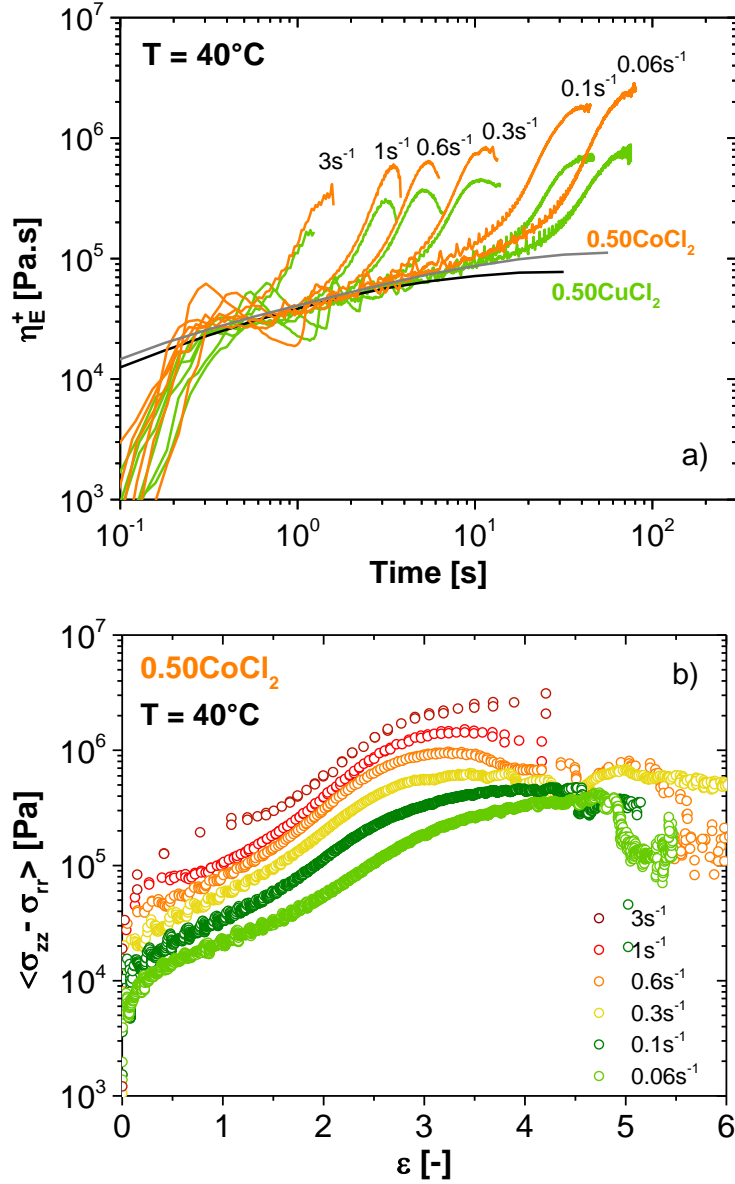
Figure 5.18 a) Comparison of the extensional stress growth coefficient η_E^+ at different constant Hencky strain rates and at 40°C for transient networks obtained with 0.50eq. of copper(II) and 0.50eq. of cobalt(II). b) The extensional $< \sigma_{zz} - \sigma_{rr} >$ at different constant Hencky strain rates and at 40°C for transient networks obtained with cobalt(II) ions.

For all deformation rates, the MSBN formed with cobalt exhibits the highest steady elongational viscosities $\eta_{E,se}$, indicating that the material displays higher capacity to resist deformation. While the proportion of free ligands is the same at 0.50eq. for both copper and cobalt, the longest effective association time differs from one ion to another. It is indeed shown in Chapter 4 that cobalt complexes have the longest effective association time τ_{final} which is equal to 70s at 40°C, whereas for copper complexes, $\tau_{final} = 50$s at the same temperature. However, this difference in timescales does not significantly affect the mechanical properties since both MSBNs have similar complex viscosities. So presumably it is the stability of the bis(terpyridine)-metal complexes that plays a major role. Herein, the cobalt complexes display high binding strength and are more stable than copper ones.[42] Therefore MSBN formed with Co(II) ions can support larger deformation and more stress is required for all the stickers to be dissociated at least once. As a direct consequence, the material can resist longer and exhibits better resistance toward extensional deformation than copper containing network because the rate of exchange and the stability differ from one type of metal ion to another. Hence, it is expected that under load the bis(terpyridine)-copper junctions will be the first to break down compared to cobalt based physical cross-links to release the stress.

On the contrary, if a more labile (or less stable) metal ions is used such as zinc(II) to form MSBN, one can easily expect that the resulting material exhibits a resistance capacity lower than transient networks obtained with copper(II) and cobalt(II) ions. Because the M-L junctions are relatively weak and will easily succumb to deformation. In fact, results shown in Figure 5.19 confirm that the physical cross-links formed with zinc(II) ions are too weak to provide any additional mechanical strength to the material due to the fact that they keep on associating and dissociating very fast with time.
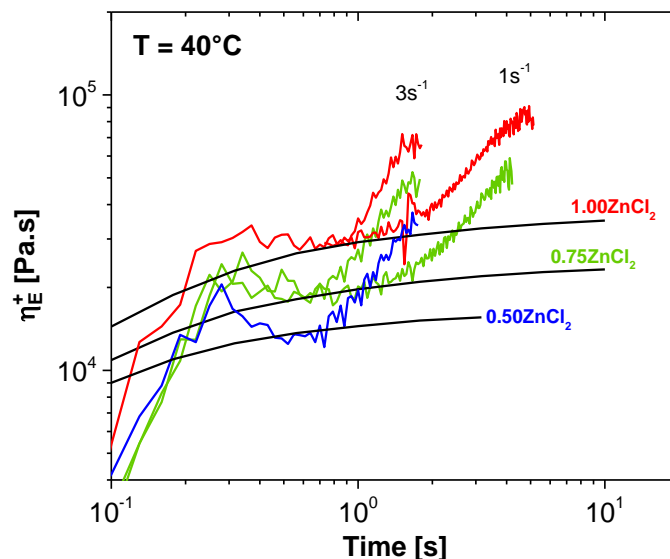
Figure 5.19 The extensional stress growth coefficient η_E^+ at different constant Hencky strain rates and at 40°C for transient networks obtained with a) 1.00eq. b) 0.75eq. and c) 0.50eq. of zinc(II) ions.

Experimentally, a set of acceptable extensional data has been collected only at the highest Hencky strain rate of 3 s^{-1} or 1 s^{-1} and yet the results are noisy, confirming the formation of a weak labile network unable to provide strong enough mechanical responses. This lability can be slightly compensated by increasing the loading of metal ions. As shown in Figure 5.19, adding more zinc(II) leads to slightly better mechanical responses of the transient networks toward extensional tests because the number of elastic chains participating to the network formation increases, but their resistance ability still remains weak compared to the other reversible networks formed with more stable metal salts such as Cu(II) or Co(II). These results indicate that the mechanical response in uniaxial extension can be finely tailored not only by varying the amount of added metal ions but also by changing the nature of the transition cations. Depending on the identity of the cations, the stability and kinetics of the physical cross-links vary accordingly, enabling to achieve a very versatile and reversible network with tunable transient viscosity, extensibility or resistance capacity under load. Ultimately the network formed with these physical cross-links displays dynamics with

273

a superior mechanical adaptability under load compared to covalently cross-linked materials.

Note that from linear rheology, it was previously reported that the telechelic star polymers cannot relax when the stickers are associated. The M-L complexes must first dissociate in order to allow the star arms to relax by fluctuation mechanisms.[34,43] In nonlinear rheology, if the deformation rate is higher than the reciprocal of the M-L dissociation time, then the breakage of the stickers can be accelerated by the imposed deformation. Therefore these M-L junctions can rupture at the timescale of the deformation, dissipating energy and facilitating the chain orientation.

5.4.3 Effect of temperature on the nonlinear viscoelasticity of MSBNs

The influence of temperature on the mechanical responses of MSBNs is also investigated for different transient networks obtained with different loadings of copper(II) ions. The temperature is increased up to 60°C and uniaxial extension measurements are performed at different Hencky strain rates. The results reported in Figure 5.20. show that at elevated temperature, the mechanical responses under extensional load are completely different from these at 40°C.
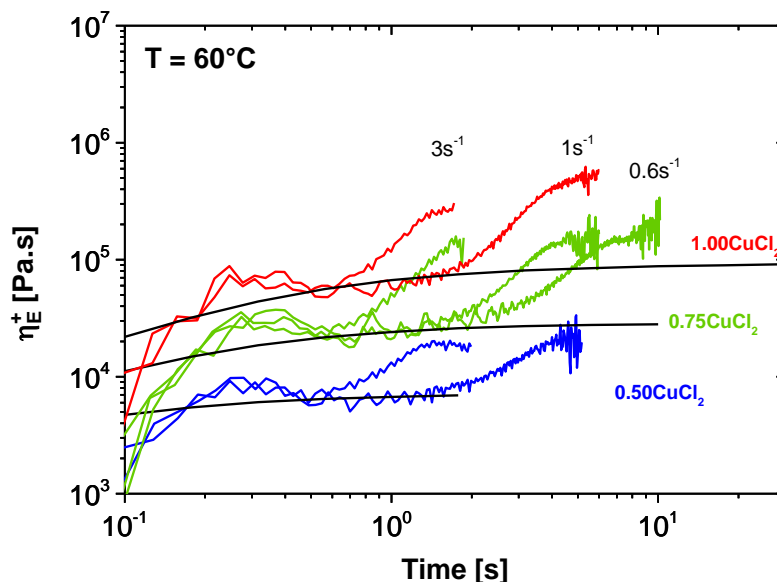
Figure 5.20 The extensional stress growth coefficient η_E^+ at different constant Hencky strain rates and at 60°C for transient networks obtained with a) 1.00eq. b) 0.75eq. and c) 0.50eq. of copper(II) ions.

Precisely, it is first observed that an acceptable set of data can be collected only at high deformation rates where the material gives strong enough mechanical response under load. Below a deformation rate of 0.6 s^{-1}, the sensitivity limit of the transducer is reached, resulting in extremely noisy data which are not considered here (data not shown). While the results are slightly noisy even at high $\dot{\varepsilon}$, the strain hardening tendency is still present and is attributed to the M-L complexes. This indicates that the stickers remain active but their effectiveness is clearly weakened with increasing temperature as mentioned in section 5.3.2. As a direct consequence, the level of transient steady elongational viscosity is lowered at 60°C with respect to $\eta_{E,se}$ obtained at 40°C for all reversible networks. These results indicate once more the dependence of the bulk nonlinear extensional viscosities on the strength and stability of the M-L complexes. The dynamics of these physical cross-links can also be engineered by varying the temperature which directly impacts the relative importance of the M-L complexes.

5.5   Conclusions

In this Chapter, a systematic investigation of the nonlinear shear and extensional viscoelastic properties was conducted on well-defined telechelic four-arm star PnBA-tpy$_4$. The latter can associate via metal-ligand coordination where bis(terpyridine) cross-links of different stability are formed with several transition metal ions (Zn^{2+}, Cu^{2+} and Co^{2+}). From the experimental data, the possibility to tailor the rheological properties of model MSBNs was demonstrated by controlling both the structure and the mechanical response of metallo-supramolecular bulk networks. Under deformation, the bulk mechanical properties of these transient networks are significantly modulated by the cross-linking density and also by the stability of the M-L complexes. Both in shear and in uniaxial extension, it was observed that M-L complexes originate and dictate the ability of the network to withstand large deformation. While the formation of metal-ligand cross-links is enhanced by addition of metal salts, the transient junctions also enhance the contribution of trapped entanglement to the mechanical properties of the material under load. Both the M-L complexes and the entanglements have a strong impact on the rheological properties of the transient networks under deformation. Additionally, the presence of uncoordinated chains, which directly influences the ligand exchange mechanism, also plays an active role and modulates the bulk mechanical properties of MSBNs.

We demonstrated that the bulk rheological properties of these systems can be engineered by varying the nature or the amount of added metal ions to form complexes. Particularly, we observed the evolution of the mechanical responses over a wide range when different ratios of metal ions were incorporated. In fact, the polymer network becomes more cross-linked with an increase in metal loadings and consequently more chains participate to the elasticity and connectivity of the network. This is why an increase in transient viscosities with increasing metal loadings was observed during shear and uniaxial extension measurements. In uniaxial extension, the model MSBNs display strain hardening behavior even at Hencky strain rates below their respective reciprocal terminal relaxation times, highlighting the contribution of the

276

physical M-L cross-links. In presence of a rotational component, strong shear thinning behavior is obtained at similar deformation rates in nonlinear shear flow. Herein, increasing the amount of added metal ions significantly reduces the fraction of uncoordinated chains from 40% for 0.50eq. of ions down to zero for 1.00eq. As a direct consequence, the rate of ligand exchange is decreased under deformation. The latter is considered extremely important since it governs the stress distribution and the chain relaxation within the reversible networks. Ultimately the extensibility or the capacity to resist deformation are influenced by this rate of remodeling the physical cross-links, allowing us to obtain a very extensible polymeric network or more rigid materials.

This ligand exchange process can also be modulated by varying the nature of the transition metal ions or by altering the temperature. For instance, zinc(II) metal ions lead to the elaboration of relatively weak MSBN with low transient viscosities, whereas networks formed with copper(II) or cobalt(II) ions lead to superior mechanical properties. This is attributed to the fact that more stable and less labile bis(terpyridine) junctions are formed with Cu(II) and Co(II) compared to Zn(II). Similarly, by altering the temperature, we systematically vary the relative importance (stability and kinetics) of the M-L complexes, which allows us to tailor their specific contribution to the network properties. Increasing the temperature results in materials with lower transient viscosities and lower resistance capacity because the M-L interactions are considerably weakened. It was previously reported that in linear rheology, the associating star polymers cannot relax when the stickers are attached. The M-L complexes must first dissociate in order to allow the star arms to relax by fluctuation mechanisms.[34,43] However, in nonlinear rheology, the sticker dissociation can also be altered by the deformation rate. For instance if the deformation rate is higher than the reciprocal of the sticker dissociation time, then the rupture of stickers might be accelerated by the imposed deformation. Consequently these M-L cross-links can rupture prior to covalent bonds at the timescale of the deformation, dissipating energy and facilitating the chain orientation. To summarize, the incorporation of terpyridine ligands within well-defined four-arm star polymers allows the elaboration of dynamically tailorable transient networks with improved mechanical properties (viscosities, extensibility, and resistance capacity). Precisely,

277

the dynamics of the metal-ligand complexes and entanglements control the structural and the temporal parameters of MSBNs. Additionally, these M-L complexes can also be used as sacrificial bonds to protect the covalent network from dramatic failure when the material is exposed to large deformation.

Note that under large deformation, flow instabilities such as shear banding or wall slip can occur at high rates of deformation. Precisely, if the shear rate is higher than the reciprocal characteristic relaxation time of the polymeric material, there might be a coexistence of different shear rates along the internal sample structure. Consequently, the polymeric material cannot respond uniformly during startup deformation, leading to unreliable set of data. In the case of entangled supramolecular polymers, it is assumed that flow instabilities happen if the deformation rate is higher than the sticker lifetime instead of the terminal relaxation time. Herein, we consider that the inverse of the sticker lifetime is higher than the range of deformation rate examined. Hence, flow instabilities should not occur. To confirm it, we tried to experimentally determine the metal-ligand lifetime via broadband dielectric relaxation spectroscopy (DRS). Details on the DRS analysis of MSBNs will be presented in Chapter 6. Results from DRS indicate that indeed the reciprocal of the sticker lifetime is higher than the deformation rate, confirming the absence of any flow instabilities during the nonlinear rheology measurements.

Bibliography

(1)   Hart, L. R.; Nguyen, N. A.; Harries, J. L.; Mackay, M. E.; Colquhoun, H. M.; Hayes, W. Perylene as an Electron-Rich Moiety in Healable, Complementary ??-?? Stacked, Supramolecular Polymer Systems. *Polymer (Guildf).* **2014**, *69*, 293–300.

(2)   Hart, L. R.; Hunter, J. H.; Nguyen, N. A.; Harries, J. L.; Greenland, B. W.; Mackay, M. E.; Colquhoun, H. M.; Hayes, W. Multivalency in Healable Supramolecular Polymers: The Effect of Supramolecular Cross-Link Density on the Mechanical Properties and Healing of Non-Covalent Polymer Networks. *Polym. Chem.* **2014**, *5*, 3680–3688.

(3)   Fu, T.; Li, Z.; Zhang, Z.; Zhang, X.; Wang, F. Supramolecular Cross-Linking and Gelation of Conjugated Polycarbazoles via Hydrogen Bond Assisted Molecular Tweezer / Guest Complexation. *Macromolecules* **2017**, *50*, 7517–7525.

(4)   Cordier, P.; Tournilhac, F.; Soulié-Ziakovic, C.; Leibler, L. Self-Healing and Thermoreversible Rubber from Supramolecular Assembly. *Nature* **2008**, *451*, 977–980.

(5)   Hentschel, J.; Kushner, A. M.; Ziller, J.; Guan, Z. Self-Healing Supramolecular Block Copolymers. *Angew. Chemie - Int. Ed.* **2012**, *51*, 10561–10565.

(6)   Appel, E. A.; Biedermann, F.; Rauwald, U.; Jones, S. T.; Zayed, J. M.; Scherman, O. A. Supramolecular Cross-Linked Networks via Host-Guest Complexation with Cucurbit[8]Uril. *J. Am. Chem. Soc.* **2010**, *132*, 14251–14260.

(7)   Harada, A.; Kobayashi, R.; Takashima, Y.; Hashidzume, A.; Yamaguchi, H. Macroscopic Self-Assembly through Molecular Recognition. *Nat. Chem.* **2011**, *3*, 34–37.

(8)   Appel, E. A.; Biedermann, F.; Hoogland, D.; Del Barrio, J.; Driscoll, M. D.; Hay, S.; Wales, D. J.; Scherman, O. A. Decoupled Associative and Dissociative Processes in Strong yet Highly Dynamic Host-Guest Complexes. *J. Am. Chem. Soc.* **2017**, *139*, 12985–12993.

(9)   Yount, W. C.; Loveless, D. M.; Craig, S. L. Strong Means Slow: Dynamic Contributions to the Bulk Mechanical Properties of Supramolecular Networks. *Angew. Chemie - Int. Ed.* **2005**, *44*, 2746–2748.

(10)   Bode, S.; Enke, M.; Bose, R. K.; Schacher, F. H.; Garcia, S. J.; van der Zwaag, S.; Hager, M. D.; Schubert, U. S. Correlation between Scratch Healing and Rheological Behavior for Terpyridine Complex Based Metallopolymers. *J. Mater. Chem.* **2015**, *3*, 22145–22153.

(11)   Bose, R. K.; Enke, M.; Grande, A. M.; Zechel, S.; Schacher, F. H.; Hager, M. D.; Garcia, S. J.; Schubert, U. S.; van der Zwaag, S. Contributions of Hard and Soft Blocks in the Self-Healing of Metal-Ligand-Containing Block Copolymers. *Eur. Polym. J.* **2017**, *93*, 417–427.

(12)   Potier, F.; Guinault, A.; Delalande, S.; Sanchez, C.; Ribot, F.; Rozes, L. Nano-Building Block Based-Hybrid Organic–inorganic

Copolymers with Self-Healing Properties. *Polym. Chem.* **2014**, *5*, 4474–4479.

(13) Huang, C.; Wang, C.; Chen, Q.; Colby, R. H.; Weiss, R. A. Reversible Gelation Model Predictions of the Linear Viscoelasticity of Oligomeric Sulfonated Polystyrene Ionomer Blends. *Macromolecules* **2016**, *49*, 3936–3947.

(14) Savage, A. M.; Walck, S. D.; Lambeth, R. H.; Beyer, F. L. Tuning the Morphology of an Acrylate-Based Metallo- Supramolecular Network: From Vesicles to Cylinders. *Macromolecules* **2018**, *51*, 1636–1643.

(15) Chen, P.; Li, Q.; Grindy, S.; Holten-Andersen, N. White-Light-Emitting Lanthanide Metallogels with Tunable Luminescence and Reversible Stimuli-Responsive Properties. *J. Am. Chem. Soc.* **2015**, *137*, 11590–11593.

(16) Williams, Z. H.; Burwell, E. D.; Chiomento, A. E.; Demsko, K. J.; Pawlik, J. T.; Harris, S. O.; Yarolimek, M. R.; Whitney, M. B.; Hambourger, M.; Schwab, A. D. Rubber-Elasticity and Electrochemical Activity of Iron(<scp>ii</Scp>) Tris(Bipyridine) Crosslinked Poly(Dimethylsiloxane) Networks. *Soft Matter* **2017**, *13*, 6542–6554.

(17) Amin, D.; Likhtman, A. E.; Wang, Z. Dynamics in Supramolecular Polymer Networks Formed by Associating Telechelic Chains. *Macromolecules* **2016**, *49*, 7510–7524.

(18) Sanoja, G. E.; Schauser, N. S.; Bartels, J. M.; Evans, C. M.; Helgeson, M. E.; Seshadri, R.; Segalman, R. A. Ion Transport in Dynamic Polymer Networks Based on Metal-Ligand Coordination: Effect of Cross-Linker Concentration. *Macromolecules* **2018**, *51*, 2017–2026.

(19) Hager, B. M. D.; Greil, P.; Leyens, C.; Zwaag, S. Van Der; Schubert, U. S. Self-Healing Materials. *Adv. Mater.* **2010**, *22*, 5424–5430.

(20) Enke, M.; Bose, R. K.; Bode, S.; Vitz, J.; Schacher, F. H.; Garcia, S. J.; Zwaag, S. Van Der; Hager, M. D.; Schubert, U. S. A Metal Salt Dependent Self-Healing Response in Supramolecular Block Copolymers. *Macromolecules* **2016**, *46*, 8418–8429.

(21) Du, L.; Xu, Z. Y.; Fan, C. J.; Xiang, G.; Yang, K. K.; Wang, Y. Z. A Fascinating Metallo-Supramolecular Polymer Network with Thermal/Magnetic/Light-Responsive Shape-Memory Effects Anchored by Fe3O4Nanoparticles. *Macromolecules* **2018**, *51*, 705–715.

(22) Kumpfer, J. R.; Rowan, S. J. Thermo-, Photo-, and Chemo-Responsive Shape-Memory Properties from Photo-Cross-Linked Metallo-Supramolecular Polymers. *J. Am. Chem. Soc.* **2011**, *133*, 12866–12874.

(23) Wang, Z.; Fan, W.; Tong, R.; Lu, X.; Xia, H. Thermal-Healable and Shape Memory Metallosupramolecular Poly(n-Butyl Acrylate-Co-Methyl Methacrylate) Materials. *RSC Adv.* **2014**, *4*, 25486.

(24) Vitvarova, T.; Svoboda, J.; Hissler, M. Conjugated Metallo-Supramolecular Polymers Containing a Phosphole Unit. *Organometallics* **2017**, *36*, 777–786.

(25) Pai, S.; Moos, M.; Schreck, M. H.; Lambert, C.; Kurth, D. G. Green-

280

to-Red Electrochromic Fe(II) Metallo-Supramolecular Polyelectrolytes Self-Assembled from Fluorescent 2,6-Bis(2-Pyridyl)Pyrimidine Bithiophene. *Inorg. Chem.* **2017**, *56*, 1418–1432.

(26) Schwarz, G.; Bodenthin, Y.; Tomkowicz, Z.; Haase, W.; Geue, T.; Kohlbrecher, J.; Pietsch, U.; Kurth, D. G.; Wu, J. U. V; Wu, D.-. Tuning the Structure and the Magnetic Properties of Metallo-Supramolecular Polyelectrolyte - Amphiphile. *J. Am. Chem. Soc.* **2011**, *133*, 547–558.

(27) Heinzmann, C.; Coulibaly, S.; Roulin, A.; Fiore, G. L.; Weder, C. Light-Induced Bonding and Debonding with Supramolecular Adhesives. *Appl. Mater. Interfaces* **2014**, *6*, 4713–4719.

(28) Bode, S.; Zedler, L.; Schacher, F. H.; Dietzek, B.; Schmitt, M.; Popp, J.; Hager, M. D.; Schubert, U. S. Self-Healing Polymer Coatings Based on Crosslinked Metallosupramolecular Copolymers. *Adv. Mater.* **2013**, *25*, 1634–1638.

(29) Rao, Y. L.; Chortos, A.; Pfattner, R.; Lissel, F.; Chiu, Y. C.; Feig, V.; Xu, J.; Kurosawa, T.; Gu, X.; Wang, C.; et al. Stretchable Self-Healing Polymeric Dielectrics Cross-Linked through Metal-Ligand Coordination. *J. Am. Chem. Soc.* **2016**, *138*, 6020–6027.

(30) Mozhdehi, D.; Neal, J. A.; Grindy, S. C.; Cordeau, Y.; Ayala, S.; Holten-Andersen, N.; Guan, Z. Tuning Dynamic Mechanical Response in Metallopolymer Networks through Simultaneous Control of Structural and Temporal Properties of the Networks. *Macromolecules* **2016**, *49*, 6310–6321.

(31) Tang, Z.; Huang, J.; Guo, B.; Zhang, L.; Liu, F. Bioinspired Engineering of Sacrificial Metal-Ligand Bonds into Elastomers with Supramechanical Performance and Adaptive Recovery. *Macromolecules* **2016**, *49*, 1781–1789.

(32) Tang, S.; Olsen, B. D. Relaxation Processes in Supramolecular Metallogels Based on Histidine-Nickel Coordination Bonds. *Macromolecules* **2016**, *49*, 9163–9175.

(33) Grindy, S. C.; Lenz, M.; Holten-Andersen, N. Engineering Elasticity and Relaxation Time in Metal-Coordinate Cross-Linked Hydrogels. *Macromolecules* **2016**, *49*, 8306–8312.

(34) Zhuge, F.; Hawke, L. G. D.; Fustin, C.-A.; Gohy, J.-F.; van Ruymbeke, E. Decoding the Linear Viscoelastic Properties of Model Telechelic Metallo-Supramolecular Polymers. *J. Rheol. (N. Y. N. Y).* **2017**, *61*, 1245–1262.

(35) Xu, D.; Hawk, J. L.; Loveless, D. M.; Jeon, S. L.; Craig, S. L. Mechanism of Shear Thickening in Reversibly Cross-Linked Supramolecular Polymer Networks. *Macromolecules* **2010**, *43*, 3556–3565.

(36) Xu, D.; Liu, C. Y.; Craig, S. L. Divergent Shear Thinning and Shear Thickening Behavior of Supramolecular Polymer Networks in Semidilute Entangled Polymer Solutions. *Macromolecules* **2011**, *44* (7), 2343–2353.

(37) Mozhdehi, D.; Ayala, S.; Cromwell, O. R.; Guan, Z. Self-Healing Multiphase Polymers via Dynamic Metal-Ligand Interactions. *J. Am.*

Chem. Soc. **2014**, *136*, 16128–16131.

(38)   Yang, B.; Zhang, H.; Peng, H.; Xu, Y.; Wu, B.; Weng, W.; Li, L. Self-Healing Metallo-Supramolecular Polymers from a Ligand Macromolecule Synthesized via Copper-Catalyzed Azide–alkyne Cycloaddition and Thiol–ene Double "Click" Reactions. *Polym. Chem.* **2014**, *5*, 1945–1953.

(39)   Jia, X. Y.; Mei, J. F.; Lai, J. C.; Li, C. H.; You, X. Z. A Highly Stretchable Polymer That Can Be Thermally Healed at Mild Temperature. *Macromol. Rapid Commun.* **2016**, *37*, 952–956.

(40)   Jia, X.-Y.; Mei, J.-F.; Lai, J.-C.; Li, C.-H.; You, X.-Z. A Self-Healing PDMS Polymer with Solvatochromic Properties. *Chem. Commun.* **2015**, *51*, 8928–8930.

(41)   Rao, Y. L.; Feig, V.; Gu, X.; Nathan Wang, G. J.; Bao, Z. The Effects of Counter Anions on the Dynamic Mechanical Response in Polymer Networks Crosslinked by Metal–ligand Coordination. *J. Polym. Sci. Part A Polym. Chem.* **2017**, *55*, 3110–3116.

(42)   Holyer, R. H.; Hubbard, C. D.; Kettle, S. F. a; Wilkins, R. G. The Kinetics of Replacement Reactions of Complexes of the Transition Metals with 2,2',2"-Terpyridine. *Inorg. Chem.* **1966**, *5*, 622–625.

(43)   Zhuge, F.; Brassinne, J.; Fustin, C.-A.; van Ruymbeke, E.; Gohy, J.-F. Synthesis and Rheology of Telechelic Entangled Bulk Metallo-Supramolecular Polymers. *Macromolecules* **2017**, *50*, 5165–5175.

(44)   Snijkers, F.; Vlassopoulos, D. Cone-Partitioned-Plate Geometry for the ARES Rheometer with Temperature Control. *J. Rheol. (N. Y. N. Y).* **2011**, *55*, 1167–1186.

(45)   Yan, Z. C.; Costanzo, S.; Jeong, Y.; Chang, T.; Vlassopoulos, D. Linear and Nonlinear Shear Rheology of a Marginally Entangled Ring Polymer. *Macromolecules* **2016**, *49*, 1444–1453.

(46)   Costanzo, S.; Huang, Q.; Ianniruberto, G.; Marrucci, G.; Hassager, O.; Vlassopoulos, D. Shear and Extensional Rheology of Polystyrene Melts and Solutions with the Same Number of Entanglements. *Macromolecules* **2016**, *49*, 3925–3935.

(47)   Meissner, J.; Garbella, R. W.; Hostettler, J. Measuring Normal Stress Differences in Polymer Melt Shear Flow. *J. Rheol. (N. Y. N. Y).* **1989**, *33*, 843–864.

(48)   Schweizer, T.; van Meerveld, J.; Öttinger, H. C. Nonlinear Shear Rheology of Polystyrene Melt with Narrow Molecular Weight Distribution—Experiment and Theory. *J. Rheol. (N. Y. N. Y).* **2004**, *48*, 1345–1363.

(49)   Schweizer, T.; Schmidheiny, W. A Cone-Partitioned Plate Rheometer Cell with Three Partitions (CPP3) to Determine Shear Stress and Both Normal Stress Differences for Small Quantities of Polymeric Fluids. *J. Rheol. (N. Y. N. Y).* **2013**, *57*, 841–856.

(50)   Huang, Q.; Mangnus, M.; Alvarez, N. J.; Koopmans, R.; Hassager, O. A New Look at Extensional Rheology of Low-Density Polyethylene. *Rheol. Acta* **2016**, *55*, 343–350.

(51)   Rasmussen, H. K.; Bejenariu, A. G.; Hassager, O.; Auhl, D. W. Experimental Evaluation of the Pure Configurational Stress

Assumption in the Flow Dynamics of Entangled Polymer Melts. *J. Rheol. (N. Y. N. Y).* **2010**, *54*, 1325–1336.

(52) Masubuchi, Y.; Watanabe, H. Origin of Stress Overshoot under Start-up Shear in Primitive Chain Network Simulation. *ACS Macro Lett.* **2014**, *3*, 1183–1186.

(53) Schweizer, K. S.; Xie, S. J. Physics of the Stress Overshoot and Chain Stretch Dynamics of Entangled Polymer Liquids under Continuous Startup Nonlinear Shear. *ACS Macro Lett.* **2018**, *7*, 218–222.

(54) Jeong, S.; Kim, J. M.; Baig, C. Effect of Chain Orientation and Stretch on the Stress Overshoot of Entangled Polymeric Materials under Start-Up Shear. *Macromolecules* **2017**, *50*, 3424–3429.

(55) Masubuchi, Y.; Ianniruberto, G.; Marrucci, G. Stress Undershoot of Entangled Polymers under Fast Startup Shear Flows in Primitive Chain Network Simulations. *Nihon Reoroji Gakkaishi* **2018**, *46*, 23–28.

(56) Stephanou, P. S.; Schweizer, T.; Kröger, M. Communication : Appearance of Undershoots in Start-up Shear : Experimental Findings Captured by Tumbling-Snake Dynamics Communication : Appearance of Undershoots in Start-up Shear : Experimental Findings Captured by Tumbling-Snake Dynamics. *J. Chem. Phys.* **2017**, *146*, 161101–161104.

(57) Cox, W. P.; Merz, E. H. Correlation of Dynamic and Steady Flow Viscosities of Food Materials. *J. Polym. Sci.* **1958**, *28*, 619–622.

(58) Shabbir, A.; Huang, Q.; Baeza, G. P.; Vlassopoulos, D.; Chen, Q.; Colby, R. H.; Alvarez, N. J.; Hassager, O. Nonlinear Shear and Uniaxial Extensional Rheology of Polyether-Ester-Sulfonate Copolymer Ionomer Melts. *J. Rheol. (N. Y. N. Y).* **2017**, *61*, 1–11.

(59) Gabriel, C.; Münstedt, H. Strain Hardening of Various Polyolefins in Uniaxial Elongational Flow. *J. Rheol. (N. Y. N. Y).* **2003**, *47*, 619–630.

(60) Arora, S.; Shabbir, A.; Hassager, O.; Ligoure, C.; Ramos, L. Brittle Fracture of Polymer Transient Networks. *J. Rheol. (N. Y. N. Y).* **2017**, *61*, 1267–1274.

Chapter 6

Dielectric relaxation spectroscopy of transient polymeric networks

Abstract

In this Chapter, the entangled telechelic four-arm star poly(*n*-butyl acrylate) end-capped with terpyridine was used to form metallo-supramolecular bulk networks (MSBNs) upon addition of copper(II) ions with different ratios. Their dielectric responses were measured via dielectric relaxation spectroscopy (DRS) to experimentally determine the lifetime of the metal-ligand coordination. DRS results reveal a high frequency α-relaxation which is attributed to the segmental motion of the chains close to the thermal glass transition temperature, followed by a low frequency α$_2$-relaxation which is presumably associated to the dynamics of the M-L complexes. These timescales are then compared with the linear viscoelastic properties of MSBNs to confirm the peak assignment and the consistency of the results.

6.1   Introduction

Supramolecular polymeric networks based on metal-ligand coordination as physical cross-links represent a promising class of materials in the field of associating polymers. The metal-ligand coordination is particularly interesting because these interactions are highly directional and versatile. The associating strength of these non-covalent interactions can be tailored by varying the nature of the ligand or the nature of the metal ions.[1,2] The use of weak metal-ligand coordination within polymer systems leads to viscous liquid-like materials. On the contrary, relatively stable and strong M-L interactions give access to rubber-like polymeric networks. Moreover, these reversible complexes display a thermal dependence. At high temperatures, M-L interactions are weakened and the associating polymers behave as Newtonian fluids because the thermodynamic stabilities and the association/dissociation kinetics of M-L complexes are altered. On the other hand, at low temperatures, metallo-supramolecular polymers behave as soft elastic networks in which a rubbery plateau covers many decades in frequency.

While lots of studies have been reported on designing metallo-supramolecular polymers with various structural building blocks, the fundamental understanding on the reversibility of these interactions and its impact on the local and the global dynamics of the metallo-supramolecular polymers is not fully established. Hence, understanding the rich mechanical properties of such metallo-supramolecular polymers is indeed challenging.[3] It can offer great opportunities to engineer the dynamics of such associating systems in the field of smart soft materials. In this Chapter, the dielectric behavior of a well-defined entangled model system is reported. The latter is based on an entangled telechelic four-arm star poly(*n*-butyl acrylate) end-capped with terpyridine ligand with low dispersity (Đ < 1.3).[4] Upon addition of different transition metal ions with various ratios (from stoichiometry to excesses), reversible metallo-supramolecular bulk networks (MSBNs) are formed. They appear completely amorphous with a glass transition temperature around -52°C and thus can be used as model systems to study their dynamics over a wide range of temperatures and

frequencies. The formation of transient networks is confirmed in rheology (small amplitude oscillatory shear measurements).

This work is inspired by the great investigations conducted by Colby et al. on ionomers to provide a molecular level understanding of dynamics of these associating systems combining several experimental techniques such as X-ray scattering, oscillatory shear and dielectric relaxation spectroscopy (DRS).[5–8] Their DRS results showed that the associating ionomers display two dipolar relaxations, one relaxation is assigned to the segmental motion of the polymer and the other one is attributed to the ionic interaction rearrangement between isolated pairs and ionic aggregates.[9,10] Similarly, this work is a continuation of the efforts to fully understand how the process of association/dissociation of the reversible M-L complexes and the mechanism of entanglement/disentanglement of the building blocks control the global dynamics of the metallo-supramolecular bulk networks. Dielectric relaxation spectroscopy is used to independently determine the lifetime of metal-ligand complexes. The dielectric spectrum of the MSBNs typically displays a prominent α relaxation at high frequencies, attributed to the segmental motion of the polymeric chain. It is followed by a slower α_2 relaxation associated to the reversible metal-ligand coordination, which is defined as the (possible) sticker lifetime. The general rheological and dielectric behavior of the entangled metal-containing transient networks is further discussed.

6.2 Materials and methods

6.2.1 Materials
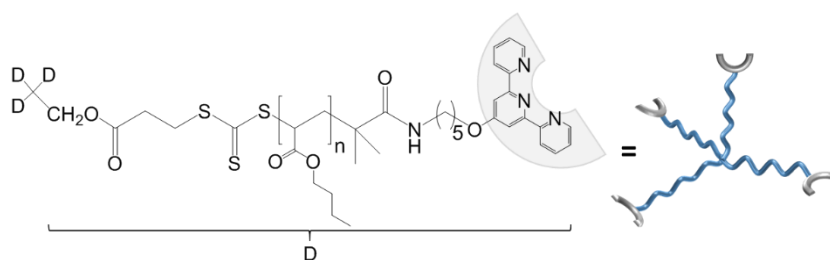
Samples	$M_{n, system}$[a]	$M_{n, arm}$[b]	M_n/M_e[c]	Đ[d]	T_g[e]
	(kg/mol)	(kg/mol)			(°C)
Star 250k	249	62	3.4/ arm	1.20	-52

Table 6.1 Structural parameters of telechelic 4-arm star PnBA-tpy$_4$ polymers. [a,b] Molar mass of the whole system determined by ^{1}H-NMR. [c] Number of entanglements calculated using M_e = 18 kg/mol. [d] Dispersity of the polymers determined by SEC, polystyrene standards were used for calibration. [e] Glass transition temperature determined by DSC.[11]

6.2.2 DRS measurements

The dielectric measurements of the MSBNs were performed using dielectric relaxation spectroscopy. Samples were prepared for measurement by allowing them to flow and cover a 40 mm diameter freshly polished brass electrode at 130°C under vacuum. To control sample thickness, a silica spacer of 50 μm thickness was placed on top of the 40 mm diameter electrode before placing the sample. Then a 10 mm diameter freshly polished brass electrode was placed on top to form a parallel plate capacitor cell which was squeezed to a gap controlled by the spacer. The MSBN/electrodes sandwiches were positioned in a Novocontrol GmbH Concept 40 broadband dielectric spectrometer, after being in a vacuum oven at 60°C for 12 h. Each sample was then annealed in the instrument at 120°C in a heated stream of nitrogen for

1 h prior to measurement to remove moisture acquired during sample loading. The dielectric permittivity was measured using a sinusoidal voltage with amplitude 1.5 V over a 10^{-1}-10^6 Hz frequency range during all experiments. Data were collected in isothermal frequency sweeps every 5°C, from (T_g + 170°C) to (T_g.- 100°C).

6.3   Results and discussion

6.3.1 Dielectric relaxation

Broadband dielectric spectroscopy is a technique which relies on the interaction between the electric dipole entities in the sample and an external field.[12] The relaxation process is related to the molecular fluctuations of dipoles originating from the movements of molecules in an electric field. Experimentally, frequency sweep measurements are typically conducted at given temperatures to measure the complex permittivity which is defined as follows:

$$\varepsilon^*(\omega) = \varepsilon'(\omega) - i\varepsilon''(\omega) \tag{6.1}$$

where ε' is the storage permittivity and ε'' is the loss permittivity. Figure 6.1 depicts the dielectric spectrum of the telechelic four-arm star precursor without metal ions at various temperatures.
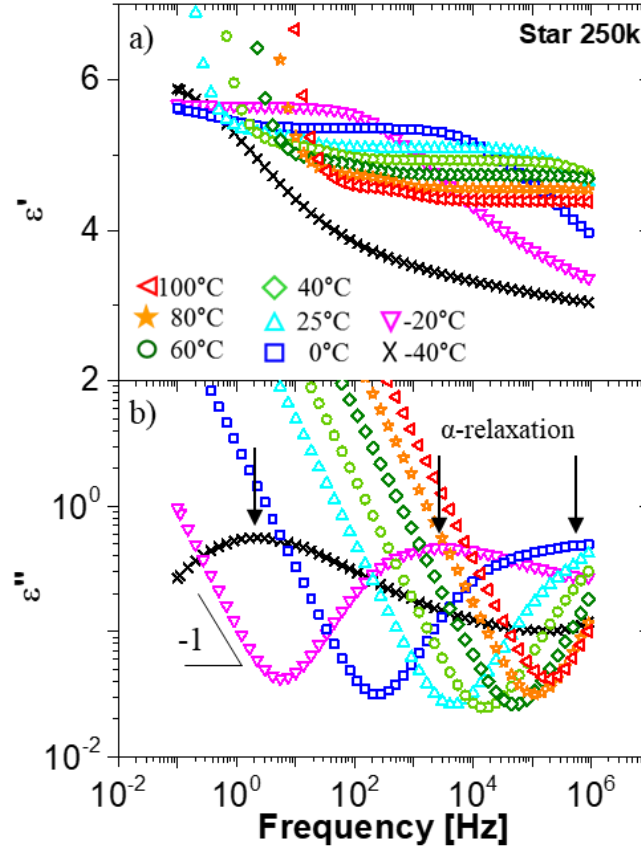
Figure 6.1 (a) Storage permittivity and (b) Loss permittivity as a function of frequency for the reference sample Star250k measured at temperature T = 100°C (red, ◄), T = 80°C (orange, ★), T = 60°C (dark green, ◊), 40°C (green, o), 25°C (cyan, Δ), 0°C (blue, □), -20°C (magenta, ∇) and -40°C (black, X). A sharp decrease of the dielectric imaginary part with a slope of -1 is observed from low to high frequency, corresponding to strong electrode polarization effect.

While the storage permittivity decreases with increasing ω till reaching a frequency-independent region, the loss permittivity exhibits a maximum peak with increasing ω. This maximum permittivity ε''_{max} is then probed at temperatures close to the T_g. The frequency corresponding to the maximum loss permittivity, f_α, determines the characteristic relaxation time, $\tau_{rel} = 1/2\pi f_\alpha$. From this result, it seems that the star precursor only shows one single relaxation peak with a

corresponding relaxation time. This single relaxation mode is attributed to the α-relaxation process which corresponds to the segmental motion of the chain near the glass transition temperature. The empirical Vogel-Fulcher-Tammann (VFT) equation is used to certify that the ε''$_{max}$ peaks probed at temperatures close to the T_g correspond to segmental motions of the chains.[13–15] To do so, the peak relaxation frequencies (ω_{max}) are plotted as a function of the inverse temperature and are compared with the VFT function as reported in Figure 6.2.
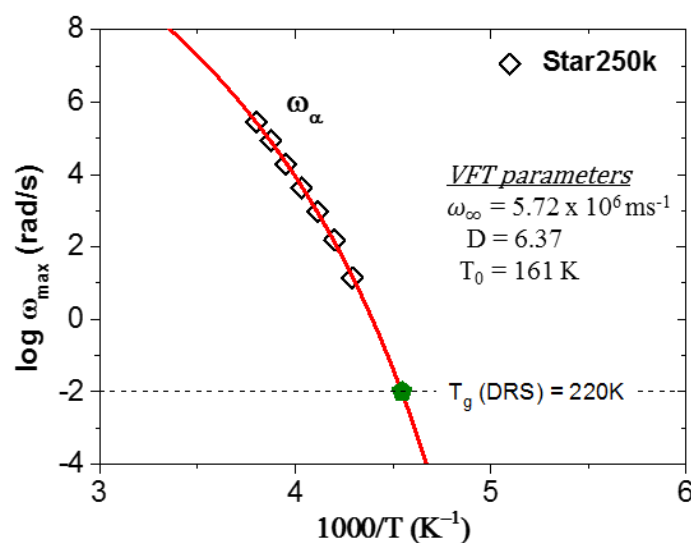
Figure 6.2 The structural α-relaxation rates for the telechelic four-arm star PnBA-tpy$_4$ as function of the inverse temperature. The solid line is a fit using the VFT equation. The green pentagon data point represents the T_g defined from DRS. The T_g (DRS) is obtained from dielectric measurements by extrapolating the VFT fit of the α-relaxation process to a value of 100 s.

The empirical VFT equation is defined as follows:

$$\omega_{max} = \omega_\infty \, exp\left(-\frac{DT_0}{T-T_0}\right) \qquad (6.2)$$

Where ω_∞ is the high-temperature limiting frequency, D is the strength parameter and T_0 is the Vogel temperature.

For the star precursor, the peak relaxation frequencies ω_{max} of the DRS α-relaxation process follows the VFT temperature dependence with a Vogel temperature T_0 equals to 161K, a strength parameter D equals to 6.37 and ω_∞ equals to 5.72 x 10^6 ms^{-1}. T_0 is also called the ideal glass transition and its value should be found to be 30-70K below T_g, which is the case here.[13] Extrapolating the α-relaxation time to 100 s using the VFT equation gives a T_g of 220 K. This value is consistent with the result of differential scanning calorimetry measurement (T_g = 221 K). This consistency confirms the assignment of the high-frequency process to the structural α-relaxation of the telechelic star precursor.

Similarly, those analyses have been performed under the same conditions for the metallo-supramolecular bulk networks obtained with different ratios of copper(II) ions. Figure 6.3 displays the storage and the loss permittivity as a function of frequency for the MSBN obtained with 0.50 equivalents of Cu(II). From low to high frequency, a sharp decrease of the dielectric imaginary part with a slope of -1 is observed in Figure 6.3.b. This sharp decrease originates from the strong electrode polarization (EP) effect. The latter is an unwanted side effect during the experiment because it screens the dielectric response of the material, influencing the dielectric properties at low frequencies.[16–18] This side effect is due to the blocking of charge carriers at the interface between the sample and the electrode. Hence the positive and negative charges are separated, leading to an additional polarization.[12] In order to overcome this issue, a derivative analysis of the real part ε' is used, which eliminates the conductivity contribution from the imaginary part ε". The derivative function is defined as follows[19]:

$$\varepsilon_{derivative} = -\frac{2}{\pi}\frac{\partial \varepsilon\prime(\omega)}{\partial \log \omega} \tag{6.3}$$

From the derivative functions presented in Figure 6.3.c, one peak is clearly observed and the onset of a second peak is highlighted. The first peak located at high frequency and probed at temperatures close to the T_g is labeled as the α-relaxation, corresponding to the segmental motion of the chains as mentioned above. One must note that in the presence of metal ions, the α-relaxation peak shows a broadening compared to the star precursor. This broadening is typical and can be considered as a characteristic of cross-linked polymers, confirming the formation of the

reversible polymeric network.[12] This broadness is due to the difference in relaxation times for segments close to and far from the transient network junctions.[20,21] The onset of the second maximum located at lower frequencies and measured at higher temperatures is referred to as the α_2-relaxation. The latter is presumably attributed to the possible metal-ligand complexe dynamics, i.e., the sticker lifetime. However, the electrode polarization effect still masks the dielectric response of the material even though a derivative analysis is performed to minimize its effect. This is probably due to the fact that the MSBN is not a highly conducting material but rather an insulating one. Consequently, when the polarization occurs, the dielectric constant ε' increases and masks the weak dielectric response of the MSBN.
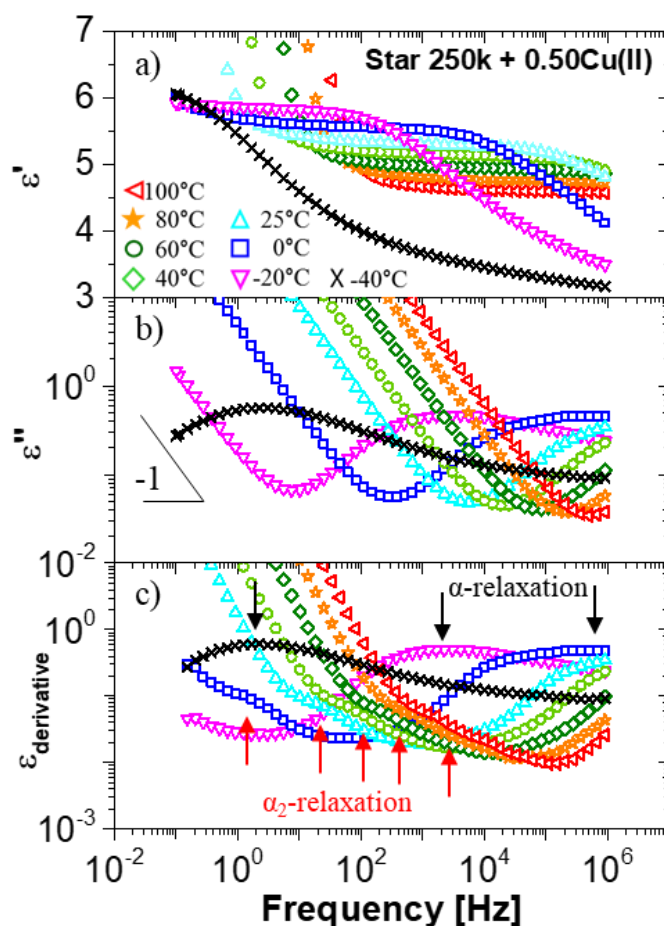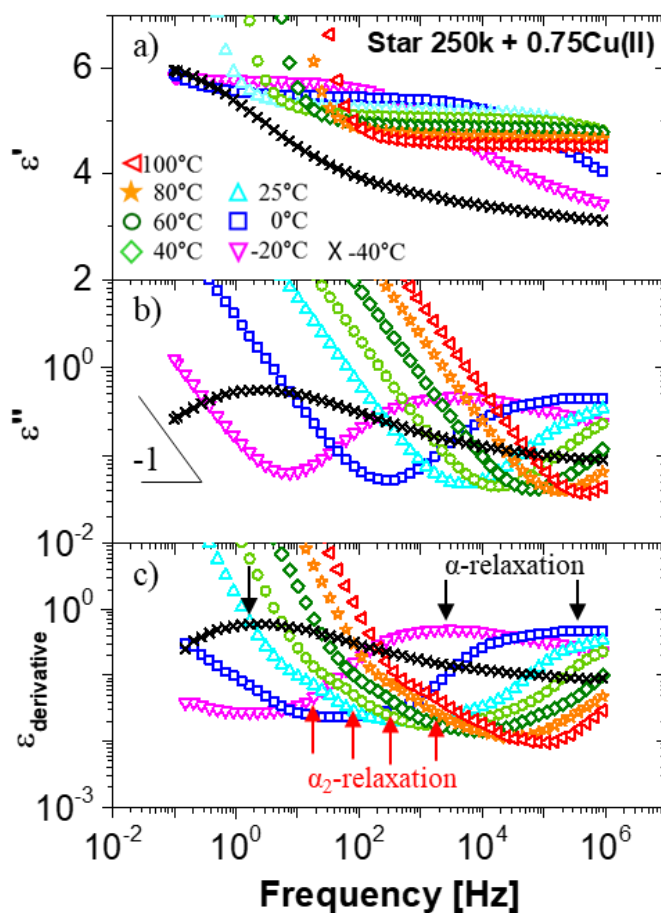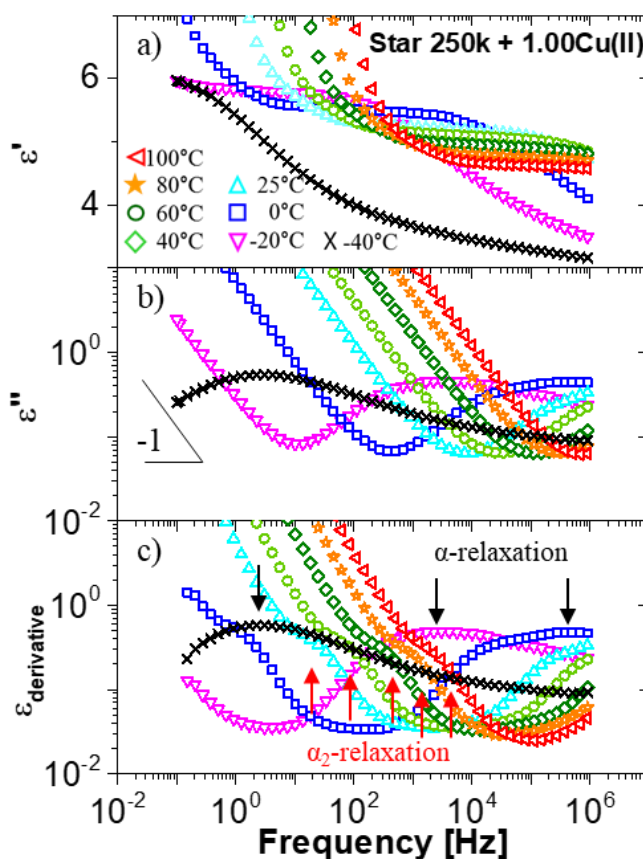

Figure 6.3 (a) Storage permittivity, (b) Loss permittivity, and (c) Derivative as a function of frequency for the reference sample Star250k

+ 0.50eq. CuCl$_2$ measured at temperature T = 100°C (red, ◄), T = 80°C (orange, ★), T = 60°C (dark green, ◊), 40°C (green, o), 25°C (cyan, Δ), 0°C (blue, □), -20°C (magenta, ∇) and -40°C (black, X).

Additionally, the scaling of the temperature dependence of the α-relaxation also fits relatively well with the VFT equation (see Figure 6.4), indicating that the peak observed at low frequencies does correspond to the segmental motion of the chains. The T$_g$ (DRS) which is equals to 216K is consistent with the value obtained from differential scanning calorimetry (T$_{g, DSC}$ = 222K).
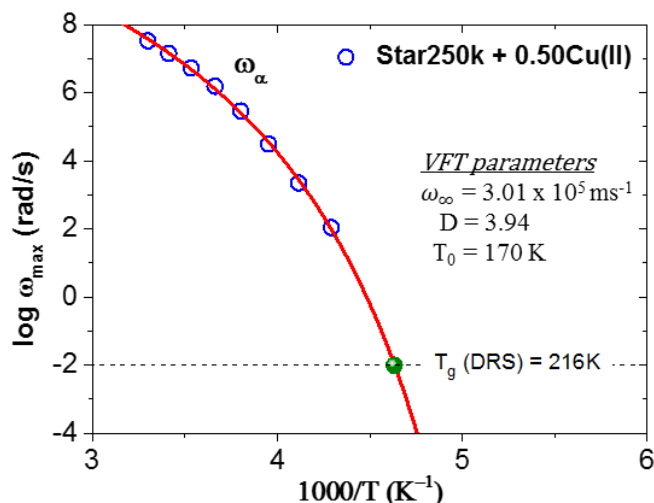
Figure 6.4 The structural α-relaxation rates for the telechelic four-arm star PnBA-tpy$_4$ + 0.50Cu(II) plotted as a function of the inverse temperature. The solid line is a fit using the VFT equation. The green filled circle data point represents the T$_g$ defined from DRS. The T$_g$ (DRS) is obtained from dielectric measurements by extrapolating the VFT fit of the α-relaxation process to a value of 100 s.

While the α-relaxation can be scaled with the VFT fit, the same procedure cannot be applied to the α$_2$-relaxation because there is no distinctive maximum in the second relaxation process. Hence, it is not possible to unambiguously determine any timescale. This is probably due to the weak dielectric response of the transient network. Note that herein, the content of the stickers is evaluated to be 0.5 wt% with respect to the polymeric matrix. Moreover, at 0.50eq. of copper(II) ions,

only 60% of the terpyridine ligands are coordinated and active, so in the end there is only 0.3 wt% of efficient metal-ligand complexes which contribute to the dielectric response. This is why when EP manifests itself, it obscures the weak response of the material. Therefore this second relaxation mode cannot be exploited and the Havriliak-Negami (HN) fitting function cannot be used due the absence of clear peaks .[22]

In order to overcome this issue, one can simply add more metal ions to increase the number of active stickers. As shown in Chapter 5, the percentage of active stickers has increased up to 80% when 0.75eq. of copper ions are added. Figure 6.5 displays the storage, the loss and the derivative permittivity as function of frequency for the MSBN obtained with 0.75 equivalents of Cu(II).

Figure 6.5 (a) Storage permittivity, (b) Loss permittivity, and (c) Derivative as a function of frequency for the reference sample Star250k

+ 0.75eq. CuCl$_2$ measured at temperature T = 100°C (red, ◄), T = 80°C (orange, ★), T = 60°C (dark green, ◊), 40°C (green, o), 25°C (cyan, Δ), 0°C (blue, □), -20°C (magenta, ∇) and -40°C (black, X).

Unfortunately, the dielectric response is still not sufficient even with 0.4 wt% of active metal-ligand coordination. Once more, only the α-relaxation can be distinctively processed and fitted with the VFT equation (data not shown), whereas the second peak is shadowed by the EP effect. The same systematic investigation is pursued on the reversible network formed with 1.00eq. of copper(II) to check if decent dielectric responses can be achieved with the maximum fraction of active and efficient metal-ligand interactions. Figure 6.6 presents the dielectric spectrum of the Star250k + 1.00eq. Cu(II) at various temperatures.

Figure 6.6 (a) Storage permittivity, (b) Loss permittivity, and (c) Derivative as a function of frequency for the reference sample Star250k

+ 1.00eq. CuCl$_2$ measured at temperature T = 100°C (red, ◄), T = 80°C (orange, ★), T = 60°C (dark green, ◊), 40°C (green, o), 25°C (cyan, Δ), 0°C (blue, □), -20°C (magenta, ∇) and -40°C (black, X).

With 1.00eq. of copper(II) ions, the second peak is still masked but it gives a strong enough dielectric response, allowing it to be further analyzed to get the lifetime of the stickers. While the α-relaxation peak can be clearly determined at various temperatures, the empirical Havriliak-Negami[22] (HN) function is needed to properly analyze the α$_2$-relaxation peak. Indeed, since the latter is not well defined and well separated from the electrode polarization effect, it is difficult to crudely determine directly the maximum from the derivative permittivity. This is why the HN function is used. The HN function is defined as follows[12]:

$$\varepsilon_{HN}^*(\omega) = \varepsilon_\infty + \frac{\Delta\varepsilon}{(1+(i\omega\tau_{HN})^\alpha)^\beta} \tag{6.4}$$

where ε_∞ is the high frequency limiting of the real part of the dielectric permittivity, $\Delta\varepsilon$ is the relaxation strength, τ_{HN} is the characteristic relaxation time, ω is the angular frequency, α and β are the shape parameters describing, respectively, the symmetric and the asymmetric broadening of the distribution of the relaxation times. An example of the fitting procedure using HN function is shown in Figure 6.7.
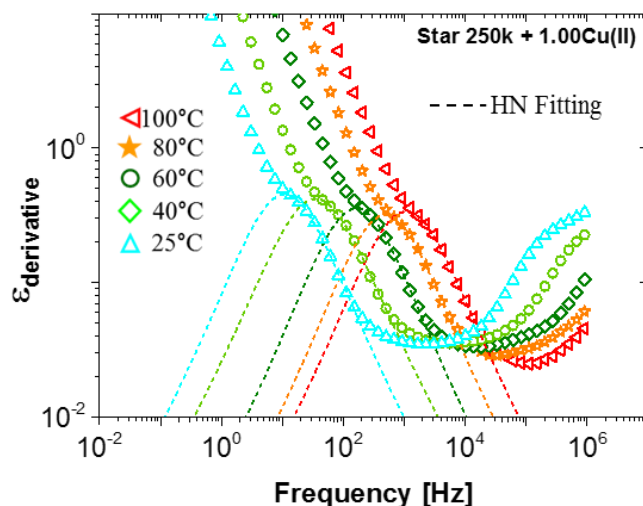
Figure 6.7 Dielectric derivative spectrum fits (dashed lines) using the Havriliak-Negami function for the α$_2$-relaxation at temperature T =

100°C (red, ◄), T = 80°C (orange, ★), T = 60°C (dark green, ◊), 40°C (green, o) and 25°C (cyan, Δ).

The shape parameters α and β in Equation 6.4 are on average α ≈ 0.81 and β ≈ 1.21 where $0 < \alpha < 1$ and $0 < \alpha.\beta \leq 1$ conditions are respected.

From the HN fitting, the peak relaxation frequencies (ω_{max}) are extracted for the α_2-relaxation and they are plotted as function of the reciprocal temperature (see Figure 6.8).
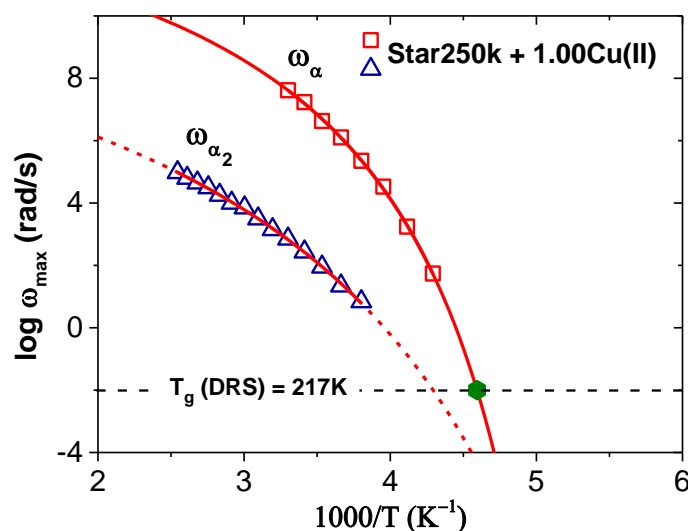

Figure 6.8 The structural α-relaxation and α_2-relaxation rates for the telechelic four-arm star PnBA-tpy4 + 1.00Cu(II) plotted as a function of the inverse temperature. The solid line and the dashed line are fits using the VFT equation. The green filled hexagon data point represents the T_g defined from DRS. The T_g (DRS) is obtained from dielectric measurements by extrapolating the VFT fit of the α-relaxation process to a value of 100 s.

Metallo-supramolecular bulk networks obtained with 1.00eq. Cu(II) display two dipolar relaxations that can be further analyzed. The first peak located at high frequency is assigned to the usual segmental motion of the polymer and is labelled as the α-relaxation. At lower frequency, the second peak which is obscured by the EP effect is attributed to the metal-ligand rearrangements and is referred as the α_2-relaxation, corresponding to M-L dissociation/association process.

These attributions can be confirmed while performing the VFT fits. Figure 6.8 clearly shows that the scaling of the temperature dependence of the α and α_2 relaxations fits with the VFT equation. This indicates that the peak observed at high frequency does correspond to the segmental motion of the chains and the second one at lower frequency is presumably related to the dynamics of the M-L coordination. Moreover, the temperature value at which the relaxation time reaches 100 s, i.e. T_g (DRS, equals to 217K) shows a good agreement with the corresponding calorimetry value (T_g = 224K). This consistency supports the peak assignments in which one peak corresponds to the segmental motion of the chain close to the glass transition and the other one to the dynamics of the M-L complexes. The VFT parameters for the Star250k + 1.00eq. Cu(II) are tabulated in Table 6.2.

	$\boldsymbol{\omega_\infty}$ (ms^{-1})	**D**	**T$_0$** (K)
α-relaxation	3.23 x 10^5	3.83	173
α_2-relaxation	2.53 x 10^3	3.72	173

Table 6.2 The Vogel-Fulcher-Tammann parameters for the α and α_2 relaxations of Star250k + 1.00eq. Cu(II).

These parameters are later on used to determine the M-L complex lifetime and will be compared with the linear viscoelastic rheology data in Section 6.3.3 to verify the consistency of the results.

6.3.2 Static dielectric constant

From these dielectric measurements performed on the precursor sample and the transient networks with different loading ratios, another parameter is also worth to mention, which is the static permittivity ε_s. The latter is defined as the low frequency plateau of the storage permittivity ε' before the onset of the electrode polarization. Figure 6.9 displays the static dielectric constant for the four-arm star precursor and the MSBNs formed with different amounts of copper(II) ions as function of the inverse temperature. The reference system exhibits ε_s = 5.1 at room temperature whereas the MSBNs have ε_s =

5.2 in average, indicating no significant difference between the systems with or without metal ions. The temperature dependence of ε_s for all systems follows the Onsager equation across the entire temperature range. Precisely, from $(T_g + 175K)$ to $(T_g + 35K)$ in which the static permittivity decreases with increase in temperature due to the thermal randomization.[23] The Onsager equation is defined as follows[5,6,12,23]:

$$\frac{(\varepsilon_s - \varepsilon_\infty)(2\varepsilon_s - \varepsilon_\infty)}{\varepsilon_s(\varepsilon_\infty + 2)^2} = \frac{1}{9\varepsilon_0 . k_B . T} \sum_i \nu_i . m_i^2 \qquad (6.5)$$

where ν_i is the number density of dipoles and m_i is their dipole moment. From a physical point of view, the permittivity defines the ability of a material to polarize in response to an applied field and can be expressed as:

$$\varepsilon_s = \varepsilon_r . \varepsilon_0 \qquad (6.6)$$

Where ε_r is the relative permittivity and ε_0 the permittivity of vacuum.
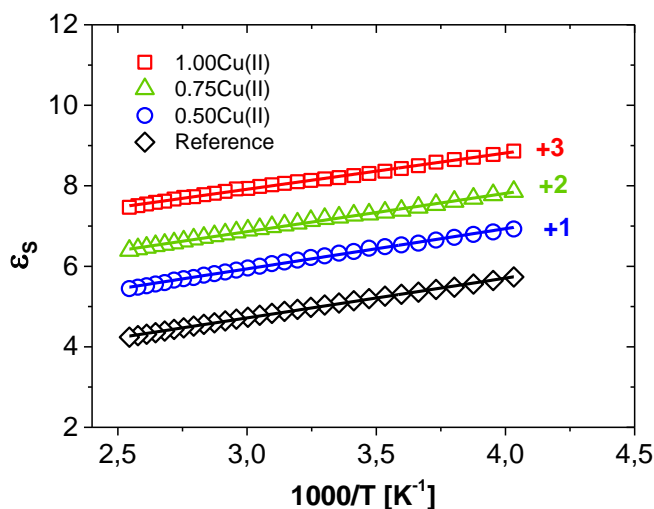
Figure 6.9 Temperature dependence of the static dielectric constant ε_s for the telechelic four-arm precursor and for the MSBNs formed with different loadings of $CuCl_2$. Data are shifted for clarity.

If a material develops a large polarization in an applied field, then its static dielectric permittivity value will be high. Herein, the reference sample and the reversible networks exhibit low ε_s, confirming the insulating properties of the associating systems. For conductive

polymers such as ionomers, these systems usually display static permittivity values ranging from 20 to 80.[5,6] The telechelic four-arm precursor and the metallo-supramolecular bulk networks are considered as insulators even though they contain aromatic groups originating from the terpyridine ligands. This is probably due to the low content of incorporated tpy moiety within the polymeric matrix (only 0.5 wt%). The latter is not sufficient to compensate the electrical insulating property of the poly(*n*-butyl acrylate) block which has a dc conductivity of 2.88 x 10^{-11} S/cm at 25°C.

6.3.3 Comparison between viscoelastic and dielectric responses

Last but not least, it is also interesting to compare the linear viscoelastic data with the dielectric responses. Figure 6.10 presents the linear viscoelastic master curves to a reference temperature of 25°C for the reversible network obtained with 1.00eq. of copper(II) ions. For comparison, the frequency dependence of the permittivity derivative $\varepsilon_{derivative}$ is also included.
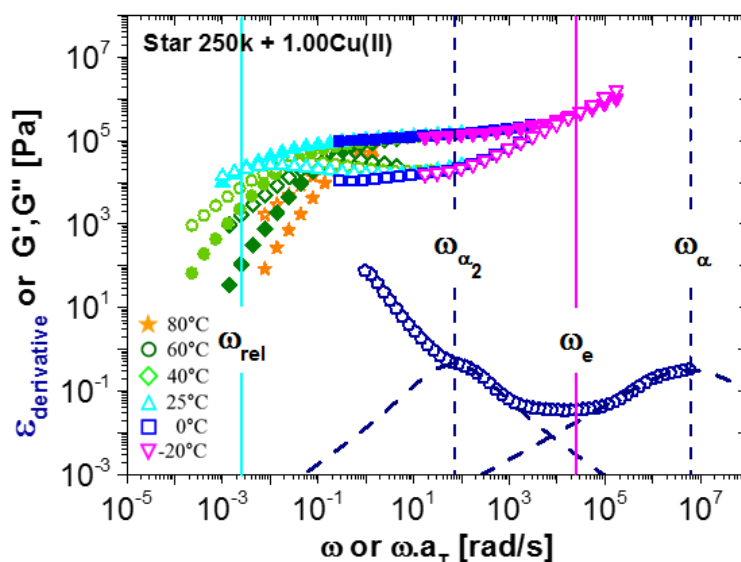
Figure 6.10 Comparison between linear viscoelastic and dielectric responses of Star 250k + 1.00eq. Cu(II) at T = 25°C. The dark blue

pentagon points represent the DRS data. The experimental linear viscoelastic data have been measured at temperature T = 80°C (orange, ★), 60°C (dark green, ◊), 40°C (green, o), 25°C (cyan, Δ), 0°C (blue, □) and -20°C (magenta, ∇). The experimental data have been shifted to a reference temperature of 25°C, based on the shift factors determined for the reference samples. The storage modulus G' is represented by filled symbols, the loss modulus G" by unfilled symbols.

From the comparison, it is clear that the dielectric α-relaxation (indicated by the vertical dashed line) does correspond to the mechanical segmental motion of the chains close to the glass transition temperature. The latter is related to the relaxation time of the monomer, i.e., the shortest relaxation time τ_0 which is indeed located in the glassy region. The reciprocal of ω_α obtained from dielectric measurements is indeed located in this monomeric relaxation region from the linear viscoelastic properties.

In Chapter 3 and 4, it was established from the linear rheology that the M-L complexes must first dissociate in order to allow the star arms to relax by fluctuation mechanisms.[4] While the lifetime of the sticker cannot be extracted from the rheological data, the dielectric measurements allow the determination of this timescale which corresponds to the dynamics of the metal-ligand complexes. In fact, the lifetime of the sticker (τ_s) is evaluated as the inverse of the frequency at which the $\varepsilon_{derivative}$ exhibits the α2- relaxation peak ($1/2\pi\omega_{\alpha2}$). Experimentally, this sticker lifetime is estimated to τ_s = 15 ms. From Figure 6.10 in the plateau region, it is indeed observed that the storage modulus G' starts to decrease from the moment $\omega = \omega_{\alpha2}$. It is assumed that the first metal-ligand complex dissociation occurs at this timescale, allowing the star arms to fluctuate and partially release some stress until the sticker re-associates again. This is why a decrease in the storage modulus can be seen starting from $\omega_{\alpha2}$.

Since there is no uncoordinated chain at 1.00eq. of copper(II), the ligand exchange mechanism (described in Chapter 4) is excluded. Most probably, the stickers have to perform several hopping processes to release the stress. In this case, it is difficult for the ligand to find a new partner to coordinate with after dissociating from the old one.[24]

302

Therefore, the ligand re-associates with its old partner and undergoes several unsuccessful searches for a new one. This failure to find a new ligand to associate, can extend the effective lifetime of the metal-ligand coordination over few orders of magnitude in frequency. Herein, the effective lifetime is at least extended to four decades in frequency if $\omega_{\alpha 2}$ and ω_{rel} are considered. Ultimately, mechanical properties of the transient networks exhibit a plateau modulus extended over a wide range of frequency with a terminal relaxation time shifted to relatively low frequency.

6.4   Conclusions

In this chapter, we have attempted to correlate morphology, viscoelasticity and dielectric response of metallo-supramolecular bulk networks based on poly(n-butyl acrylate) blocks and terpyridine associating units with different amount of copper(II) ions. From the dielectric relaxation analyses, it is clearly observed that the star precursor simply displays an α-relaxation peak at high frequency and at temperatures close to T_g. This latter follows a Vogel-Fulcher-Tammann (VFT) temperature dependence and is referred to as the segmental motion of the chains near the glass transition temperature. Upon addition of metal cations, this α-relaxation peak broadens, indicating the formation of the transient networks. Moreover, the onset of an α_2-relaxation peak is probed at lower frequencies, which is presumably labelled as the dynamics of the M-L complexes. This second peak cannot be properly distinguished from the electrode polarization (EP) effect which obscures the α_2-relaxation peak. This masking is still present even though a derivative of the real permittivity is performed to remove the conductivity contribution from the imaginary permittivity. This highlights the insulating features of the systems which give relatively weak dielectric responses.

However, when 1.00eq. of copper(II) ions is used to obtain the transient network, the α_2-relaxation peaks are slightly more visible and can be exploited to determine the lifetime of the M-L coordination. Since these peaks are still not well-defined, the empirical Havriliak-Negami (HN) function is used to analyze them. Similarly, the α_2-

relaxation also displays a VFT temperature dependence, confirming that the α$_2$ is related to the dynamics of the M-L interactions. When those dielectric data are compared with the linear viscoelastic measurements, both inputs are consistent and the peak assignments are confirmed. Hence, the metal-ligand coordination lifetime can only be experimentally determined via DRS for the transient network formed with 1.00eq. of Cu(II) which is evaluated to τ_s = 15 ms. It is also observed that the incorporation of bis(terpyridine)-copper complexes within the polymeric matrix has no effect on the dc conductivity and the static dielectric permittivity. This indicates that the incorporation of 0.5 wt% of aromatic-containing terpyridine ligand within polymeric matrix are clearly not sufficient to counter-balance the insulating properties of the poly(n-butyl acrylate) block.

Dielectric relaxation spectroscopy is a powerful method to investigate the molecular dynamics of polymeric systems over a very broad frequency range. Depending on the studied polymeric system, different relaxation processes can be investigated. Herein, DRS is an excellent complementary tool to not only experimentally determine the lifetime of the M-L coordination but also to confirm and to check the consistency between different characterization methods. For instance, the combination of the DRS with the different scanning calorimetry analysis and the oscillatory shear measurements can be very insightful.

Bibliography

(1)   Mozhdehi, D.; Neal, J. A.; Grindy, S. C.; Cordeau, Y.; Ayala, S.; Holten-Andersen, N.; Guan, Z. Tuning Dynamic Mechanical Response in Metallopolymer Networks through Simultaneous Control of Structural and Temporal Properties of the Networks. *Macromolecules* **2016**, *49*, 6310–6321.

(2)   Grindy, S. C.; Holten-Andersen, N. Bio-Inspired Metal-Coordinate Hydrogels with Programmable Viscoelastic Material Functions Controlled by Longwave UV Light. *Soft Matter* **2017**, *13*, 4057–4065.

(3)   Wang, R.; Sing, M. K.; Avery, R. K.; Souza, B. S.; Kim, M.; Olsen, B. D. Classical Challenges in the Physical Chemistry of Polymer Networks and the Design of New Materials. *Acc. Chem. Res.* **2016**, *49*, 2786–2795.

(4)   Zhuge, F.; Brassinne, J.; Fustin, C.-A.; van Ruymbeke, E.; Gohy, J.-F. Synthesis and Rheology of Telechelic Entangled Bulk Metallo-Supramolecular Polymers. *Macromolecules* **2017**, *50*, 5165–5175.

(5)   Choi, U. H.; Lee, M.; Wang, S.; Liu, W.; Winey, K. I.; Gibson, H. W.; Colby, R. H. Ionic Conduction and Dielectric Response of Poly(Imidazolium Acrylate) Ionomers. *Macromolecules* **2012**, *45*, 3974–3985.

(6)   Choi, U. H.; Ye, Y.; Salas De La Cruz, D.; Liu, W.; Winey, K. I.; Elabd, Y. A.; Runt, J.; Colby, R. H. Dielectric and Viscoelastic Responses of Imidazolium-Based Ionomers with Different Counterions and Side Chain Lengths. *Macromolecules* **2014**, *47*, 777–790.

(7)   Chen, Q.; Bao, N.; Wang, J. H. H.; Tunic, T.; Liang, S.; Colby, R. H. Linear Viscoelasticity and Dielectric Spectroscopy of Ionomer/Plasticizer Mixtures: A Transition from Ionomer to Polyelectrolyte. *Macromolecules* **2015**, *48* (22), 8240–8252.

(8)   Chen, Q.; Tudryn, G. J.; Colby, R. H. Ionomer Dynamics and the Sticky Rouse Model. *J. Rheol. (N. Y. N. Y).* **2013**, *57*, 1441–1462.

(9)   Fragiadakis, D.; Dou, S.; Colby, R. H.; Runt, J. Molecular Mobility, Ion Mobility and Mobile Ion Concentration in Poly (Ethylene Oxide)-Based Polyurethane Ionomers. *Macromolecules* **2008**, *41*, 5723–5728.

(10)   Lee, M.; Choi, U. H.; Colby, R. H.; Gibson, H. W. Ion Conduction in Imidazolium Acrylate Ionic Liquids and Their Polymers. *Chem. Mater.* **2010**, *22*, 5814–5822.

(11)   Zhuge, F.; Hawke, L. G. D.; Fustin, C.-A.; Gohy, J.-F.; van Ruymbeke, E. Decoding the Linear Viscoelastic Properties of Model Telechelic Metallo-Supramolecular Polymers. *J. Rheol. (N. Y. N. Y).* **2017**, *61*, 1245–1262.

(12)   Kremer, F.; Schönhals, A. *Broadband Dielectric Spectroscopy*; Heidelberg, Springer-Verlag Berlin: Berlin, 2003.

(13)   Vogel; H. Das Temperaturabhangigkeitsgesetz Der Viskositat von Flussigkeiten. *Phys. Z.* **1921**, *22*, 645–646.

(14)   Fulcher, G. S. Analysis of Recent Measurements of the Viscosity of

Glasses. *J. Am. Ceram. Soc.* **1992**, *75*, 1043–1055.

(15) Tammann, G.; Hesse, W. Die Abhängigkeit Der Viscosität von Der Temperatur Bie Unterkühlten Flüssigkeiten. *Anorg. Allg. Chem* **1926**, *156*, 245–257.

(16) Fuoss, R. M.; Kirkwood, J. G. Electrical Properties of Solids. VIII. Dipole Moments in Polyvinyl Chloride- Diphenyl Systems*. *J. Am. Chem. Soc.* **1941**, *63*, 385–394.

(17) Klein, R. J.; Zhang, S.; Dou, S.; Jones, B. H.; Colby, R. H.; Runt, J. Modeling Electrode Polarization in Dielectric Spectroscopy: Ion Mobility and Mobile Ion Concentration of Single-Ion Polymer Electrolytes. *J. Chem. Phys.* **2006**, *124*, 144903–144908.

(18) Emmert, S.; Wolf, M.; Gulich, R.; Krohns, S.; Kastner, S.; Lunkenheimer, P.; Loidl, A. Electrode Polarization Effects in Broadband Dielectric Spectroscopy. *Eur. Phys. J. B* **2011**, *83*, 157–165.

(19) Wübbenhorst, M.; Van Turnhout, J. Analysis of Complex Dielectric Spectra. I: One-Dimensional Derivative Techniques and Three-Dimensional Modelling. *J. Non. Cryst. Solids* **2002**, *305*, 40–49.

(20) Roland, C. M. Constraints on Local Segmental Motion in Poly(Vinylethylene) Networks. *Macromolecules* **1994**, *27*, 4242–4247.

(21) Casalini, R.; Roland, C. M. Effect of Crosslinking on the Secondary Relaxation in Polyvinylethylene. *J. Polym. Sci. Part B Polym. Phys.* **2010**, *48*, 582–587.

(22) Havriliak, S.; Negami, S. A Complex Plane Representation of Dielectric and Mechanical Relaxation Processes in Some Polymers. *Polymer (Guildf).* **1967**, *8*, 161–210.

(23) Onsager, L. Electric Moments of Molecules in Liquids. *J. Am. Chem. Soc.* **1936**, *58*, 1486–1493.

(24) Semenov, A. N.; Rubinstein, M. Dynamics of Entangled Associating Polymers with Large Aggregates. *Macromolecules* **2002**, *35*, 4821–4837.

Chapter 7

Relaxation process of transient polymeric networks moving in a linear polymer matrix

Abstract

This Chapter focuses on the linear viscoelastic properties of entangled metallo-supramolecular bulk networks diluted in linear poly(*n*-butyl acrylate)s with two different molar masses. Binary blends with various ratios of the transient network are investigated both experimentally and theoretically using small amplitude oscillatory shear (SAOS) and a modified version of the tube-based time marching algorithm (TMA) respectively. The experimental data reveal that reversible network relaxation depends on both disentanglement and association dynamics, with the respective importance of these two processes depending on the nature and the amount of the metal ion or on the temperature but also on the length and the ratio of the linear matrix. A good description of the data is achieved using the modified TMA model. The latter contains two fitting parameters, i.e. the probability of an initially associated arm to dissociate and the time during which the dissociated arm remains free. This work provides early results on binary blends based on reversible networks diluted in linear matrices. The interpretations of the results can be reconsidered and are completely open for discussions.

7.1   Introduction and Objective

As presented in the previous chapters, metallo-supramolecular networks composed of entangled telechelic star molecules display highly tunable rheological properties, which are sensitive to temperature as well as to the nature and proportion of the metal ions added to the system. The objective of the present work is to explore how the dynamics of such transient networks can be altered if we dilute them in a matrix of linear polymer, in various proportions.

Based on our previous works, we first expect that the linear matrix will affect the probability of a ligand to be involved in the supramolecular network.[1] Indeed, blending the telechelic stars to non-sticky molecules will decrease the amount of added metal ions and therefore, should favor the presence of dangling ends. We would like to investigate the consequence of this dilution effect, and see if it can be compensated by using an excess of metal ions, compared to this stoichiometric amount. In addition to decreasing the proportion of metal ions present in the sample, mixing the telechelic star in a linear matrix will also lead to a reduction of the proportion of supramolecular groups. Therefore, it should also affect the associating probability of a ligand since this last one will have a lower density of ligands in its surrounding, with which it can form new complex. It is thus interesting to investigate how this variation in ligands and metal ions density will influence the dynamics of the resulting transient network.

Second, an important point that we would like to address in this chapter is the role played by the motion of the linear matrix on the dynamics of the transient network. Indeed, several works on binary blends of linear polymer chains have shown that for such blends, the relaxation process of the long polymer is highly governed by the motion of the short chains, with the long chains moving at the rhythm of the entanglement/disentanglement process of the short component.[2–4] In a way, a similar picture can be used here: before its relaxation, the entangled supramolecular network will move at the rhythm of the reptation of the linear matrix, leading to its partial relaxation through Constraint Release (CR) process. Furthermore, it is presently not clear if the mobility of the linear matrix influences the capability of the

dissociated arms of the stars to move around in order to create new supramolecular associations. In such a case, the lifetime of the transient network should depend on the length of the linear matrix, which offers another way to control the dynamics of the supramolecular network.

In order to address these questions, three different sets of samples have been prepared, as illustrated in Figure 7.1: The first set is composed of the pure supramolecular telechelic four-arm star P*n*BA 'Star250k', which has been already used in Chapters 5 and 6. Different samples have been prepared, by varying the amount and the nature of the added metal ions to the polymeric material. In the second set of samples, these telechelic star molecules are blended to a relatively well entangled linear P*n*BA polymer with a molar mass of 100 kg/mol in various proportions. Finally, the third set of samples comprisse the mixture of the Star 250k with the short unentangled linear matrix, of molar mass 18 kg/mol.
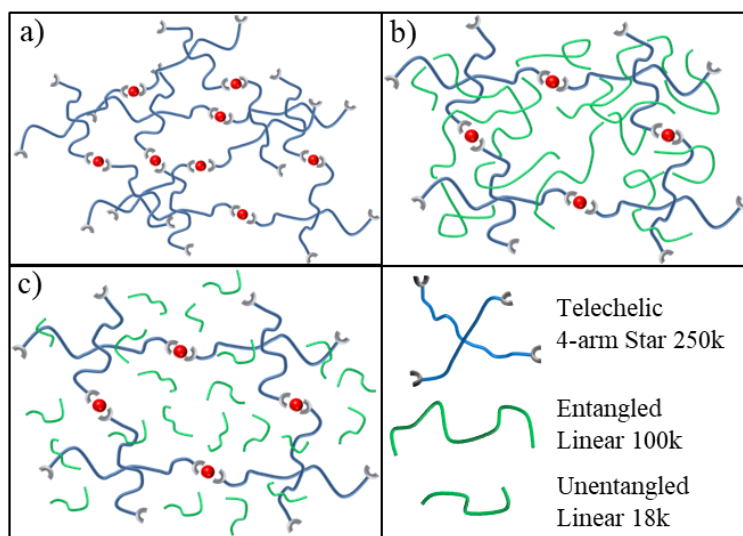
Figure 7.1 Schematic representation of the three sets of samples analyzed in this work with (a) Transient network composed of pure telechelic star polymer, (b) The supramolecular stars are blended to an entangled linear matrix, and (c) The supramolecular stars are blended to an unentangled short chains matrix.

The rest of this chapter is organized as follows. In section 7.2 the experimental procedures to synthesize and characterize the associating four-arm star mode and the linear polymers are described. In the same section the methods are summarized. Section 7.3 presents the linear viscoelastic properties of the studied materials via small amplitude oscillatory shear (SAOS) measurements. Several conclusions are drawn from the experimental results and they are further used in the next section. A tube-based model is developed in Section 7.4 to describe the viscoelastic properties of these transient networks blended to a linear polymeric matrix. In section 7.5, we use this model to analyze further the experimental data and discuss the influence of several parameters, such as the amount or the nature of metal ions, the proportion and the length of the linear matrix but also the temperature. The conclusions are drawn in section 7.6.

7.2   Materials and methods

7.2.1 Materials

The synthesis of the telechelic four-arm star ($M_n = 249$ kg/mol) poly(n-butyl acrylate) end-capped with terpyridine ligand (4-arm star PnBA-tpy$_4$) was achieved by reversible addition-fragmentation chain-transfer (RAFT) polymerization in bulk condition as explained in Chapter 2.[5] Similarly, the linear PnBAs ($M_n = 100$ kg/mol and $M_n = 18$ kg/mol) were synthesized via RAFT polymerization. Details on the studied polymeric samples are provided in Table 7.1.
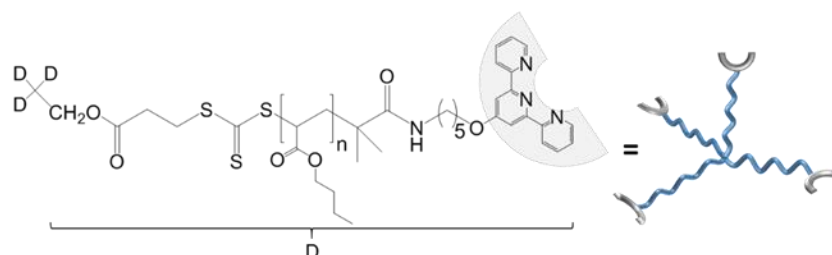
a) Telechelic four-arm star PnBA-tpy$_4$
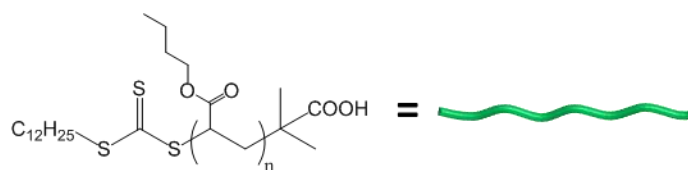
b) Linear (un-)entangled PnBA

Samples	$M_{n, system}$[a] (kg/mol)	$M_{n, arm}$[b] (kg/mol)	M_n/M_e [c]	Đ[d]
Star 250k	249	62	3.4/ arm	1.20
Lin100k	100	/	5.6	1.16
Lin18k	18	/	1	1.09

Table 7.1 Structural parameters of the telechelic 4-arm star PnBA-tpy$_4$ polymer and the linear PnBAs. [a,b] Molar mass of whole system determined by ^{1}H-NMR. [c] Number of entanglements calculated using $M_e = 18$ kg/mol. [d] Molar mass dispersity of the polymers determined by SEC, polystyrene standards were used for calibration.

7.2.2 Sample preparation

7.2.2.1 Metallo-supramolecular bulk networks

Samples were prepared by dissolving a given amount of the telechelic four-arm star PnBA-tpy$_4$ in acetone. The sealed reaction vessels were mixed via vortex for 30 min at room temperature to obtain concentrated polymeric solutions with a concentration of 500g.L^{-1}. The

metallo-polymers were then readily obtained by adding different equivalents of transition metal ions (with respect to the terpyridine content) dissolved in acetone. The reaction vessels were again mixed via vortex for 30 min and left to rest for 1 hour at room temperature to ensure total complexation of the metal. The solvent was evaporated under reduced pressure at 40°C then the sample was dried under vacuum at 40°C for 24 hours to obtain metallo-supramolecular bulk networks (MSBNs).

7.2.2.2 Binary blends of MSBNs and linear P*n*BA

Binary blend samples were prepared by dissolving a given amount of linear P*n*BA in acetone then a given amount of MSBNs was added. The sealed reaction vessels were mixed via vortex for 30 min and left to rest for 1 hour at room temperature to form concentrated polymeric solutions with a concentration of $500g.L^{-1}$. The solvent was evaporated under reduced pressure at 40°C then the sample was dried under vacuum at 40°C for 24 hours to obtain metallo-supramolecular bulk networks blended to linear poly(*n*-butyl acrylate) at various weight percent (wt %) ratio.

7.2.3 Methods

The linear viscoelastic properties of the materials were investigated by performing shear rheological experiments in the linear regime on an Ares (TA Instruments) rheometer equipped with a air/nitrogen convection oven that ensure an accurate temperature control (± 0.1°C). Dynamic meachanical measurements were carried out at given temperatures, using stainless steel 8 mm plate–plate geometries. The gap was adjusted between 400 and 500 μm so that the geometry was completely filled. Normal forces were checked to be relaxed prior any measurement. Dynamic frequency sweeps were performed at a deformation amplitude of 3% over a temperature range of -20°C to 80°C and a frequency range of $10^2 – 10^{-3}$ rad/s. All dynamic measurements were performed within the linear viscoelastic region, which was determined from dynamic strain sweep experiments. At each temperature, dynamic time sweep measurements of 1 hour were performed. The collected data were shifted along the frequency axis

using the time-temperature superposition (TTS), yielding master curves that were constructed at the same reference temperature T_{ref} = 25°C.

7.3   Experimental Results

7.3.1 Influence of the ion content

For the following systematic investigation, different ratios of copper(II) ions (from 0.25eq. to 1.00eq.) are incorporated into the telechelic four-arm star precursor to from the transient networks with different cross-linking densities. Figure 7.1. demonstrates the large influence of the amount of metal ions added into the sample to form the reversible network. In particular, by adding a stoichiometric amount of copper ions (i.e. 0.50eq.), a large fraction of the sample relaxes at high frequencies. As discussed in Chapters 4 and 5, it corresponds to uncoordinated arms which are not participating to the network formation.
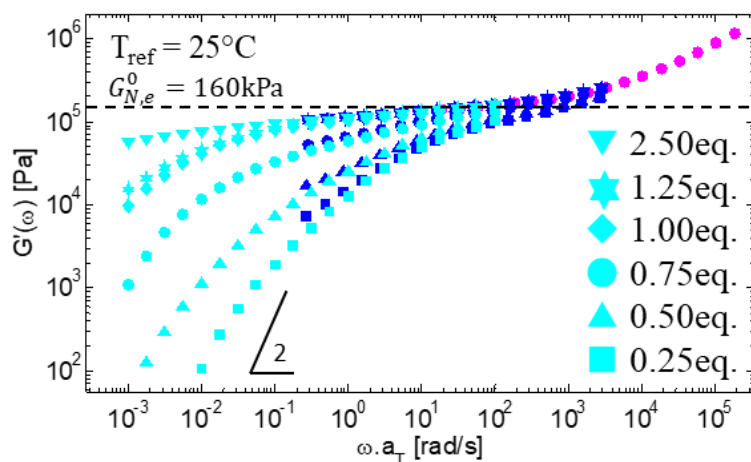
Figure 7.1 Storage modulus versus frequency at a reference temperature of 25°C. Data have been measured at T_{ref} = 25°C (cyan), 0°C (blue) or -20°C (magenta) for the Star250k with different ratio of copper(II) ions with 2.50eq. (∇), 1.25eq. ($\bigstar$), 1.00eq. ($\Diamond$), 0.75eq. (o), 0.50eq. (Δ) and 0.25eq. ($\square$).

Only with 1.00eq. of ions or more, the curves reach the level of the entanglement plateau modulus, of 160 kPa, which means that most of the sticky arms are involved in the supramolecular network. This last one is close to a well cross-linked transient network, containing a low amount of dangling arms. Furthermore, we see that adding a larger amount of metal ions strongly influences the terminal relaxation time of the network. As previously mentioned in Chapters 4 and 5, the metallo-supramolecular bulk networks relax via ligand exchange mechanism in which a fraction of uncoordinated has an active role in the stress relaxation. It was observed that this fraction of dangling arms decreases with increasing the amount of added copper(II) ions because more arms are cross-linked to form the reversible network. Hence, the rate of the ligand exchange is reduced, extending the relaxation time of the resulting materials. Therefore, the fraction of uncoordinated arms is an important parameter to control.

In Figure 7.1, one can also observe that with Cu(II) ions, the samples containing 1.00eq., 1.25eq. or 2.50eq. have their respective storage modulus superimposed relatively well at high frequency, e.g. from 10^5 to 10^2 rad/s. This means that at time shorter than 0.01s, the data are mostly not affected by the dynamics of the metal-ligand complexes. It is therefore tempting to consider this time as an estimation of the association lifetime of the complexes, which is consistent with the timescale found by dielectric relaxation measurement (reported in Chapter 6). This is further discussed in Section 7.5. From these first results, we conclude that a minimum of 1.00eq of cations must be added to the pure star precursor in order to ensure that most of the telechelic arms are involved in the elaboration of the reversible network. Since blending the star molecules in a linear matrix reduces this weight fraction of added metal ions, it was decided to perform the experiments with 2.50eq. of ions to compensate this dilution effect and to ensure that the majority of the chains are coordinated.

7.3.2 Influence of the temperature

Figure 7.2 shows the influence of temperature on the relaxation of the transient networks obtained by adding 1.00eq. of copper(II) ions.

As explained in Chapter 4, the curves have been shifted according to the shift factors found for the reference sample. In such a case, the temperature effect on the segmental dynamics is taken into account. Obviously, based on these shift factors, the data cannot be shifted into a well-fitted master-curve. This demonstrates the large influence of temperature on the dynamics of the supramolecular interactions, e.g. metal-ligand coordinations.
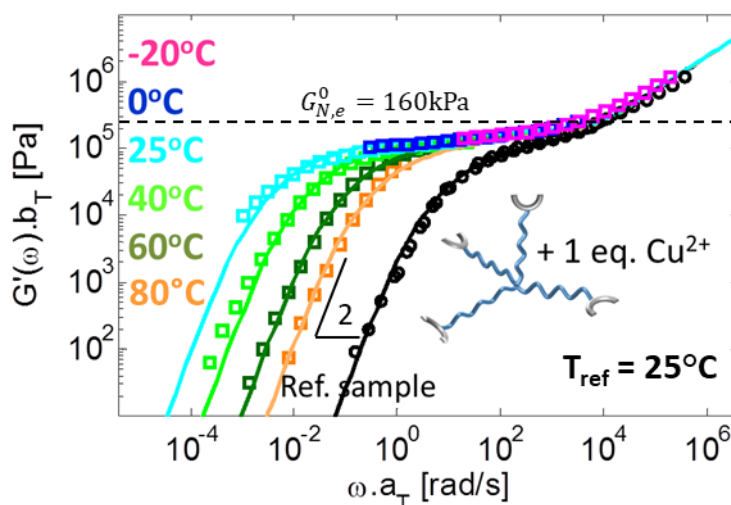

Figure 7.2 Storage modulus as function of the frequency measured at different temperatures (from 80°C to -20°C) for the Star250k containing 1.00eq. of Cu(II) ions. For comparison, the storage modulus of the reference sample without metal ions (black, o) is also plotted. The symbols represent the experimental data while the solid lines have been obtained based on the Equation 7.2.

However, one can notice the possibility to build a superimposed master-curve by using different shift factors. Such behavior was already observed in literature.[6–8] In fact Chen et al. showed that by defining the necessary shifts to build a master-curve and by removing the contribution from the segmental dynamics, the authors could determine the activation energy related to the supramolecular bonds.[6] In the present work (as discussed in Chapter 4) using the same approach to perform data shifting is more delicate since the molecules are entangled. Therefore, it is preferable to incorporate this effect directly in the modelling part.

Since the main effect of the stickers is an overall delay of the star relaxation, i.e., the stickers are acting as extra friction points located at the arm extremity, this can be taken into account in our model by considering that the star arms can effectively relax only during a short fraction of time, i.e., the time during which their end groups are dissociated. Consequently, the survival probability of a molecular segment x (going from 0 at the arm extremity to 1 at the branching point) relaxing by Contour Length Fluctuations (CLF), which is usually defined as (see Chapter 4):

$$p(x,t) = exp\left(\frac{-t}{\tau_{fluc}(x)}\right) \quad , \tag{7.1}$$

with $\tau_{fluc}(x)$ being the fluctuations time of the segment x, is now re-defined as follows:

$$p(x,t) = exp\left(\frac{-p_{free}\, t}{\tau_{fluc}(x)}\right) \tag{7.2}$$

Thus, in Equation 7.2, the parameter p_{free} takes into account the overall delay of the star relaxation. It is one of the two parameters required in the modelling to model the supramolecular dynamics of the telechelic stars. As already shown in Figure 7.2 (and further discussed in Section 7.4), by taking into account this overall delay as function of the temperature, it allows us to correctly describe the relaxation modulus of this specific sample. It is considered as a fitting parameter and further analyzed in detail and discussed in Section 7.5.

The viscoelastic responses of the transient networks become much more complex when the amount of added metal ions is above 1.00eq. As illustrated in Figure 7.3, the relaxation time spectrum broadens and the storage moduli cannot be described by simply shifting the data to lower frequency. While the data are presented with copper ions, similar results have been obtained with other metal ions such as the cobalt ions.
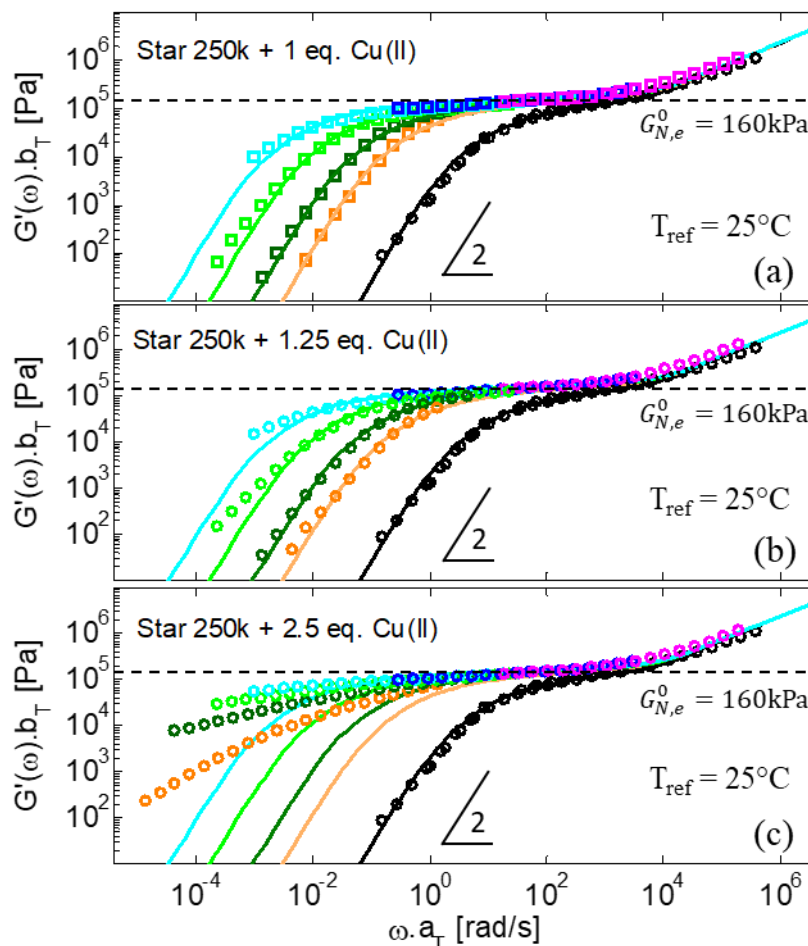
Figure 7.3 Storage modulus as a function of frequency measured at different temperatures for the Star250k containing (a) 1.00eq., (b) 1.25eq. and (c) 2.50 eq. of Cu(II) ions. Experimental data are measured at T = -20°C (magenta), 0°C (blue), 25°C (cyan), 40°C (green), 60°C (dark green) and 80°C (orange). For comparison, the storage modulus of the reference sample without metal ions (black, o) is also plotted. The symbols represent the experimental data while the solid lines have been obtained, based on the Equation 7.2. Same values of $p_{free}(T)$ have been used for the three samples.

We attribute this complex relaxation to the fact that the time during which a supramolecular end group stays free, τ_{free}, is extremely reduced. The latter time is so short that it starts to compete with the fluctuations time of the arm. Indeed, an arm which dissociates from the transient network is then able to disentangle and relax its carrying stress. However, this requires that the corresponding sticker stays free during a time longer than the fluctuations time of the deeper arm segments. Otherwise, as illustrated in Figure 7.4, the latter (i.e. deeper arm segments) will not be able to relax in a single dissociation step and may need several steps instead.
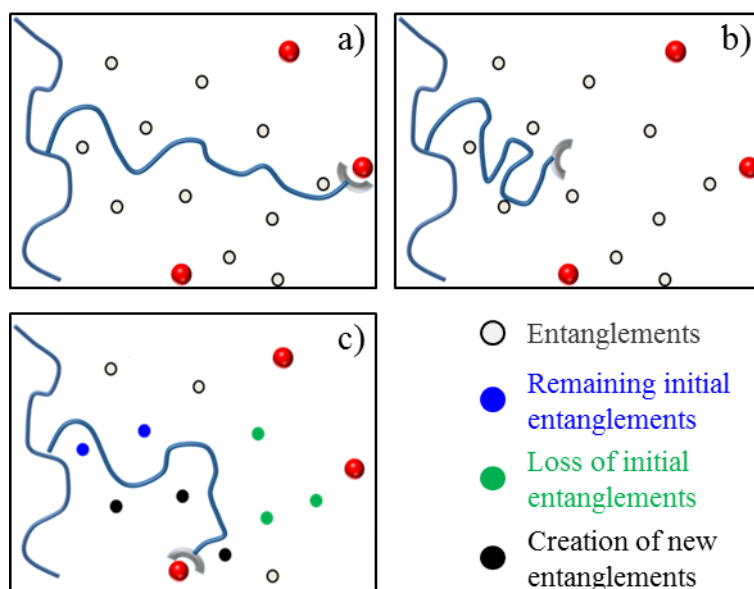
Figure 7.4 Cartoon which represents the relaxation of an arm by fluctuations (a) at t = 0, (b) at t = t_1 and c) at t = t_2 > t_1. The relaxation can takes place only during the time the chain end is dissociated from a complex. If this dissociation time is relatively short, a new complex will be formed before the arm had relaxed its deeper segments.

As detailed in Section 7.4, depending on the ratio between the fluctuation time and the free time, the relaxation by fluctuations of the deeper arm segments can require several dissociation/association events before taking place. In an extreme case, the relaxation of these deeper arm segments may never occur.

7.3.3 Influence of the linear matrix

In this section, we investigate the influence of the proportion and the length of the linear matrix on the relaxation of the transient network. Experimentally, the transient network formed with 2.50eq. of cobalt(II) ions is mixed with linear PnBAs at various weight ratios. The linear viscoelastic results are presented in Figure 7.5 for the supramolecular network blended into linear matrices at a reference temperature of 0°C. Similarly, Figure 7.6 presents the experimental data at a reference temperature of 40°C for the transient network mixed with linear matrices (Lin18k or Lin100k). Same x- and y- scales have been used in the two figures in order to facilitate the comparison between the viscoelastic properties of these two sets of samples.
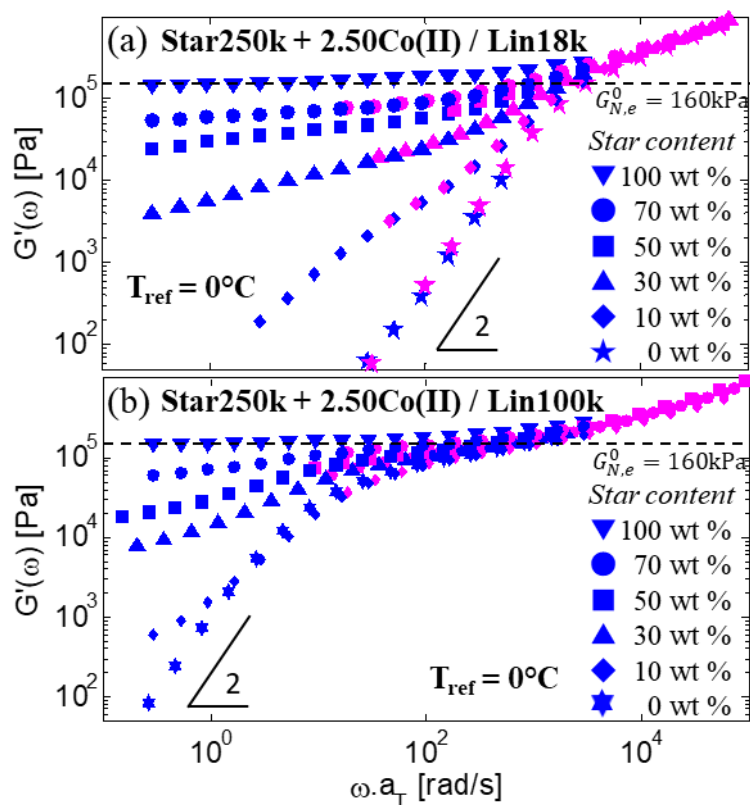
Figure 7.5 Storage modulus as a function of frequency at a reference temperature of 0°C for the Star250k + 2.50eq. Co(II) diluted in the linear matrix (a) Lin18k and (b) Lin100k with different proportions:

100 wt% (∇), 70 wt% (o), 50 wt% (□), 30 wt% (Δ), 10 wt% (◊) and 0 wt% (★).
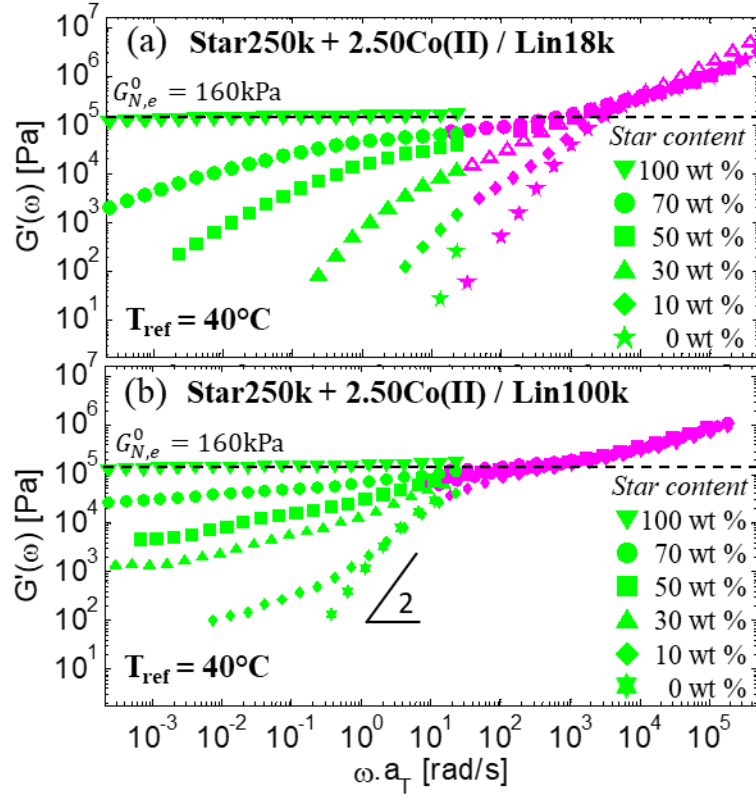
Figure 7.6 Storage modulus as a function of frequency at a reference temperature of 40°C for the Star250k + 2.50eq. Co(II) diluted in the linear matrix (a) Lin18k and (b) Lin100k with different proportions: 100 wt% (∇), 70 wt% (o), 50 wt% (□), 30 wt% (Δ), 10 wt% (◊) and 0 wt% (★).

     With both sets of samples, we can highlight the relaxation of the linear matrix at intermediate frequency range, leading to a first decrease of the storage modulus from the entanglement plateau (G_N^0 =160 kPa) to lower values. Additionally, this decrease is dependent on the proportion of the linear chains. At low frequency, this first relaxation is followed by a slow decrease of G'(ω). On the other hand, in the low frequency region, most of the samples show a secondary plateau, which can be attributed to the fraction of the unrelaxed

transient network. The importance of this fraction increases with increasing the proportion of telechelic stars. In case of 100 wt% of star molecules, the sample displays a fully elastic behavior, with a module close to 160 kPa, i.e. the entanglement rubbery plateau. It must be noted here that for all samples, the density of entanglements (1 per 18 kg/mol) is much more important than the density of strands located between two branching points in case of a perfect network (of 1 per $2M_a$, M_a being the molar mass of a star arm) for the pure telechelic star polymer). Therefore, the corresponding storage and loss moduli indicate the disentanglement process of the telechelic stars rather than the dissociation mechanism of the stickers.

By comparing the relaxation of the transient network in the two different linear matrices, an interesting difference is observed at 40°C. At this temperature, the metal-ligand complexes become more labile and less stable. Hence, at the same proportion, the transient network relaxes much faster in the short unentangled chains matrix (Lin18k) than in the matrix composed of entangled linear chains (Lin100k). Indeed, the terminal regime or a significant decrease in the storage modulus can be observed with all the blends obtained with the short matrix. On the other hand, the second plateau remains constant at low frequency for the blends composed of the long linear matrix. Even if the network is composed of only 10 wt% of telechelic stars, one can observe that the transient network based on the metal-ligand cross-links does not reach its terminal relaxation within the experimental frequency window.

From this result, it is thus concluded that the mobility of the linear matrix has a large influence on the relaxation dynamics of the supramolecular network. While the origin of this difference is not clear, we attribute it to a stabilizing effect coming from the entangled matrix which can hamper the motion of a dissociated arm. Thus it reduces the surrounding that a dissociated arm can explore within its free time, τ_{free}. In consequence, a newly dissociated ligand will have a larger probability to stay at the same vicinity of the other free ligand, increasing its probability to associate again and reform the complex which has been just destroyed (i.e. with the same old partner). This is further discussed in section 7.5.

By heating the samples, faster relaxation of the transient network diluted in the Lin100k matrix is expected (as shown in Figure 7.7. panel (a). However, while temperature strongly affects the blend composed of 70 wt% of star polymer, it has only a tiny influence on the two other blends containing 30 wt% or 50 wt% of stars. This result differs from the viscoelastic behavior of the blends based on the unentangled matrix, in which a large temperature effect is observed for low concentration of telechelic stars (see Figure 7.7 panel (b)). Furthermore, when the long linear matrix is used, no terminal flow is reached even at 100°C. Instead, the storage modulus slowly decreases with decreasing the frequency. This behavior is further investigated and discussed in Section 7.5.
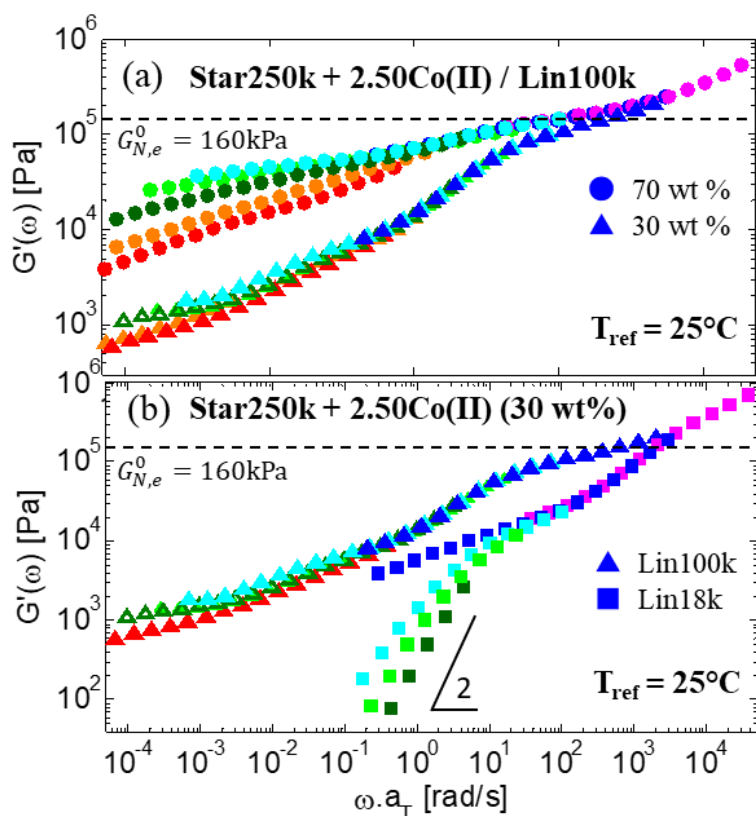
Figure 7.7 Storage modulus as a function of frequency for (a) the Star250k + 2.50eq. Co(II) diluted in the linear matrix Lin100k, at 70 wt% (o) or 30 wt% (Δ), (b) the Star250k + 2.50eq. Co(II) diluted in the linear matrix Lin100k (Δ) or Lin18k (□) at 30 wt%. Data have been

measured at different temperatures: T = -20°C (magenta), 0°C (blue), 25°C (cyan), 40°C (green), 60°C (dark green), 80°C (orange) and 100°C (red).

7.4   Modelling

7.4.1 Linear viscoelastic properties of a transient network composed of telechelic monodisperse star molecules

Based on the experimental results described in Section 7.3, we now extend our tube model in order to describe the relaxation of binary blends composed of entangled transient networks (formed with telechelic star precursors) diluted in a linear matrix. As explained in Section 7.3, the main influence of the supramolecular end group on the relaxation of the star molecules is an overall delay of their fluctuations time. The functional group acts as an extra friction point that the arm has to carry in order to move and relax. The effect of supramolecular groups is somehow similar to the effect of the branches of a H-like polymer. Precisely, the relaxation of its inner backbone is strongly slowed down by the presence of the branches. In the present model, this overall delay is taken into account by using Eq. 7.2, through the parameter p_{free}. This first parameter which informs us about the probability for a sticker to be free. Additionally, one needs to define a second parameter which is related to the frequency at which the sticker is blinking between dissociated and associated states. To this end, we define the parameter τ_{free}, as the average time during which a dissociated end group will stay free before re-associating again.

Based on τ_{free}, we can now determine the total time $\tau_{rel}(x)$ during which an arm segment will be free before being considered as relaxed. If a sticker has to blink several times between associated and dissociated states, $\tau_{rel}(x)$ is thus obtained by summing up the different free times of the different events. To do so, assuming that τ_{free} is known, we first statistically determine the probability that the time during which a sticker stays free before associating again is equal to a specific

323

time t. Even if on average, this time is equal to τ_{free}, the real free time can significantly differ from this value and therefore this polydispersity effect must be accounted for. The distribution of free times is determined by considering a large ensemble of stickers and assuming that they all became free at time $t = 0$. For each sticker, we then go step by step through time, with a very small time steps of Δt ($<< \tau_{free}$) and look if the stickers stay free during each of these steps. This is easily achieved by generating random numbers between 0 and 1 and comparing them to the probability $p_{free-free}$ that a free sticker stays free during a step of Δt:

$$p_{free-free} = \exp(\frac{-\Delta t}{\tau_{free}}) \qquad (7.3)$$

As soon as a sticker associates again, the total time during which it has stayed free is stored. Later on it is used to build the distribution of free times. An example of such distribution is shown in Figure 7.7 panel (a). On the other hand, the fluctuation times of the segments x belonging to an unassociated arm are determined, based on our usual TMA model (see Figure 7.7 panel (b)). This allows us to compare each of these fluctuations times with the distribution of free times. As illustrated in Figure 7.7, we can then determine what is the probability that a single dissociation event suffices to allow the arm segment x to relax by fluctuations. The latter is defined as $p_{retract}$. This probability is represented by the blue area below the distribution curve. Otherwise, if the dissociation time is shorter than the fluctuations time of the arm segment (see the white area below the distribution curve), the relaxation of the arm segment cannot take place. Then the arm will have to associate again and to do go through a second attempt, a third attempt and so on till finding a dissociation event long enough to allow the arm segment to relax.
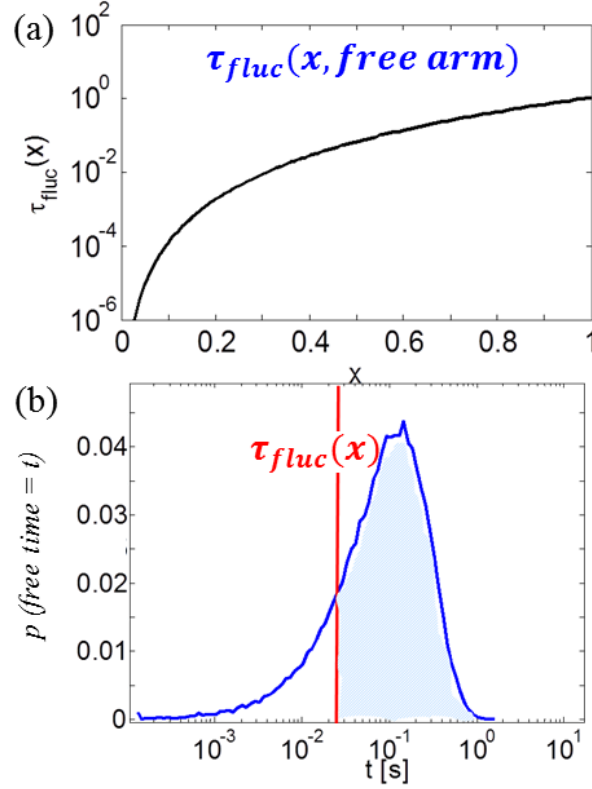
Figure 7.7 (a) Fluctuations time of the arm segments for the Star 250k, considering that it is unassociated. (b) Distribution of free time determined by considering that $\tau_{free} = 0.1$ s. The red line represents the fluctuation time of the segment x which has been chosen as example. The blue area represents the probability $p_{retract}$ that this segment can relax during one dissociation event.

This simple mechanism, which is illustrated in Figure 7.4, is taken into account in the model by increasing the relaxation time of an arm segment x, $\tau_{rel}(x)$, which represents the total time during which an arm must stay free in order to observe the relaxation of the arm segment x. It is then required to determine on average the number of dissociation events that the M-L complex has to go through, before the arm segment x can relax:

$$\#_{events}(x) = \frac{1}{p_{retract}} \qquad (7.4)$$

325

Adding this parameter to the fluctuations time of the arm segment x, the total time during which an arm must stay free before relaxing is then equal to:

$$\tau_{rel}(x) = (\#_{events}(x) - 1).\,\tau_{free} + \tau_{fluc}(x) \qquad (7.5)$$

This extra penalty on the segment relaxation must be added to the overall delay of the relaxation. Therefore, the survival probability of an arm segment x (see Eq. 7.2) is now defined as:

$$p(x,t) = exp\left(\frac{-p_{free}\,t}{\tau_{rel}(x)}\right) \qquad (7.6)$$

This last equation contains the two new parameters of the model, τ_{free} and p_{free}, which are needed to describe the dynamics of the supramolecular bonds. In section 7.5, their values, which are determined by best-fitting procedure, are presented and discussed.

It must be noted that in the case of a brief free time τ_{free}, it is possible that some arm segments will never manage to relax. Because the corresponding fluctuation time $\tau_{fluc}(x)$ of these segments is longer than the whole distribution of possible free times, leading to ($p_{retract}$ = 0). This is illustrated in Figure 7.8, where the relaxation times of the arm segments are represented while using two different values of τ_{free}. It is seen that if τ_{free} is equal to 1 s, the retraction of arm segments from $x = 0.75$ to $x = 1$ requires an extensive time to make it possible. Therefore, such situation will lead to the appearance of a second low frequency plateau in the storage modulus curve.
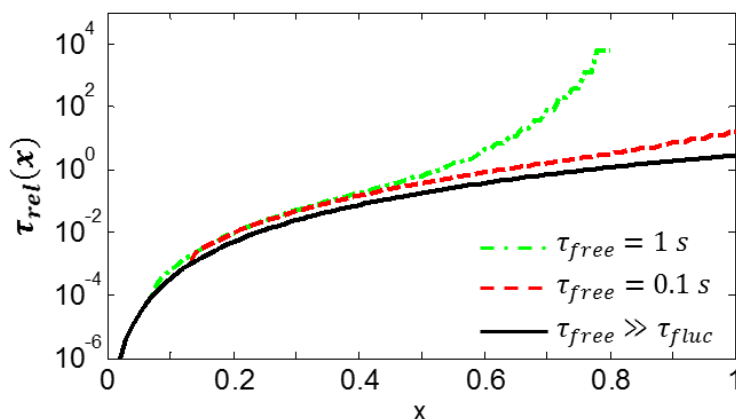
Figure 7.8 Relaxation times of the arm segments for the Star250k, considering that $\tau_{free} \gg \tau_{fluc}(x)$ (see the dashed red curves – in such a case, $\tau_{free} = \tau_{fluc}$), $\tau_{free} = 0.1$ s (continuous red curve), or $\tau_{free} = 1$ s (continuous green curve).

Then, knowing the survival probability of each arm segment, the relaxation modulus of the transient network can be determined, as usually done with our TMA tube model (see Section 7.4.3).

7.4.2 Linear viscoelastic properties of telechelic star polymer blended with an unentangled matrix

Similar approach as the one for the monodisperse telechelic star polymer can be used in case of a binary blend of telechelic stars diluted linear chains. However, it is required to take into account the relaxation of the short chain matrix. Furthermore, since the relaxation of the transient network is much longer than the relaxation of the linear matrix, it is expected that the reversible network relaxes part of its stress by a Constraint Release Rouse (CRR) process, in a similar way as it has been described by Hawke et al.[9] This process is illustrated in Figure 7.9: before its relaxation by dissociation of the stickers, the transient network relaxes first by intrinsic Rouse process, until molecular segments of size M_e are relaxed. Then, it relaxes by CRR process, i.e. Rouse relaxation which can take place only at the rhythm of the motions of the linear matrix. Therefore, these Rouse modes, which concern the Rouse relaxation of molecular segments of molar mass between M_e and

$M_{e, trapped} = M_e/\upsilon_{star}$ (with υ_{star}, the proportion of star molecules), are slower than the intrinsic Rouse modes and are assumed to be delayed by a specific delay factor, θ_{matrix}. Once the segments of mass $M_{e, trapped}$ are relaxed by CRR, the transient network cannot relax further and needs to wait until its transient bonds start to dissociate, allowing the star arms to slowly disentangle.
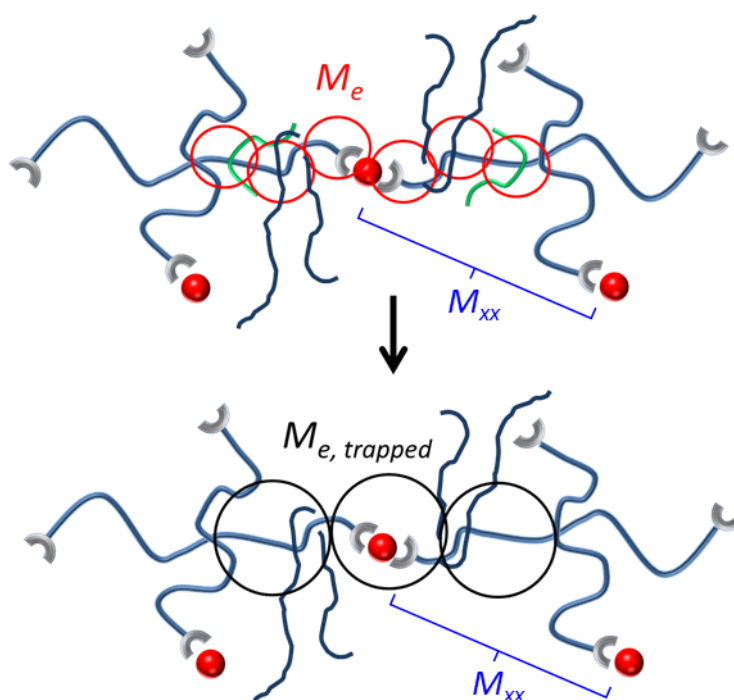
Figure 7.9 Rouse Relaxation of the molecular segments: while the segments shorter than M_e relax by their intrinsic Rouse mechanisms, the relaxation of longer segments by CRR, from M_e to $M_{e, trapped}$ can only take at the rhythm of the short linear chains (represented in green).

Thus, for the blends obtained with the matrix Lin20k, the relaxation modulus $G(t)$ can be modelled as[10]

$$G(t) = G_{star}(t) + G_{lin}(t) \qquad (7.7)$$

Where $G_{lin}(t)$ describes the contribution of the unentangled linear matrix:

$$G_{lin}(t) = v_{lin} \left[\frac{\rho RT}{M_{lin}} \cdot \left(\sum_{p=1}^{N} exp \left(\frac{-2\,p^2 t}{\tau_{Rouse}(M_{lin})} \right) \right) \right] \qquad (7.8)$$

and $G_{star}(t)$ takes into account the contribution from the telechelic stars to the modulus:

$$G_{star}(t) = G_{Rouse,star}(t) + G_{d,star}(t) \qquad (7.9)$$

The first term of the right part of this equation describes the Rouse and Constraint Release Rouse relaxation of the star polymer:

$$G_{Rouse,star}(t) = v_{star} \left[\frac{\rho RT}{2M_{arm}} \cdot \left(\sum_{p=Z+1}^{N} exp \left(\frac{-2\,p^2 t}{\tau_{Rouse}(2M_{arm})} \right) + \right.\right.$$

$$\left.\left. \sum_{p=Z_{trapped}}^{Z} exp \left(\frac{-2\,p^2 t}{\theta_{matrix} \cdot \tau_{Rouse}(2M_{arm})} \right) \right) \right] \qquad (7.10)$$

where Z is the number of entanglements and star-star entanglements per arm and $Z_{trapped} = Z.\upsilon_{star}$. On the other hand, the second term of Eq. 7.9 describes the relaxation by dissociation and disentanglement of the transient network:

$$G_{d,star}(t) = G_N^0 \cdot \upsilon_{star}{}^2 \sum_{x=1/100}^{x=1} p(x,t)\,\Delta x, \qquad (7.11)$$

with $\Delta x = 1/100$ and the survival probability $p(x, t)$ is described as for monodisperse telechelic star (see Eq. 7.6). The parameter G_N^0 is the plateau modulus, which accounts for both the entanglements and the branching points of the transient network:

$$M_{XX} = (2M_{arm})/\upsilon_{star} \qquad (7.12)$$

$$G_N^0 = \frac{4}{5} \frac{\rho RT}{M_e} + \frac{\rho RT}{M_{XX}} \qquad (7.13)$$

While $(G_N^0 . v_{star}^2)$ is the level of the second low frequency plateau, considering that all the telechelic arms are participating to the transient network and that they all had the time to relax by CRR process before starting to relax by sticker dissociation and fluctuations process.

The influence of the CRR process illustrated in Figure 7.10 for the blend composed of 30 wt% of telechelic stars in 70 wt% of the short chain matrix Lin18k. Predictions are compared to experimental data in Figure 7.10, while considering that the transient network is permanent ($G_{d,star}(t) = G_N^0 . v_{star}^2$). In the case of such a short linear matrix, the delay factor θ_{matrix} is expected to be small since the matrix is almost unentangled ($M_e = 18$ kg/mol). From the experimental data, one can observe a second Rouse regime, characterized by a slope of ½, at frequencies between 10^2 and 10^3 rad/s. Since this regime appears after the relaxation of the linear matrix, it can be attributed to the longest Rouse relaxation modes of the network, corresponding to molecular segments of mass between M_e to $M_{e, trapped}$ (see Figure 7.9). If this CRR regime is predicted without considering delay in the long modes of Rouse relaxation ($\theta_{matrix} = 1$), the star network is predicted to relax immediately after the relaxation of the matrix, which is too fast compared to the experimental data (see the dashed curve). In order to well capture the viscoelastic data, these long Rouse modes must be delayed by a factor $\theta_{matrix} = 4$ (see the continuous curve). Since this parameter does not depend on the weight fraction of the telechelic star polymer, this value is used for all blends based on the short chain matrix.
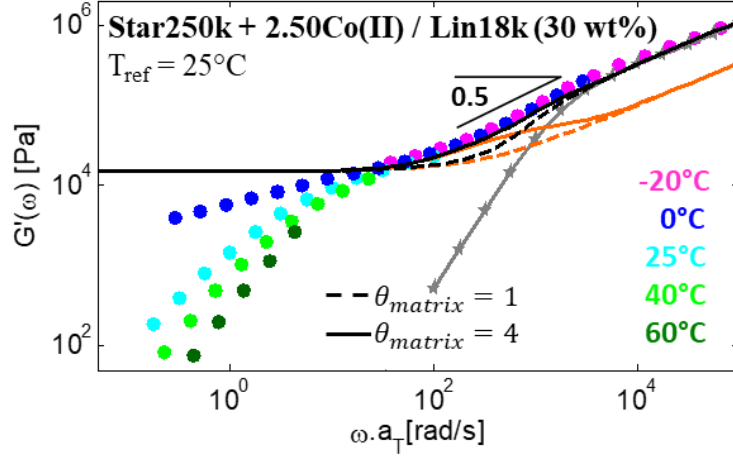
Figure 7.10 Storage modulus as a function of frequency for the Star250k + 2.50eq. Co(II) diluted in the linear matrix Lin18k, at 30 wt%. Data have been measured at different temperatures: T = -20°C (magenta), 0°C (blue), 25°C (cyan), 40°C (green), 60°C (dark green). For comparison, the viscoelastic response of the matrix is plotted (★, grey, 25°C). The theoretical curves have been obtained by assuming that the star network is permanent, and $\theta_{matrix} = 1$ (dashed black curve) or $\theta_{matrix} = 4$ (continuous black curve). The solid and dashed lines in orange show the contribution from the star polymer only to the storage modulus.

7.4.3 Linear viscoelastic properties of telechelic star polymer blended to an entangled matrix

For the star polymer diluted in the long, entangled matrix, the relaxation modulus is determined, following the usual equation of the Time Marching Algorithm (TMA)[10]:

$$G(t) = G_{Rouse}(t) + G_N^0 \varphi'(t)\phi(t)^\alpha \qquad (7.14)$$

The function $G_{Rouse}(t)$ describes the high frequency Rouse relaxation and the function $\varphi'(t)$ represents the survival fraction of molecular segments which are still in their initial tube:

$$\varphi'(t) = v_{lin}\varphi'_{lin}(t) + v_{star}\varphi'_{star}(t) \qquad (7.15)$$

331

The survival fraction of the linear matrix, $\varphi_{lin}{}'(t)$ accounts for both reptation and CLF relaxation (see Section 7.3), while the survival fraction of the telechelic star, $\varphi_{star}{}'(t)$, is described based on Eq. 7.6:

$$\varphi'_{star} = \sum_{x=1/100}^{x=1} exp\left(\frac{-p_{free}\,t}{\tau_{rel}(x)}\right) \Delta x \qquad\qquad (7.16)$$

On the other hand, the dilation factor $\phi(t)^{\alpha}$ is the number of entanglement segments per dilated segment and corresponds to a tube diameter of $a(t)=a(t=0)\ \phi(t)^{-\alpha/2}$. In this case, the CRR process is taken into account by adding the condition that the chains cannot explore their surrounding faster than a Rouse process:

$$\phi(t) = max\left(\varphi'(t), \phi(t-\Delta t)\left(\frac{t-\Delta t}{t}\right)^{\frac{1}{2}}\right) \qquad . \qquad (7.17)$$

7.5   Results and Discussion

7.5.1 Reference polymer melts

In order to determine the material parameters for the model, we first compare the experimental and the theoretical data of the reference samples (see Table 7.1). Following our previous works on PnBA polymers, the entanglement plateau modulus and the molar mass between two entanglements are fixed to 160 kPa and 18 kg/mol, respectively. The last parameter, which is the Rouse relaxation time of an entanglement segment, τ_e, is fixed to 5.10^{-4} s at a reference temperature of 25°C. In order to easily extend this approach to the viscoelastic properties of a transient network, the reference samples are considered as monodisperse. Figure 7.11. shows that there is a very good agreement between the predicted curves and the experimental results.
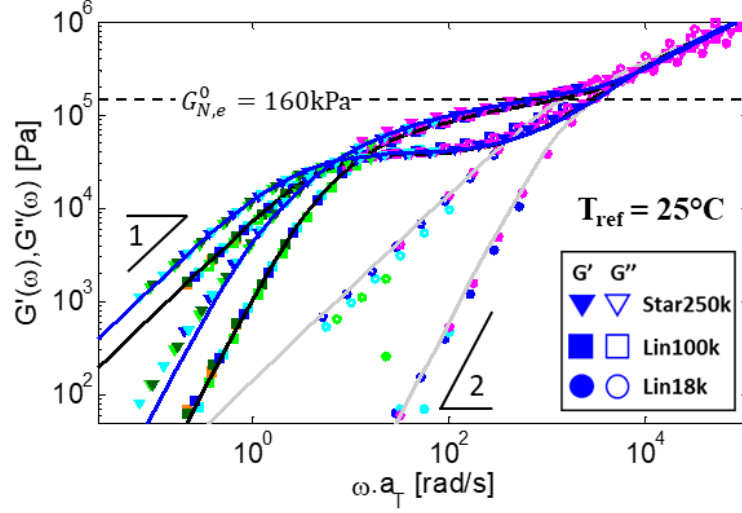
Figure 7.11 Storage and loss moduli as a function of frequency for the reference samples Star250k (∇), Lin100k ($\square$) and Lin18k (o) measured at different temperatures: T = 80°C (orange), 60°C (dark green), 40°C (green), 25°C (cyan), 0°C (blue) and -20°C (magenta). Symbols are experimental data and solid lines are model predictions. Master curves have been built at 25°C.

7.5.2 Transient networks composed of telechelic star polymers

We then focus on the viscoelastic properties of the transient networks obtained with pure telechelic stars, while considering different amount of metal ions. As mentioned in Section 7.3, a minimum of one equivalent of ions must be used in order to ensure that most of the star arms are involved in the formation of the transient network. As shown in Figure 7.3, the main influence of adding 1eq. Cu^{2+} or 1.25eq. Cu^{2+} into the telechelic star polymer is an overall delay of the data, which is taken into account by the parameter p_{free} in Eq. 7.6. However, in addition to this overall shift of the data, broadening of the relaxation time spectrum has been observed at lower temperatures (T < 40°C). We attributed this effect to a too short average times τ_{free} during which a free sticker stays free, which forces the arm to dissociate and associate again several times. Until the arm reaches a dissociation event

long enough to allow the fluctuation of the deeper arm segments. By taking into account this effect (see Eq. 7.6), a good description of the experimental curves can be obtained as presented in Figure 7.12.
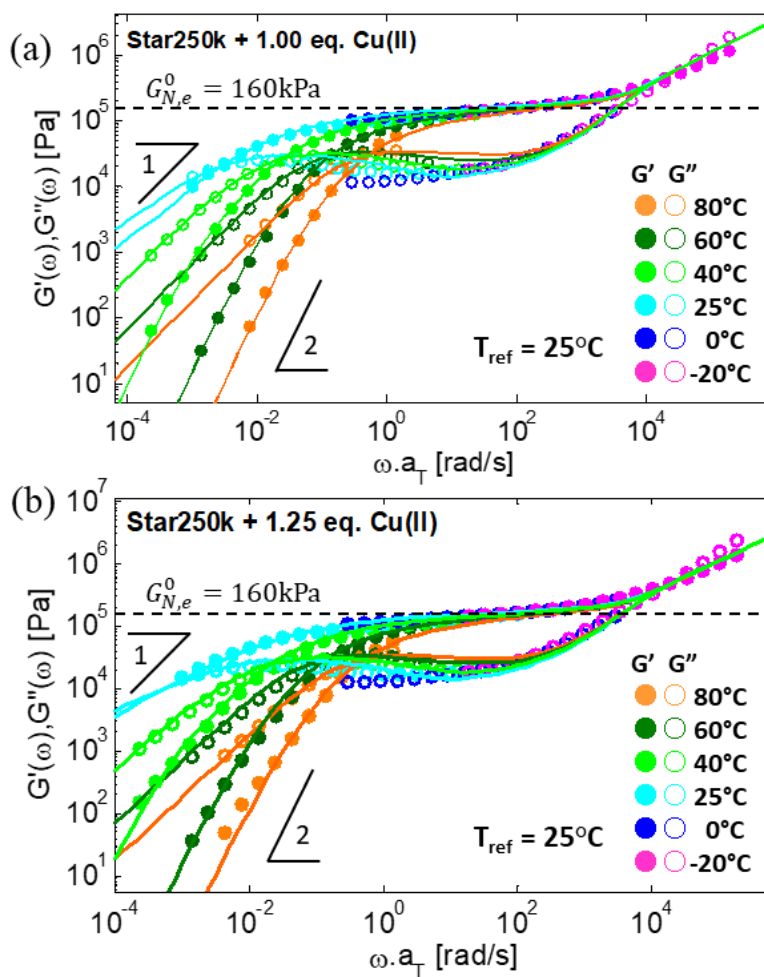
Figure 7.12 Storage and loss moduli as a function of frequency for (a) Star250k + 1eq. Cu(II) and (b) Star250k + 1.25eq. Cu(II) measured at different temperatures: T = 80°C (orange), T = 60°C (dark green), 40°C (green), 25°C (cyan), 0°C (blue) and -20°C (magenta). The experimental data (symbols) have been shifted to a reference temperature of 25°C and they are compared with the theoretical curves (solid lines).

The influence of a short τ_{free} is even more pronounced when 2.50eq. of copper or of cobalt ions are added. In such a case, the transient network does not reach its terminal flow regime within the accessible experimental frequency window and a second low frequency plateau is observed at low frequency, as discussed in section 7.3. Furthermore, as shown in Figure 7.13, when 2.5eq. Co^{2+} ions are added to the telechelic star polymer, an extra relaxation peak appears at intermediate frequency around 10 rad/s.
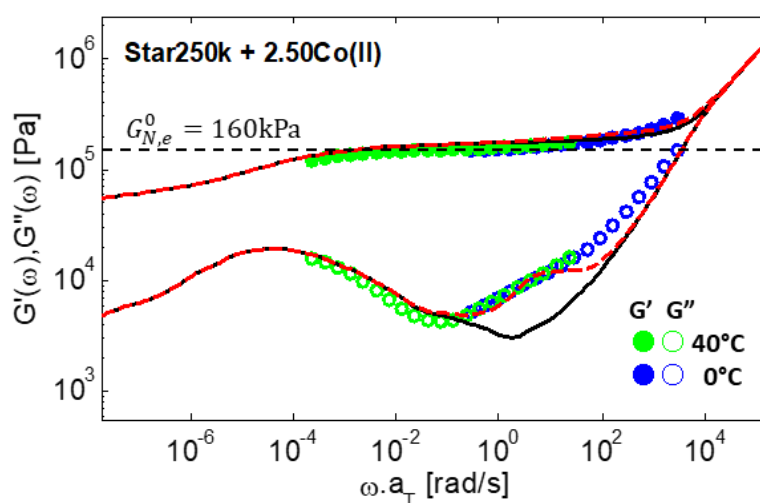
Figure 7.13 Storage and loss moduli as a function of frequency for the Star250k + 2.5eq. Co(II). Experimental data (o) have been measured at 0°C (blue) and 40°C (green). Theoretical results have been obtained with (--) or without (—) considering that the segments cannot relax before the average association time of the complexes, $\tau_{complex}$.

There are several possibilities to explain the origin of this extra relaxation peak. First, it could be attributed to dangling arms. Indeed, since the sample has a large excess amount of metal ions, the formation of mono-complexes could be favored, leading to free arms unable to form junctions with another arm. However, the relaxation peak is slightly too quick to well match the relaxation time of free arms. Furthermore, adding dangling arms would lead to a fast decrease of G' and a lower G" peak at low frequency, which is not the case observed herein. Therefore, we rather attribute the extra relaxation peak to the

335

association time of the complexes, $\tau_{complex}$. Before this time, which is estimated to be around 0.25 s in the case of Star250k + 2.5eq. Co^{2+}, the associated complexes are stable. Since these complexes link two arms together, they allow an extra strand to carry some stress (see Figure 7.14) and participate to the modulus for an amount of $\rho RT/(2M_{arm})$. But as soon as these complexes open, the associated extra stress vanishes. Therefore, their contribution to the modulus through time can be expressed as equal to $\rho RT/(2M_{arm}) \, exp\left(-t/\tau_{complex}\right)$.
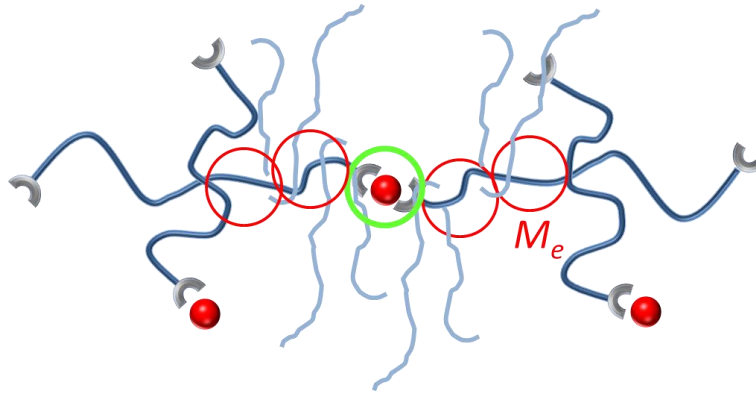
Figure 7.14 Cartoon, which represents in green the extra strand able to carry some stress when the complexes are formed. As soon as the complex opens, the corresponding stress is lost.

Besides affecting the modulus, $\tau_{complex}$ also fixes a minimum time before which the relaxation of the arms cannot take place. Therefore, it is considered that the arm relaxation start at $\tau_{complex}$ rather than at time ($t = 0$). As shown in Figure 7.13, taking into account the association time of the complexes allows a better description of the data at intermediate frequency. However, further tests should be performed in order to validate this explanation.

In Figure 7.15, this approach is applied to the transient network at different temperatures. As it is shown, a good agreement between experimental and theoretical curves is obtained if $\tau_{complex}$ is assumed to decrease exponentially with the temperature T:

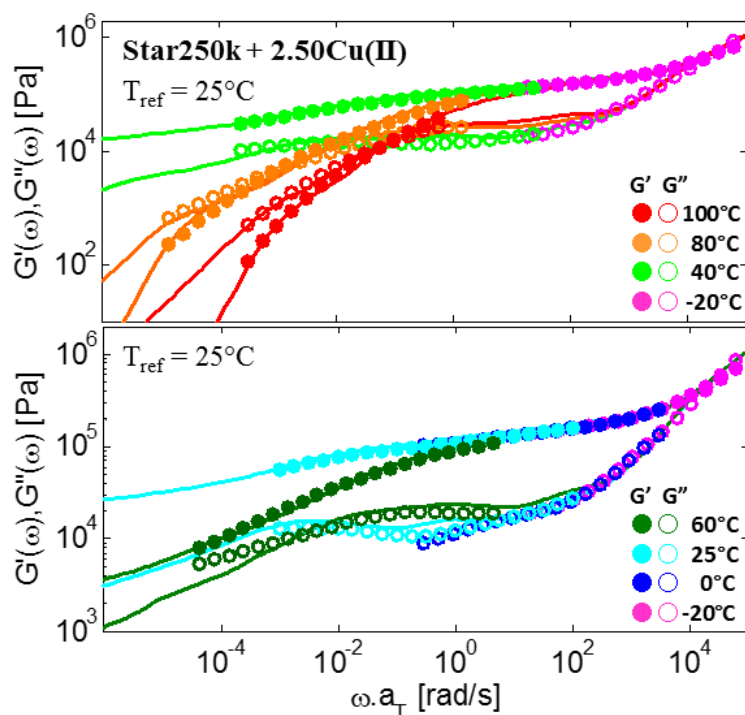$$\tau_{complex} = 1.5 \, exp\left(\frac{-T}{22}\right) \tag{7.18}$$
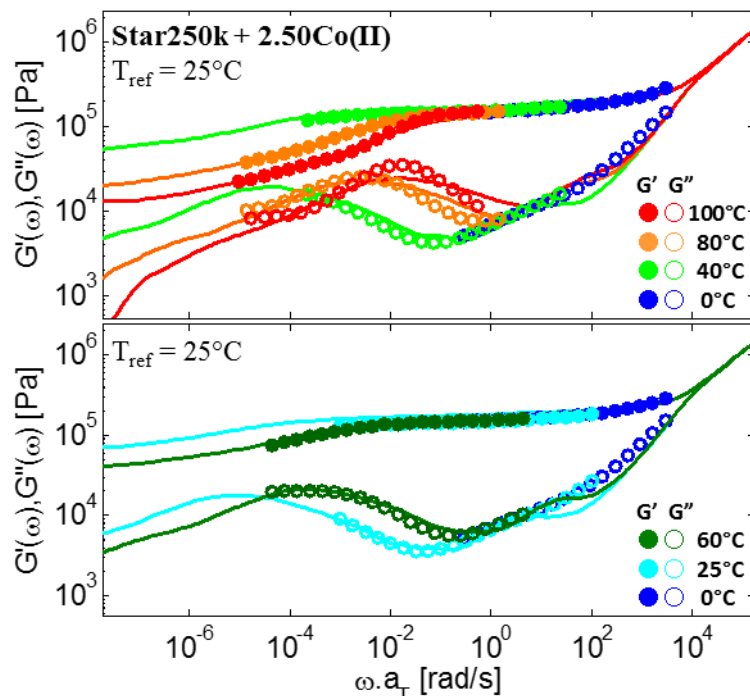
Figure 7.15 Storage and loss moduli as a function of frequency for the Star250k + 2.5eq. Co(II) measured at different temperatures: T = 100°C (red), 80°C (orange), 60°C (dark green), 40°C (green), 25°C (cyan) and 0°C (blue). The experimental data (symbols) have been shifted to a reference temperature of 25°C and they are compared with the theoretical curves (solid lines).

Same approach can be applied to the transient network containing 2.5eq. Cu^{2+}. However, in such a case, the association time of these complexes seems too short to strongly influence the data. Only at low temperatures, its effect can be observed, as it is shown in Figure 7.16 for the data measured at 25°C. In this case, $\tau_{complex}$ has been fixed to 16 ms, as suggested by the dielectric relaxation spectroscopy results (see Chapter 6). In contrast to the networks containing Co^{2+} ions, the transient network formed with 2.5eq. Cu^{2+} exhibit no clear plateau in the *G'* curve at intermediate frequencies, as it is predicted by the model. Moreover, the G" relaxation peak at low frequencies is much less pronounced than expected (see the red dashed curves). From these two observations, we conclude that this sample contains a larger amount of

dangling arms, most probably related to the formation of mono-complexes. The fact that the formation of mono-complexes is more promoted with copper ions than cobalt ions is probably due to the difference in their binding constants to form mono- (K_1) and bis-complexes (K_2 and β). Co(II) ions display a $K_1 = 10^{8.4}$ M^{-1} which is lower than $K_2 = 10^{9.9}$ M^{-1} and $\beta = 10^{18.3}$ M^{-2}, indicating that the formation of bis-complexes is indeed more promoted. For Cu(II) ions, $K_1 = 10^{12}$ M^{-1} is still lower than $\beta > 10^{18}$ M^{-2} but its value is higher than $K_2 > 10^6$ M^{-1}, meaning that the mono-complexes tend to remain in this state once they are formed. Good agreement with the theoretical data is obtained if 15 wt% of mono-complexed dangling arms are considered (see Figure 7.16).
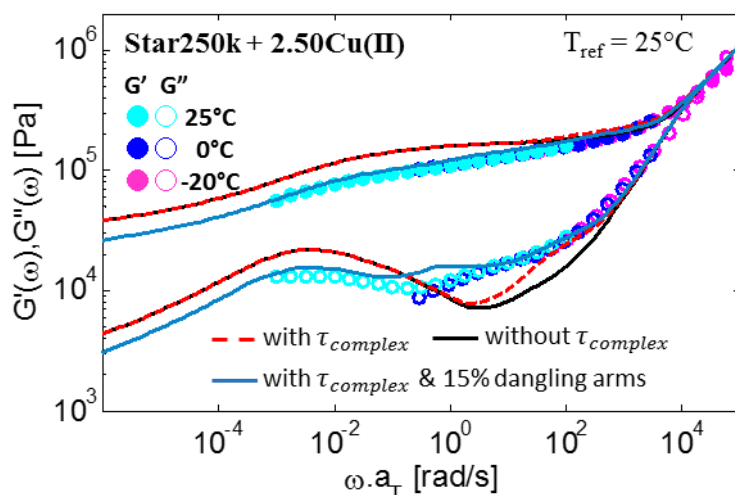
Figure 7.16 Storage and loss moduli as a function of frequency for the Star250k + 2.5eq. Cu(II) measured at T = -20°C (magenta), 0°C (blue) and 25°C (cyan). The experimental data (symbols) have been shifted to a reference temperature of 25°C. Theoretical results (solid or dashed lines) have been determined with (--, red) and without (—, black) considering the complex association time $\tau_{complex}$ and no dangling arms, or by considering both $\tau_{complex}$ and 15% of dangling arms (—, blue grey).

At higher temperatures, the same amount of dangling arms was found, based on the modelling (see Figure 7.17), while the association

time of the complex is too fast to significantly affect the data. From this result, it is concluded that the transient network based on copper ions has a larger tendency to create mono-complexes, compared to the network built from ligand-cobalt complexes.

Figure 7.17 Storage and loss moduli as a function of frequency for the Star250k + 2.5eq. Cu(II) measured at different temperatures: T = -20°C (magenta), 0°C (blue), 25°C (cyan), 40°C (green), 60°C (dark green), 80°C (orange) and 100°C (red). The experimental data (symbols) have been shifted to a reference temperature of 25°C. Theoretical results are shown by the continuous curves.

In these results, the two model parameters p_{free} and τ_{free} are fixed by best-fitting procedure, it is then interesting to look at their dependence on temperature and density of metal ions. Results are presented in Figure 7.18. Both parameters seem to increase exponentially with temperature.[1] With Co^{2+} ions, much lower values of p_{free} are found. This last parameter decreases even more when a higher amount of ions is

339

added, indicating that the overall delay on the arm relaxation strongly depends on both the nature and amount of ions.
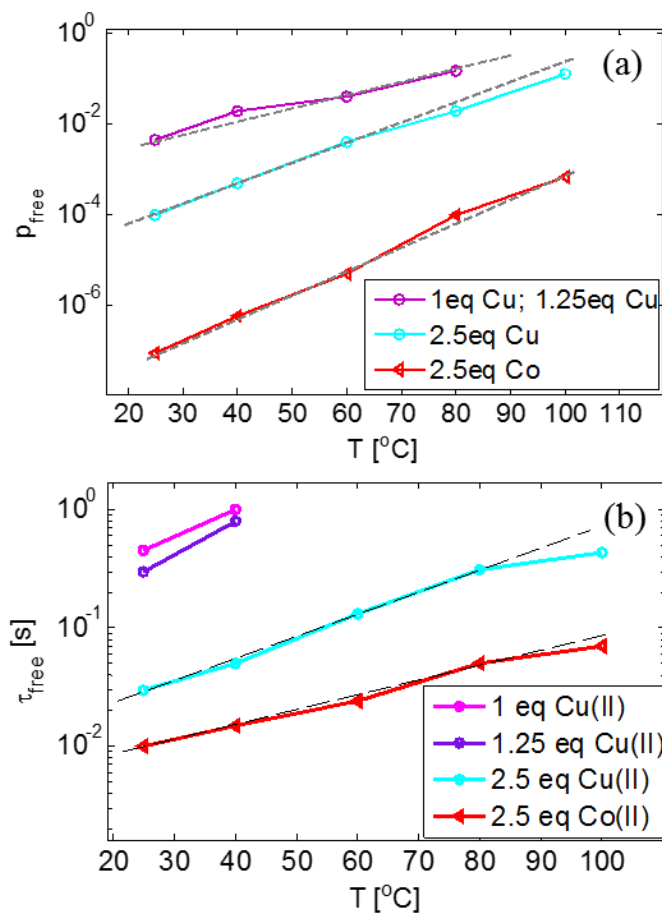
Figure 7.18 Evolution of (a) p_{free} and (b) τ_{free} as function of temperature for the pure transient network by varying the nature and amount of metal ions.

7.5.3 Transient networks composed of telechelic star polymers blended with an unentangled linear matrix

We now apply the model proposed in section 7.4.2 on the transient networks diluted in an unentangled matrix. In the case of monodisperse telechelic star polymer with 2.5eq. Co(II), an extra

contribution to the modulus, $\upsilon_{star}\ \rho RT/(2M_{arm})\ exp\left(-t/\tau_{complex}\right)$, is considered in addition to the relaxation modulus described in Eq. 7.7. The latter is considered in order to take into account the contribution of the additional segment which are formed by the association of two arms. Moreover, it is assumed that the relaxation of the transient network does not start before $\tau_{complex}$, allowing to correctly capture the data. The exact value of this time could not be determined due to the low sensitivity of the model. But also due to the lack of experimental data in the frequency range where this process takes place. Therefore, we fix it to 0.015 s for all samples.

Results are shown in Figure 7.19 for all the blends, composed of 30 wt% (panel a), 50 wt% (panel b) or 70% (panel c) of telechelic stars, while the corresponding parameters used to describe the data are shown in Figure 7.20. First, it is observed that the parameter p_{free} strongly decreases with decreasing the proportion of the linear matrix. This is expected since the transient network is more and more diluted, therefore the probability for a ligand to find another ligand in its surrounding becomes lower. Compared to the pure transient networks (with 100 wt% star), the values of p_{free}, are significantly larger for all the blends. Moreover, the maximum value ($p_{free} = 1$) is reached at high temperatures. This suggests that diluting the network in a short chain matrix also largely decreases the overall delay effect originating from the association/dissociation of the stickers. This is confirmed by the fact that all these blend samples reach their terminal regime, contrary to the pure transient network.

On the other hand, it is found that the parameter τ_{free} only depends on the sample composition (see Figure 7.20) and it is temperature independent. This suggests that τ_{free} is affected by temperature exactly as the linear matrix, i.e. only depends on the segmental dynamics of the chains. Precisely, the time during which a sticker stays free depends on how fast the dissociated arm and its surrounding can move. Since this effect is already taken into account in the WLF shift factors which were used to present the data at a reference temperature of 25°C, it leads to a constant τ_{free}. However, the fact that τ_{free} increases with increasing the proportion of telechelic stars is a priori counter-intuitive, but in the context of unentangled linear matrix,

increasing υ_{star} also largely affects the entanglement state and thus, the fluctuations times of the telechelic stars. Therefore, even if τ_{free} increases with increasing υ_{star}, the ratio $\tau_{free}/\tau_{fluc}(x)$ decreases as expected. The latter ratio governs the number of association/dissociation events ($\#_{event}$) needed before the relaxation of an arm segment.
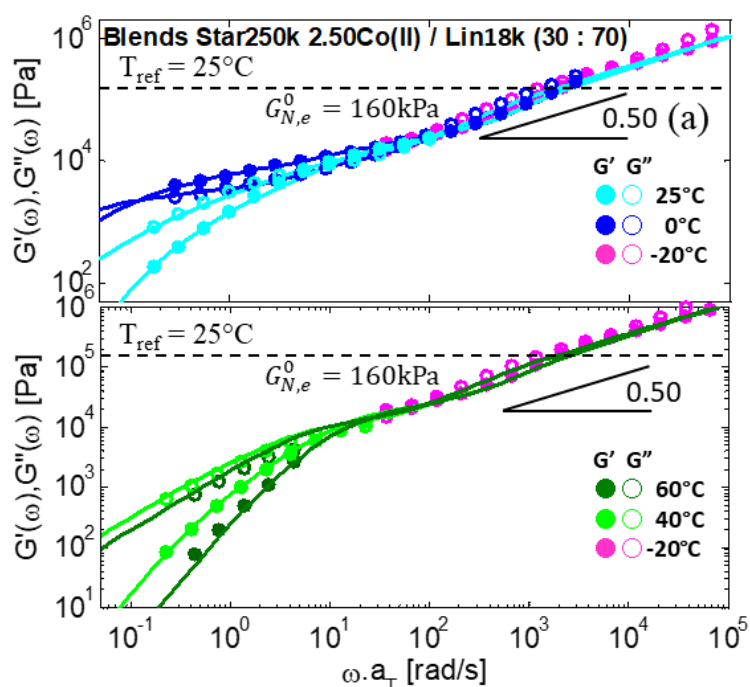

Figure 7.19 (a) Storage and loss moduli as a function of frequency for the Star250k + 2.5eq. Co(II) diluted in the short chain matrix Lin18k at 30 wt%. Experimental data (symbols) have been measured at different temperatures: T = -20°C (magenta), 0°C (blue), 25°C (cyan), 40°C (green), 60°C (dark green), 80°C (orange) and 100°C (red). The experimental data have been shifted to a reference temperature of 25°C. Theoretical results are shown by the continuous curves.
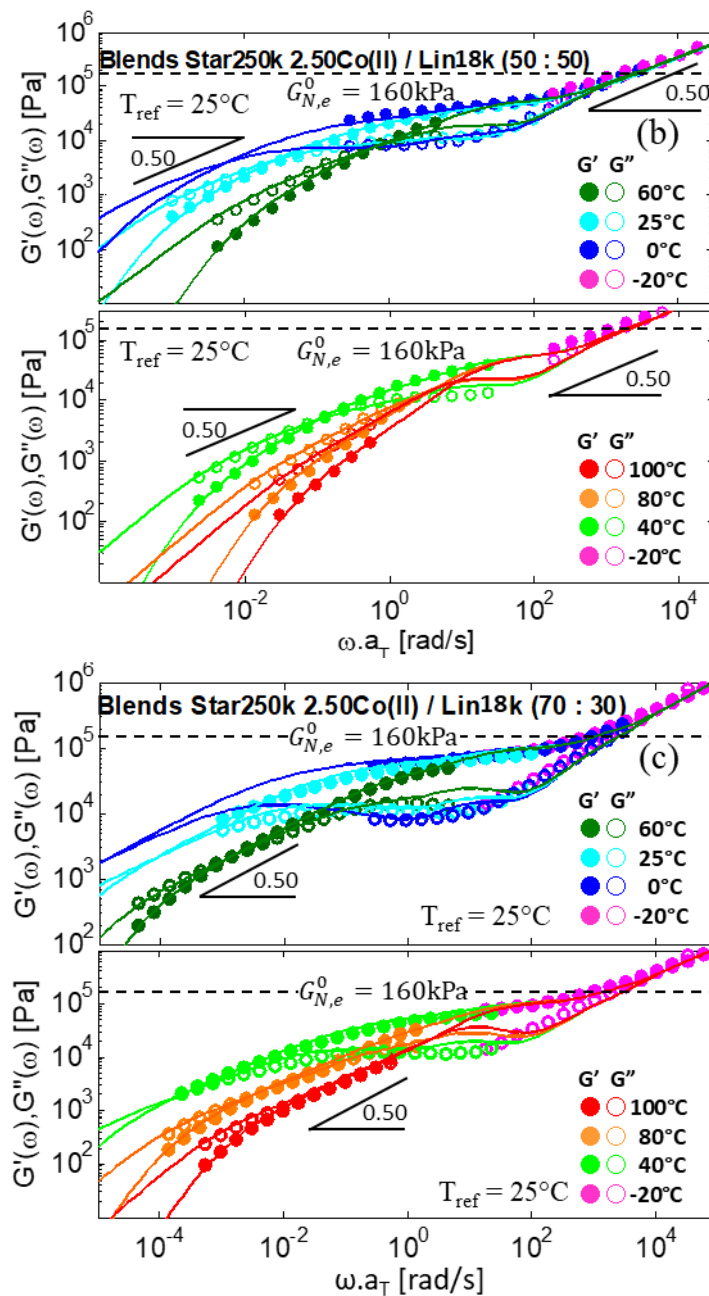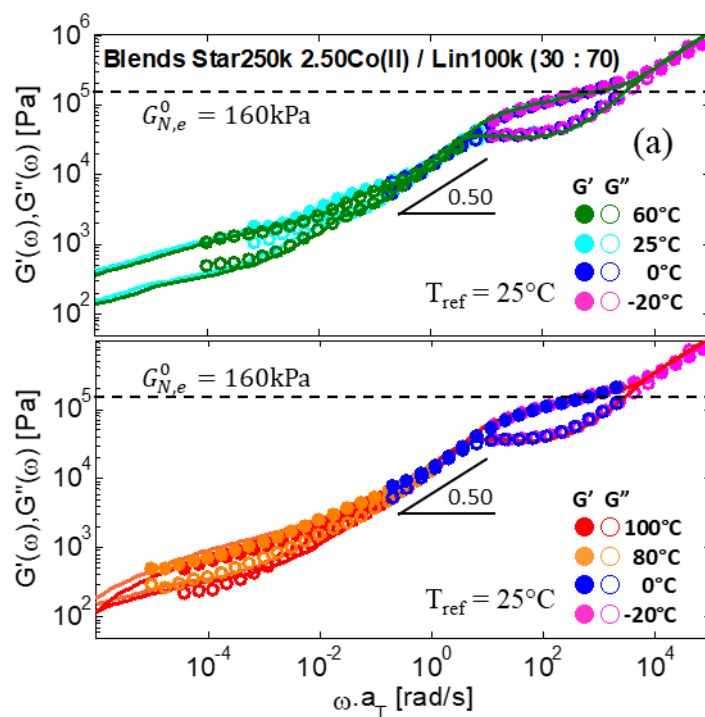
Figure 7.19 Storage and loss moduli as a function of frequency for the Star250k + 2.5eq. Co(II) diluted in the short chain matrix Lin18k at (b) 50 wt% and (c) 70 wt%. Experimental data (symbols) have been measured at different temperatures: T = -20°C (magenta), 0°C (blue),

343

25°C (cyan), 40°C (green), 60°C (dark green), 80°C (orange) and 100°C (red). The experimental data have been shifted to a reference temperature of 25°C. Theoretical results are shown by the continuous curves.
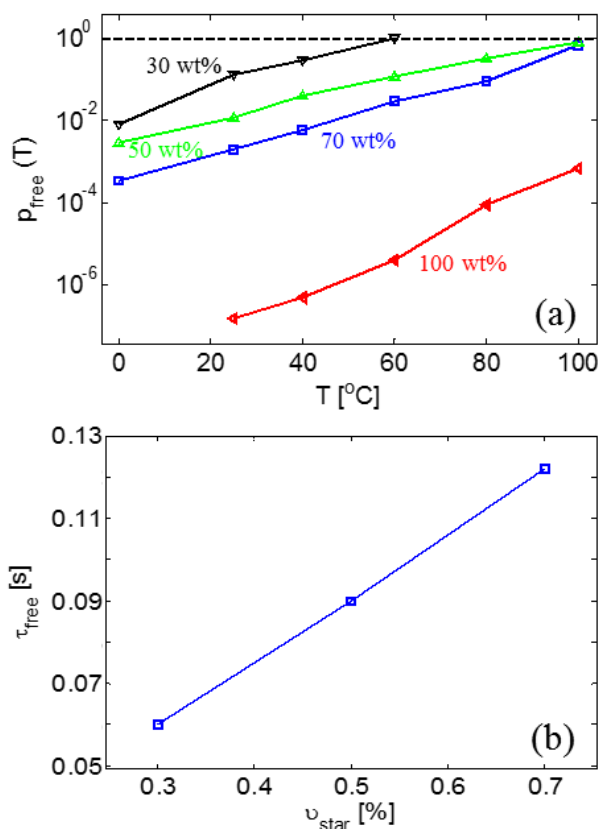

Figure 7.20 (a) Evolution of p_{free} as function of the temperature for the transient network diluted in the short chain matrix (Lin18k) at different proportions: 30wt% (∇), 50wt% (Δ), 70wt% ($\square$) or 100wt% ($\triangleleft$). (b) Evolution of τ_{free} as function of the star proportion.

7.5.4 Transient networks composed of telechelic star polymers blended with an entangled linear matrix

As presented in section 7.3, blending the transient network in a longer linear matrix strongly affects the relaxation of the reversible network. In this section, we model the experimental data and discuss

the obtained results. Comparison between theoretical and experimental curves is shown in Figure 7.21. Here again, it is possible to determine the parameters p_{free} and τ_{free} to well capture the experimental data. However, at low frequencies, a large discrepancy is observed. The fact that this discrepancy does not appear in the storage modulus seems to indicate that the sample is still slightly evolving through time, i.e. it did not reach its full equilibrium prior to measurements, despite a long waiting time of 10 hours as shown in Figure 7.22. Thus, this indicates that a transient network diluted in a long matrix takes an extensive time to equilibrate when compared to the corresponding case in a short linear matrix.

Figure 7.21 (a) Storage and loss moduli as a function of frequency for the Star250k + 2.5eq. Co(II) diluted in the short chain matrix Lin100k at 30 wt%. Experimental data (symbols) have been measured at different temperatures: T = -20°C (magenta), 0°C (blue), 25°C (cyan), 40°C (green), 60°C (dark green), 80°C (orange) and 100°C (red). The experimental data have been shifted to a reference temperature of 25°C. Theoretical results are shown by the continuous curves.
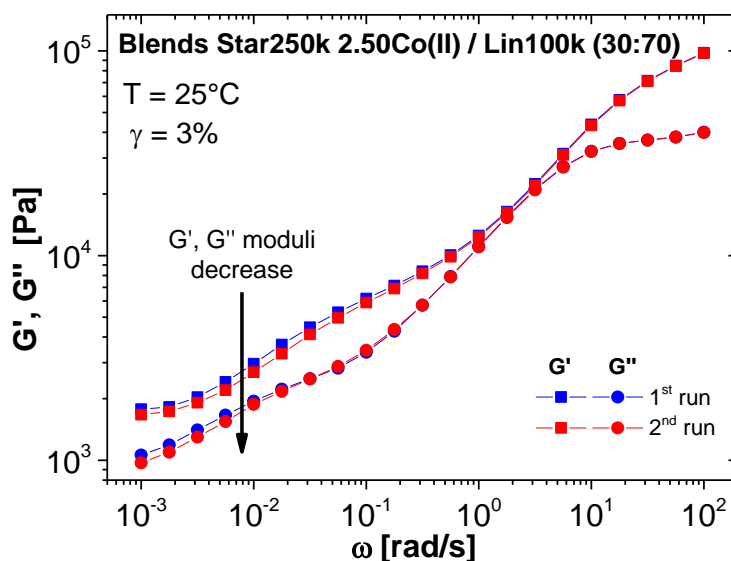
345
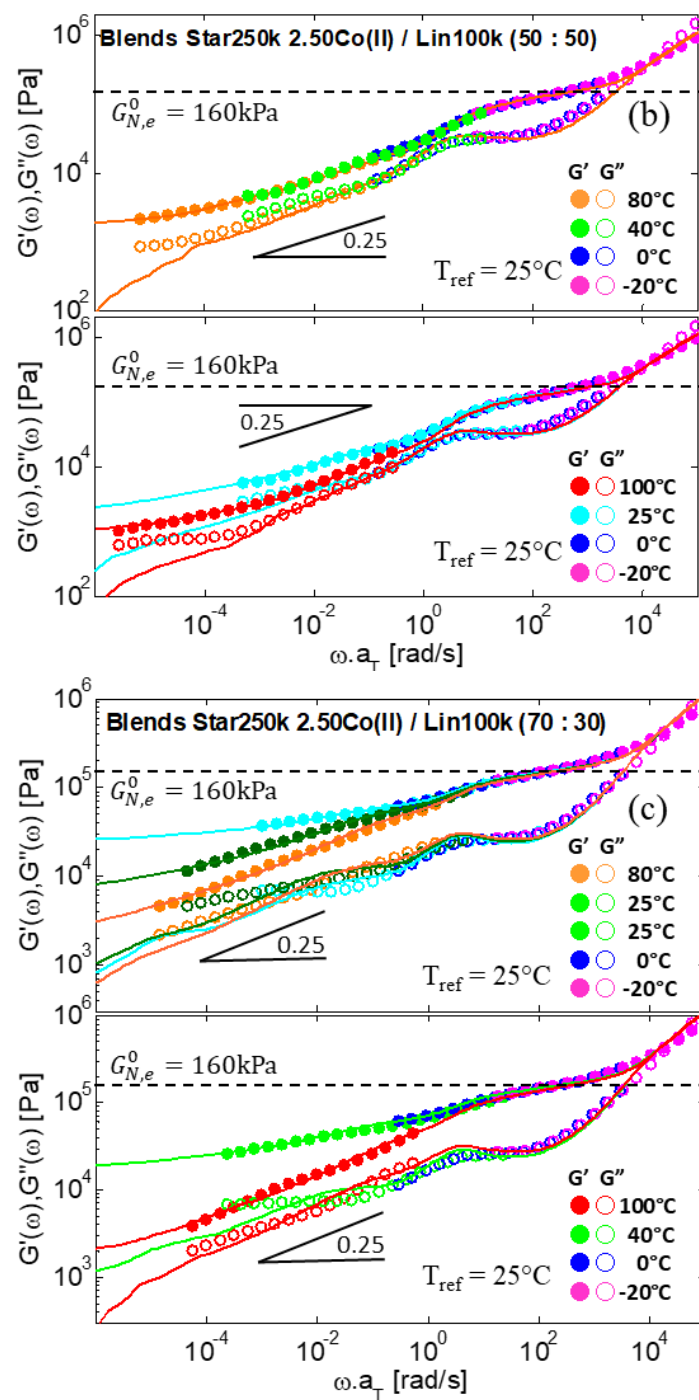
Figure 7.21 Storage and loss moduli as a function of frequency for the Star250k + 2.5eq. Co(II) diluted in the short chain matrix Lin100k at

346

(b) 50 wt% and (c)70 wt%. Experimental data (symbols) have been measured at different temperatures: T = -20°C (magenta), 0°C (blue), 25°C (cyan), 40°C (green), 60°C (dark green), 80°C (orange) and 100°C (red). The experimental data have been shifted to a reference temperature of 25°C. Theoretical results are shown by the continuous curves.

Figure 7.22 Storage and loss moduli as a function of frequency for the Star250k + 2.5eq. Co(II) diluted in the short chain matrix Lin100k at 30 wt% measured at 25°C. The second dynamic measurement does not overlap well with the first run at low frequencies, indicating that the system keeps evolving despite a long waiting time of 10 hours which is the duration of one frequency sweep experiment.

Furthermore, it is also observed in the case of entangled linear matrix, none of the blend samples reach their final relaxation regime at high temperatures. This long relaxation process is reflected in the values of p_{free}: as shown in Figure 7.23. While p_{free} is larger than the value found with pure telechelic stars, it is much lower than the values found with the unentangled matrix (see Figure 7.20) with the same blend proportion. This means that the relaxation of the star arms are much more affected by the sticker dynamics when an entangled linear matrix is used. A possible explanation is that the long entangled matrix around the sticky arms combined with the slow fluctuations of the dissociated

arms tend to decrease the probability of the metal-ligand complexes to dissociate efficiently.

On the other hand, it is observed in Figure 7.23 that p_{free} and τ_{free} for the blends composed of 30 wt% or 50 wt% of star polymer do not exhibit a large temperature dependence. This is consistent with Figure 7.7, where it was shown that the viscoelastic data of these blends nearly superimpose. This may suggest that the complexes are extremely stable, due to the low proportion of ligands in their surroundings to form new complexes combined with the low mobility of the chains. It must be noted that these results must be further validated. In particular, the importance in reaching the equilibrium state of the transient network prior to any experimental measurements.
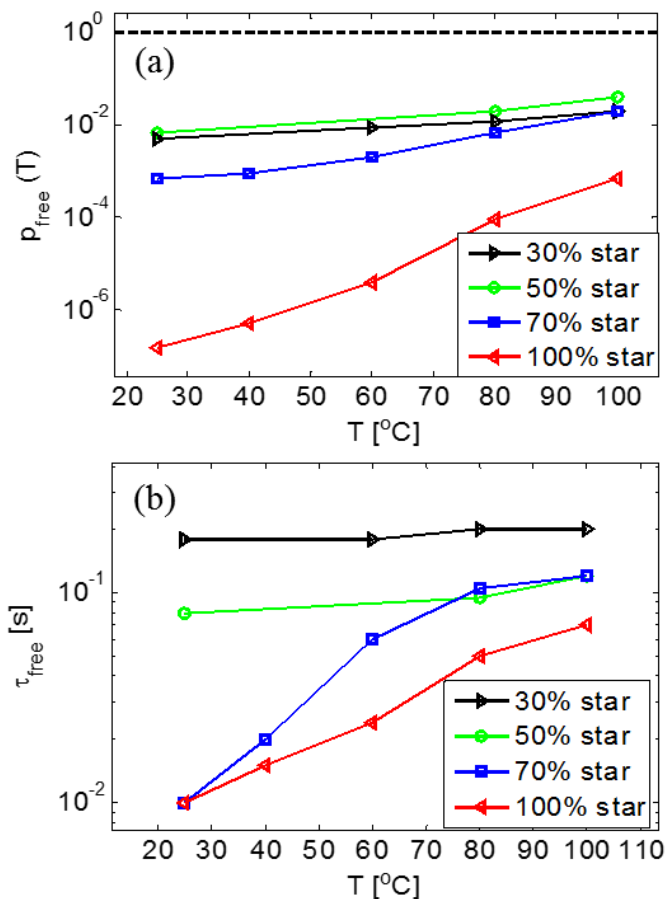
Figure 7.23 Evolution of (a) p_{free} and (b) τ_{free} as function of temperature for the transient network diluted in the long entangled chain matrix

(Lin100k) at different proportions: 30wt% (>), 50wt% (o), 70wt% (□) or 100wt% (<).

7.6   Conclusions

In this chapter, we discussed the viscoelastic properties of a transient network based on the telechelic star molecules able to associate through metal-ligand coordination at the extremities. We first investigated the influence of the amount and the nature of the metal ions used to build the reversible network on the dynamics of the resulting material. It was shown that an excess of metal ions must be used in order to reduce the proportion of dangling arms. The dynamics of these transient bonds lead to two major effects on the viscoelastic behavior of the network. First, they induce an overall delay on the network relaxation, which is well captured by decreasing the efficiency of time via the parameter p_{free}. Second, they broaden the relaxation time spectrum. Sometimes they even lead to the appearance of a second low frequency plateau in the storage modulus. This effect is attributed to the competition between the time needed for a free arm to relax by fluctuations and the time during which the arm stays free, τ_{free}.

Based on these observations, we developed a model in order to describe the data and quantify these two parameters. It was found that they both increase exponentially with the temperature. Then, we investigated the influence of diluting the transient network in a linear matrix. Specifically, two different matrices were used: one was unentangled and the other was entangled in order to investigate the influence of the network environment on its relaxation. It was found that this environment has a significant impact on the network stability. Indeed, the network diluted in the short chains matrix relaxed much faster than the one mixed in the long chains matrix.

We then extended our model to describe the relaxation of these blends. When the short chain matrix was used, it was found that the average time during which a sticker stays free, τ_{free}, mostly depends on the dynamics of the linear chains, while p_{free} is strongly affected by the strength of the supramolecular bonds, as reflected by its large dependence on temperature. On the other hand, the results found with

the longer linear matrix showed very different trend with low or high proportion of telechelic star polymers. Therefore, we need to further validate these results before drawing more conclusions to deeper understand the linear viscoelastic properties of metallo-supramolecular networks diluted in linear matrices (e.g. the dilution effect with linear unentangled matrix and the double network effect with linear entangled matrix). Hence, the interpretations of these results are open to further discussions.

Note that the model presented in this chapter exhibits few similarities and differences with the theoretical model described in Chapter 4. In fact, the upgraded TMA model alpha reported in Chapter 4 might be used to predict the linear viscoelastic properties of associating star polymers with an excessive amount of metal ions by changing the values of the fitting parameter p_{ass}, i.e., the fraction of associated stickers. These values should be close to 1 since more metal ions are added to form the bis(terpyridine) complexes. However, there is a possibility that the alpha model fails to predict the broad relaxation spectrum due to the fact that the whole star arm fully relax during one dissociation event. Moreover, this last model does not take into account the transient network environement, e.g. the dilution effect while blended with linear (un-)entangled matrices. Hence it cannot be exploited to model the linear viscoelastic properties of blends. Whereas using the upgraded TMA model beta of Chapter 7 to predict the linear rheology of associating systems with (sub-) stoichiometric amounts of metal ions should be feasible by cancelling the network environment effect (θ_{matrix}) and also by reducing the number of association-dissociation event to 1, allowing the star arm to fully relax during one dissociated state. One should also metion that the alpha model was used as a reference to build the upgraded TMA beta model.

Bibliography

(1)   Zhuge, F.; Hawke, L. G. D.; Fustin, C.-A.; Gohy, J.-F.; van Ruymbeke, E. *J. Rheol.* **2017**, *61*, 1245–1262.

(2)   Watanabe, H.; Matsumiya, Y.; van Ruymbeke, E. *Macromolecules* **2013**, *46*, 9296–9312.

(3)   van Ruymbeke, E.; Shchetnikava, V.; Matsumiya, Y.; Watanabe, H. *Macromolecules* **2014**, *47*, 7653–7665.

(4)   Read, D. J.; Jagannathan, K.; Sukumaran, S. K.; Auhl, D. W. *J. Rheol.* **2012**, *56*, 823–873.

(5)   Zhuge, F.; Brassinne, J.; Fustin, C.-A.; van Ruymbeke, E.; Gohy, J.-F. *Macromolecules* **2017**, *50*, 5165–5175.

(6)   Zhang, Z.; Huang, C.; Weiss, R. A.; Chen, Q. *J. Rheol.* **2017**, *61*, 1199–1207.

(7)   Gold, B. J.; Hövelmann, C. H.; Lühmann, N.; Wischnewski, A.; Richter, D. *J. Rheol.* **2017**, *61*, 1211–1226.

(8)   Zhang, Z.; Chen, Q.; Colby, R. H. *Soft Matter* **2018**, *14*, 2961–2977.

(9)   Hawke, L. G. D.; Ahmadi, M.; Gondansaz, H.; van Ruymbeke, E. *J. Rheol.* **2016**, *60*, 297–310.

(10)   Ebrahimi, T.; Taghipour, H.; Grießl, D.; Mehrkhodavandi, P.; Hatzikiriakos, S. G.; van Ruymbeke, E. *Macromolecules* **2017**, *50*, 2535–2546.

Conclusions and Perspectives

In this thesis, a systematic investigation on entangled associating polymers based on metal-ligand (M-L) coordination has been conducted to address the link between the molecular level and the macroscopic properties of associating polymers for material designs and tailoring rheological features. This investigation was achieved by combining the synthesis (RAFT polymerization), the rheology (linear shear, nonlinear shear and uniaxial extensional), the dielectric relaxation spectroscopy, the structural characterizations (DSC, X-rays scattering) with theoretical models (upgraded TMA models). In the state of the art, it was shown that there are several synthetic strategies to build supramolecular polymers. Among a plethora of techniques, a combination of a pre-modification approach with a controlled radical polymerization is used to elaborate metallo-supramolecular polymers (MSPs). In particular, entangled supramolecular poly(*n*-butyl acrylate)s (P*n*BAs) were obtained via reversible addition-fragmentation chain transfer (RAFT) polymerization. Different chain transfer agents (CTAs) bearing terpyridine (tpy) ligands were synthesized and further used for the polymerization of *n*-butyl acrylate monomers. After polymerization, the chemical structure of the CTA was included within the polymeric system, allowing the incorporation of tpy moieties at specifically targeted locations of the polymer chains. Hence, a set of well-defined entangled linear (semi-)telechelic and telechelic four-arm star P*n*BAs functionalized with tpy units at chain ends with various molar masses was synthesized. Furthermore, a terpyridine acrylate (TPA) monomer was also elaborated and polymerized with *n*BA monomers via RAFT process to obtain a set of entangled linear sticky copolymers with the terpyridine groups randomly located along the polymer backbone. All these associating polymeric precursors were synthesized with low dispersity (Đ < 1.3) and with molar masses ranging from 100 to 250 kg/mol.

These polymeric precursors were then used to form metallo-supramolecular bulk polymers (MSBPs) upon addition of transition metal ions. While linear (semi-)telechelic P*n*BAs form longer chains,

the telechelic four-arm stars and the linear sticky copolymers self-assemble into reversible networks in which M-L complexes act as physical cross-links. Different metal cations were used such as zinc(II), copper(II), cobalt(II) or nickel(II) with the same counter anion which is the chloride. These metal cations have the same charge and similar ionic radius, making them suitable for comparison. What differs from one metal ion to another ion is its binding strength and kinetics to form the bis(terpyridine)-metal complex.

The linear viscoelastic properties of these MSBPs were systematically investigated via small angle oscillatory shear (SAOS). The results obtained from linear rheology highlight the impacts of M-L complexes combined with entanglements on the mechanical properties. In the case of linear mono-functional PnBA, in which chain length extension occurred, the chains mainly relaxed as relatively stable assemblies and their viscoelasticity was close to Maxwell predictions. For linear telechelic PnBA systems, their complex viscoelasticity originated from the combination of the reptation of the linear supramolecular molecular assemblies and the dissociation of stickers. Then, it is followed by the relaxation of more complex architectures such as polymer loops resulting in the presence of a second plateau modulus and an increase in modulus. In the case of four-arm star polymers, transient networks were formed by the combination of covalent cross-linking nodes, which came from the polymer cores, along with dynamic physical bridges which originate from the metal-ligand complexes. The star arm extremities must first dissociate, allowing the arms to relax via fluctuations. Depending on the thermodynamic stability and kinetics of the M-L complexes, the reversible bulk networks were able to behave as soft solids in a large frequency range. These experimental data reveal that the relaxation of MSBPs depends on both disentanglement and association dynamics, with the respective importance of these two processes depending on the nature of the metal ion and on the temperature. Hence, the incorporation of terminal active M-L complexes in polymers shows that the linear mechanical responses of the MSBPs can be finely engineered.

These systems were also theoretically investigated using a modified version of the tube-based time marching algorithm (TMA). A good description of the linear viscoelastic properties was achieved by

using a modified TMA model in which the dynamics of the stickers was taken into account. Particularly, it was considered that the M-L dissociations occur via a ligand exchange mechanism. The original TMA is a tube based model which comprises the reptation, the contour length fluctuations and constraints release mechanisms and can be used to describe the polymeric precursors without metal ions. In order to provide a good description of the MSBPs experimental viscoelastic data, two additional fitting parameters, such as the fraction of uncoordinated ligand and the longest time required to ensure that all chains were dissociated at least once, were introduced to the TMA model. The latter time was found to be independent of the chain architecture/topology and was well described by an Arrhenius equation, which allows us to derive the related activation energy. Therefore, it is possible to determine in advance this timescale for polymers based on the same terpyridine-ion complexes, leaving the modified TMA model with only one unknown parameter which is the average fraction of associated arms. One should mention that these results are valid as long as the samples contain a fraction of uncoordinated arms and that M-L association/dissociation events occur via ligand exchanges.

To achieve a systematic investigation of the rheological behaviors of the associating polymers based on M-L interactions, nonlinear rheological studies were conducted on the metallo-supramolecular bulk networks (MSBNs). Precisely, start-up shear measurements were performed using a home-made cone-partitioned plate (CPP) geometry and uniaxial extension tests were conducted on a filament stretching rheometer (FSR). In extension, the MSBNs exhibited strain hardening at extension rates below their respective terminal relaxation times. Since the transient viscosity of MSBNs was measured at low strain rates, the strain hardening was attributed to the physical crosslinks originated from the M-L complexes. On the other hand, strong shear thinning behavior was observed at similar deformation rates in nonlinear shear flow. From the experimental data, it was observed that M-L complexes dictate the ability of the reversible network to withstand large deformation. While the formation of M-L cross-links was enhanced by addition of metal salts, the transient junctions were also enhancing the contribution of trapped entanglements on the mechanical properties of the material under

355

deformation. Both M-L complexes and entanglements have a strong impact on the rheological properties of the transient networks under deformation. Additionally, the fraction of uncoordinated chains plays an active role in the stress distribution and modulates the bulk mechanical properties of MSBNs. The nonlinear viscoelastic properties of these associating systems can be tailored by varying the nature or the amount of added metal ions to form complexes. But also by altering the temperature which directly influences the relative importance of the metal-ligand complexes within the polymeric materials.

For covalently bonded polymers, if the applied shear rates are higher than the reciprocal characteristic relaxation time of the polymers, flow instabilities might be present. In the case of entangled supramolecular polymers, it is assumed that the deformation rates should be compared with the M-L coordination lifetime instead of the terminal relaxation time. Hence, dielectric relaxation spectroscopy (DRS) experiments were conducted on the MSBNs to experimentally determine the sticker lifetime. DRS results revealed a high frequency α-relaxation which was attributed to the segmental motion of the chains close to the thermal glass transition temperature. It was followed by a low frequency α_2-relaxation which was presumably associated to the dynamics of the M-L complexes. These timescales were then compared with the linear viscoelastic properties of MSBNs to confirm the peak assignments and the consistency of the results. However, the metal-ligand coordination lifetime was only experimentally determined via DRS for the transient network formed with 1.00eq. of Cu(II) which was evaluated to $\tau_s = 15$ ms. For the other transient networks, the electrode polarization effect was masking the majority of the α_2-relaxation, prohibiting the determination of the metal-ligand coordination lifetime at 0.50 and 0.75eq. of copper(II). Therefore, it was shown from the DRS data that the sticker lifetime was higher than the deformation rates, suggesting the absence of flow instabilities during the nonlinear rheology tests.

Additionally, the influence of diluting the transient network in a linear polymeric matrix was investigated. Two different matrices were used, one is unentangled and the other one is entangled, to study the influence of the network environment on its relaxation. It was found that this environment has a significant impact on the network stability.

356

Indeed, the network diluted in the short chains matrix relaxes much faster than the one mixed in the long chains matrix. When the short chain matrix was used, it was found that the average time during which a sticker stays free, τ_{free}, mostly depends on the dynamics of the linear chains, while p_{free} is strongly affected by the strength of the supramolecular bonds.

To summarize, we have developed model metallo-supramolecular networks functionalized with transition metal−ligand coordination complexes. Particularly, the rheological properties of terpyridine end-functionalized four-arm star poly(n-butyl acrylate) polymer are readily modulated over a wide spectrum by varying the temperature, the transition metal ion stoichiometry or the type of metal cation which directly affect the binding strength of the resulting M-L complexes. Furthermore, the dynamic nature of these transient coordination bondings lead to a promising pathway for engineering stimuli-responsive polymeric materials. With this work, it is hoped that a fundamental understanding on the structure-properties relationships of the entangled metallo-supramolecular bulk polymers has been gained. More precisely, on how the entanglements combined with M-L interactions influence the structure, the relaxation dynamics and the mechanical properties of different metallo-supramolecular entangled polymers over a wide range of timescales or temperatures. With this framework, we should be able to explore other transient networks based on M-L complexes and provide general guidelines for the design of novel MSPs with specific and tunable mechanical features. In particular, it would be interesting to have a complete study over the viscoelastic behavior of a reversible networks formed with only transient cross-links, for instance, the linear sticky copolymers presented in Chapter 3. The latter exhibited promising rheological behavior in which the cumulative effect of the stickers was highlighted, allowing the elaboration of relatively stable transient networks using bis(terpyridine)-zinc complexes as physical junctions. The linear viscoelastic properties of these reversible networks is studied and the results are reported in the Figure S1.
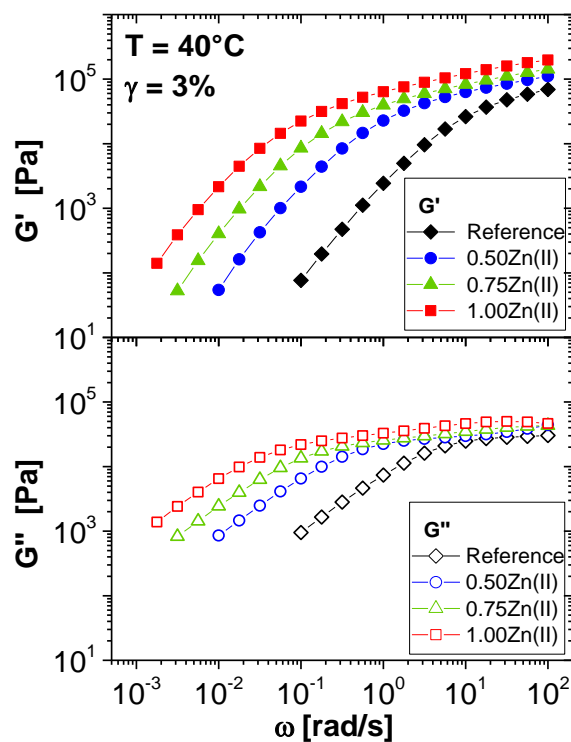
Figure S1 Linear rheology curves at 40°C of linear sticky PnBA$_{110k}$-co-PTPA$_{15}$ with different ratio of zinc(II) ions. The diamond symbols correspond to the reference polymer without metal ions. The storage modulus G' is represented by filled symbols, the loss modulus G" by unfilled symbols.

To the contrary, the nonlinear rheology of these systems still needs to be performed in order to achieve a complete systematic investigation over the mechanical properties of the transient networks formed with only physical M-L cross-links. Then, it would be interesting to compare the dynamics of the MSBNs formed with the telechelic four-arm star polymer with the ones obtained with the linear sticky copolymers. The experimental data may be further characterized using the modified TMA model presented in Chapter 4 as a starting point to describe the linear viscoelasticity. In a next step, it would be interesting and challenging to develop a tube based model to characterize the complex nonlinear viscoelastic properties of these metallo-supramolecular bulk polymers. Once the dynamics of these MSBPs are well characterized and well understood, it would be also

interesting to study the viscoelastic behavior of binary blends of two types of telechelic polymers as well as blends of telechelic precursors with linear sticky copolymers, and to be able to modulate the modulus of these associating systems on demand. Similar approach can be exploited by adding binary blends of metal ions to form metallo-supramolecular bulk polymers with M-L interactions displaying double dynamics. Other metal cations such as lanthanide ions can also be extremely interesting to use for the elaboration of light-emitting metallo-supramolecular polymers. In fact, the formed complexes not only act as transient junctions but they also exhibit luminescence properties, allowing one to track changes in molecular structures as a function of deformation or temperature. This optical property can be particularly promising to visually track the structural evolution of a material under small or large deformation.

Note that, for the linear sticky copolymers, zinc ions were purposely selected for their ability to form labile M-L complexes. Moreover, Zn(II) cations do not exhibit any toxicity, allowing the resulting MSBNs to be applicable for concrete applications such as coatings or adhesives. Indeed, the utilization of the metal-ligand interactions within poly(n-butyl acrylate) can be promising for the elaboration of the supramolecular adhesives with advanced functionalities such as stimuli-responsive features and reversible association/dissociation events. On one hand, the adhesive forces at the interface of two substrates can be engineered. On the other hand, the mechanical and the stimuli-responsive bulk properties of these materials can also be finely tailored. Therefore, it is possible to obtain supramolecular adhesives exhibiting a wide range of adhesion strengths in which dissociation can be triggered on demand with various external stimuli such as temperature or irradiation. However, one should note that these adhesives properties are highly complex and involve several mechanisms spanning different length scales. Hence, fundamental studies are needed in order to be able to exploit the use of the MSPs as supramolecular adhesives. For instance, macroscopic adhesive properties can be characterized by several experimental methods ranging from probe tack, tape peel or shear tests. Additionally, it is also important to study the fracture of reversible networks for understanding how these materials fail under large deformation.

Acknowledgments

In this last part, I would like to express my acknowledgments towards all the people that I have met during these past four years and who helped me to complete this thesis. First I would like to thank the jury members Jacques Devaux, Charles-André Fustin, Michel Cloître and Dimitris Vlassopoulos for the time they have spent to review this manuscript, the interest that they have put on this work and for their constructive comments. Your precious advices helped me a lot to improve the quality of the manuscript.

I am thankful to Jacques Devaux for chairing this session and sharing his brillant idea of blending the mono-associating systems of different molar mass and track the time needed to reach the equilibrium ratio of different systems. I would like to thank Charles-André for his supervision during these years. You are always involved in my projects and you always bring up relevant questions with instructive advices to reinforce the validity and the quality of the works. Even though it is not official, somehow you always acted as my third Ph.D supervisor and it was very helpful. I am very grateful to Michel Cloître for taking place in this graduation committee. As always, your relevant comments were extremely useful for me to improve the manuscript. I am extremely thankful for your generosity, your kindness and your straightforwardness.

I would like to express my gratitude to Dimitris Vlassopoulos who gave me the opportunity to visit his group to learn nonlinear shear rheology with the great help of Salvatore and Daniele. Your working pace inspires me and motivates me a lot. I am extremely grateful for your hospitality and your generosity. It goes without saying that the nonlinear rheology chapter is written only thanks to your strong support. I am so thankful for all your kind advices during each discussion. Special thanks to Salvatore and Daniele (amici miei) for helping me to easily settle down in Crete during my visit. I learned a lot from both of you and I sincerely spent great cheerful moments with you guys. Daniele I really miss our early morning session in the lab to settle the measurements and then we go enjoy a nice espresso on the terrace.

during my third year of Ph.D. I was extremely proud of you for the great works you have accomplished on your own.

To my rheology labmates Hamid, Taisir, Ashwin and Sina, it was a pleasure sharing the same office with you and having numerous discussions during these years. Especially to my friend Hamid, you have to be careful with your neck now that I am about to leave. Many thanks to Taisir for fruitful discussions on uniaxial extensional rheology. Your expertise helped me a lot to quickly understand the basics. To Sina, I will most probably miss all your jokes.

My sincere appreciations go to Filip, Luigi and Frank for your time and all your advices. I am so grateful to all of you for giving me such a great oppurtinity to join the group. E sopratutto a Luigi per il tuo aiuto e la tua generosità. Ti sarò sempre grato.

In this last page, I would like express my sincere gratitude to my promoters Evelyne and Jean-François for their guidance, their encouragment and for giving me freedom on this project. To Jean-François, thank you for receiving me at UCL during my first visits, for your great help during my registration and also for arranging my industrial secondment with Jean-Marc. I am thankful to Patrice for accepting me in his group at Allnex. To Evelyne, I am so greatful for your invaluable insights, your teachings, your patience and your tremendous generosity that I received during these years. You have been a constant model for me and your cheerfulness always inspires me to work at my best and to go beyond my limits. I am so thankful for all the great opportunities (conferences, visits to other group) that you offered me to improve myself not only as a researcher but also as a person. A special thought goes to your wonderful family as well: Xavier, Victor, Diego and Martin. All the joyful moments that we had together will forever be engraved in my memories and I hope we will continue to share other ecstatic moments.

Finally, I wish to dedicate this thesis to my family: my beloved mother, Fadoi, Patrick, Kamel and Jean-Baptiste (sisi la famille) for all their sacrifice, encouragement and support during these past four years. Special thanks to Fadoi for her tremendous help and patience till the very end. It was indeed a long journey with ups and down but it was definitely worth it as I luckily found new family members.